Transcranial Magnetic Resonance-Guided Focused Ultrasound (tcMRgFUS): An Investigation of the Key Factors to Enhance Treatment Outcomes for Patients with Tremor

A thesis submitted in fulfilment of the requirements for the degree of Doctor of Philosophy

by

Kain Kyle

Faculty of Medicine and Health

University of Sydney

2023

Statement of originality

This is to certify that to the best of my knowledge, the content of this thesis is my own work. This thesis has not been submitted for any degree or other purposes.

I certify that the intellectual content of this thesis is the product of my own work and that all the assistance received in preparing this thesis and sources have been acknowledged.

Kain Kyle

Authorship attribution statement

This thesis contains material published in several journals for which I was corresponding author, responsible for project conception, data analysis and manuscript preparation.

Section 3.4 contains material published in the following journal article:

Kyle, Kain, Joel Maamary, Benjamin Jonker, James Peters, Yael Barnett, Michael Barnett, Arkiev D'Souza, Jerome Maller, Chenyu Wang, and Stephen Tisch. 2023. "Consistency Is Key: Influence of Skull Density Ratio Distribution on the Formation of Clinically Effective Lesions and Long-Term Tremor Suppression Following Treatment with MR-Guided Focused Ultrasound." *Journal of Neurosurgery* 1–9. doi: https://doi.org/10.3171/2023.6.JNS231153.

Section 4.4 contains material published in the following journal article:

Kyle, Kain, Jerome Maller, Yael Barnett, Benjamin Jonker, Michael Barnett, Arkiev D'Souza, Fernando Calamante, Joel Maamary, James Peters, Chenyu Wang, Stephen Tisch, Arkiev D. Souza, Fernando Calamante, Joel Maamary, James Peters, Chenyu Wang, and Stephen Tisch. 2023. "Tremor Suppression Following Treatment with MRgFUS: Skull Density Ratio Consistency and Degree of Posterior Dentatorubrothalamic Tract Lesioning Predicts Long-Term Clinical Outcomes in Essential Tremor." Frontiers in Neurology 14(April):1–10. doi: 10.3389/fneur.2023.1129430.

Kain Kyle 29/09/2023

As supervisor for the candidature upon which this thesis is based, I can confirm that the authorship attribution statements above are correct.

Chenyu Wang 29/09/2023

Acknowledgments

Firstly, I would like to acknowledge and extend my deepest respect to the Aboriginal people, both past and present, as the traditional custodians of the land on which this research was conducted. I pay homage to the Gadigal people of the Eora Nation, upon whose ancestral lands the University of Sydney and St Vincent's Hospital Sydney stand.

I am sincerely grateful for the mentorship, guidance and support provided by my supervisor, Chenyu Wang. Thank you for the countless hours you have spent working with me on the material presented in this thesis. Your encouragement, vision and incredible gift for distilling an overwhelming amount of information into a cohesive idea have been pivotal in the completion of this work. I look forward to continuing our research journey together.

I am deeply thankful for the extraordinary support provided by Michael Barnett. Your passion, knowledge and wisdom have significantly influenced my development as a researcher, for which I will always be grateful.

I would like to thank the team at St Vincent's Hospital Sydney for their support, particularly Yael Barnett, without whom I would not be in the position I am today. Thank you to Stephen Tisch, Ben Jonker, Joel Maamary and James Peters for your guidance and generosity in sharing your knowledge. I would also like to thank the Medical Imaging team, especially Kirsten Moffat, Karen Chisnell, Joanne Ross and Nicole Welsh, for all of your assistance and encouragement. Your contribution underpins not just my own work but that of the entire research group.

Thank you to Arkiev D'Souza for your assistance. You have been an incredible source of knowledge over the course of this project. Thank you to Linda Ly for your advice and guidance throughout this journey, I sincerely appreciate all you have done for me in the time we have worked together.

I would like to express my gratitude to the team at GE Healthcare Australia, in particular Jerome Maller and Daneh Turner. Thank you for your mentorship and for providing such a supportive research environment.

I would also like to thank my family, especially my parents, for their unconditional support and for fostering my innate curiosity. I am sorry if you were hoping my academic pursuits might have answered some of the many questions I had; I am afraid it has only generated more.

Finally, I would like to thank my wife, Tess Novak. Without your boundless encouragement and unwavering support, this work simply would not have been possible. I am eternally grateful, and I feel profoundly fortunate to have you by my side.

Thesis Abstract

Transcranial magnetic resonance-guided focused ultrasound (tcMRgFUS) is a minimally invasive surgical procedure for the treatment of tremor in movement disorders such as essential tremor (ET), dystonic tremor (DT) and tremor dominant Parkinson's Disease. This PhD thesis investigates the patient-specific and treatment-related factors that influence tremor improvement following treatment with tcMRgFUS. Patient-specific factors such as the disease type, and properties of the skull were analysed to investigate the relationship with clinical outcomes. Treatment factors such as the tcMRgFUS lesion location was also investigated with advanced neuroimaging techniques such as diffusion tensor imaging (DTI). The comprehensive study of these factors offers the potential to enhance patient outcomes via improved patient screening and treatment strategy.

Thesis outcomes

Journal Articles

- **Kain Kyle**, Joel Maamary, Benjamin Jonker, James Peters, Yael Barnett, Michael Barnett, Arkiev D'Souza, Jerome Maller, Chenyu Wang, and Stephen Tisch. 2023. "Consistency Is Key: Influence of Skull Density Ratio Distribution on the Formation of Clinically Effective Lesions and Long-Term Tremor Suppression Following Treatment with MR-Guided Focused Ultrasound." *Journal of Neurosurgery* 1–9. doi: https://doi.org/10.3171/2023.6.JNS231153.

- **Kain Kyle**, Jerome Maller, Yael Barnett, Benjamin Jonker, Michael Barnett, Arkiev D. Souza, Fernando Calamante, Joel Maamary, James Peters, and Chenyu Wang. 2023. "Tremor Suppression Following Treatment with MRgFUS : Skull Density Ratio Consistency and Degree of Posterior Dentatorubrothalamic Tract Lesioning Predicts Long-Term Clinical Outcomes in Essential Tremor." (April):1–10. doi: 10.3389/fneur.2023.1129430.

- **Kain Kyle**, James Peters, Joel Maamary, Benjamin Jonker, Yael Barnett, Michael Barnett, Jerome Maller, Chenyu Wang and Stephen Tisch. "Magnetic resonance-guided focused ultrasound for treatment of essential tremor: Ventral intermediate nucleus ablation alone or additional posterior subthalamic area lesioning?" (In submission with Movement Disorders: Clinical Practice).

- **Kain Kyle**, James Peters, Benjamin Jonker, Yael Barnett, Joel Maamary, Michael Barnett, Jerome Maller, Chenyu Wang PhD, and Stephen Tisch. "Validation of automated spiral analysis for assessment of tremor severity during MR-guided focussed ultrasound. (In submission with British Journal of Neurosurgery).

- Wilson, David N., Yael Barnett, **Kain Kyle**, Stephen Tisch, and Benjamin P. Jonker. 2021. "Predictors of Thermal Response and Lesion Size in Patients Undergoing Magnetic Resonance-Guided Focused Ultrasound Thalamotomy." *Journal of Clinical Neuroscience* 91:75–79. doi: 10.1016/j.jocn.2021.06.019.

- Maamary, Joel, James Peters, **Kain Kyle**, Yael Barnett, Benjamin Jonker, and Stephen Tisch. 2023. *Effective Subthalamic Nucleus Deep Brain Stimulation Following MRgFUS for Tremor Dominant Parkinson's Disease*. Vol. 10. doi: 10.1002/mdc3.13662.

Conference Abstracts

- **Kain Kyle**, Jerome Maller Yael Barnett, Stephen Tisch, Benjamin Jonker, Michael Barnett, Arkiev D'Souza, and Chenyu Wang. Comparison of Automated Thalamic Segmentation Techniques: Applications in MRgFUS Planning. ISMRM & SMRT Annual Meeting Online May 2021

- **Kain Kyle**, Yael Barnett, Stephen Tisch, Ben Jonker, Arkiev D'Souza, Jerome Maller, Michael Barnett, Joel Maamary, and Chenyu Wang. Acute Global Structural and Diffusivity Changes Following Treatment with MRgFUS. 31st Joint Annual Meeting ISMRM-ESMRMB & ISMRT London 2022

- Arkiev D'Souza, Fernando Calamante, **Kain Kyle**, Stephen Tisch, Ben Jonker, Yael Barnett, Joel Maamary, Jerome Maller, Justin Garber, Michael Barnett, and Chenyu Wang. Immediate changes in graph metrics following MRgFUS - an investigation using state-of-the-art diffusion image analysis. 31st Joint Annual Meeting ISMRM-ESMRMB & ISMRT London 2022

- Zihao Tang, Mariano Cabezas, **Kain Kyle**, Arkiev D'Souza, Stephen Tisch, Ben Jonker[4], Yael Barnett, Joel Maamary, Jerome Maller, Michael Barnett, Weidong Cai, and Chenyu Wang. Towards a personalized MRgFUS treatment for tremor disorders: A study on the number of ablations using deep learning and structural connectivity. 31st Joint Annual Meeting ISMRM-ESMRMB & ISMRT London 2022

Table of Contents

List of Figures

List of Tables

Glossary of abbreviations

SD	Standard Deviation
Hz	Hertz
AC	Anterior Commissure
AD	Alzheimer's disease
AE	Adverse Effect
AER	Adverse Effect Rate
AFD	Apparent Fibre Density
AIC	Akaike information criterion
ATD	Accumulated Thermal Dose
ATTD	accumulated therapeutic thermal dose
COG	Centre of Gravity
CI	Confidence Interval
CRST	Clinical Rating Scale for Tremor
CT	Computed Tomography
DBS	Deep Brain Stimulation
dMRI	Diffusion MRI
DPI	Dots per inch
DRTT	Dentatorubrothalamic tract
DT	Dystonic Tremor
DTI	Diffusion Tensor Imaging
EEG	Electroencephalography
EMG	Electromyography
ET	Essential Tremor
ETP	Essential Tremor Plus
FA	Fractional Anisotropy
FDR	False Discover Rate
fMRI	Functional MRI
FOD	Fibre Orientation Distribution

FTM	Fahn-Tolosa-Marin tremor rating scale
FUS	Focused Ultrasound
GE	Gradient Echo
GK	Gamma Knife
GPi	Globus Pallidus Internus
HE	Heating Efficiency
HFS	High Frequency Stimulation
HIFUS	high-intensity FUS
HTS	Hand Tremor Score
ION	Inferior Olivary Nucleus
L-dopa	Levodopa
M1	Primary Motor Cortex
MEG	Magnetoencephalography
mm	Millimetres
MPD	Mean Percentage Difference
MPRAGE	Magnetization-Prepared Rapid Acquisition Gradient Echo
tcMRgFUS	Transcranial Magnetic Resonance-guided Focused Ultrasound
MRI	Magnetic Resonance Imaging
NAE	Number of Active Elements
PC	Posterior Commissure
PD	Parkinson's Disease
PET	Positron Emission Tomography
PSA	Posterior Subthalamic Area
QUEST	Quality of Life in Essential Tremor
RF	Radiofrequency
RN	Red Nucleus
ROI	Region of Interest
SDR	Skull Density Ratio
SNR	Signal to Noise Ratio
ST	Skull Thickness
T1-WI	T1-Weighted Image
TAWD	Tremor Associated with Dystonia

TMS	Transcranial Magnetic Stimulation
TRIG	Tremor Investigation Group
US	Ultrasound
VC	Ventralis caudalis Nucleus
Vim	Ventral Intermediate Nucleus
VLa	Ventral Lateral Anterior Nucleus
VLp	Ventral Lateral Posterior Nucleus
Voa	Ventralis Oralis Anterior
Vop	Ventralis Oralis Posterior
WMnMPRAGE	White Matter Nulled Magnetization-Prepared Rapid Acquisition Gradient Echo
ZI	Zona Incerta

1 Introduction

1.1 Tremor

1.1.1 Background

Tremor, defined as the "involuntary, rhythmic, oscillatory movement of any body part" [1], is one of the most prevalent movement disorders. Tremor itself is not inherently dangerous, however, tremor can cause significant disability, affecting daily activities and negatively impacting quality of life[2]. The psychological impact of tremor is thought to be greater than the physical disabilities [3–5]. Tremor has been associated with social isolation and depression [3], as well as difficulty in gaining and maintaining employment [3,6–8], with up to 25% of patients forced to retire prematurely due to the severity of tremor[9].

All adults exhibit some degree of physiological tremor[10], and it is important to distinguish physiological tremor from pathological tremor. Tremor is often distinguished by the phase of movement, distribution and frequency [11], which together with the patient history typically form the basis of clinical diagnosis. Tremor can be divided into 2 types: Resting tremor: "tremor present in a body part that is fully supported against gravity and that is not associated with any voluntary activity", and action tremor: "tremor present with any voluntary movement of a body part"[12]. Action tremor can be further subdivided into postural, kinetic, intention, task-specific and isometric tremor, definitions of which are summarised in *Table 1-1*. Tremor frequency is often characterised as slow(<4Hz), medium (4-7 Hz) or high (>7 Hz), while severe tremor amplitude is considered around 4cm[13].

Table 1-1 Definition of tremors as defined by Elias et al.[12]

Tremor type	Definition
Resting	Tremor present in a body part that is fully supported against gravity and not associated with any voluntary activity
Action	Tremor present with any voluntary movement of a body part
Postural	Tremor while holding a position against gravity
Kinetic	Tremor with volitional movement that is unchanged throughout all phases of movement
Intention	Tremor that increases in amplitude at the target
Task-specific	Tremor that is appears or is exacerbated by a specific movement
Isometric	Tremor with contraction of muscles against resistance without movement of the affected body part

Tremor can be associated with several neurological diseases, neurodegenerative conditions, medications, lesions and traumatic injuries - some common tremor types and their characteristics are summarised in *Table 1-2*. The remainder of this thesis will focus on two commonly encountered tremors – essential tremor (ET) and dystonic tremor (DT).

1.1.2 Essential Tremor

Definition

Table 1-2 Tremor definitions per the 2018 international Parkinson and Movement Disorder Society consensus statement[1]

Tremor subtype	Definition
Essential tremor	"Isolated tremor syndrome of bilateral upper limb action tremor, of at least 3 years duration, with or without tremor in other locations (such as the head, voice or lower limbs), and in the absence of other neurological signs (such as dystonia, ataxia or parkinsonism)"
Essential tremor plus	"Tremor with the characteristics of ET and additional neurological signs of uncertain significance such as impaired tandem gait, questionable dystonic posturing, memory impairment, or other mild neurologic signs of unknown significance that do not suffice to make an additional syndrome classification or diagnosis. ET with tremor at rest should be classified here."
Dystonic tremor	"Tremor in a body part affected by dystonia"
Tremor associated with dystonic	"Tremor in body parts that are not dystonic"

Due to the heterogeneity in the presentation of ET, and the evolution of symptoms over time, which may include the development of other neurological conditions, there is continued debate over whether ET should be considered a "syndrome" or a "family of diseases". While ET was often thought of as a "benign tremor syndrome", some studies have found an association with cognitive impairment[14], and there is evidence of increased mortality in people with ET[15,16], however, the exact mechanism underlying this observation remains unclear.

The first use of the term "Essential Tremor" can be traced back to Pietro Burresi of the University of Siena, Italy, where the term was used to describe the isolated action tremor in an 18-year-old man [17]. The term featured more regularly through the early 1900s and the first review of ET was published in 1949[18], where the condition was described as a "monosymptomatic peculiarity" in a majority of cases, with frequent familial occurrence. By

1983, it was recognised that ET was not a "single entity", with dystonic tremor and postural parkinsonian tremor also included in the early definition [19]. The Tremor Investigation Group (TRIG) published criteria for ET diagnosis in 1994 [20], where the term "Classic ET" was used to describe definite and probable cases of ET, while cases not meeting the criteria for Classic ET were classified as "possible ET". Classic ET was defined as "bilateral, largely symmetric postural or kinetic tremor involving hands and forearm with additional or isolated head tremor but in the absence of abnormal posturing".

The first consensus statement tremor classification was published in 1998 and included the TRIG criteria for diagnosis, stating that ET is a "tremor syndrome, classically defined by a mostly hereditary, mainly postural tremor of the hands and sometimes head"[11]. The consensus statement did not, however, include the duration of tremor in the definition of ET, arguing that the durations of 3 years (probable ET) and 5 years (definite ET) recommended by the TRIG criteria were arbitrary[11]. The tremor classification was further refined in the most recent consensus statement, published in 2018[21]. Here tremor was classified according to two axes: Axis 1 – based on the clinical characteristics, and Axis 2 – based on the aetiology. The task force divided the axis 1 tremor syndromes into 2 groups: isolated tremor, where tremor is the only abnormal sign, and combined tremor, where additional signs such as dystonia and ataxia are present. ET was defined as an "isolated tremor syndrome of bilateral upper limb action tremor, of at least 3 years duration, with or without tremor in other locations (such as the head, voice or lower limbs), and in the absence of other neurological signs (such as dystonia, ataxia or parkinsonism)"[1]. The exclusion criteria for ET were defined as isolated focal tremors, orthostatic tremor with a

frequency greater than 12Hz, task and position specific tremor, and sudden onset and stepwise deterioration.

In the updated consensus statement, the concept of ET-plus was also proposed. ET-plus was defined as “tremor with characteristics of ET, with additional neurological signs of unknown significance, such as questionable dystonia, impaired tandem gait and memory impairment, which includes ET with tremor at rest” [21]. The introduction of this new classification led to the reclassification of up to 83% of patients from ET to ET-plus[22,23] with indications that ET-plus may be more common than ET [1,23,24]. In the latest consensus statement, the task force acknowledged that the clinical signs and symptoms in ET may evolve over time, including the development of new symptoms such as dystonia and parkinsonism, which may result in a change in diagnosis. This, together with observed associations between patient age and ET-plus, has led to speculation that ET-plus is simply a later stage of ET, however, whether the additional neurological signs in ET-plus are coincidental or aetiologically related remains unclear.

Demographics

Accurate estimation of the prevalence of ET is made challenging by the number of people suffering from tremor who choose not to seek medical attention [25]. Additionally, inconsistent application of the diagnostic criteria may have impacted some studies of the epidemiology of ET, where the inclusion of patients with mild tremor potentially contributed to the higher reported prevalence of the condition [26]. Nonetheless, Essential tremor is

known to be one of the most prevalent movement disorders [27], affecting up to 800,000 individuals in Australia[28], and 3.2 cases per 1000 individuals afflicted globally, increasing to 28.7 cases per 1000 individuals in people over 80 years old [29].

The prevalence of ET with respect to age displays a bimodal distribution, with cases of ET onset peaking in early adulthood and in people over the age of 65. The age at onset has been shown to be an important prognostic factor, with Louis et. al. demonstrating in their study of 195 ET patients that the mean age at onset was 40.9 years in familial ET, compared with 57.3 years in sporadic ET. Sporadic ET is also associated with more rapid progression[30] due to the reduced reserve and neuronal loss associated with ageing[31]. The prevalence of ET is similar between men and women, however, research has shown that women tend to have a greater prevalence of, and more severe, head tremor, while men may experience more severe postural tremor. [32,33]

Risk Factors

Family history has been identified as an important factor in the development of ET. Approximately 50-70% of patients with ET have a family history of tremor [34], and first-degree relatives are approximately 4.7 times more likely to be diagnosed with ET[35]. While inheritance patterns vary, it appears to follow an autosomal dominant pattern with incomplete penetrance [36]. An association between ET and Parkinson's Disease (PD) has also been identified, with ET patients at a higher risk of developing PD than the general population [37].

Studies of ET in monozygotic twins have found that, while concordance is high, it is not complete, suggesting non-genetic factors in the development of ET [38,39]. Several environmental factors have been linked to ET, including diet[40], exposure to agricultural work [41] and pesticides [42,43]. Some studies have also found an association between lead exposure and ET, with lead blood concentrations found to be greater in patients with ET [44,45]. Smoking has been found to have a protective effect in ET, which is believed to be due to the effect of nicotine on acetylcholine receptors[46], with non-smokers at a higher risk of ET than smokers[47,48]. Sleep duration has also been linked with ET[49]. Studies of the relationship between alcohol consumption and ET have returned mixed results, possibly due to the high rates of chronic alcoholism in ET populations [50]. Ethanol has been shown to have short-term tremor-relieving effects via suppression of the inferior olivary nucleus (ION) [51] and GABA transmission [52]; however, increased alcohol consumption has also been suggested as a risk factor [41,53] due to the degenerative effect on the cerebellum, including atrophy and loss of Purkinje cells[54].

Pathophysiology

The pathophysiology of ET is not well understood, with ongoing debate over whether ET is a neurodegenerative disease or primarily a disorder of electrical network dysfunction. ET is a chronic disorder with an observed progressive clinical course, with some studies estimating a 3.1% – 5.3% increase in tremor severity per year[55]. Studies have shown that age is a risk factor for ET, consistent with other neurodegenerative diseases such as PD and Alzheimer's disease (AD)[31]. While post-mortem studies in ET have been limited, there have been reports of morphological changes in the cerebellum, including Purkinje cell (PC) loss and an increase

in the number of PC axonal swellings (PC torpedoes)[56], loss of spines in PC dendrites, remodelling of PC axons and PC death[57].

Imaging studies of ET have suggested functional and structural abnormalities in the brain, particularly in the cerebellum and cerebellar-thalamic network. Some studies have suggested possible atrophy in the cerebellum in ET patients[58,59], however, results have been mixed, and recent meta-analysis did not find a systematic difference in grey matter morphology between ET and healthy controls[60]. Diffusion MRI (dMRI) studies have identified structural changes in the white matter tracts in the cerebellum and cerebellar peduncles[61,62], as well as more widespread microstructural alterations in the corticospinal tract, corpus callosum and cortico-pontine tracts[63–65] and in the fibre tracts connecting the ventral intermediate (Vim) nucleus of the thalamus with the motor and supplementary motor cortical regions[66]. Studies employing functional MRI (fMRI) and positron emission tomography (PET) have identified neuronal activity changes in cerebellum, thalamus, motor cortex and red nucleus, with abnormal functional connectivity of the cortico-cerebello-thalamic tract has been a consistent finding in fMRI studies of ET [67–79].

Electrophysiological studies employing electroencephalography (EEG) or magnetoencephalography (MEG) have provided data linking the oscillations in neuronal activity with the oscillations in peripheral muscle activity. EEG/MEG studies have demonstrated rhythmic cortical activity in the primary motor cortex (M1) region in ET. Other EEG/MEG studies have implicated the cerebellum, thalamus and motor cortex as nodes in an interconnected tremor network[80], and demonstrated that involvement of the cortex is intermittent[81].

While the findings of neuroimaging and electrophysiological studies of ET are varied, which may reflect the clinical and pathophysiological heterogeneity of ET, the data supports the structural and functional changes in the cerebellum and a wider tremor-related network as the pathophysiological substrate of ET.

1.1.3 Dystonic Tremor

Definition

Dystonia is defined as "a movement disorder characterised by the sustained or intermittent muscle contractions causing involuntary postures, often with repetitive movements or jerky oscillations, and often worsened by voluntary action"[82]. The term dystonia is a broad umbrella term for several clinically heterogeneous disorders.

Dystonia may occur in an isolated body part (focal dystonia) in several contiguous regions (segmental dystonia), or multifocal and generalised dystonia [83–86], and the distribution of affected regions may progress over time. Dystonia may also be categorised by aetiology, where dystonia in the context of no secondary cause or associated brain pathology is considered primary dystonia, and all other forms of the condition considered secondary dystonia [87], which can be further divided into inherited, complex and acquired subtypes.

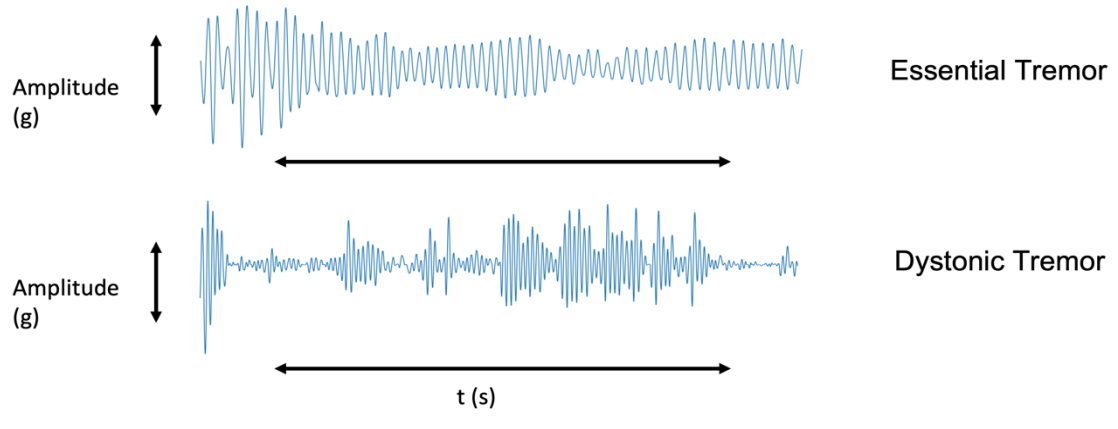

*Figure 1-1 Example of tremor measured with accelerometry in a patient with ET (**top**) and DT (**bottom**).*

Tremor has only recently been recognised as forming part of the clinical spectrum of dystonia [88,89]. Dystonia was first reported in 1911, when "dystonia musculorum deformans" was described by Hermann Oppenheim[90]. Studies in the 1960s [91] and 1970s [92,93] also reported tremor in dystonia, however, tremor was not included in the first consensus definition of dystonia in 1984 [94]. Dystonic tremor was first included in the 1998 Movement Disorders Society consensus statement, where the term tremor associated with dystonia (TAD), was also first proposed [11], and by 2013 the MDS committee proposed an updated definition stating the dystonic movement may be tremulous [82]. The latest Movement Disorders Society consensus statement, published in 2018, defines dystonic tremor (DT) as tremor in a body part affected by dystonia, while tremor in a body part not affected by dystonia was termed tremor associated with dystonia (TAD). The definition of DT is based on the phenomenology of movement, where DT is typically characterised by jerky, coarse, irregular and asymmetric oscillations with saw-tooth appearance (*Figure 1-1*); however, small regular ET-like oscillations have also been described.[95] DT is most often observed

during postural, holding and reaching tasks, [96,97] however, tremor at rest is also possible [97], which can be difficult to distinguish from PD[98].

Recent studies have shown that tremor in dystonia most frequently involves the head [99], followed by the upper limbs, and appears to be associated with the spread of dystonia to previously unaffected regions of the body[96,100,101]. The peak frequency of DT is similar to ET and ET-plus at around 4-10Hz [102]. TAD has been shown to be a relatively symmetric postural and kinetic tremor, with higher frequency than DT [103], and can be difficult to distinguish from ET[104].

Accurate diagnosis of DT can be difficult, and the updated definitions of DT remain controversial. There is considerable inter-rater disagreement in the diagnosis of DT, with one study reporting a Fleiss kappa of only 0.34 between 4 expert raters [105], however, the effect of sensory tricks on tremor, as well as the presence of null points where tremor is significantly diminished or disappears in certain positions, may help distinguish DT from ET [106]. Studies employing EMG and accelerometry have demonstrated that DT can be distinguished from ET by greater variability in the tremor frequencies over time [107,108] , as well as increased variation in the intensity and duration of muscular activity [109].

Demographics

The true prevalence of dystonia remains unclear; however, the literature suggests that dystonia is a relatively rare disease[110]. The reported prevalence of late-onset and early-onset primary dystonia is estimated as 30-7320 cases per million people and 2-50 cases per

million –respectively [111–120]. A recent meta-analysis estimated the prevalence of primary dystonia to be 16.43 cases per 100,000 people[121]. Dystonia may present at any age, however, age at onset is known to be a relevant prognostic factor [122].

The reported prevalence of tremor in those diagnosed with dystonia ranges from 14-87% [123], with an average prevalence of 53%[99], according to a recent study. Head tremor in patients with cervical dystonia is the most common form of DT [99], with one study estimating that 68% of patients exhibited tremor [124], and studies have estimated that 20% of patients with dystonia experience postural tremor of the upper limbs [125] .

The prevalence of tremor in dystonia has been shown to be associated with increased age and longer dystonia duration [102]. Some studies have suggested that there is a greater prevalence of DT in females compared with males [96,126]. Higher age at onset has been reported in patients with tremor compared with those without tremor [126]. There is evidence that tremor is more frequently seen in segmental and multifocal dystonia, compared with focal dystonia [96]. Patients with primary dystonia appear to be more likely to have tremor than those with secondary dystonia [123]

Risk Factors

There is clear evidence of genetic factors in dystonia, with several genetic loci linked with primary dystonia[127]. The phenotypic heterogeneity observed in dystonia suggests that environmental factors may play an important role, however, little research in this area has been conducted. There is evidence that infection or fever may be associated with early-

onset generalised dystonia[128] , while traumatic injury has also been linked with dystonia[128,129] however, this remains controversial. Cigarette smoking has been reported to have a negative association with primary dystonia[130].

Pathophysiology

Traditionally, DT was considered a disorder primarily associated with dysfunction of the basal ganglia, however, as in ET, more recently the prevailing view has shifted to that of more widespread motor network dysfunction [102,131,132]. It remains unclear whether dystonia and DT are the result of unique pathophysiology, however, there is evidence that the jerky oscillatory motion in dystonia and DT share similar neuroanatomical and physiological features [103,133–136], including impaired inhibition at the cortical, subcortical and spinal level [137]. Whether DT and TAD are distinct entities remains unclear, however, there is evidence that DT may be more similar to non-tremulous dystonia, while TAD shares more features with ET[108].

Recent studies have implicated both the basal ganglia and cerebello-thalamo-cortical networks in DT [138–140], however, it remains unclear if tremor is driven by a single network or a combination of both. Dystonia has been known to occur in the context of focal cerebellar lesions [141,142], as well as degenerative cerebellar disease [143–145]. Pathological changes to the cerebellum, including cerebellar lesions and atrophy, as well as functional abnormalities in the cerebellum have been identified in DT patients [146–149].

1.1.4 The Tremor Network

Early models of ET focused on a central oscillator as the source of tremor, with the inferior olivary nucleus (ION) thought to be involved due to the potential for rhythmic excitation [150]. The neurons of the ION carry unique calcium channels that are capable of producing rhythmic discharges at tremor frequencies. The olivary hypothesis for ET was based on the similarity between ET and tremor induced by the β-carboline harmaline in primates [151], and it was thought that oscillatory activity originated in the ION and was transmitted and amplified through the cerebellum, resulting in entrainment of the thalamus, motor cortex and brainstem nuclei [152]. This view, however, has since been refuted [153], based on the lack of structural alterations in the ION in ET and neuroimaging and electrophysiological studies that instead implicate several structures in a tremor-related network, including the cerebellum, thalamus and motor cortex (*Figure 1-2*).

The Cerebellum

The cerebellum has been the subject of many studies on movement disorders, particularly in ET. Deep cerebellar nuclei and Purkinje cells of the cerebellar cortex connect to the contralateral ION via the olivocerebellar pathway, crossing the contralateral inferior cerebellar peduncle. The cerebellum also provides the Vim nucleus of the thalamus with glutaminergic input through deep cerebella nuclei[154] via the dentatorubrothalamic tract. Together with the rubro-olivary tract, which connects the ipsilateral ION and red nucleus (RN), these 3 tracts form the Guillain Mollaret Triangle.

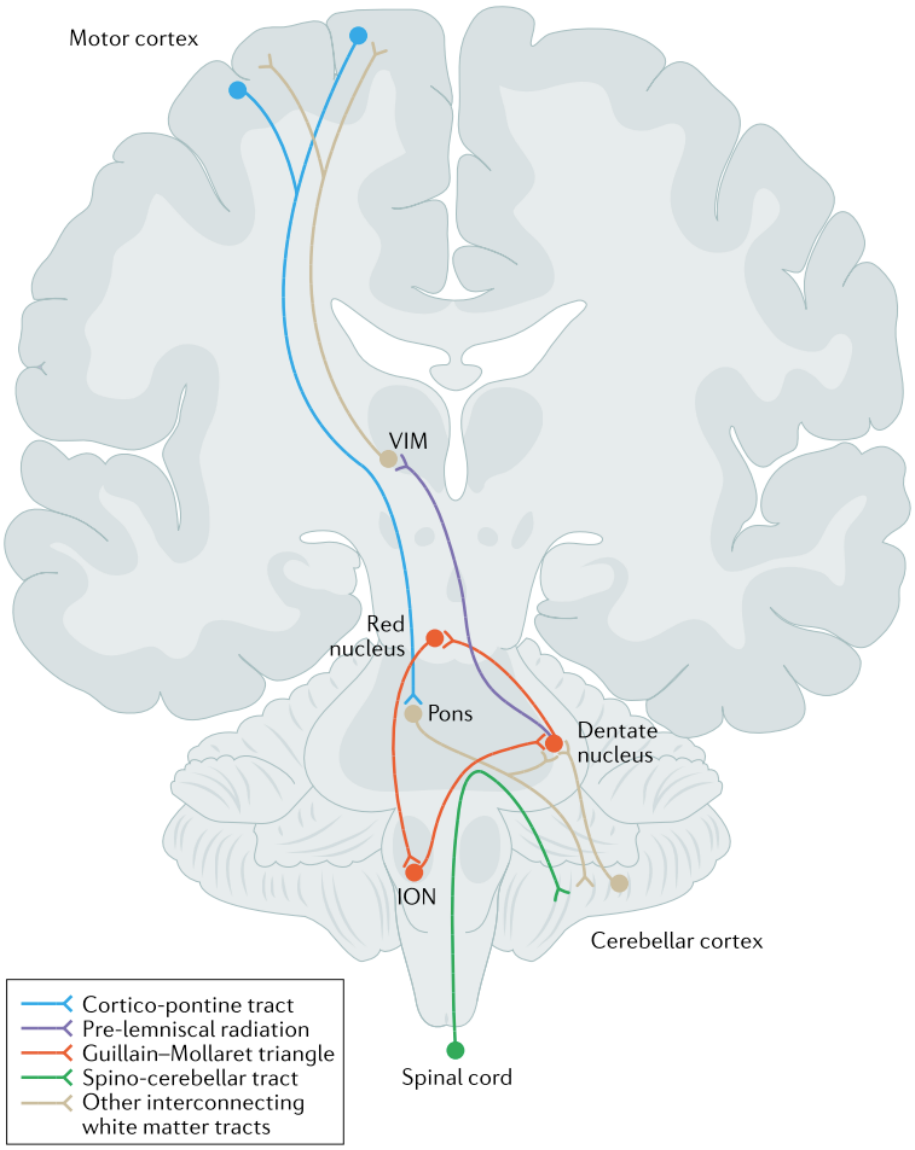

Figure 1-2 Illustration of structures implicated in the propagation of tremor. Adapted from [450].

Early studies of harmaline tremor in mice demonstrated that tremor severity was decreased when the cerebellum was not intact[155], highlighting the relationship between the ION and cerebellum in the generation of tremor. The involvement of the cerebellum in ET has since been confirmed by a number of physiological and neuroimaging studies.

Electrophysiological studies employing EEG have demonstrated oscillatory activity in the cerebellum at 4-12Hz, which correlated with tremor severity [156]. Early fMRI and PET studies

observed bilateral cerebellar activation in ET patients during postural tremor[75,157,158], which have been confirmed in more recent studies [159,160]. Furthermore, recent studies employing combined electromyography (EMG) and fMRI concluded that cerebello-dentato-thalamic activity and cerebello-cortical connectivity were disturbed in ET[74].

While the involvement of the cerebellum in ET has been well established, studies have also implicated the cerebellum as a key component in dystonic tremor, with fMRI studies investigating the inter-regional coupling of the cerebello-thalamic pathway in DT [161] producing similar results to studies in ET [71,74]. fMRI studies in DT have demonstrated abnormal network activity in DT, with cerebellar connectivity during grip-force induced tremor similar to ET [139,162], and the cerebellum often implicated as a key node within the pathological tremor network [131,132,163]. Furthermore, dMRI studies have demonstrated microstructural changes in the cerebello-thalamic pathway in dystonia [164], and transcranial magnetic stimulation (TMS) studies targeting the cerebellum have been shown to improve dystonic symptoms in patients with cervical dystonia [165,166]. Taken together, there is significant evidence that the cerebellum is involved in both ET and DT.

The Thalamus

Connected to several regions implicated in tremor networks, including the cerebellum, motor cortex and basal ganglia, the thalamus has been identified as a key region in the genesis of tremor[167]. The thalamus is composed of multiple grey matter nuclei, each with unique histological features, structural connections and functional roles. The principal thalamic nuclei involved in the motor circuit, and the most relevant for stereotactic

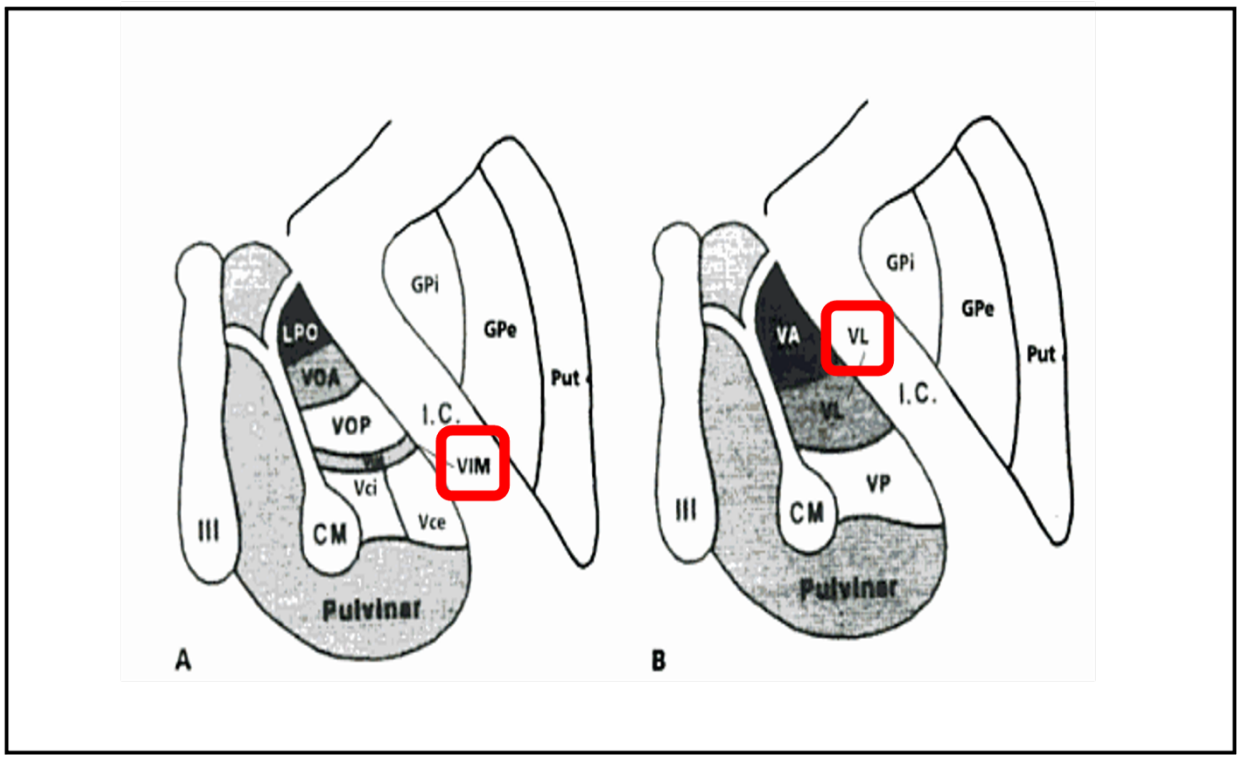

Figure 1-3 Axial view of thalamic atlas schemes. ***A*** *- Hassler classification system with Vim circled in red.* ***B*** *- Anglo-American classification system with ventral lateral (VL) motor thalamus circled in red. Adapted from* Osenbach et al.[451]

treatment of tremor, are those of the ventrolateral tier of the thalamus, known collectively as the motor thalamus. The motor thalamus is the principal relay point between the ascending and cerebellar inputs, and the motor regions of the cerebellar cortex. In surgical literature, it is defined as the region bounded by the internal medullary lamina medially, the external medullary lamina, reticular nucleus and internal capsule laterally and the somatosensory thalamic nuclei posteriorly. The nuclei of the motor thalamus are distinguished by the target/source of their afferent/efferent projections and have long been the focus in the treatment of movement disorders.

Several thalamic parcellation schemes have been proposed, with the nomenclature of Hassler finding popularity amongst neurosurgeons, while the atlas proposed by Morel et al.

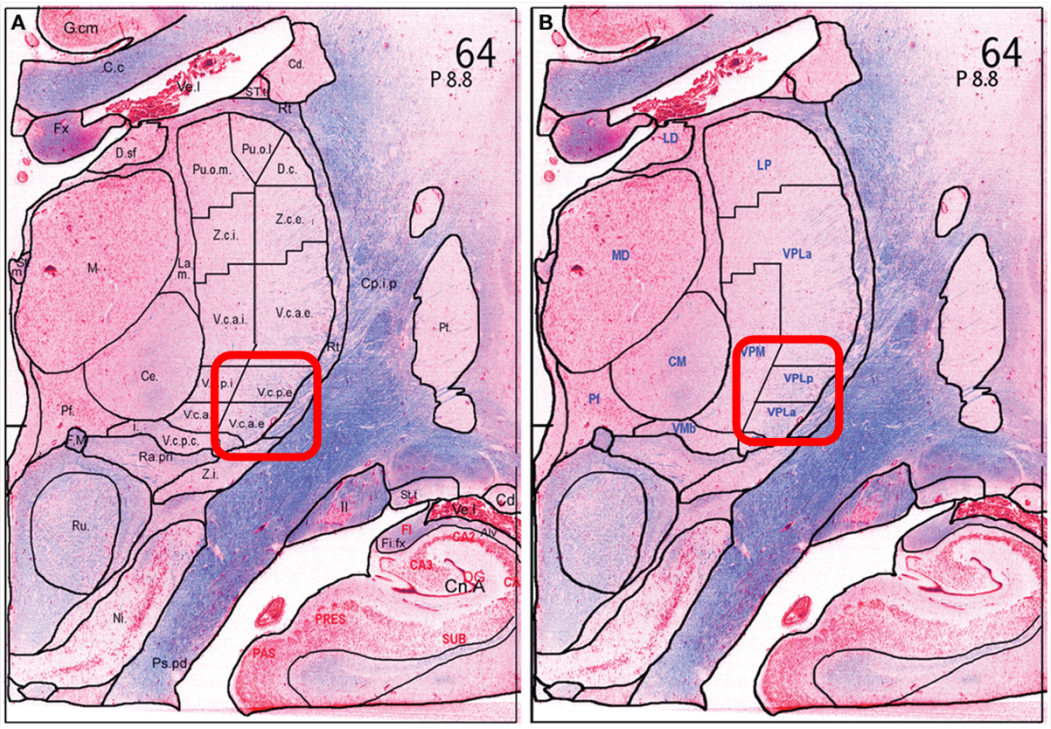

*Figure 1-4 Coronal view of thalamic nuclei as defined with the Schaltenbrand atlas (**A**) and the terminology of Hirai and Jones (**B**). Ventral lateral (VL) motor thalamus circled in red. Adapted from Sadikot et al.* [450].

features more prominently in neuroimaging research. The most important nuclei of the motor thalamus for neurosurgical treatment of tremor are the ventral oralis posterior nucleus (Vop) and ventral intermediate nucleus (Vim), as labelled by Hassler (*Figure 1-3*), and Schaltenbrand (*Figure 1-4*), which corresponds approximately with the ventral component of the posterior portion of the ventral lateral nucleus (VLp) as defined in the Morel atlas.

The Vim is a wedge-shaped structure of relatively sparse cell zone, with medium to large sized neurons, measuring approximately 8-9mm in the dorsoventral and mediolateral directions, and with rostrocaudal thickness of 3-3.5mm in the lateral region, and 1.5-2mm in the medial region.

The Vim receives primarily excitatory input from the cerebellum and projects to the primary motor cortex (M1) of the cerebral cortex and is thought to function as a relay for sensory motor-integration[168]. Microelectrode recordings have demonstrated that tremor-related activity is present in the Vim[169–172]. Deep brain stimulation targeting the Vim is known to reduce tremor severity in both ET and DT[173,174], and the Vim has long been a target of stereotactic lesioning for treatment of tremor[175]. Results of fMRI studies in ET have observed increased cerebellar activity during tremor and at rest, while tremor in ET is typically an action tremor. This observation has led to speculation that the Vim may act as a gate between the cerebellum and motor cortex[176]. This gating function is thought to be responsible for the reduction in tremor severity during stimulation of the Vim with deep brain stimulation (DBS), where stimulation is thought to reset the oscillatory rhythm in the cerebello-thalamo-cortical pathways, preventing propagation of tremor to the limbs[177].

While cerebello-thalamic projections have been implicated in both ET[74] and DT[161], connections between the thalamus and basal ganglia are also thought to play a role in DT. fMRI studies have shown that activity in the basal ganglia circuits was related to jerky oscillations in dystonia [178], and greater reduction in functional connectivity in the cortical-basal ganglia-cerebellar pathway in DT, compared with ET [139,162]**.** DBS studies in DT have demonstrated that a stimulation volume with greater overlap with the cerebello-thalamic pathway correlated with reduced tremor severity [138], consistent with studies in ET [179,180]. However, the optimal stimulation region in DT was found to be further anterior, towards the Vop [138], which receives input from the globus pallidus interna (GPi) [181]. fMRI studies in DT have also found increased tremor-related activity in the cerebello-thalamo-cortical network,

Vop and pallidum[161]. These findings support the hypothesis that DT involves dysfunction of both the cerebello-thalamo-cortical and pallido-thalamic pathways.

The Motor Cortex

The primary motor cortex (M1) received projections from the thalamus as well as extensive connections with other cortical regions, including the premotor cortex, the supplementary motor area, and multiple parietal regions. EEG/MEG studies have implicated the motor cortex in ET, with cortical activity found to be coherent with ET [81,159,182], with one MEG study finding that the M1 exhibited the strongest cerebro-muscular coupling in ET[159]. Furthermore, transcranial magnetic stimulation (TMS) studies have demonstrated that the application of TMS to the M1 region can reset tremor in ET [183,184] , while inhibitory repetitive TMS (rTMS) has been shown to reduce tremor amplitude in ET [185,186]. While the M1 has been implicated in tremor, some studies have shown only intermittent corticomuscular coherence [81,187], suggesting that the motor cortex may not directly drive tremor activity in ET.

1.1.5 Assessing Tremor Severity

Several clinical scales have been developed for the assessment of tremor severity, which have been employed in clinical trials to measure treatment efficacy [188,189]. The Clinical Rating Scale for Tremor (CRST), originally proposed by Fahn, Tolosa and Marin in 1988 [13], and further revised in 1993 [190], has been employed in several clinical trials for ET [191–197]. This rating scheme is composed of 3 parts, part A, B and C. Part A scores tremor by body region,

including rest and action tremor of the face, tongue, voice, head, trunk, upper limbs and lower limbs. Part B scores task performance by assessing kinetic tremor of the upper limbs during writing, as well as drawing and water pouring tasks. Part C scores tremor-related disability, and includes assessment of speaking, eating, drinking, hygiene, dressing, writing, working and social activities. Each item is scored individually, with scores ranging between 0 and 4, with 4 indicating maximum severity, and the scores of the part A, B and C are summed to give the total CRST, with a maximum possible score of 156 [189].

Additionally, the Hand Tremor Score (HTS), which is derived from CRST parts A and B, is a useful scheme for assessing hand-specific tremor severity[198]. HTS is calculated by summing scores from resting, posture and action components of CRST part A, and the handwriting, drawing and pouring components of CRST part B, with a maximum score of 32 for the

dominant hand, and 28 for the non-dominant hand as handwriting is assessed for the dominant hand only.

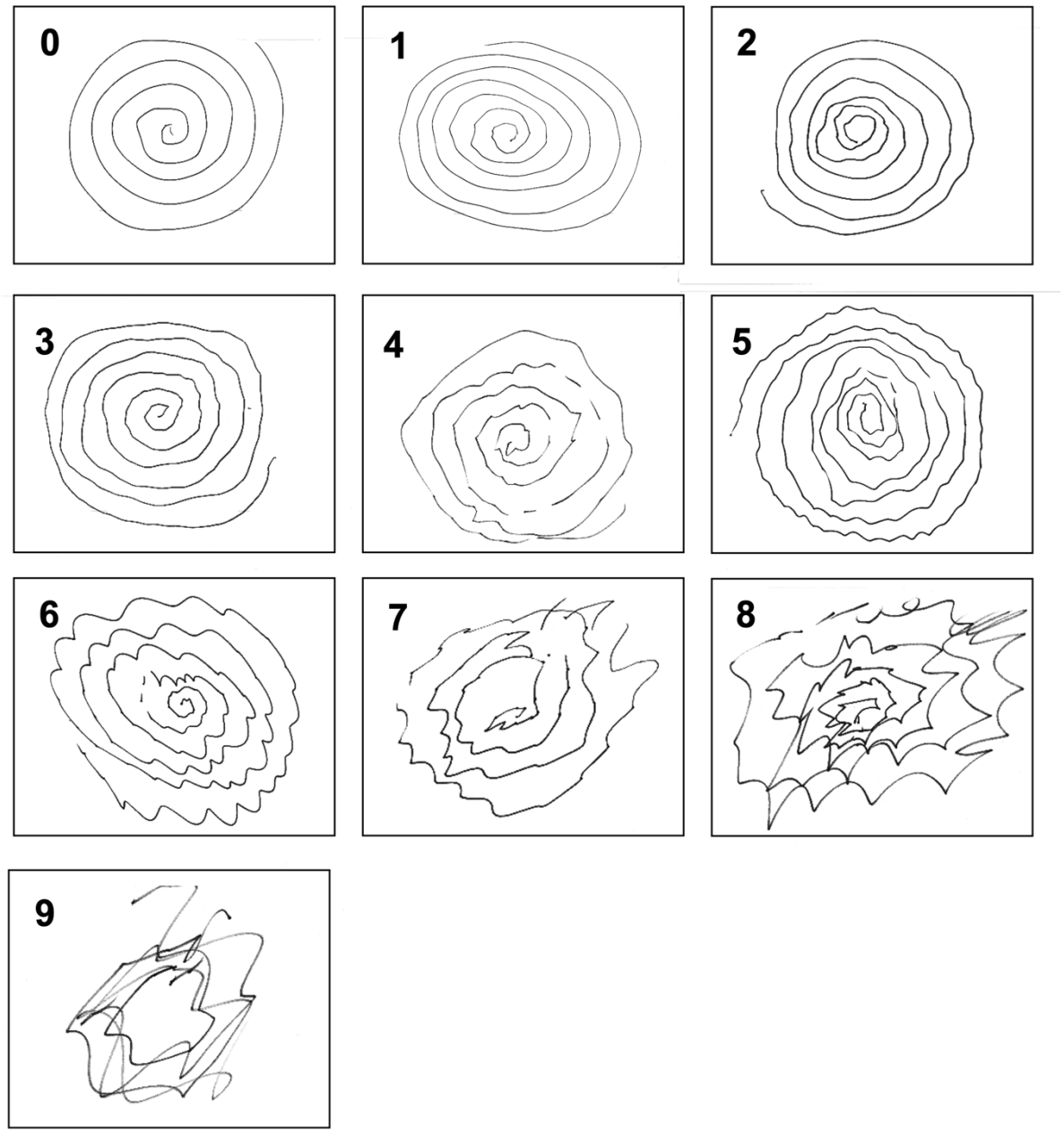

Figure 1-5 Example of spirals rated with Bain and Findley spirography scale.

The Quality of Life in Essential Tremor (QUEST) questionnaire was also designed specifically for ET [199], to quantify the impact of tremor on patient quality of life not captured by CRST or HTS. While the values provided in the self-reported QUEST questionnaire are based on the individual patient's experience and thus may be a more subjective measure of tremor severity, the QUEST scores provide a meaningful measure of the impact of tremor on the patient well-being [200], and have been employed in several studies of ET. QUEST is composed of 30 items related to the impact of tremor on everyday activities; each scored on a 5-point scale ranging from 0-4 for a maximum score of 120 points. For binary items, such as "I had to quit my job because of tremor", scores of 0 or 4 are used, with a score of 4 indicating the statement was true.

Rating of Archimedes spirals drawn by patients with tremor is also a common method for estimation of tremor severity. Several rating schemes have been developed, including the Fahn-Tolosa-Marin (FTM) tremor rating scale were developed, which rates spirals on a 0–4-point scale[13], which was further developed by Bain et al., who developed a 0–10-point rating scale, which has been widely adopted by clinicians in trials on ET[201], with a higher score indicating more severe tremor. An example of spirals in the Bain and Findley spirography scale is shown in *Figure 1-5*.

1.1.6 Summary

While our understanding of the structures and networks involved in tremor continues to evolve, there is substantial evidence implicating several structures as nodes in a connected tremor network. While the pathophysiology of DT and ET remains unclear, it has been

demonstrated that several common structures in this tremor network are implicated in the pathogenesis of tremor in both disorders. Thus, these structures and the white matter pathways that connect them have become common targets in the stereotactic treatment of tremor.

1.2 Treating Tremor: Targeting the Tremor Network

1.2.1 A Brief History of Stereotactic Surgery

There is a long history of surgical procedures targeting specific regions of the brain for the treatment of movement disorders. Some of the earliest research into stereotactic surgery for tremor occurred in 1908 when Horsley and Clarke attempted to target the deep cerebellar nuclei and subcortical structures in primates [202]. In these early experiments, the stereotactic head frame was developed, which, together with external landmarks, was used to introduce probes into the primate brain for the creation of electrolytic lesions.

By the late 1940s, the procedure had started to resemble that of modern stereotactic procedures when Spiegel et al. published a procedure using a modified head frame used by Horsley et al., as well as the use of encephalography to record brain activity during the procedure, allowing the probe to be inserted through a small burr hole in the skull and removing the need for direct visualisation of the target [203]. In this study, lesioning was performed with injections of alcohol, however, these advancements stimulated significant research into methods of lesion creation, including chemothalamotomy, cryothalamotomy, electrolytic lesioning and radiofrequency lesioning [204]; by the 1950s a significant improvement in the mortality rate of treatment was observed [205].

A majority of the work across the 1950s and 1960s was focused on targeting the pallidum [206–208] for the treatment of rigidity and tremor in Parkinson's disease, however, some groups

had begun to recognise the motor thalamus as an important target in the treatment of tremor. [209–211]. Hassler et al. would further refine the nomenclature of the thalamic nuclei and demonstrate the effectiveness of the Vim as a target for the treatment of tremor [210,212].

By the end of the 1960s, stereotactic ablative procedures had found widespread popularity amongst many neurosurgeons [213], however, the success of the medication Levodopa (L-dopa) for the treatment of parkinsonism in the 1970s saw a significant decrease in the use of stereotactic procedures for the treatment of movement disorders. [214] However, side effects such as drug-induced dyskinesia and gait freezing [215] led to renewed interest in surgical treatments, particularly after Laitinen et al. in 1992 successfully demonstrated that rigidity in Parkinson's disease, as well as L-dopa induced dyskinesia, could be treated with pallidotomy [216,217]. The 1990s also saw the extension of stereotactic surgery for the treatment of additional movement disorders such as ET[218–221].

Functional neurosurgery had relied up to this point on radiofrequency lesioning for the surgical treatment of tremor, however, there remained hesitance to return to stereotactic surgery due to the invasive nature of the procedure and unpredictable lesion size, with associated risks of haemorrhage and permanent deficits [222]. For decades, neurosurgeons performing RF thalamotomy for the treatment of tremor had used high-frequency electro-stimulation (HFS) at the intended target site to test the effectiveness. [223] However, it was not until 1987 when Benabid et al conducted trials on the chronic stimulation of the motor thalamus for the treatment of tremor in patients with PD or ET. These studies revealed that high-frequency (>100Hz) stimulation of the thalamus could achieve similar clinical effects as lesioning of the same area. In 1993, the first clinical trial of deep brain stimulation (DBS) was

undertaken in the treatment of patients with Parkinson's disease, and DBS was subsequently approved by the FDA in 1997 and 2001 for the treatment of tremor in ET and severe tremor in PD, respectively. Since DBS targeting the motor nuclei of the thalamus could achieve similar effects to lesioning without the need for permanent tissue destruction, and aided by technological advances in brain stimulation hardware, particularly in power supply, it quickly became the preferred option over lesional approaches [224,225], owing to its reversibility, tuneability, low morbidity and potential for bilateral treatment.

While DBS has been proven effective in the management of tremor and remains the most popular treatment option for advanced ET, the underlying stereotactic methodology remains similar to that of RF ablation, requiring the insertion of a probe through the skull and intervening brain to the treatment target, and is associated with similar risks due to the invasiveness of electrode insertion, including the risk of infection, haemorrhage or hardware related complications [226].

The limitations of DBS and recent advances in lesioning technology have seen a recent resurgence in stereotactic lesioning with incisionless neurosurgical procedures for the treatment of tremor. Using such techniques, the tissue of the brain can be precisely ablated through an intact skull without the need for craniotomy or the drilling of burr holes for the passage of probes into the brain. Several incisionless lesioning techniques are currently performed. Lesioning with gamma knife (GK) radiotherapy employs ionizing radiation focused on a target in the brain to denature cellular DNA, causing cell death within the treated area. However, the effect of treatment with GK is not instantaneous and can often

take up to several months before a clinical effect may be observed[227–229]; thus, intraoperative verification of target efficacy is not possible with GK.

More recently, transcranial magnetic resonance-guided focused ultrasound (tcMRgFUS) has emerged and has become a rapidly developing incisionless surgical option for the modulation and thermal ablation of tissue. The procedure employs ultrasound to deliver acoustic energy to the tissue of the brain, increasing the tissue temperature and leading to thermocoagulation at the treatment target. Guidance in real-time with MRI imaging allows precise placement of the heated volume to ablate structures relevant for tremor control. The immediate treatment effects allow intraoperative evaluation of target efficacy and the presence of any adverse effects. tcMRgFUS does not employ ionizing radiation and is thus not associated with the risk of radiation-induced tumorigenesis. Importantly, the ultrasound waves employed in tcMRgFUS can target tissue in the brain through in intact skull, reducing the risks associated with RF lesioning and stimulation with DBS.

1.2.2 Transcranial Magnetic Resonance-guided Focused Ultrasound

While the use of ultrasound for in vivo thermal ablation of tissue has been explored since the 1940s[230], recent technological advances have seen focused ultrasound (FUS) employed in the treatment of several pathologies. Low-intensity FUS has been used for opening of the blood brain barrier for targeted drug delivery[231], while high-intensity FUS (HIFUS) has been used in the treatment of bone tumours and uterine fibroids [232–237], and more recently as a minimally invasive method for the creation of

focal brain lesions in the treatment of movement disorders including ET, DT and PD [192,238,239]. The first studies of tcMRgFUS for the treatment of tremor occurred in 2013, when tcMRgFUS was used to treat tremor in ET [192,238]. This was followed by several larger studies that demonstrated significant tremor reduction in both ET and PD [198,240], however, tremor re-occurrence in PD has been observed [241,242]. The promising tremor suppressing effects of these early studies have seen, as of 2020, the global adoption of neurological tcMRgFUS at more than 50 institutions [243] where it has replaced previously developed stereotactic lesioning procedures (RF, GK), particularly in the unilateral treatment of mediation refractory ET [198,238,244,245]. Since 2013 there has been a significant increase in the number of publications confirming tremor reduction following tcMRgFUS (*Table 1-3*).

Table 1-3 List of studies with follow-up clinical tremor improvement in patients with Essential Tremor (ET) treated with tcMRgFUS.

Study	Year	Number of Patients	Mean age at treatment (years)	Treatment Target	Longest Clinical Follow-up (months)	Tremor Improvement (Score %)
Elias[192]	2013	15	66.6	Vim	12	CRST 56.0
Lipsman[238]	2013	4	70.8	Vim	3	HTS 81.3
Huss[195]	2015	15	67.2	Vim	12	CRST 55.7
Chang[191]	2015	8	66.1	Vim	6	$CRST_A$ 73.5
Elias[246,247]	2016	76	70.8	Vim	12	HTS 39.8
Gallay[248]	2016	18	69.1	PSA	12	ETRS 55.2
Schreglmann[249]	2017	6	70.7	PSA	6	HTS 83.0
Jung[197]	2018	20	65.1	Vim	12	CRST 67.3
Chang[250]	2018	67	71.0	Vim	24	HTS 55.6
Sinai[251]	2019	24	70.5	Vim	12	HTS 78.9
Gasca-Salas[194]	2019	23	64.1	Vim	12	CRST 49.5
Park[252]	2019	12	61.7	Vim	48	HTS 55.7
Halpern[253]	2019	52	71.0	Vim	36	HTS 52.7
Krishna[254]	2019	179	71.1	Vim	12	HTS 57.9
Su[255]	2020	14	75.5	Vim	1	HTS 59.0
Fukutome[193]	2020	15	62.9	Vim	12	CRST 80.0
Zur[256]	2020	22	72.0	Vim	6	HTS 79.2
Wu[257]	2021	48	59.14	Vim	24	HTS 49.6
Purrer[258]	2022	37	69.4	Vim	12	HTS 82.0
Yamamoto[259]	2022	17	71.6	Vim	24	HTS 56.9
Kato[260]	2022	15	72.8	Vim	6	HTS 59.5
Pae[261]	2022	85	65.3	Vim	6	HTS 72.0
Jameel[196]	2022	13	69.0	Vim/PSA	24	CRST 52.6

Abbreviations used: Vim (Ventral Intermediate Nucleus), PSA (Posterior Subthalamic Area), CRST (Clinical Rating Scale for Tremor), $CRST_A$ (Part A of CRST), HTS (Hand Tremor Score)

The high frequency (650 kHz) ExAblate 4000 system (InSightec Inc) received FDA approval for intracranial treatment of ET in 2016[262] and is currently the only FUS device approved for

thermoablation of the brain. The key advantages of tcMRgFUS over other lesion-based treatment approaches are the use of ultrasound for the creation of a precise focal lesion through an intact skull with immediate therapeutic effects, negating the need for the invasive probes employed in RF lesioning, or ionizing radiation as used in GK radiosurgery (*Table 1-4*). Additionally, the MRI compatibility of the device allows MR imaging to be used for target localisation and real-time monitoring to ensure accurate lesion placement.

tcMRgFUS Mode of Action

High-intensity transcranial MRgFUS (tcMRgFUS) makes use of high-intensity focused ultrasound waves to deposit energy in the tissue of the brain. Sound waves are mechanical vibrations that occur in a medium in which the molecules oscillate in the direction of wave propagation. Ultrasound (US) waves are sound waves with frequency greater than the human auditory limit of 20 kHz[263]. Conventional imaging with ultrasound typically uses US waves with frequencies between 2-15 MHz, while focussed US (FUS) employs lower frequencies between 200kHz – 1MHz [264]. US waves are generated with piezoelectric transducers, which expand and contract in response to an applied voltage. These transducers can be designed with focusing components such as radiators, lenses or reflectors to focus and direct the generated US wave. As the US wave propagates through tissue, the US is attenuated due to absorption,

Table 1-4 Summary of available stereotactic procedures for the treatment of tremor.

Technique	**RF Lesioning**	**DBS**	**GK Lesioning**	**tcMRgFUS Lesioning**
Description	Probe inserted into the brain to ablate tissue at selected region to create a permanent focal lesion.	Electrodes connected to implantable pulse generator are inserted into the brain, providing electrical stimulation at selected regions to modulate neuronal activity.	Ionizing radiation is directed to the selected region of the brain through an intact skull to create a permanent focal lesion.	Ultrasound waves are focused on a selected region of the brain through an intact skull to create a permanent lesion
Worldwide experience	>50 years	>30 years	> 20 years	<10 years
Reversible	No	Yes	No	No
Adjustable	No	Yes	No	No
Cranial burr hole required	Yes	Yes	No	No
Implantation of hardware	No	Yes	No	No
Bilateral treatment	No	Yes	No	No
Treatment effect	Immediate	Delayed (dependant on programming may take up to 6 months)	Delayed (up to 12 months)	Immediate
Target confirmation	Neuroimaging, intraoperative stimulation, intraoperative test lesions, microelectrode recording, procedural evaluation	Neuroimaging, intraoperative stimulation, intraoperative test lesions, microelectrode recording	Planning neuroimaging, indirect anatomical targeting	Planning neuroimaging, indirect anatomical targeting, real-time MRI thermometric maps, intraoperative test lesions, procedural evaluation

Abbreviations used: RF (Radiofrequency), DBS (Deep Brain Stimulation), GK (Gamm Knife), tcMRgFUS (Transcranial MRI-guided Focused Ultrasound)

reflection and refraction. The absorption of US energy in the tissue of the brain causes an elevation of temperature. If the temperature of the tissue reaches a threshold temperature of approximately 44°C for several seconds, irreversible thermocoagulation and tissue necrosis will occur[265]. To achieve targeted tissue temperature elevation, tcMRgFUS employs an array of US transducers that each focus an US wave on a single point. The combination of US waves from each transducer are combined and amplified at this focal spot, resulting in a

sharp increase in tissue temperature at the target, within a region typically between 4-5mm in diameter [266], leading to thermocoagulation and the creation of a focal lesion, while the tissue along the path of each individual beam is unaffected.

Delivering US through the skull

Key to successful focal lesioning of the brain with tcMRgFUS is accurate heating of tissue at the focal spot to temperatures high enough to cause thermocoagulation. In order to achieve efficient heating at the focal spot with a completely transcranial method, obviating the need for craniotomy, there were several challenges to be overcome. The skull represents a major barrier to the penetration of US into the brain, with acoustic attenuation approximately 30-60 times greater in bone compared with soft tissue [264] (attenuation of 13.0dB/cm in bone compared with 0.6dB/cm in brain tissue at 1MHz[267]. Thus, a significant amount of energy is lost before reaching the brain. Attenuation of US by the skull is influenced by the frequency of US wave, with greater frequency delivering increased energy but also increased attenuation and distortion resulting in a loss of intensity at the target[267]. Lowering the US frequency mitigates these issues, however, lower frequencies are associated with an increased prevalence of cavitation. Cavitation is the creation and collapse of bubbles in the tissue of the brain induced by the mechanical effects of US, which can lead to undesirable large temperature changes[268]. tcMRgFUS is performed with an US frequency of 650 kHz, chosen to reduce the effects of skull-induced US attenuation and phase errors while remaining high enough to reduce the risk of cavitation[266].

Additionally, the composition of the skull is heterogeneous, varying in density and thickness, which affects the propagation of the US beams. The speed of a sound wave through a medium is governed by its density. As the density of bone is greater than soft tissue, the velocity of the US wave through the skull is greater than in the brain. However, since the thickness and density of the skull is not consistent, the wave from each transducer may experience differences in the path length through the skull or differences in density and thus, wave velocity, leading to relative changes in the phase of each wave upon exiting the skull. These phase differences lead to a reduction in intensity at the focal spot due to the loss of phase coherence. One of the key advancements in the development of tcMRgFUS was the development of a phased-array US transducer, which allows for the independent modulation of phase of the US wave from each element to correct for the phase changes introduced by the skull. This phase modulation, in anticipation of the phase change due to the path through the skull, results in greater intensity at the focal spot and a more well-defined heated volume. In order to accurately apply a phase modulation to each element, a computed tomography (CT) scan is acquired prior to treatment and is used to estimate the relative phase change experienced by each US beam.

The Skull Density Ratio

In addition to the estimation of phase errors, pre-treatment CT is also acquired for estimating of the patient skull density ratio (SDR). The SDR is a key metric used to assess patient suitability for treatment with tcMRgFUS. The skull SDR is defined as the ratio of the density of trabecular bone to cortical bone[269] as measured on CT imaging. At the interface of two distinct media, a greater mismatch in the acoustic impedance will cause greater

attenuation due to the increased reflection of energy. Thus, a greater mismatch in density of the trabecular and cortical bone, reflected as a lower SDR value, is indicative of increased US attenuation by the skull. The SDR value is typically estimated on CT prior to treatment for patient screening, and again during treatment planning by measuring the skull CT intensities along the path from each US transducer to the target, producing an SDR value for each US element which are averaged to provide a single patient SDR value. In patients with lower SDR values, to achieve ablative temperatures at the focal spot, the intensity of US must be increased to compensate for the loss of energy in the skull, however, the intensity increase is limited by the risk of focal heating at the scalp. In patients with extremely low SDR, it may not be possible to reach therapeutic temperatures without risk of burns, and these patients may be deemed unsuitable for treatment with tcMRgFUS. An SDR of 0.40 has traditionally been used as a cut-off for patient inclusion [270], although it has been shown that treatment is possible in patients with low SDR by delivery of long-duration low-intensity sonications [271–275]. While there is little literature on the distribution of SDR values in the general population, one study reported 50% of participants with SDR lower than the empirical threshold of 0.4 [269].

Real-time temperature monitoring

The MRI compatibility of tcMRgFUS represents a distinct significant advantage of the technique, by allowing the tissue temperature increase to be monitored in real time with MR thermometry. As the tissue is heated during each US sonication, the change in temperature changes the resonant frequency of the protons in the heated volume. This change in frequency can be detected in gradient echo (GE) MRI as a phase shift relative to the baseline phase and provides a 2D cross-section of temperature increase, centred on the sonication target. This allows the maximum and average temperature increase to be calculated (Equation 1-1) for confirmation of adequate tissue heating, as well as providing verification of the accuracy of the treatment target.

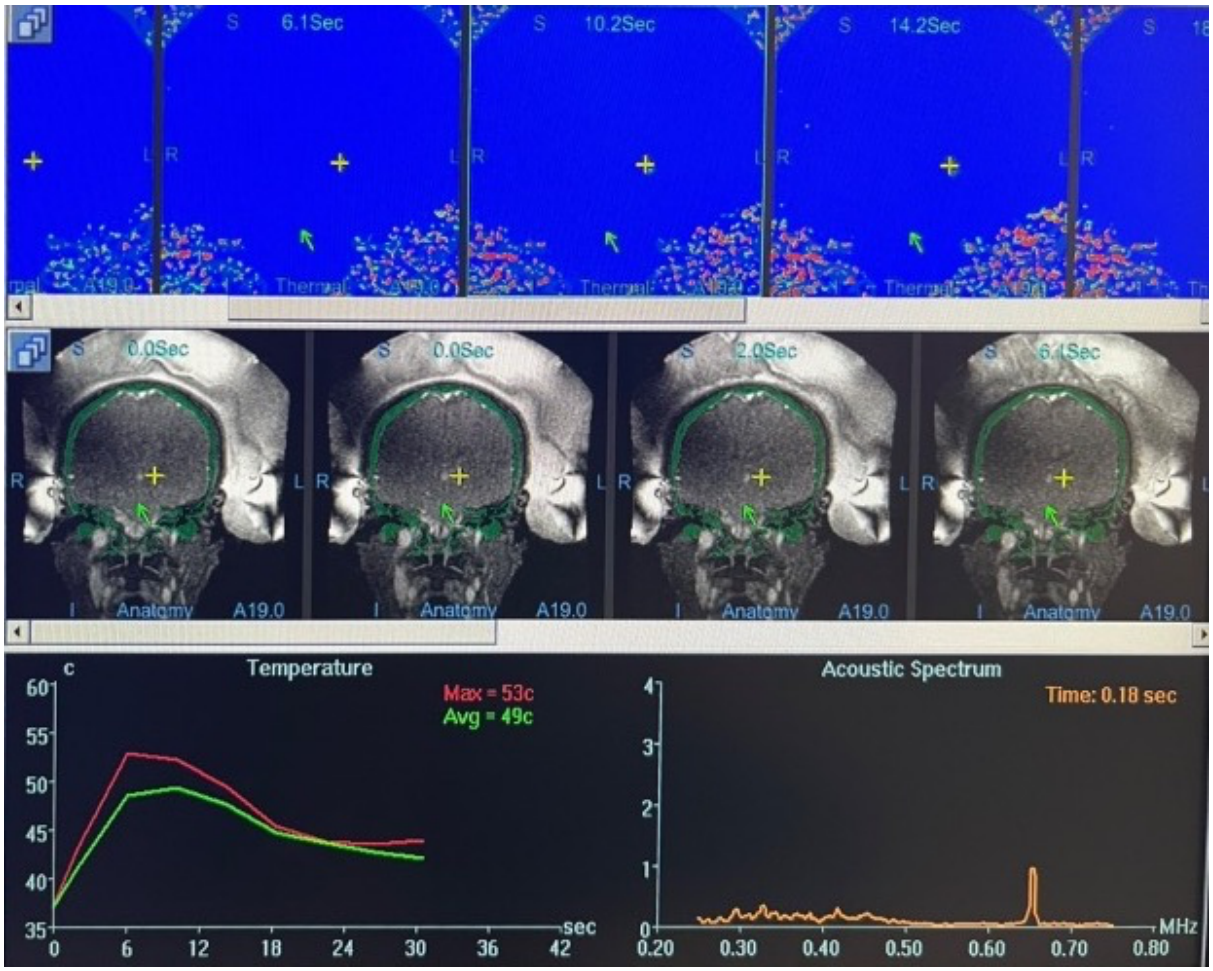

Figure 1-6 tcMRgFUS console during temperature monitoring. Maximum temperature at treatment target shown with red curve and average temperature with green curve.

$$\Delta T = \frac{\phi(t) - \phi(t_0)}{\gamma \alpha B_0 T_E}$$ Equation 1-1

Where T is the change in tissue temperature, ϕ is the phase, γ is the gyromagnetic ratio α is the temperature sensitivity of the PRF shift (-0.00909 ppm/°C) B is the magnetic field the TE is the echo time.

The MR thermometry acquired during each sonication provides a 2D map of tissue heating across the entire brain, which is then used to calculate the tissue temperature elevation at the target coordinates. Typically, both the maximum temperature elevation and the average temperature increase in the 9 voxels centred on the sonication coordinates are monitored (*Figure 1-6*).

Disadvantages of treatment with tcMRgFUS

While treatment of tremor with tcMRgFUS presents several distinct advantages over more invasive techniques such as DBS, there remains a number of disadvantages that are yet to be addressed by technological advances. The use of US transducer, with accompanying water bath for scalp cooling precludes the use of a conventional MRI receiver coil, severely impacting the quality of imaging acquired during treatment. The low-quality imaging has implications for treatment targeting. Accurate targeting is reliant on the accurate mapping of coordinates defined on pre-treatment planning imaging, with the intra-operative imaging. Thus, any inaccuracies in the intra-operative imaging can cause targeting errors. Furthermore, the low bandwidth required to increase SNR in the intra-operative imaging leads to off-resonance effects in the MR thermometry, leading to errors in the location of the ablated volume, further impacting the accuracy of treatment targeting.

Treatment with tcMRgFUS has also been associated with several treatment-induced sensory and motor adverse effects including paraesthesia, dysarthria, dysmetria, and gait disturbance [196,276]. Boutet et al. demonstrated that encroachment of the tcMRgFUS lesion into the posterior ventralis caudalis (VC) nucleus was associated with increased incidence of sensory side effects, while lesioning of the later internal capsule was associated with motor side effects[276]. The permanent nature of tcMRgFUS makes mitigation of these adverse effects particularly important, and represents a key advantage of DBS over tcMRgFUS, owing to its tunability and reversibility. Improved target identification may aid in avoiding adverse effects by reducing the impact on the surrounding structures associated with these adverse effects.

1.2.3 The ExAblate System

The tcMRgFUS system (ExAblate 4000 Neuro system, InSightec, Tirat Carmel, Israel) is integrated into the MRI scanner (***Figure 1-7***). The system is comprised of a 30cm diameter hemispherical US transducer helmet, with 1024 individual US elements distributed across the helmet, positioned to direct US waves to a single focal spot at the geometric focus. The US transducer is MRI compatible and is integrated into the MR scanning table. The US transducer helmet is designed to allow a stereotactic head frame to be attached, immobilising the patient and ensuring a fixed spatial relationship between the transducer

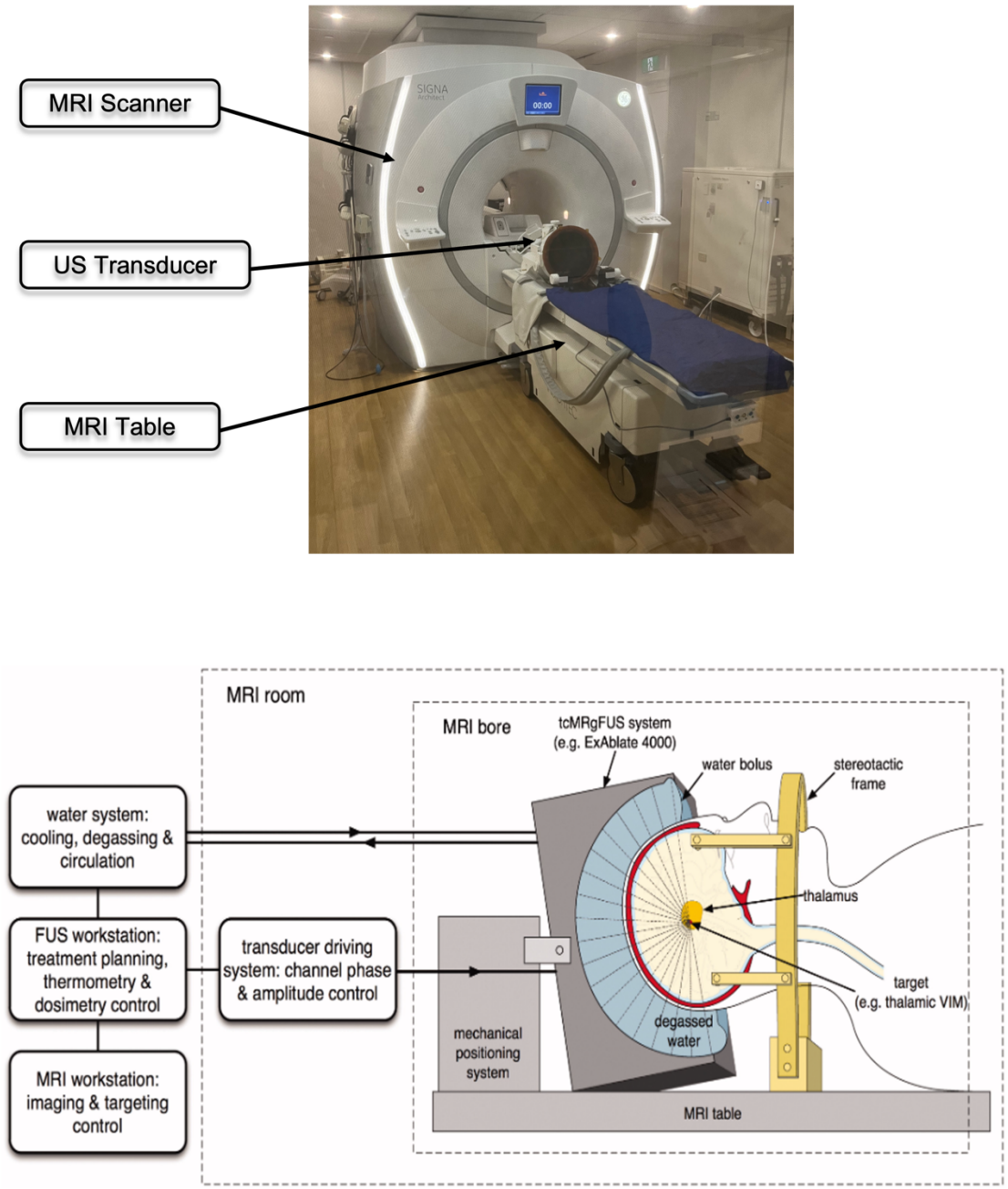

Figure 1-7 MRI scanner and US transducer. Bottom - Summary of components in tcMRgFUS system. Adapted from (Kyriakou et al. 2014).

and the patient's head for accurate treatment targeting. The US transducer features a mechanical positioning system that can be adjusted manually to ensure the geometric focus corresponds with the treatment target. Degassed and chilled water (15-20°C) is circulated

through the space between the patients scalp and the US transducers, providing acoustic coupling between the transducer and scalp, as well as active cooling of the scalp. In addition to the generation of US waves, there are additional elements in the transducer that can detect cavitation and automatically terminate the sonication if required.

In the MRI control room, the US transducer connects to the FUS workstation, which is also linked to the MRI scanner console, allowing communication between the FUS and MRI systems. On the FUS console, pre-treatment imaging can be co-registered with planning MRI acquired after the patient is positioned in the transducer. The target location is defined on the FUS console and transformed to coordinates relative to the FUS transducer. The sonication parameters, including the power, duration and energy, are defined on the FUS console, and the individual element amplitudes and phase offsets are calculated and fed into the transducer driving system, which controls the generation of US from each transducer element. While the US amplitude can be modulated individually to maximise the intensity at the focus, in tcMRgFUS, the amplitude is often designed to ensure a unform distribution of energy across the surface of the skull [277], minimising skull heating [278].

1.2.4 The tcMRgFUS Procedure

The tcMRgFUS procedure for treatment of tremor is approximately 3 hours in duration and typically requires the coordinated involvement of experts in neurosurgery, neurology and radiology. The ExAblate system is tested on a gel phantom to ensure proper system operation prior to the commencement of the procedure. The patient's head is shaved, and the scalp is examined for any lesions or scars that may affect US propagation. A local

anaesthetic is administered prior to the attachment of an MR-compatible stereotactic head frame to the patient's head, with screws placed over the lateral orbits above the eyebrows and in the occipital bone. A circular plastic diaphragm with a central opening is then stretched over the patient's head, ensuring a tight seal against the patient's head. The patient is positioned supine on the MRI scanner table, with their head towards the MRI bore. The stereotactic head frame is fixed to the base plate of the US transducer. The plastic diaphragm is fixed tightly to the transducer helmet and the space between the patient's head and the transducer is filled with chilled and degassed water. The patient is accompanied in the MRI room by a registered nurse during the treatment, and the patient's vital signs are monitored throughout. If required, a light sedative may be administered. The patient is provided with a button connected to the FUS console, which will terminate the sonication if required.

The use of the US transducer helmet precludes imaging with a conventional MRI head coil; thus, all intra-procedural imaging is thus acquired with the MRI body coil. A three-plane localiser is acquired, followed by a tracking scan to localise the US transducer and detect the central frequency. A 3D T1-weighted image (BRAVO) is then acquired and is co-registered to pre-treatment CT and MRI for treatment planning and target localisation (*Figure 1-8*). Using the pre-treatment MRI, the treatment target coordinates are defined by the treatment

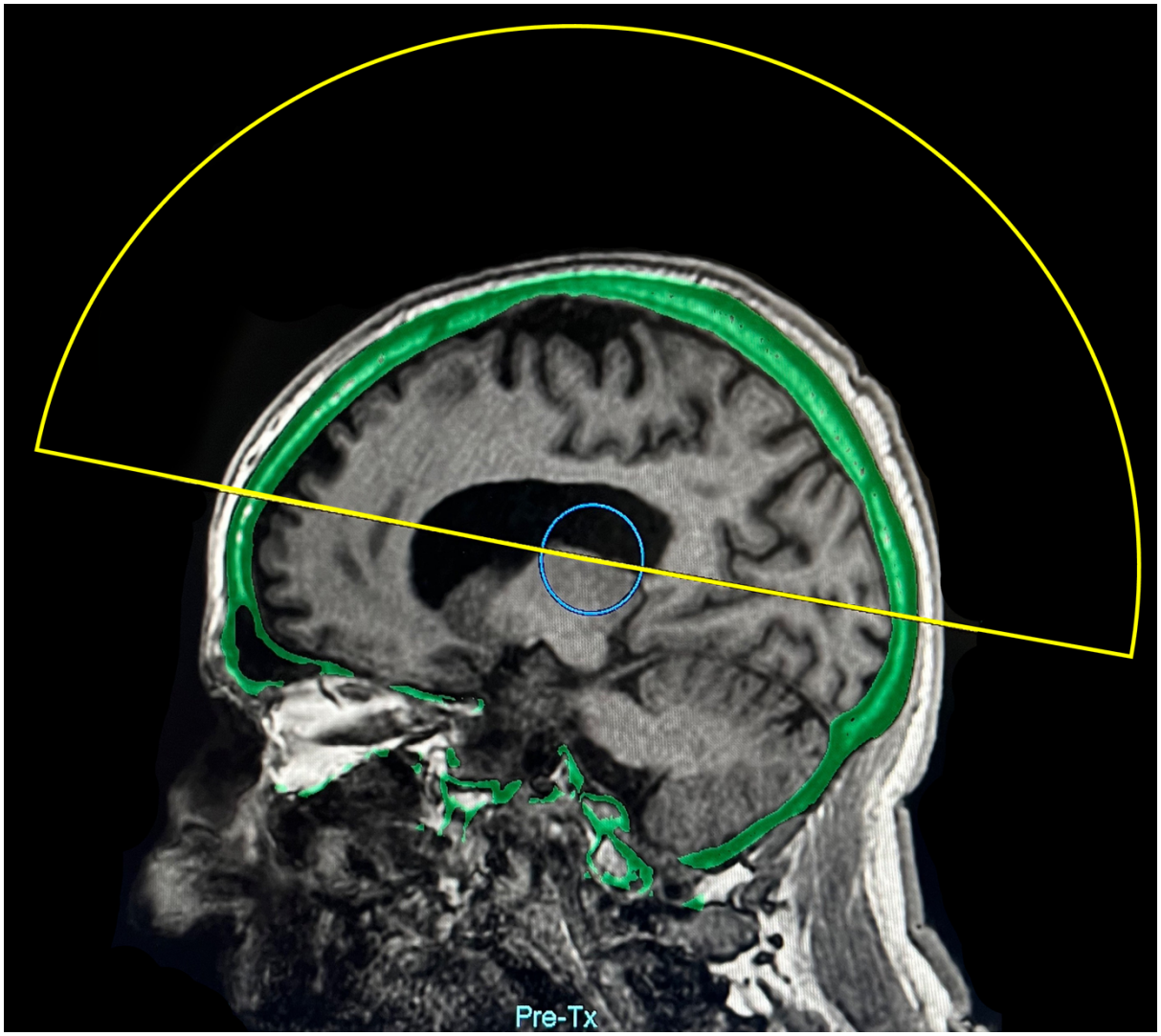

Figure 1-8 Sagittal view of planning T1-WI acquired with MRI body coil. Skull segmentation from co-registered planning CT shown in green, US transducer shown in yellow, and transducer focal point indicated by blue circle.

neurosurgeon on the FUS console. Intra-cerebral calcifications are identified (*Figure 1-9*), and any additional "no pass" regions, such as air-filled sinuses, are defined, reducing the number of active elements available for treatment. Upon evaluation of the treatment plan, the number of active elements, and the mean SDR and skull area of those elements are calculated from the pre-treatment CT. Typically, at least 700 active elements are required for successful treatment, and the US energy must be delivered over at least 250 cm^2.

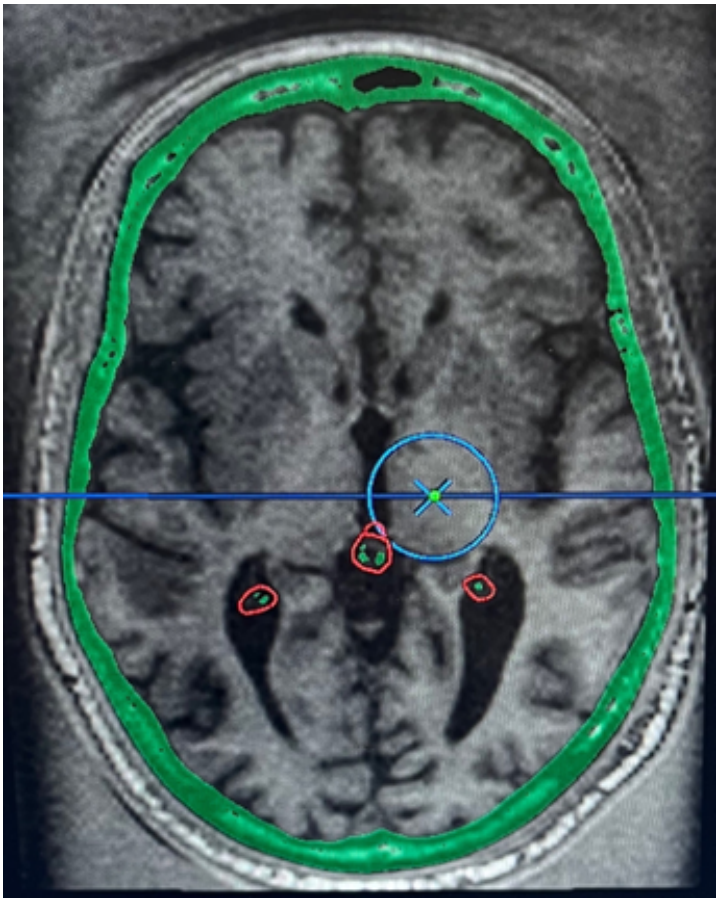

Figure 1-9 Axial view of planning T1-WI with treatment target indicated by blue cross. Calcifications indicated by red circles.

Additionally, fiducial markers are placed to identify any patient head movement during the treatment.

If all treatment requirements are met, the neurosurgeon will commence US sonications. There are three sonication phases in treatment: alignment, verification and treatment. In the alignment phase, short duration low energy sonications (1300-3000 joules dependent on patient SDR) are delivered, which are sufficient to observe a temperature increase on MR thermometry, but below the threshold required to create any biological effects, typically between 40-45°C. The purpose of these sonications is to confirm the heated volume

corresponds with the treatment target coordinates. Multiple alignment sonications are performed with MRI thermometry acquired in different orientations and phase encoding directions. Acquisition in multiple orientations is necessary since the MR thermometry is a single 2-dimensional slice; thus, to examine the three-dimensional extent of the heated volume, acquisitions need to be acquired in multiple orthogonal planes. Modification of the frequency encoding direction is required to account for the errors in the position of the focal "hot spot". Spatial misalignments of the heated volume can occur in the frequency encoding direction due to the off-resonance effects caused by tissue heating[279], which are exacerbated by the low receiver bandwidth required with imaging using the MRI body coil. Thus, for a given alignment sonication, the hot spot position can be confirmed in the phase encoding direction only. Modifications to the target coordinates may be adjusted in the alignment step, or when necessary, the physical position of the transducer may be adjusted manually to ensure the focal spot of the US array is aligned with the treatment target.

The second phase is verification, where the sonication power and duration are gradually increased across multiple sonications to reach temperatures between 46-52°C. At these temperatures, a neuromodulatory effect may be observed in order to verify the efficacy of the treatment target. The target coordinates may again be modified at this step to improve the patient response.

The final sonication phase is treatment, where sonication power and duration are increased to achieve ablative temperatures (>53°C). To ensure the creation of a permanent, durable lesion, the target is consolidated with at least 2 sonications at high temperatures. [280]

Following each sonication in the verification and treatment phase of treatment, the patient is evaluated by a movement disorders neurologist. This evaluation focuses on the changes in tremor severity by instructing the patient to hold several postures and tasks that typically elicit a tremulous response, such as drinking or extension of the upper limbs. The evaluation also includes drawing of a freeform Archimedes spiral on paper with an unsupported arm, which is a validated method for assessing tremor severity.[281] An example of the improvement of freeform spirals over the course of the treatment is shown in *Figure 1-10*.

Following the final sonication, the water is drained from the transducer helmet, the head frame is detached, and the patient is removed from the MRI scanner table. A complete neurological evaluation is undertaken immediately post-treatment to assess the clinical response, followed by the acquisition of post-treatment MRI to confirm the location and size of the tcMRgFUS lesion.

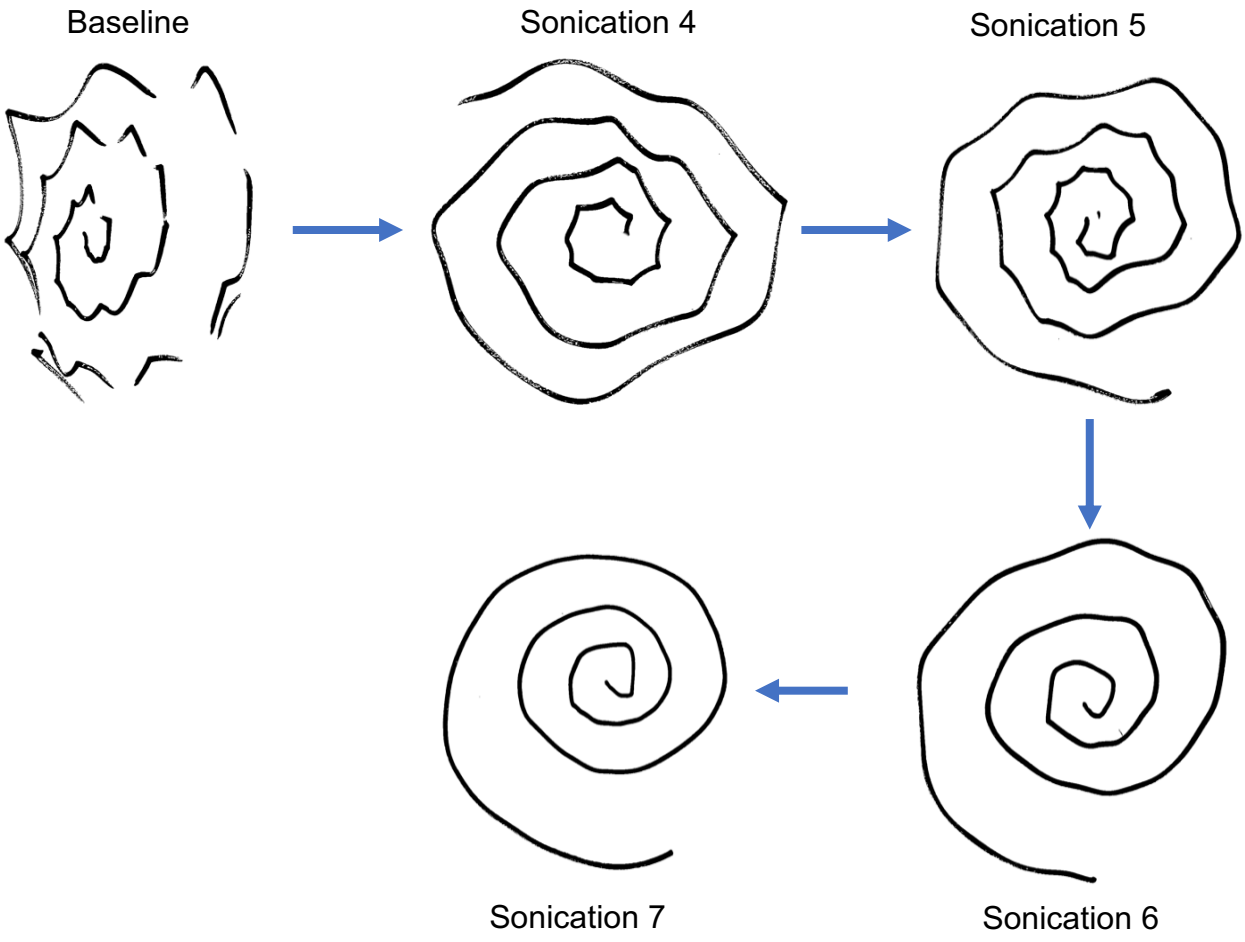

Figure 1-10 Examples of intraoperative spirals drawn during treatment with tcMRgFUS. Each spiral was drawn immediately after the indicated sonication.

1.2.5 The tcMRgFUS Target

In addition to correction of skull-induced phase errors, phase modulation is also employed to steer the beams, shifting the US focal spot by several millimetres, however, for larger positional adjustments in target coordinates the US transducer must be mechanically adjusted. While there is flexibility in the treatment coordinates within the brain, the

treatment envelope is limited to the centre of the brain, as targeting structures off-centre results in large incidence angles between the US waves and skull, which leads to increases US reflection and a significant reduction in heating[266].

The Vim of the thalamus has been targeted in the stereotactic treatment of tremor since the 1950s and remains the most frequently targeted structure in the treatment of tremor[282]. Unlike other common targets for stereotactic surgery such as the globus pallidus interna (GPi) or subthalamic nucleus, the Vim is not easily visible on standard structural MRI sequences, making determination of the exact coordinates for treatment challenging. DBS and thalamotomy studies have provided a wealth of data on the optimal coordinates for targeting of the Vim with indirect targeting methods, which remain the gold standard method for Vim localisation[283,284]. Indirect targeting defines the coordinates of the Vim relative to easily identifiable intracerebral landmarks. Typically, this is the anterior and posterior commissures (AC and PC, respectively). With this method, the coordinates of the Vim are defined as approximately 25% of the AC-PC distance anterior to the PC, 13-14mm lateral to the midline and 0-2mm superior to the AC-PC plane (*Figure 1-11*). However, while indirect targeting continues to be employed for treatment with DBS and lesion-based approaches, it does not take into account the anatomical variability between patients, or the effects of global and region atrophy on the spatial relationship between structures of the brain [285–287].

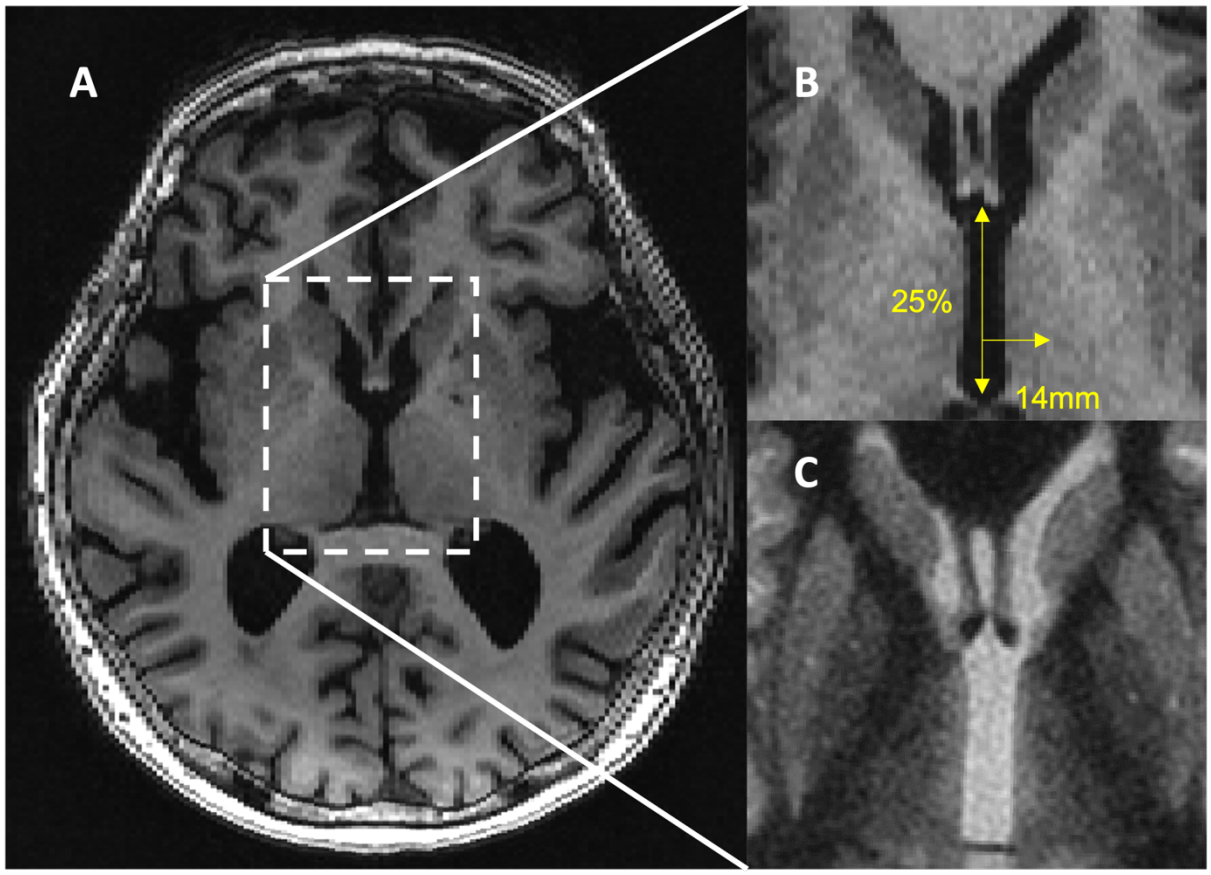

Figure 1-11 ***A*** *– Axial T1-WI.* ***B –*** *Conventional target coordinates for the Vim shown on T1-WI.* ***C****-Corresponding contrast with WMnMPRAGE showing increased thalamic contrast.*

Several MRI sequences have shown potential for providing direct targeting of the Vim. White matter nulled MPRAGE (WMnMPRAGE) is a modification of the conventional magnetization-prepared rapid acquisition with gradient echo (MPRAGE) sequence, with an inversion time optimised for visualisation of grey matter by nulling of the signal from white matter and provides significantly improved intra-thalamic contrast. Excellent visualisation of the individual thalamic nuclei with WMnMPRAGE acquisitions has been reported at high field (7T)[288], and many centres routinely acquire the older fast gray matter acquisition T1 inversion recovery (FGATIR)[289] for treatment targeting at clinical field strengths (1.5 and 3T).

Diffusion MRI (dMRI) has also shown promise in the identification of the optimal treatment coordinates. dMRI employs powerful diffusion gradients to sensitise MRI contrast to the diffusion of water along the direction of the applied gradient. By collecting data with diffusion direction oriented along a number of directions, the microstructural environment of the tissue can be explored. Several dMRI-based approaches for target localisation have been proposed, including those that parcellate the thalamus into discrete nuclei based on cortical connectivity [290–292], or clustering of the diffusion fibre orientation distribution (FOD)[293]. Diffusion tractography, which can be used to reconstruct the trajectory of white matter pathways in the brain based on the orientation of diffusivity within each voxel, has shown particular promise in localisation of the DRTT, the involvement of which several studies have shown is crucial for effective treatment of tremor [294–296].

While direct targeting of the Vim on MRI is a promising area of development and has the potential to improve the accuracy of tcMRgFUS lesion placement, and some centres have begun including dMRI tractography into the tcMRgFUS targeting procedure [297,298], indirect targeting remains the preferred method for neurosurgeons. Further validation of these methods of direct targeting is needed before widespread clinical adoption can be expected.

1.2.6 The tcMRgFUS Lesion

The temperature increase at the focal spot is influenced by a number of physical factors, including the skull SDR, thickness and density, technical factors such as the ultrasound intensity and duration and accuracy of phase correction, as well as physiological factors such as tissue perfusion and diffusion (Equation 1-2). The biological effects of thermal increase

$$\rho C_V \frac{\partial T}{\partial t} = \nabla \cdot \kappa \nabla T - \rho_b C_b W (T - T_a) + Q$$ Equation 1-2

Where ρ is the tissue density, C is the specific heat capacity, κ is the thermal conductivity, ρ_b C_b, and W are the density, specific heat capacity and perfusion rate of blood, T_a is the ambient temperature, and Q is the absorbed power density

from tcMRgFUS depend on the sonication temperature and the duration of elevated temperature experienced by the tissue, as well as tissue specific properties. The temperature elevation over time can be estimated with the bio-heat equations[299].

For sonications of short duration the effect of perfusion is generally ignored[300], however, at longer durations perfusion effects may be more relevant and lead to the development of a steady state between energy deposition in tissue and heat sink effects via blood perfusion. [301]. The concept of accumulated thermal dose (ATD) was developed as a metric to standardise the evaluation of the extent of tissue damage from thermal exposure[302]. The most popular method for calculating ATD is by expressing the thermal dose as the cumulative minutes at 43°C that would be required to achieve an equivalent biological effect [243]. The value of 43°C was chosen from in vitro experiments, where the time required for coagulative necrosis is reduced by 50% for every additional degree above 43°C [303]. Data from tcMRgFUS studies has shown that in humans the thalamus requires approximately 100 CEM_{43} to cause tissue necrosis [304,305].

Studies on the characteristics of tcMRgFUS lesions in the brain have demonstrated that the typical tcMRgFUS lesion is circular in shape and similar in appearance to RF lesions but significantly different from GK lesions [306], however, it is often elongated along a single axis to form a prolate spheroid shape, particularly in the supero-medial to infero-lateral direction[297], however, the exact shape differs between patients and is also influenced by any repositioning of the sonication coordinates. On post-treatment MRI, the lesion appears as multiple concentric zones (*Figure 1-12*), the appearance of which evolves over time (*Figure 1-13*). Zones 1 and 2 are the innermost regions exhibiting restricted diffusion at 24 hours post-treatment and are thought to represent areas of coagulation and cytotoxic edema [307,308]. Zone 1 appears hypo-intense on T2-WI, and iso-intense on T1-WI, while zone 2 appears as a T2 hyper-intense T1 hypo-intense rim around zone 1. Cavitation of the lesion

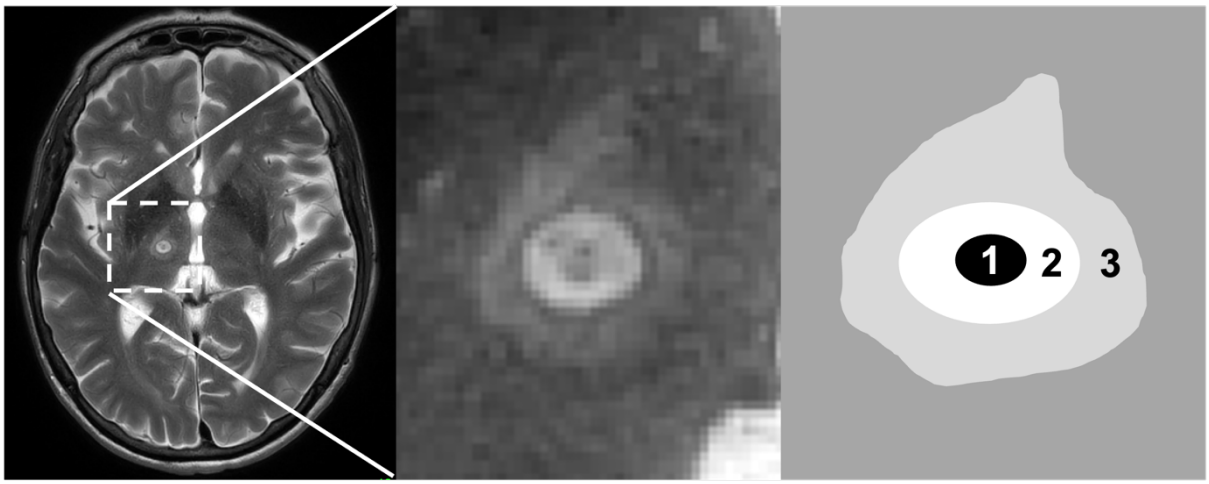

Figure 1-12 Axial view of tcMRgFUS lesion with concentric zones.

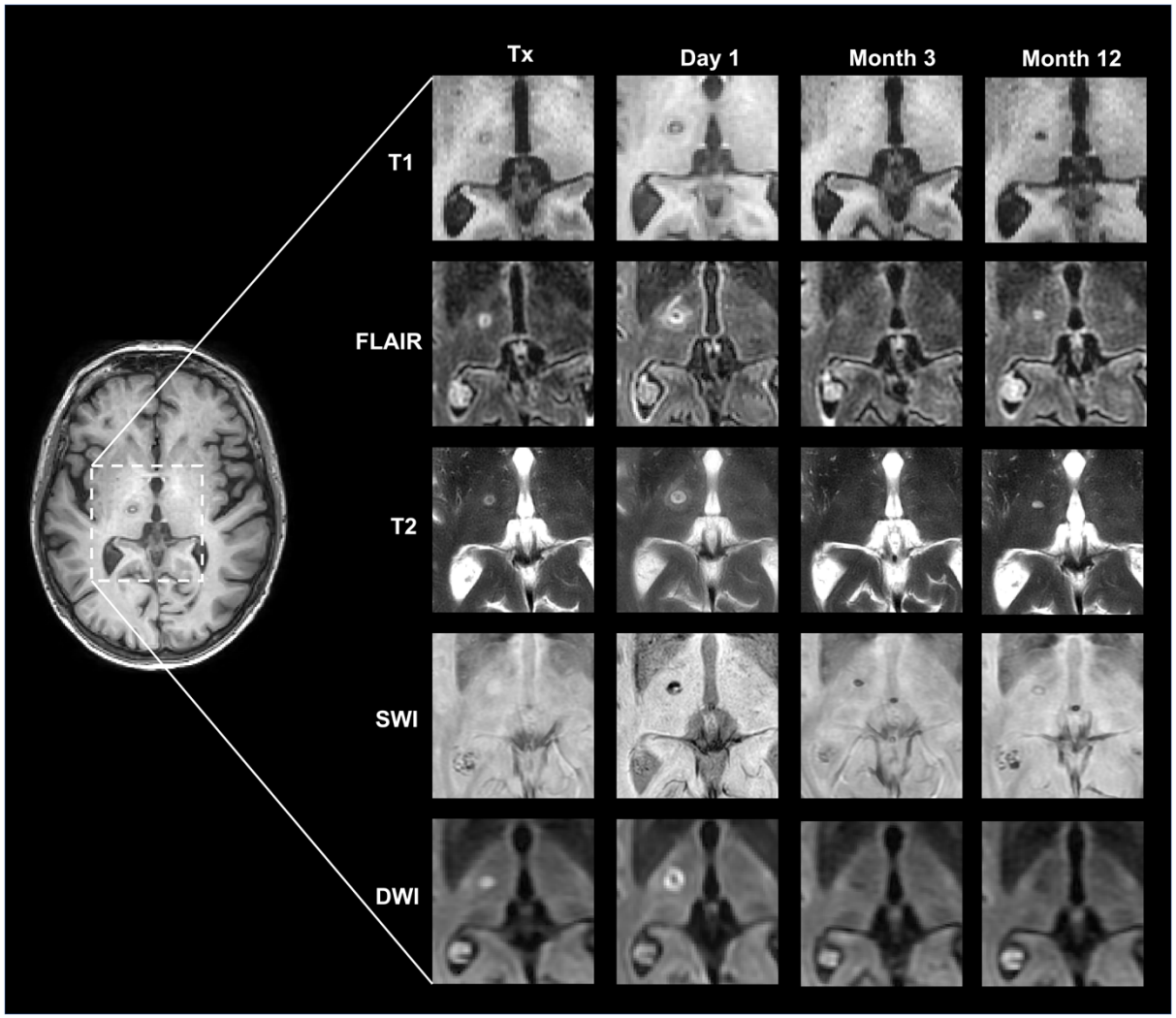

Figure 1-13 Evolution of tcMRgFUS lesion on MRI over a period of 12 months.

Abbreviations used: Tx (Day of treatment), SWI (Susceptibility Weighted Imaging), FLAIR (Fluid Attenuation Inversion Recovery), T1 (T1 Weighted Image), T2 (T2 Weighted Image), DWI (Diffusion Weighted Image)

in zones 1 and 2 frequently occurs within 1-week post-treatment, followed by cavity collapse and pseudonormalisation of the diffusion imaging. Zone 3 appears as a slightly T2 hyper-intense and T1 hypo-intense region on the periphery of zone 2 and is consistent with vasogenic edema. Zone 3 appears approximately 24 hours to 1 week following treatment and is typically resolved by 1-month post-treatment.

The diameter of zone 1 in the axial plane is approximately 2.7mm, and the thickness of zones 2 and 3 are 2.2mm and 3.0mm respectively[309]. However, there is significant variation between subjects, dependent on the physical characteristics of the patient and sonication parameters. Some studies have indicated that a minimum lesion volume of 40mm^3 is required to achieve adequate tremor benefit, and indeed several studies on tcMRgFUS have demonstrated a relationship between lesion size and clinical improvement[276,309]. However, larger lesions have also been shown to be associated with adverse events due to encroachment on surrounding structures[276]. In addition to the focal structural changes at the lesioned site, microstructural [310] changes in regions distal to the lesion have also been shown in dMRI studies, particularly along the DRTT at the level of the superior cerebellar peduncle and in the subcortical white matter below the motor cortex, which were correlated with clinical improvement[310].

1.3 Thesis motivation and aim

tcMRgFUS is an emerging surgical option for the treatment of tremor in movement disorders such as ET and DT. However, while a significant treatment effect of tcMRgFUS has been demonstrated, particularly in patients with ET, there remains a spectrum of observed clinical outcomes, and suboptimal outcomes continue to be reported. The exact reason for the range in tremor improvement remains unclear. However, the current tcMRgFUS literature, and lessons learned from treatment with DBS, point to the influence of tremor subtype, patient-specific characteristics and the treatment target as potential explanatory factors. Further investigation of the factors that influence the degree of tremor benefit experienced by patients following treatment with tcMRgFUS is of paramount importance for the continued improvement of patient screening and treatment strategy, as well as the identification of areas of technological improvement for future research and development.

The primary objective of this thesis was to investigate the key factors that influence the improvement in tremor experienced by patients treated with tcMRgFUS. This investigation was undertaken with a tiered approach that mirrored the typical tcMRgFUS process, from patient screening through to treatment. The thesis begins with the investigation of the patient-specific factors that may contribute to successful treatment outcomes and continues to the treatment-specific factors that are controlled by the treating team.

1.4 Organisation of thesis

This thesis is organised into five chapters: one introductory chapter (**Chapter 1**), three results chapters (**Chapters 2, 3 and 4**) and one summary chapter (**Chapter 5**). Each results chapter is divided into several sections, with each section representing a discrete study written in manuscript style, which together contribute towards the research focus of that chapter.

The overarching theme of this thesis is the investigation of factors that contribute to greater clinical improvement following the treatment of tremor with tcMRgFUS, with each results chapter focusing on the relationship between tremor improvement and a single patient or treatment-related factor. The multi-faceted nature of this thesis reflects the complex nature of the treatment of tremor with tcMRgFUS, in acknowledgment that there is no single factor that is determinant of outcome – rather it is the interplay of disease characteristics, patient characteristics, and decisions made at the time of treatment that may influence the degree of improvement experienced by patients. Subsequently, each of these three factors are further explored in the results chapters of this thesis.

Chapter 1 provides essential background information on the pathophysiology, aetiology and characteristics of the two main tremor subtypes considered in this thesis: essential tremor and dystonic tremor. The structures of the brain implicated in an inter-connected tremor network are introduced, and the history of stereotactic surgical targeting of this network for

the treatment of tremor is described. Finally, the development of tcMRgFUS is presented, as well as an overview of the technical aspects of the tcMRgFUS procedure.

In **Chapter 2**, the clinical tremor benefit of treatment with tcMRgFUS is investigated. The primary objective of this chapter was to compare the tremor benefit experienced by patients diagnosed with differing tremor subtypes to determine if there was a significant difference in tremor improvement, both intraoperatively and at long-term follow-up. Intraoperative tremor improvement was explored with the development a novel automated algorithm to analyse the tremor severity captured in the freeform spirals drawn by patients during tcMRgFUS. The chapter continues to assess long-term tremor suppression by evaluation of standardised tremor and quality of life scores at regular follow-up intervals.

Chapter 3 explores the effect of the skull on the effective deposition of US energy in the tissue of the brain. The first section in **Chapter 3** focuses on the effect of patient SDR on the intraoperative changes in sonication heating efficiency by investigating the persistent effects of sonication history on heating efficiency change. The second section in **Chapter 3** explores the influence of regional SDR values on the formation of clinically effective lesions and how this influences long-term tremor suppression.

Chapter 4 investigates the impact of the location of the tcMRgFUS lesion on tremor suppression and evaluates several potential neuroimaging tools to provide improved targeting methods. In the first section, two automated thalamic segmentation tools are investigated, and the degree of concordance with the conventionally placed Vim lesions is assessed. Additionally, a probabilistic targeting method for target identification is replicated

with an independent dataset. The second study of **Chapter 4** employs dMRI tractography to define the DRTT connecting the cerebellum with the Vim of the thalamus. The clinical utility of each targeting method is explored by comparison with the observed tremor improvement. In the final section of **Chapter 4**, the lesion location in patients requiring secondary lesioning of the posterior subthalamic area (PSA) is compared to those requiring lesioning of the Vim only to investigate any systematic differences in the Vim lesion location between the two groups. Additionally, the tremor benefit and adverse effects are compared across the two groups to determine if either targeting strategy is superior.

In **Chapter 5**, the main findings from each results chapter are summarised, and the key research outcomes of the thesis are presented, and the study limitations are discussed. Additionally, based on the results presented in this thesis, a number of future research directions are identified and discussed that may further improve understanding of the key factors that influence tremor suppression following treatment with tcMRgFUS.

2 Influence of Tremor Subtype on Clinical Outcomes

Based on:

- **Kain Kyle**, James Peters, Benjamin Jonker, Yael Barnett, Joel Maamary, Michael Barnett, Jerome Maller, Chenyu Wang PhD, and Stephen Tisch. “Validation of automated spiral analysis for assessment of tremor severity during MR-guided focussed ultrasound. (In submission with British Journal of Neurosurgery).

2.1 Abstract

While there is substantial literature on the stereotactic treatment of tremor with existing methodologies such as DBS and RF thalamotomy, particularly in the treatment of ET, as a relatively new surgical procedure for the treatment of tremor, there is relatively little literature comparing the outcomes across different tremor subtypes following treatment with tcMRgFUS. This chapter investigates any differences in tremor benefit experienced by patients with different tremor subtypes, including ET, ET-plus and DT, following treatment with tcMRgFUS. Section 2.2 begins with the development of a novel algorithm for the estimation of tremor severity in intraoperative hand-drawn spirals. The algorithm is applied to the spirals drawn by patients during tcMRgFUS, and the tremor improvement is compared across tremor subtypes. In section 2.3, the improvement in clinical tremor scores at long-term follow-up visits are investigated, and the improvement in scores are compared across the tremor subtypes.

2.2 Background

Essential tremor (ET) is one of the most common movement disorders; and there is a long history of stereotactic neurosurgical interventions for treatment of the disorder [218–221]. Decades of research into DBS and RF lesioning of the Vim have demonstrated the efficacy of these treatments in people with ET. More recently, stereotactic lesioning with tcMRgFUS has been used to treat ET. The first pilot study of tcMRgFUS, conducted in 2013, demonstrated the efficacy of the procedure [192,238]; and several subsequent studies reported significant tremor benefit in patients with ET [198,238,244,245], leading to increased adoption of the procedure worldwide[243].

Tremor has only recently been formally recognised as a component of the clinical spectrum of dystonia [88,89]. In its 2018 consensus statement, the International Parkinson and Movement Disorder Society defined dystonic tremor (DT) as tremor in a part of the body affected by dystonia [21]. In the same statement, the concept of ET-plus (ETP) was first defined, defined as tremor with characteristics of ET and additional neurological signs of unknown significance. While the pathophysiology of ET, ETP and DT are not well understood, several structures in a common tremor network, including the cerebellum, thalamus and primary motor cortex, have been implicated [80,138–140], and thus the same stereotactic interventions targeting this network, as pioneered in treatment of ET, have been applied to and DT[239]. However, while several studies have reported on the efficacy of tcMRgFUS for the treatment of ET [198,238,244,245], the literature comparing the relative tremor

improvement across the tremor subtypes following treatment with tcMRgFUS remains scant.

One of the key advantages of tcMRgFUS over other incisionless surgical options, such as gamma knife (GK) radiosurgery, is the immediate tremor suppressive effect observed in tcMRgFUS. The intraoperative improvement in tremor is used to assist clinicians in the identification of the optimal treatment coordinates, and typically involves a clinical evaluation of the patient by a movement disorders neurologist while the patient remains on the MRI table positioned with their head within the US transducer. Assessment of tremor severity via evaluation of freeform Archimedes spirals drawn by tremor patients is a validated method and is often included in the intraoperative evaluation [311]. Several manual rating scales for spirals in the context of tremor have been developed, however, they suffer from a lack of inter- and intra-rater consistency [312,313]. Thus, automated methods of spiral rating may aid clinicians by providing an unbiased and reproducible means of assessing tremor improvement over the course of the tcMRgFUS procedure.

2.3 Validation of automated spiral analysis for assessment of tremor severity during tcMRgFUS

2.3.1 Introduction

ET and DT are two common movement disorders, typically characterised by postural and kinetic tremor of the upper limbs [24,314,315], which can lead to difficulty in performing daily activities such as eating, drinking, and handwriting[316]. Tremor severity is often assessed by visual evaluation of handwriting or drawing, including the drawing of spirals, with spiral assessment forming part of the CRST scores[13]. To standardise the assessment of spirals, visual assessment schemes such as the Fahn-Tolosa-Marin (FTM) tremor rating scale were developed, which rates spirals on a 0–4-point scale[13]. This was expanded upon by Bain et al., who developed a 0–10-point rating scale, which have been widely adopted by clinicians in trials on ET. Ratings based on visual inspection, however, are subject to intra and interrater variability[201]. More recently, digital analysis of tremor during spiral drawing has been demonstrated using digitising tablets, which has been shown to correlate well with expert visual ratings [201,317,318]. Such techniques, however, require specialised equipment to capture the data for analysis.

As described in section 1.2, tcMRgFUS has recently emerged as a promising surgical procedure for the treatment of tremor in patients with movement disorders, including ET and DT [246,253,319]. One of the key advantages of tcMRgFUS is that it allows for the evaluation of tremor severity during the procedure, to confirm that the targeted coordinates are providing adequate tremor suppression, prior to the creation of a permanent lesion,

allowing clinicians to fine tune the target coordinates. Quantitative analysis of tremor severity in the MR environment is made challenging by the permanent magnetic field and imaging gradients, which makes the use of electronic equipment a potential hazard. Clinicians commonly employ hand-drawn spirals on paper to assess tremor improvement over the course of the procedure, due to the simplicity of implementation and validation in other treatments of tremor such as DBS [311].

Several groups have proposed automated algorithms for the quantification of tremor amplitude in hand-drawn spirals. The technique published by Legrand et al. is based on the calculation of the distance of each point in the spiral from the underlying template spiral[317]. Spirals drawn on a template, however, are impractical during tcMRgFUS due to the position of the patient's head within the ultrasound transducer, hindering visibility, and necessitating the use of freeform spirals. Kraus et al. demonstrated an algorithm applied to freeform spirals with an extremely high correlation with the manually rated spirals in the original Bain and Findley dataset, by comparing each point in the spiral to the intended location, approximated by calculation of a moving average of the drawn spiral[320]. The authors, however, fail to explain how the algorithm is able to derive a score from spirals that feature crossing or kissing lines, where the desired path of the spiral is difficult to infer in an automated fashion, particularly in the context of severe tremor. We present an algorithm to quantitatively measure tremor amplitude in spirals, which is fully automated in spirals without crossing lines, and can be applied to spirals with disconnected or crossing/kissing with manual input. We validate this algorithm against the blinded visual ratings of expert movement disorder neurologists. Additionally, we apply this algorithm to the intraprocedural spirals collected during treatment with tcMRgFUS, to compare the

trajectory of spiral improvement over the course of the procedure between patients with ET and DT and compare with long-term tremor score improvement.

2.3.2 Methods

This study was a retrospective analysis of data collected from patients treated with tcMRgFUS for medication refractory tremor at St Vincent's Hospital, Sydney, Australia, between November 2018 and March 2022. The study inclusion criteria included a tremor subtype diagnosis of ET, ET-plus (ETP) or DT, availably of original intraoperative spirals, and availability of pre- and post-treatment clinical tremor data. The study was conducted in accordance with the Helsinki Declaration on human experimentation. Informed consent was obtained from all subjects and the study was approved by St Vincent's Hospital Ethics Review Committee (ETH00670).

For optimisation of the spiral analysis algorithm described in detail below, a validation dataset of 100 spirals were selected at random using the RAND function in Microsoft Excel (Microsoft Corporation, 2018. *Microsoft Excel*, Available at: https://office.microsoft.com/excel) from a pool of spirals drawn by patients during the tcMRgFUS procedure. The spirals were visually rated by two blinded expert movement disorder neurologists. The spirals were also analysed with the automated algorithm, employing varying filter cut-off ratios and spiral error metrics to determine which combination provided the best agreement with the visual ratings. The optimised algorithm was then retrospectively applied to the spirals of all subjects who met the study inclusion criteria.

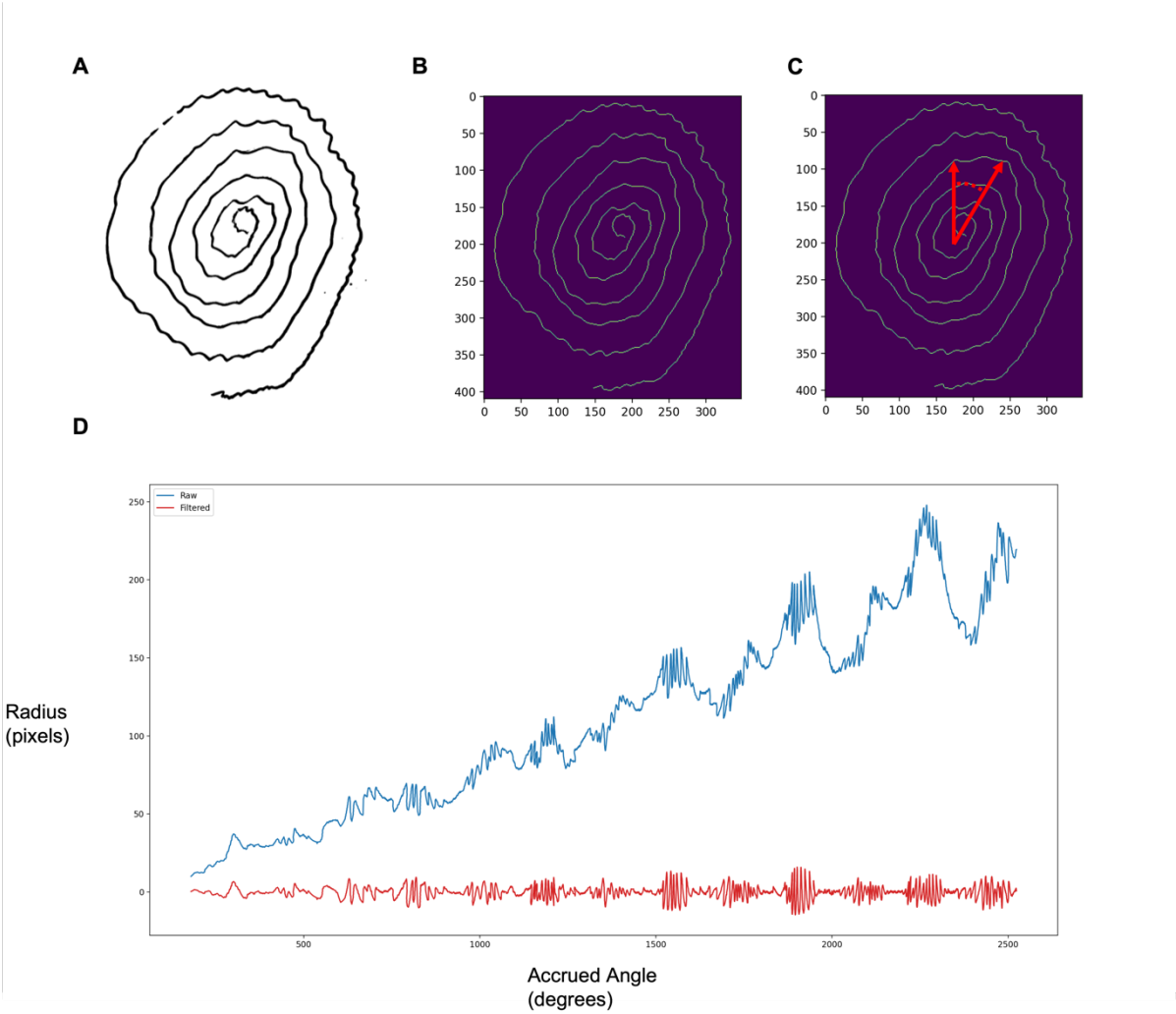

Figure 2-1 Summary of spiral analysis pipeline. ***A*** *- digitised spiral,* ***B*** *- Spiral after binarization, skeletonization and joining of individual line segments,* ***C*** *- Unravelling of the spiral by conversion to polar coordinates. For each point in the spiral, the radius and angle subtended with respect to the spiral centre and vertical axis is calculated, indicated by the red arrows, and the total accrued angle is calculated.* ***D*** *- Spiral in polar coordinates, blue line shows raw spiral after conversion, and red line shows polar coordinates after passing through a high-pass filter.*

Spiral Analysis Algorithm

Each spiral was digitised by scanning with a Hewlett-Packard scanner (HP DeskJet 2700) with automatic paper feed. Scan settings were set to black and white, with a resolution of 600 dpi (dots per inch), for a final resolution of 4961 × 7016. The raw images were manually

edited to remove the manual annotations added at the time of collection. The digitised image was then resampled to 362 × 512 pixels, to decrease processing time while maintaining the image aspect ratio. In cases that featured crossing or kissing lines that could not be analysed in an automated fashion, the spiral was manually edited and separated into individual spiral components at the point of line crossing. These components were recombined after conversion to polar coordinates, described below at step 4. Manual image editing was performed with the image manipulation software package GIMP (version 2.10.24) (https://www.gimp.org).

The spiral processing pipeline was performed as follows:

(1) The greyscale image was rescaled to values between 0 – 1. Pixels below a cut-off value of 0.5 were set to zero, and the image was binarized.
(2) The binarized image was skeletonized, reducing the image to a 1-pixel wide representation.
(3) If the skeletonized spiral consisted of several disconnected line segments, the end points were identified, and joined to the nearest segment with linear extrapolation to create a single curve.
(4) The spiral was unravelled by converting each point in the spiral from cartesian to polar coordinates (*Figure 2-1*).
    i. The centre of the spiral in cartesian coordinates was identified by taking the mean value of all points in the spiral along the horizontal and vertical axes.
    ii. Starting from the centremost point of the spiral, the angle and radius of each point in the spiral relative to the spiral centre was calculated. The change in angle from one point to the next was calculated and the sum of accrued angle was plotted against the radius for each point (blue curve in *Figure 2-1*C).

iii. If the spiral was manually separated into individual components, the start of one component was appended to the end of the previous after conversion to polar coordinates, resulting in a single curve (*Figure 2-2*).

iv. Due to tight curvature at the centre of the spiral, which can be undiscernible from tremor, the first 180° of the spiral was discarded.

(5) The data in polar coordinates was passed through a high-pass Butterworth filter, removing both the low frequency variations in radius associated with the underlying spiral shape and oscillations due to parallax errors resulting from inaccurate centering of the spiral, leaving only the high frequency deviations from the smooth curve due to tremor (red curve in *Figure 2-1*D).

i. As this study was investigating the tremor amplitude only, not the tremor frequency, the choice of filter cut-off frequency was arbitrary – the filter response is determined by the ratio between the sampling frequency and cut-off frequency. Subsequently, the sampling rate was estimated by calculating the average difference in angle between each point in the transformed data set, and the filter cut-off frequency was calculated by division of the sampling rate by a constant factor, defined as the cut-off frequency ratio.

(6) For each point in the filtered data, the absolute deviation from zero was calculated, resulting in a list of deviation values for each spiral. This perturbation of the drawn line from the ideal spiral path was defined as the spiral error and was used as a measure of tremor severity.

(7) For the list of spiral error values, both the mean and maximum values were calculated, and compared during the optimisation step.

All image processing was performed using the sci-kit image processing module (version 0.19.3) in Python (version 3.8.15). Signal processing was performed with SciPy (version 1.10.1) in Python.

Spiral Validation

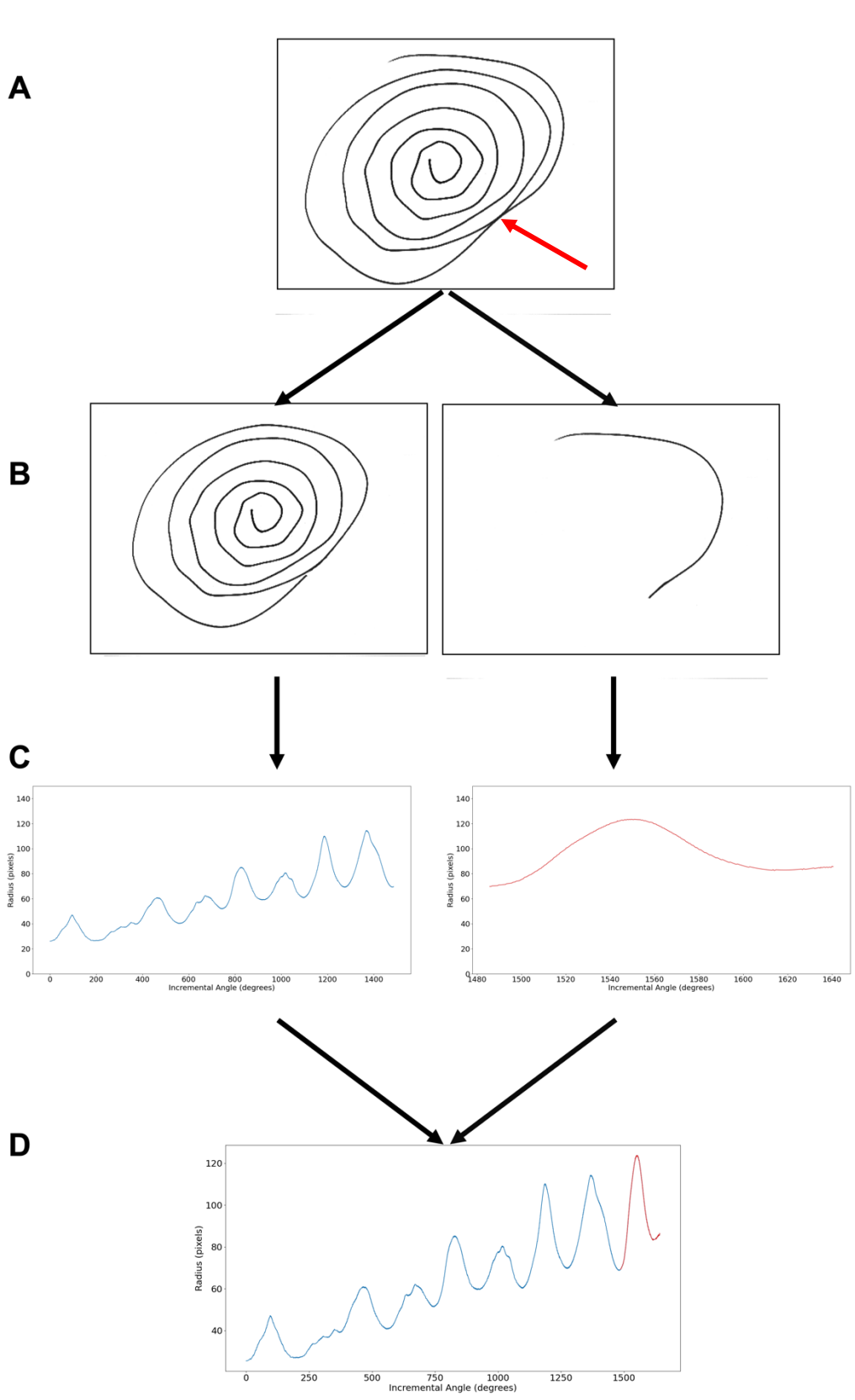

Figure 2-2 Example workflow for spirals with crossing lines. ***A*** *– Raw spiral with crossing lines, indicated by red arrow.* ***B*** *– Spiral is separated into non-crossing components.* ***C*** *– Each component is converted to polar coordinates individually.* ***D*** *– Each component (shown in red and blue) in polar coordinates is recombined prior to high-pass filtering.*

100 spirals were selected at random from a pool of 619 spirals drawn by patients who underwent tcMRgFUS for treatment of tremor. The spirals were rated by two movement disorder neurologists using the Bain and Findley rating scale for free form spirals[321], which rates spirals on a scale of 0 to 10, where 10 corresponds to the inability to draw a spiral due to the severity of tremor. Analysis was restricted to spirals for which automated analysis was possible, thus the maximum possible rating of spirals in the validation set was 9.

The same 100 spirals were analysed with the automated spiral error algorithm described above. To determine the optimal filter cut-off frequency ratio, ratios of 75, 100, 125 and 150 were used and the results compared. For each cut-off frequency ratio, both the mean and maximum spiral error was calculated, resulting in total of 8 measurement of spiral error for each spiral. As a consequence of the Weber-Fechner law of psychophysics, which predicts a logarithmic relationship between the perceived tremor magnitude, and the true tremor amplitude[322,323], spiral error was log-transformed and rescaled to between 0-9, to match the range of Bain and Findley spiral ratings, consistent with other studies on spiral analysis[317].

Inter-rater agreement between the visual ratings provided by the 2 expert clinicians, and agreement between the averaged expert visual rating and the 8 spiral error metrics computed with the automated spiral algorithm were assessed with Spearman's rank correlation analysis. Additionally, bias between the automated spiral error, and the average visual spiral ratings was assessed with Bland-Altman analysis.

For analysis of reproducibility, 10 spirals from the existing validation dataset were selected at random with the RAND function in Microsoft Excel, and flipped around 1 axis, converting

clockwise spirals to anti-clockwise, or anti-clockwise to clockwise. These duplicated flipped spirals were distributed randomly in the validation dataset for visual rating and were analysed with the optimised spiral algorithm for comparison with the original spiral. Due to the greater precision of the automated method compared with the manual ratings, the spiral error was then rounded to the same rating increments (0.5) as the averaged visual rating.

tcMRgFUS Procedure

The tcMRgFUS procedure was performed as described in section 1.2.4. Briefly, prior to treatment the patient's head was shaved and a stereotactic frame was affixed to the head. The patient was positioned headfirst in the MRI scanner in the supine position, with the head positioned within the ultrasound transducer. A T1-weighted image (T1-WI) was acquired with the body coil of the MRI scanner and fused to pre-treatment MR and CT imaging for landmark identification and target planning. Ultrasonic lesioning was performed using the ExAblate Neuro system (InSightec, Tirat Carmel, Israel) 650kHz, with a 1024-element phased array ultrasound transducer. Sonication temperature increase was monitored via intraprocedural 2D MR thermometry, acquired at 3 second intervals during each sonication. The sonication target and heating spot shape were confirmed with a series of low energy sonications, such that the temperature increase was below the threshold to permanently destroy brain tissue. Following target confirmation, sonication power and energy were gradually increased to therapeutic temperatures (>53^{o}C), causing thermal necrosis of brain tissue at the treatment target. Following the initial index sonications, each

patient was evaluated immediately after each sonication to monitor improvements in tremor severity, and the appearance of any side effects.

The Vim was targeted using coordinates of approximately 25% of the distance between the anterior (AC) and posterior commissure (PC), plus approximately 0.5mm in the AC-PC plane, and 14mm lateral to the midline. Coordinates were adjusted for individual patient anatomy. Any patients treated in additional regions outside of the Vim, such as the PSA, were excluded from this study.

Spiral Collection

All spirals were drawn with the patient supine in the MRI scanner, and head positioned within the ultrasound transducer. The spirals were drawn with a black felt marker on a standard A4 (210 $\times$ 297 mm) white sheet of paper, supported on a plastic clipboard held by the treating neurologist. The clipboard was held in position above the patient to allow comfortable supine writing position with extension of the arm such that the arm and hand were unsupported. The patient was asked to draw an Archimedes spiral to the best of their abilities, with no instructions given on the size of the spiral, speed with which to draw, or spiral direction (clockwise or anticlockwise).

For each patient, a baseline spiral was drawn immediately prior to the first sonication. A spiral was drawn again after the first clinical evaluation following the initial index sonications, and again after every subsequent sonication until the completion of treatment. Each spiral was annotated with the time and sonication number after which it was collected.

Intra-procedural Spiral Improvement

Following validation of the spiral analysis, the optimised algorithm was used to analyse all 619 spirals collected during treatment with tcMRgFUS, with the aim of exploring the trajectory of spiral improvement over the course of the tcMRgFUS procedure, and to determine if the trajectory differed by tremor subtype. The linear transform defined during the rescaling step of the spiral validation was used to rescale the spiral error of all spirals. Spirals were separated into baseline, first intra-procedural examination, first spiral after reaching a therapeutic temperature of 53°C, and the spiral following the final sonication. Patients were factored into 3 tremor subtype groups: ET, ETP and DT. ETP was defined as a patient with ET and featuring additional neurological symptoms such as impaired gate, dystonia, or memory impairment. Absolute spiral error, and percentage improvement from baseline, at each examination was compared across the three tremor subtypes to determine if there was a significant difference. The normality of the spiral error distribution was assessed with Shapiro-Wilk test of normality. Absolute and percentage improvement in spiral error was compared across the 3 groups at each examination with the non-parametric Kruskal-Wallis test. Pairwise Wilcoxon tests with false discovery rate (FDR) correction for multiple comparisons were used for pairwise comparisons of spiral error between tremor subtypes at each examination.

Pearson correlation was used to assess the relationship between the absolute spiral error at baseline and post treatment, with the baseline and long-term follow-up tremor scores, respectively. For comparison with long-term tremor score improvement, percentage

improvement in spiral error between the baseline and post-treatment spirals were used to group the patients into above and below average treatment response groups. Percentage improvement in tremor scores at long-term follow-up were compared across the two groups with independent t-tests, to determine if the spiral error improvement measured on the day of treatment was associated with long-term tremor score improvement.
All statistical analysis was performed using the statistical software package R (version 4.2.2) in RStudio (Version 1.4.1717, RStudio, Inc., Boston, MA URL, http://www.rstudio.com).

Clinical Evaluation

Clinical tremor scores were calculated for each patient by a trained movement disorders neurologist prior to treatment, and again at intervals of 1-, 3-, 6-, 12-, 24- and 36-months post-treatment. The evaluation included CRST, HTS and QUEST scores, as summarised in section 1.1.5. For investigating of long-term outcomes, as not all patients returned for every follow-up clinical evaluation, the most recent score for each patient was used as the follow-up tremor score. Tremor score improvement was assessed by calculation of the percentage change of the follow-up score relative to the baseline score and inverted such that a positive value represents tremor score improvement.

2.3.3 Results

tcMRgFUS and Patient Characteristics

114 subjects who were treated with tcMRgFUS were identified. From this dataset, 27

subjects were excluded due to missing spiral data, 16 were excluded due to not meeting the tremor subtype criteria, and 19 were excluded due to missing pre/post treatment clinical tremor data, leaving 52 subjects for inclusion in the study. The cohort included 19 subjects with ETP, 21 patients with DT and 12 subjects with ET. The mean patient age and disease duration at the time of treatment was 73.11 ± 8.64 and 28.31 ± 16.31 years, respectively. There was not found to be a significant difference in age or disease duration between tremor subtypes. The mean time between the baseline and most recent clinical evaluations was 18.20 ± 12.52 months.

The mean number of sonications delivered over the course of the treatment was 9.75 ± 2.97, and the mean maximum sonication temperature was 56.73 ± 1.89°C, reaching at least

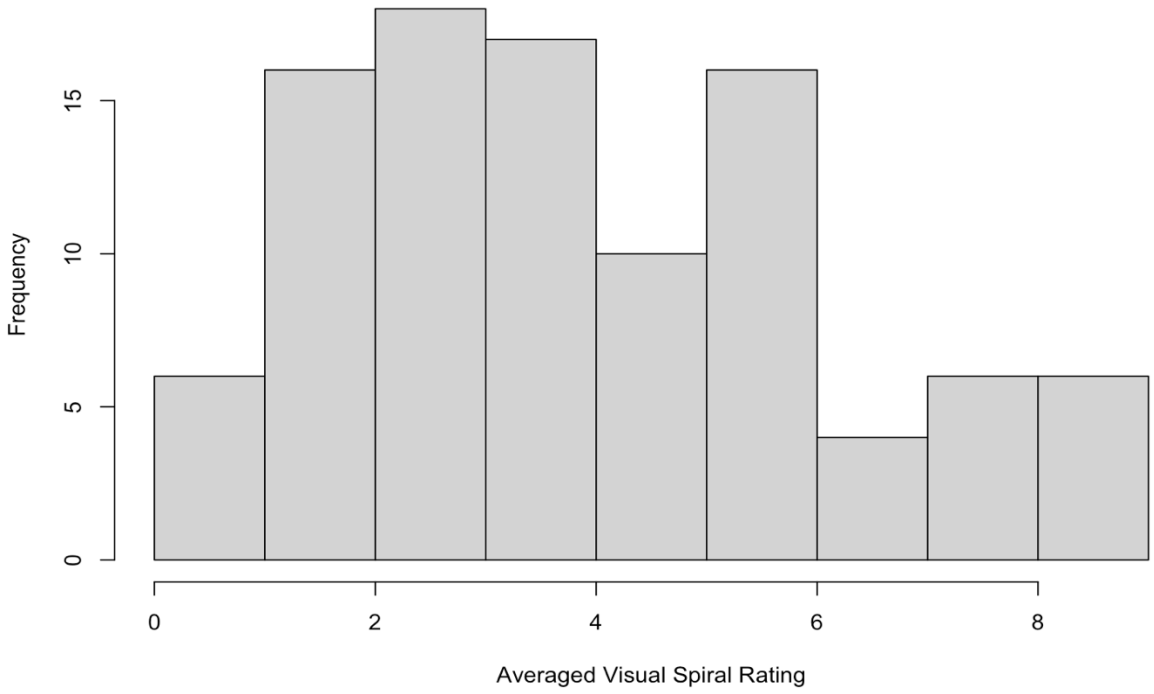

Figure 2-3 Histogram of the averaged spiral ratings from the blinded expert movement disorder neurologists used in the spiral validation.

Table 2-1 Patient and tcMRgFUS treatment characteristics.

Variable	All patients N=52
Sex, n(%)	
Male	32 (62)
Female	20 (38)
Tremor Subtype , n(%)	
ET	12 (23)
ETP	19 (37)
DT	21 (40)
Age, mean ± SD, years	73.11 ± 8.64
Disease Duration, mean ± SD, years	28.31 ± 16.31
Treatment Side, n(%)	
Left	44 (85)
Right	8 (15)
Number of Sonications	9.75 ± 2.97
Max. Average Temperature (°C)	56.73 ± 1.89°C

Abbreviations used: ET (Essential Tremor), ETP (Essential Tremor Plus), DT (Dystonic Tremor), SD (Standard Deviation)

53°C in all subjects. On average, the first evaluation was performed after 4.02 ± 0.98 sonications, with an average sonication temperature of 50.50 ± 2.51°C. The first therapeutic sonication occurred on average after 5.65 ± 1.67 sonications, with an average temperature of 55.44 ± 1.91°C. There was not found to be a significant difference in the number of sonications, or maximum sonication temperatures between tremor subtypes. Patient and treatment characteristics are summarised in *Table 2-1*.

Spiral Analysis Validation

Of the 100 spirals in the validation set, the mean averaged Bain and Findley rating was 4.21 ± 2.28 (minimum 0, maximum 9), the distribution is shown in *Figure 2-3*. Inter-rater agreement was excellent (r=0.90, p<0.001). The spiral ratings provided by the two clinicians were identical in 55 (55%) of the presented cases. The correlation between the averaged clinician spiral ratings, and the automated spiral error are summarised in *Table 2-2* . A

*Table 2-2 Summary of Pearson correlation and Bland-Altman analysis for the automated spiral analysis algorithm employing high-pass frequency cut-off ratios of 75, 100, 125 and 150. For each frequency cut-off ratio, the mean and maximum spiral error was calculated. *Indicates best performing algorithm parameters.*

Frequency Ratio	Pearson Correlation	Bland-Altman Bias
75		
Mean	r=0.89, CI: 0.84 - 0.93, p<0.001	0.35 ± 1.06, CI: 0.14 - 1.56
Max	r=0.82, CI: 0.74 - 0.88, p<0.001	-0.63 ± 1.27, CI: -0.88 - 0.28
100		
Mean	r=0.84, CI: 0.76 - 0.88, p<0.001	0.28 ± 0.95, CI: 0.10- 0.47
Max	r=0.91, CI: 0.87 - 0.94, p<0.001	-0.60 ± 1.22, CI: -0.8 - 0.37
125		
Mean	**r=0.94, CI: 0.89 - 0.95, p<0.001***	**0.04 ± 0.87, CI: -0.14- 0.21***
Max	r=0.91, CI: 0.87 - 0.94, p<0.001	0.38 ± 1.17, CI: -0.61 - 0.15
150		
Mean	r=0.91, CI: 0.87 - 0.94, p<0.001	-0.16 ± 0.94, CI: -0.34 - 0.02
Max	r=0.84, CI: 0.77 - 0.89, p<0.001	-0.07 ± 1.21, CI: -0.31 - 0.17

combination of high-pass filter cut-off frequency ratio of 125, and tremor amplitude calculated using the mean spiral error resulted in the greatest correlation. Notably, the Pearson correlation (r=0.94, p<0.001) between the automated spiral error and averaged clinical ratings were greater than the inter-rater correlation. Bland-Altman analysis indicated the mean difference between the spiral error and the average visual rating was 0.04 (95% CI - 0.14-0.21). Bland-Altman plots and scatter plots illustrate the relationship between the automated spiral error and visual ratings are shown in *Figure 2-4*.

In the reproducibility analysis, the averaged expert visual rating of the flipped spiral differed from the rating of the original spiral by 0.5 rating points in 5 (50%) cases, and Pearson correlation between the rating of the original and flipped spirals was 0.82. When analysed

with the optimised spiral algorithm, the Pearson correlation between the original and flipped spirals was 0.97. After rounding of spiral error values to the nearest multiple of 0.5, for consistency with the precision of the averaged visual ratings, the rounded spiral error of the original and flipped spirals were identical in all 10 cases.

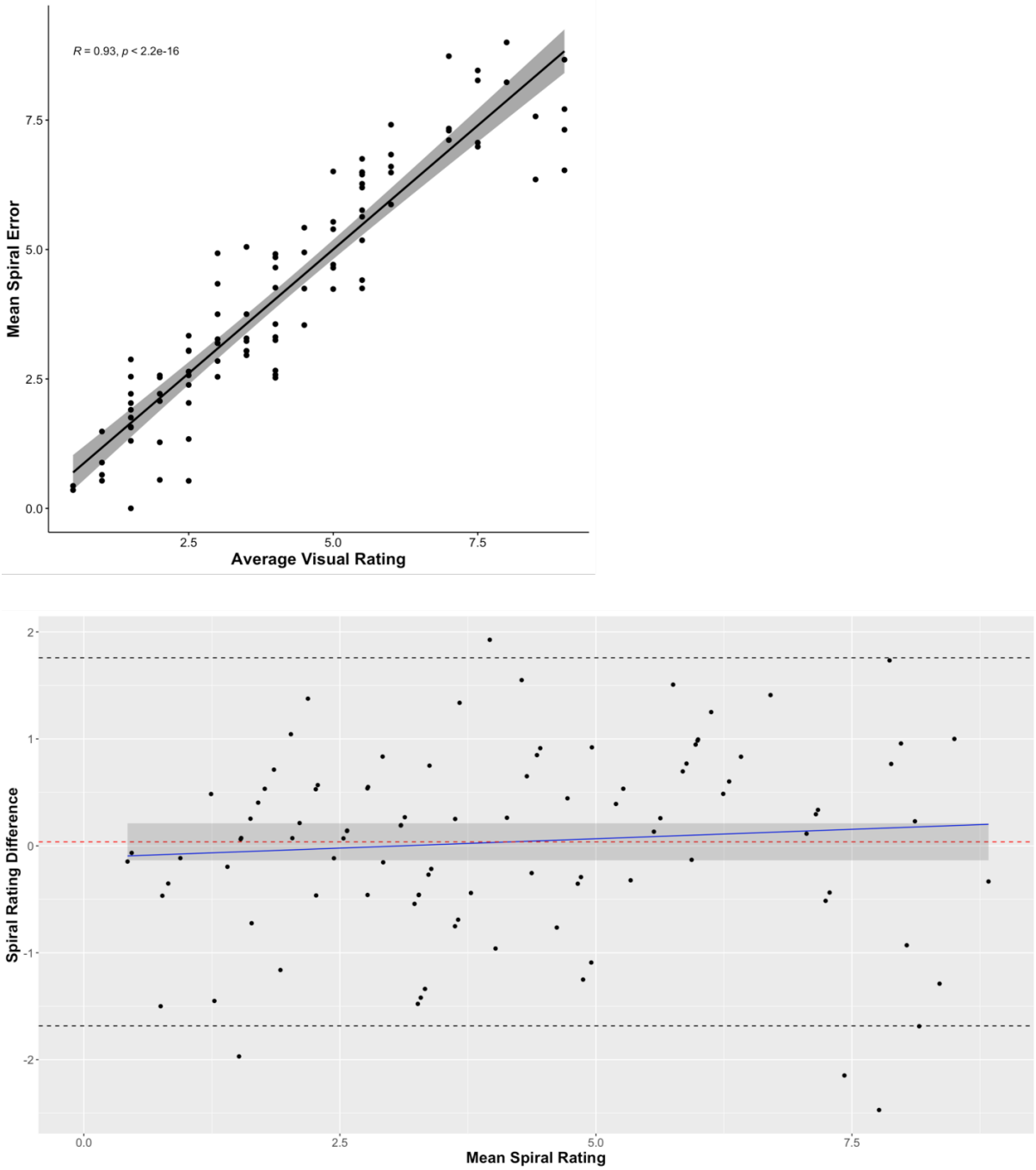

Figure 2-4 Correlation between the averaged visual spiral ratings and the log-transformed automated spiral error. ***Bottom –*** *Bland-Altman plot of averaged visual spiral ratings and automated mean spiral error. Bias indicated by red dashed line with 95% confidence intervals (shaded region), black dashed line indicates limits of agreement, and regression fit of the difference indicated by blue line.*

Correlation of spiral error with clinical scores

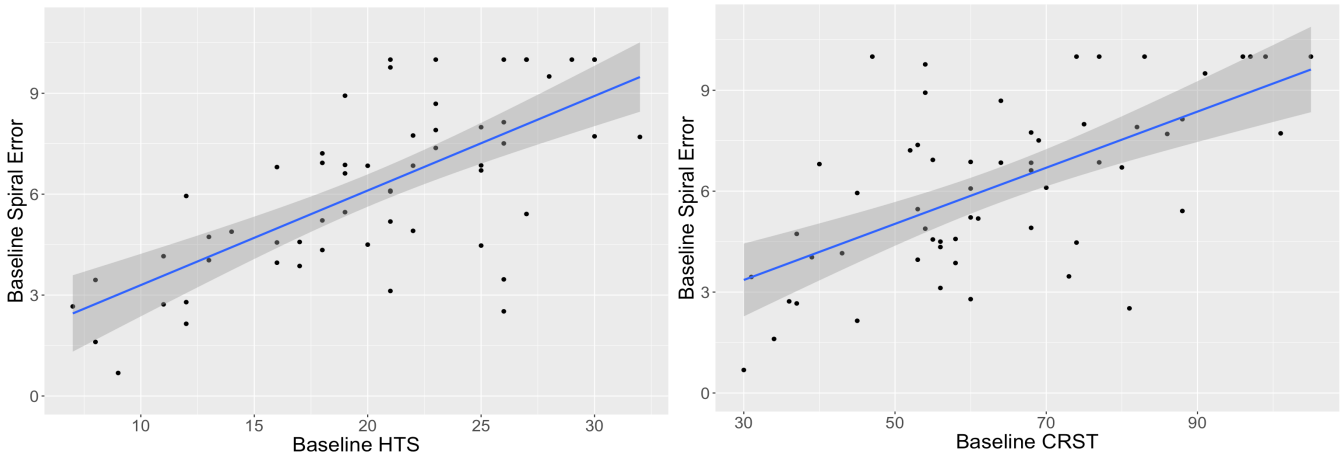

*Figure 2-5 Correlation between baseline HTS (**left**) and CRST (**right**) and the baseline mean spiral error. Line of best fit indicated by blue line, and shaded region indicates 95% confidence interval.*

Baseline absolute spiral error was significantly correlated with baseline HTS (r=0.696, p<0.001), and CRST (r=0.623, p<0.001), shown in *Figure 2-5*. Absolute spiral error measured on the post-treatment spiral was also significantly correlated with HTS (r=0.569, p<0.001) and CRST (r=0.721, p<0.001) at long-term follow-up. Patients in the greater than average spiral improvement group experienced significantly greater improvement in HTS (67.14 ± 21.70% vs. 51.23 ± 21.85%, p=0.009) and CRST (48.94 ± 14.18 vs. 36.31 ± 17.50%, p=0.004) at long-term follow-up, compared with those in the low spiral improvement group, shown in *Figure 2-6*.

Intra-procedural spiral measurements

The mean spiral error across all subjects prior to the first sonication was 6.07 ± 2.46, which improved to 1.97 ± 1.42 post-treatment (paired t-test p<0.001). Baseline spiral error was lowest in ET patients (5.16 ± 1.51), followed by ETP (5.96 ± 2.12) and DT (6.90 ± 2.96), however, these differences were not found to be statistically significant.

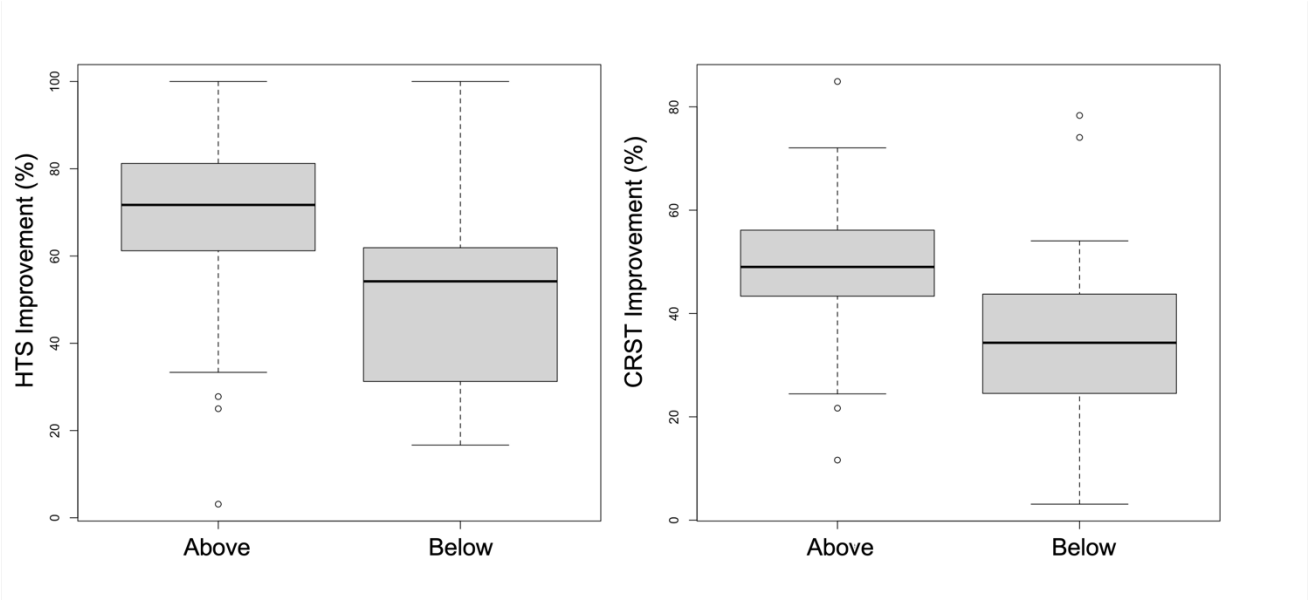

*Figure 2-6 Percentage improvement in HTS (**left**) and CRST (**right**) at the most recent clinical follow-up, grouped by those with above and below average final spiral improvement. Box indicates interquartile range, whiskers indicate standard deviation, solid line indicates median value and outliers represented by dots.*

The percentage spiral error improvement at the first evaluation was significantly lower in patients with DT (31.95 ± 24.24%, p=0.005) and ETP (26.10 ± 33.94%, p=0.002), compared with patients with ET (56.33 ± 15.14%). After the spiral drawn following the first therapeutic sonication, percentage improvement in DT patients (35.21 ± 26.15, p=0.013) was again significantly lower than in ET patients (64.94 ± 24.03). Improvement in ETP patients (44.94 ± 30.71, p=0.081) was also lower compared with ET, however, this difference did not reach statistical significance. Spiral error measured on the spiral following the final sonication of the treatment followed the same pattern as the first therapeutic sonication, with spiral improvement significantly lower in DT patients (56.17 ± 23.10, p=0.038) compared with ET patients (75.30 ± 18.49). Improvement was again lower in ETP patients (63.49 ± 24.15, p=0.174), however, the difference was not statistically significant. Absolute spiral error after

the final sonication was significantly greater in DT patients (2.37 ± 1.56, p=0.019) compared with ET patients (1.17 ± 0.88), while the error in ETP patients was greater (1.94 ± 1.36, p=0.122), it was not statistically significant. The mean improvement in spiral error at each evaluation are shown in *Figure 2-7*.

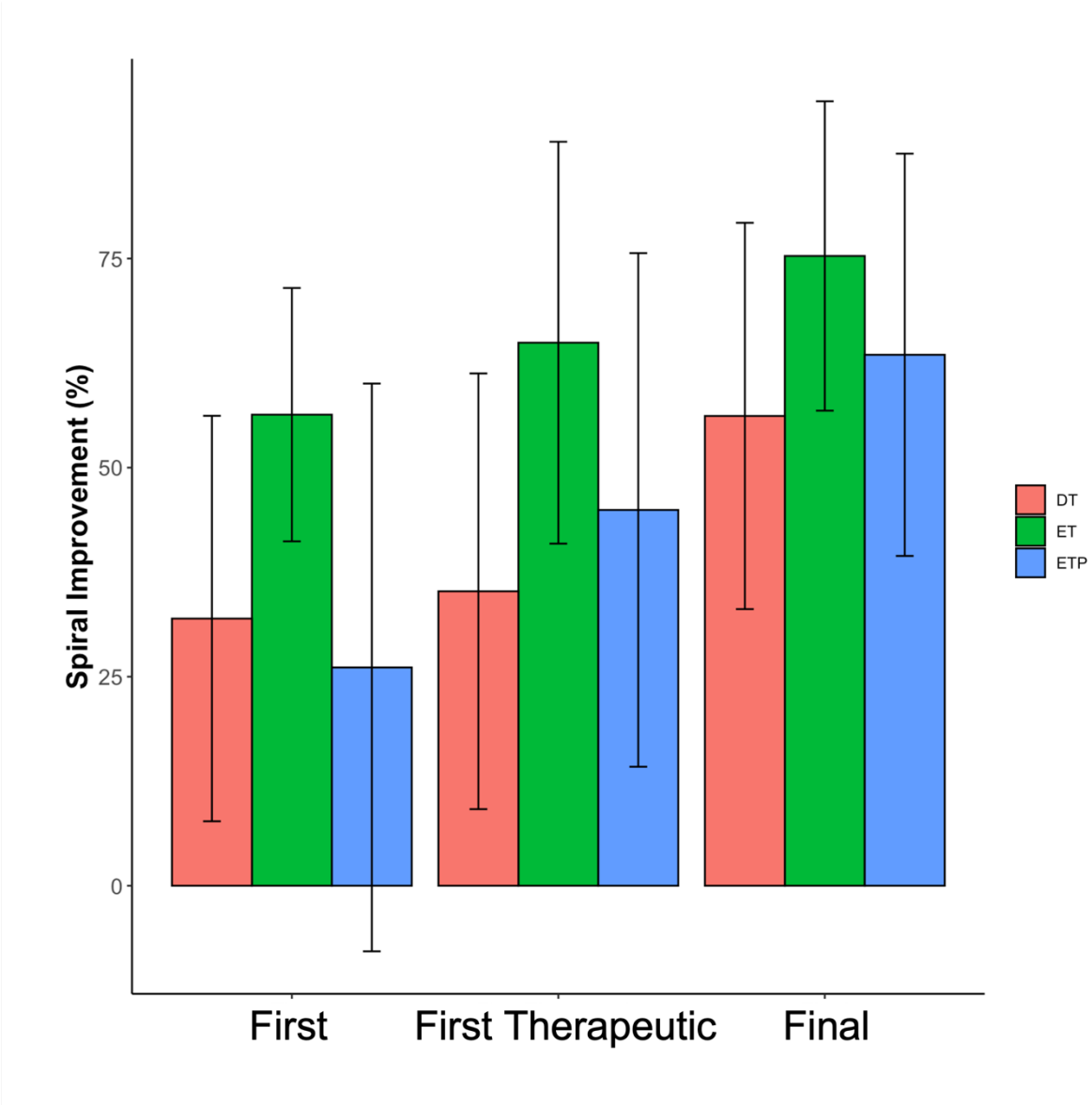

Figure 2-7 Mean spiral improvement at the first evaluation, first evaluation after reaching therapeutic sonication temperatures, and the final evaluation during tcMRgFUS. Whiskers indicate standard deviation for each tremor subtype at each evaluation. Note negative improvement indicates increased spiral error.

2.3.4 Discussion

Development of an objective and reproducible method of tremor severity measurement provides benefits for clinicians evaluating the changes to tremor during tcMRgFUS, and for research into tremor improvement during tcMRgFUS treatment. The aim of this study was twofold; the primary aim was to validate a semi-automated spiral analysis algorithm against a validation dataset of manually derived spiral ratings from two neurologists trained in movement disorders. The secondary objective was to use the spiral analysis to examine the trajectory of spiral improvement over the course of the tcMRgFUS procedure, to determine if there was a significant effect of tremor subtype on spiral improvement.

The results of the validation analysis found that there was excellent agreement (r=0.94) between the spiral error, and the average visual spiral rating, indicating the automated spiral analysis metrics are reflective of the same characteristics of the spiral used by clinicians to rate the spiral. Moreover, the agreement with the averaged spiral ratings was greater than the interrater agreement, suggesting that the automated spiral analysis algorithm may provide a more reproducible measure of the impact of tremor on spiral quality. Results of the reproducibility analysis highlight the impact of human error in visually rated spirals, where 50% of the duplicated spirals were rated differently to the original spiral, while the automated algorithm demonstrated a correlation of 0.97, and identical ratings when the spiral error was rounded to the same increments as the manual ratings. Thus, use of the automated analysis may help reduce variance due to both inter and intra-rater variability. Furthermore, we demonstrate that spirals that are drawn with crossing or

kissing lines can be included in analysis. The algorithm is open source and has been made publicly available on GitHub (github.com/kkyle193/spiral_rating).

We show that the spiral error measured prior to treatment was significantly correlated with pre-treatment HTS and CRST, providing further validation that the spiral error measured with this algorithm provides a meaningful measure of tremor severity. Our findings that the spiral error improvement measured post treatment was significantly associated with improvement in HTS and CRST measured at long-term follow-up provides validation of the use of spirometry for evaluation of intra-procedural tremor improvement and suggests that post-treatment spiral error improvement is a significant indicator of the long-term tremor suppression following treatment with tcMRgFUS.

To the author's knowledge, this is the first study to directly compare the spiral improvement measured during tcMRgFUS across different tremor subtypes. The lower spiral improvement experienced by DT patients in this study, relative to ET, may suggest that the acute treatment benefit following tcMRgFUS is lower in patients with DT. This interpretation, however, requires further validation with additional techniques to capture the severity of other forms of tremor, such as postural tremor.

Additionally, we show that patients with a diagnosis of ETP exhibited a different trajectory of spiral improvement, compared with patients with pure ET, with less improvement at the first evaluation. ETP is a relatively new concept, defined in the 2018 consensus statement of the Movement Disorder Society on tremor, characterised as essential tremor with additional neurological symptoms such as impaired gait, dystonia, or memory impairment[324]. There is

currently little literature on how the re-classification of patients as ET or ETP may affect the response to treatment with tcMRgFUS. We show that the trajectory of ETP patients is between ET and DT, with a slow initial response, similar to patients with DT. However, ETP patients exhibited significant improvement following the initial spiral, to the point that the spiral error improvement after the final sonication was not significantly different from ET patients. The difference in trajectory between ETP and ET patients emphasizes the importance of this new classification and may be of use for future clinical trials on patients treated with tcMRgFUS for tremor. Importantly, we show that the improvement in post-treatment spirals was not significantly different between ET and ETP patients, indicating the long-term clinical outcomes may be similar, however, this requires further investigation.

The characterisation of tremor improvement during tcMRgFUS may provide benefit to treating clinicians in making treatment strategy decisions such as targeting, primarily by highlighting that tremor subtype should be considered when evaluating the tremor response to treatment at early evaluations. For example, a lack of response to early sonications in a patient with pure ET may be more alarming than in a patient with DT, and suggest a change to coordinates may be necessary, given ET patients typically respond early. Conversely, a small relative spiral improvement in a patient with DT may not indicate a target adjustment is necessary, given they generally appear to show less improvement on the initial evaluation, and tremor suppression may still be achieved following subsequent sonications of therapeutic temperatures.

Automated analysis of tremor using spirals drawn on paper is hindered by the inherent limitation of 2D analysis of tremor, which cannot quantify tremor that is perpendicular to

the paper on which the spiral is drawn. This limitation is particularly evident in the poor relationship between spirals rated greater then 8 by clinicians, where this effect can be considered by clinicians in their rating but cannot be captured by the automated analysis. Furthermore, analysis of spirals drawn on paper does not capture any information on the speed with which the spiral was drawn; thus, the true frequency of tremor cannot be determined, in contrast to tremor analysis using digital tablets where the pen velocity can be tracked to deduce the frequency. The use of accelerometry may compliment spiral evaluation for the intraoperative assessment of tremor by providing information on tremor amplitude in 3 dimensions, as well as capturing tremor frequency. Nonetheless, we demonstrate that the spiral error estimated by the presented algorithm exhibited excellent agreement with the visual rating. The presented algorithm is fully automated for the analysis of non-crossing spirals, and can be run in minutes, offering the potential to provide unbiased intraoperative data on tremor severity. The benefits of the presented algorithm are twofold; firstly, the algorithm can be applied on a retrospective dataset, providing unbiased data on the intra-operative tremor improvement without the need to blind expert raters or consult multiple experts to address inter-rater variability. Secondly, as the algorithm is fully automated and can be run a standard computer with computation time less than 1 minute, the algorithm may be used to provide real-time data on tremor improvement during treatment.

Furthermore, the improvement in spiral error measured with this algorithm was a significant predictor of the improvement in clinical scores at long-term follow-up, further validating the use of the spiral analysis in evaluating the outcome of tcMRgFUS.

2.3.5 Conclusion

We present a semi-automated spiral analysis algorithm, that can be applied to fully connected spirals, disconnected spirals, and spirals with crossing lines. The spiral error measured using this algorithm exhibited greater agreement with the average visual spiral rating, compared to the inter-rater agreement. The improvement in spiral error between the baseline and post-treatment spiral error was shown to have a significant effect on the long-term clinical outcomes, indicating that spiral improvement is a meaningful predictor of long-term outcomes. Additionally, we present a significant effect of tremor subtype on the trajectory of spiral improvement over the course of the tcMRgFUS procedure, with patients diagnosed with DT experiencing significantly less spiral improvement, compared with ET. The relationship between tremor subtype and spiral improvement, may suggest that long-term tremor benefit is associated with the tremor subtype diagnosis, however, this requires further investigation. In the following section, the change in long-term tremor scores is investigated with a more rigorous statistical model.

2.4 Comparison of long-term tremor change in essential tremor and dystonic tremor following treatment with transcranial tcMRgFUS.

2.4.1 Introduction

ET is one of the most common neurological disorders, with a prevalence between 0.4-3.9% of the population globally[27]. Disease symptoms commonly feature a tremor of the arms during voluntary movement or posture[314], or less frequently at rest [325,326]. While the pathophysiology underlying ET is not completely understood, several studies have implicated dysfunction of the cerebellar-thalamo-cortical pathways and basal ganglia in the generation and propagation of tremor signals [327–329]. Neurosurgical procedures targeting the Vim of the thalamus, which receives cerebellar afferents, have demonstrated a significant reduction in tremor in patients with ET[330].

Tremor has only recently been recognised as forming part of the clinical spectrum of dystonia [88,89]. DT typically features tremor during voluntary movement and posture, although tremor is commonly more irregular and asymmetric, compared with ET[108]. While ET and DT share similar clinical features, their pathophysiology differs substantially [162,315]. Despite this, there is emerging evidence of involvement of the cerebellum and basal ganglia in DT; and treatments proven to be effective in treatment of ET have been applied to DT with promising results [331,332].

While several studies have reported on the long-term effectiveness of tcMRgFUS on tremor control in patients with ET [319,333,334], there remains a distinct lack of literature on outcomes in patients with DT. In section 2.3 the intraoperative tremor improvement measured from freeform spirals drawn by patients was investigated and compared across tremor subtypes. Intraoperative improvement was found to be significantly lower in patients diagnosed with DT, and spiral error measured immediately post-treatment was found to be associated with long-term improvement, suggesting DT patients may experience lower long-term improvement. Building on the results of section 2.3, the aim of this investigation was the compare the long-term tremor suppression experienced by ET and DT patients, treated with tcMRgFUS at a single centre.

2.4.2 Methods

This investigation was a retrospective analysis of data from 66 patients with medication-refractory ET or DT, who underwent tcMRgFUS for treatment of tremor at St Vincent's Hospital, Sydney Australia, between January 2019 and November 2022. All DT patients met the criteria for DT[1], and all ET patients met the 2018 consensus criteria for ET or ETP[21] considered collectively as ET. Informed consent was obtained from all participants, and the study was approved by the St Vincent's Hospital ethics review committee (ETH00670).

tcMRgFUS Procedure

tcMRgFUS was performed as described in sections 1.2.4 and 2.3.2. In all subjects, the Vim was the first treatment target, using the coordinates of 25% of the AC-PC distance anterior

to the PC plus approximately 0.5mm, 14mm lateral to the midline at the level of the intercommissural line. The final coordinates were adjusted for individual patient anatomy, included the 3rd ventricle width and proximity to the visualised internal capsule. In 17 subjects, a secondary region was targeted after tremor suppression was considered sub-optimal following adequate lesioning of the Vim. In 13 patients, the posterior subthalamic area (PSA) was lesioned by targeting the white matter equidistant between the medial border of the STN and lateral border of the red nucleus at its equator, corresponding to AC-PC coordinates of approximately x=9.5 mm, y=-6.0 mm, z=-5.5 mm. In 4 patients, the Ventralis oralis anterior (Voa) was targeting using coordinates of approximately 13 mm lateral to the AC-PC line and 33.3% anterior to the PC, at the level of the AC-PC line.

Vim Ablation Volume

MRI data was acquired the day immediately following treatment. The post treatment imaging was acquired on a 3T Philips Ingenia (Philips Inc, Amsterdam, The Netherlands) and included a T1-WI (sequence: IR-FFE, imaging plane: axial, TI: 450 ms, TR: 7.9 ms, TE:2.6 ms, Flip Angle: 8^{o}, FOV: 240 mm, acquisition matrix: 240 $\times$ 240, slice thickness: 1.0 mm, slices: 170). The Vim ablation was manually segmented on the day-1 T1-WI and used for calculation of the ablation volume. The segmentation included both the T1 iso-intense core, and hypointense rim, corresponding to zones 1 and 2 per Wintermark et al[309]. The segmentation was performed using ITK-SNAP[335]. An example Vim segmentation is shown in *Figure 2-8*.

Clinical Evaluation

Subjects were evaluated prior to treatment by a neurologist, and again at intervals of 1-, 3-, 6-, 12-, 24- and 36-months post treatment. The clinical evaluation included scoring of the clinical rating scale for tremor (CRST) [336], which is divided into three parts (A, B and C), with each sub-score combined to give a total CRST score. Part A measures tremor at rest, posture, and action in 9 parts of the body. Part B measures action tremor in the upper limbs, and part C measures functional disability. As CRST part C can be considered a less objective measure of tremor, CRST was calculated as the subtotal of CRST parts A and B only, consistent with previous investigations of tremor following tcMRgFUS[337]. HTS in the treated hand was calculated from CRST parts A and B, comprising tremor in the upper limbs including rest, postural, action, pouring, handwriting and constrained spirals. Tremor scores at follow-up visits were converted into percentage change from the corresponding baseline

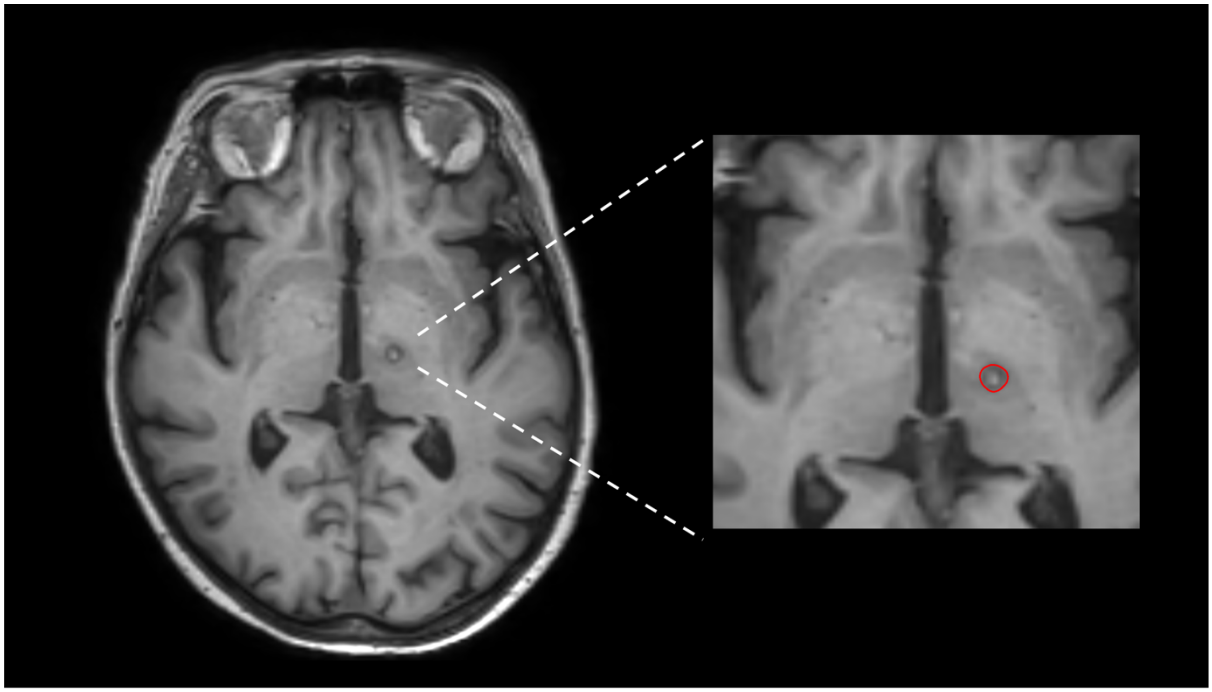

Figure 2-8 Example axial view of left Vim ablation segmentation. Vim segmentation shown in red.

score and inverted such that a positive value indicates a reduction in tremor score, relative to baseline. Self-reported QUEST scores were also collected at each evaluation. While QUEST scores are a subjective measure of tremor severity, the scores are an important tool for monitoring the change in quality-of-life following treatment[338].

Statistical Analysis

To increase sample size and simplify direct comparison of tremor scores at clinical follow-up visits, the follow-up data was re-grouped into short-term (1-3 months), medium-term (6-12 months) and long-term (24-36 months) visits. When a subject had scores for both visits in the re-grouped timepoint, the score from the later visit was used. Due to the non-normal distribution of tremor scores, absolute tremor scores were compared within subjects between baseline and follow-up with a paired Wilcoxon signed-rank test. Change in percentage tremor improvement between short- and long-term visits within subjects was compared with a paired Wilcoxon signed-rank test. Absolute and percentage change in tremor scores at each timepoint were compared across disease types with a Mann-Whitney U test.

Percentage improvement in each tremor score at each follow-up visit was also analysed with a linear mixed-effects model, leveraging data from all follow-up timepoints to increase statistical power. The model included tremor score data from the original clinical visit scheme (1-, 3-, 6-, 12-, 24- and 36-months post-treatment), with time included as a continuous variable to capture any effect of longer follow-up times on tremor improvement. A model was constructed with percentage change in tremor score at each follow-up clinical

Table 2-3 Patient and tcMRgFUS treatment characteristics.

Variable	**All patients N=66**
Sex, n(%)	
Male	46 (70)
Female	20 (30)
Disease Type, n(%)	
ET	37 (56)
DT	29 (44)
Age, mean ±SD, years	73.43 ± 8.29
Disease Duration, mean ±SD, years	27.45 ± 17.04
Treated Side n(%)	
Left	52 (79)
Right	14 (21)
Treatment Target, n(%)	
Vim	49 (74)
Vim & PSA	13 (20)
Vim & Voa	4 (6)
Number of Sonications	10.01 ± 2.78
Max. Average Sonication Temperature (°C)	58.25 ± 1.97

Abbreviations used: ET (Essential Tremor), DT (Dystonic Tremor), Vim (Ventral Intermediate Nucleus), PSA (Posterior Subthalamic Area), Voa (Ventralis Oralis Anterior).

visit as the response variable, and a random slope and intercept to account for the repeated tremor measurements per subject. Disease type (ET or DT) and patient sex were included as categorical predictors, and patient age and time from baseline for each tremor score were included as continuous predictors. The model was run using data from all subjects, and then again independently for ET and DT subjects, with disease type removed from the model. The residuals of each model were manually inspected to ensure normality.

All statistical analysis was performed using the R (version 4.2.2) statistical software package in RStudio (Version 1.4.1717, RStudio, Inc., Boston, MA URL, http://www.rstudio.com).

2.4.3 Results

Study Participants

Participant characteristics were summarised in *Table 2-3*. Out of the total of 66 participants, 37 were diagnosed with ET, and 29 with DT. 46 (69.70%) of the subjects were male. The mean patient age and disease duration at the time of treatment was 73.43 $\pm$ 8.29 and 27.45 $\pm$ 17.04 years, respectively. All participants included in the study returned for at least 1 follow-up clinical evaluation. The mean time elapsed between the most recent clinical evaluation and the treatment was determined as 16.63 ± 12.61 months. Statistical analysis did not reveal any significant differences in age or disease duration between the ET and DT patient groups.

The number of patients who returned at each follow-up visit are summarised in *Table 2-4*. When the data was re-grouped into short-, medium- and long-term follow-up visits, 32 patients who completed evaluations at both short- and long-term visits were identified. This subset of patients was comprised of 18 patients with ET and 14 patients with DT. 17 of the 32 patients were treated in the Vim only, while 6 patients were also treated in regions outside the Vim, including the PSA(N=4), and the Voa (N=2). The mean age and disease

Table 2-4 Summary of patient numbers at each clinical visit. Re-grouped visits indicated in columns with grey shading.

	Time (months)									
	Baseline	1	3	Short-term	6	12	Mid-term	24	36	Long-term
ET	37	28	23	32	20	22	25	14	12	18
DT	29	20	21	26	17	19	24	10	5	14

Table 2-5 Mean tremor scores for ET and DT patients at baseline and follow-up. Mean absolute scores shown in the top section of the table, and mean percentage change from baseline in the bottom section.

	Baseline	Short-term	Medium-term	Long-term
		Absolute Values		
HTS				
ET (mean ± SD)	19.19 ± 5.37	5.91 ± 4.71	6.44 ± 3.53	6.33 ± 5.40
DT (mean ± SD)	20.28 ± 7.74	8.15 ± 7.51	8.08 ± 5.95	7.83 ± 5.11
CRST				
ET (mean ± SD)	44.65 ± 13.80	25.34 ± 9.75	24.16 ± 8.20	26.00 ± 11.06
DT (mean ± SD)	48.10 ± 17.83	31.11 ± 14.75	31.12 ± 14.46	28.08 ± 13.35
QUEST				
ET (mean ± SD)	44.47 ± 14.21	10.94 ± 13.10	15.32 ± 10.33	20.00 ± 20.68
DT (mean ± SD)	51.00 ± 15.71	21.29 ± 22.53	28.08 ± 22.19	27.29 ± 20.17
		Percentage Change		
HTS				
ET (mean ± SD)	-	70.64 ± 19.57	64.38 ± 15.57	62.85 ± 25.80
DT (mean ± SD)	-	63.32 ± 24.69	58.59 ± 23.52	51.93 ± 20.29
CRST				
ET (mean ± SD)	-	44.14 ± 14.14	41.54 ± 11.50	37.59 ± 19.53
DT (mean ± SD)	-	37.59 ± 14.62	33.80 ± 19.78	31.50 ± 18.26
QUEST				
ET (mean ± SD)	-	73.55 ± 34.02	62.57 ± 29.48	64.52 ± 34.37
DT (mean ± SD)	-	59.51 ± 39.98	45.05 ± 38.51	34.71 ± 50.81

Abbreviations used: HTS (Hand Tremor Score), CRST (Clinical Rating Scale for Tremor), QUEST (Quality of life in Essential Tremor), ET (Essential Tremor), DT (Dystonic Tremor).)

duration in this patient subset was 70.57 ± 8.79 and 27.67 ± 16.46 years, respectively. There was not a significant difference in age or disease duration between ET and DT patients.

Treatment Parameters

Table 2-6 Results of linear mixed-effects model, run on entire subject cohort.

	β	95% CI	p	t
HTS				
Age	-0.40	-0.61, -0.22	<0.001***	-4.18
Time	-0.22	-0.29, -0.11	<0.001***	-4.40
Disease Type	0.49	0.14, 0.95	0.029*	2.68
Sex	-0.49	-0.87, -0.02	0.030*	-2.05
CRST				
Age	-0.24	-0.41, -0.07	0.006*	-2.78
Time	-0.17	-0.28, -0.06	<0.001***	-3.01
Disease Type	0.57	0.29, 0.98	0.010*	3.59
Sex	-0.52	-0.89, -0.16	0.005**	-2.82
QUEST				
Age	-0.14	-0.36, 0.09	0.231	-1.20
Time	-0.18	-0.27, -0.09	<0.001***	-3.89
Disease Type	0.51	0.05, 0.98	0.031*	2.17
Sex	-0.23	-0.71, 0.26	0.356	-0.93

***significance < 0.001, ***significance < 0.01, ***significance < 0.05

An average of 10.01 $\pm$ 2.78 sonications were delivered over the course of the treatment. The average peak sonication temperature reached was 58.25 $\pm$ 1.97°C. An average of 4.10 $\pm$ 1.41 sonications per patient reached temperatures in excess of the therapeutic threshold of 53°C, reaching at least 53°C in all subjects. The mean ablated Vim volume was 132.41 $\pm$ 49.14 mm^3. There was not found to be a significant difference in the total number of

Table 2-7 *Results of linear mixed-effects model, run for ET and DT patients independently.*

	β	95% CI	p	t
		ET		
HTS				
Age	-0.57	-0.81, -0.33	<0.001***	-4.70
Time	-0.19	-0.31, -0.08	<0.001***	-3.33
Sex	-0.22	-0.78, 0.33	0.426	-0.80
CRST				
Age	-0.34	-0.57, -0.10	0.006*	-2.79
Time	-0.20	-0.33, -0.05	<0.001***	-2.72
Sex	-0.60	-1.15, -0.04	0.036*	-2.13
QUEST				
Age	-0.13	-0.45, 0.20	0.439	-0.78
Time	-0.18	-0.32, -0.02	<0.001***	-2.25
Sex	0.02	-0.72, 0.75	0.965	0.04
		DT		
HTS				
Age	-0.27	-0.59, 0.04	0.089	-1.72
Time	-0.22	-0.37, -0.07	0.040	-2.94
Sex	-0.57	-1.23, 0.08	0.086	-1.73
CRST				
Age	-0.14	-0.40, 0.12	0.282	-1.08
Time	-0.16	-0.35, 0.03	0.100	-1.66
Sex	-0.44	-0.97, 0.08	0.098	-1.67
QUEST				
Age	-0.17	-0.50, 0.17	0.322	-1.00
Time	-0.21	-0.33, -0.08	0.107	-3.29
Sex	-0.43	-1.13, 0.27	0.226	-1.22

***significance < 0.001, ***significance < 0.01, ***significance < 0.05

sonications, the maximums sonication temperature or the Vim ablation volume between disease types.

Tremor

Mean absolute tremor scores at baseline and each re-grouped follow-up visit are summarised in *Table 2-5*, and the distribution in values are shown in *Figure 2-9*. At baseline, the mean HTS, CRST and QUEST for patients with ET was 19.19 ± 5.37, 44.65 ± 13.80 and 44.47 ± 14.21, respectively. For patients with DT, the mean baseline scores were and 20.28 ± 7.74, 48.10 ± 17.83 and 51.00 ± 15.71, for HTS, CRST and QUEST, respectively. The mean QUEST scores at baseline were significantly greater in DT patients (p=0.034). There were no other significant differences in absolute scores between ET and DT patients at baseline or follow-up.

Absolute tremor scores were significantly reduced at all follow-up visits in both ET and DT patients (*Table 2-5*). The mean percentage improvement in HTS, CRST and QUEST scores at long-term follow-up for patients with ET was 62.85 ± 25.80, 37.59 ± 19.53 and 64.52 ± 34.37%, respectively. In DT patients, the mean change in tremor scores at long-term follow-up were 51.93 ± 20.29, 31.50 ± 18.26 and 34.71 ± 50.81%, for HTS, CRST and QUEST, respectively. Improvement in HTS at long-term follow-up was maintained to a level of 50% in 13 (72%) ET patients, and 8 (57%) DT patients. While ET patients experienced, on average, greater percentage improvement in all 3 tremor scores at long-term follow-up, the

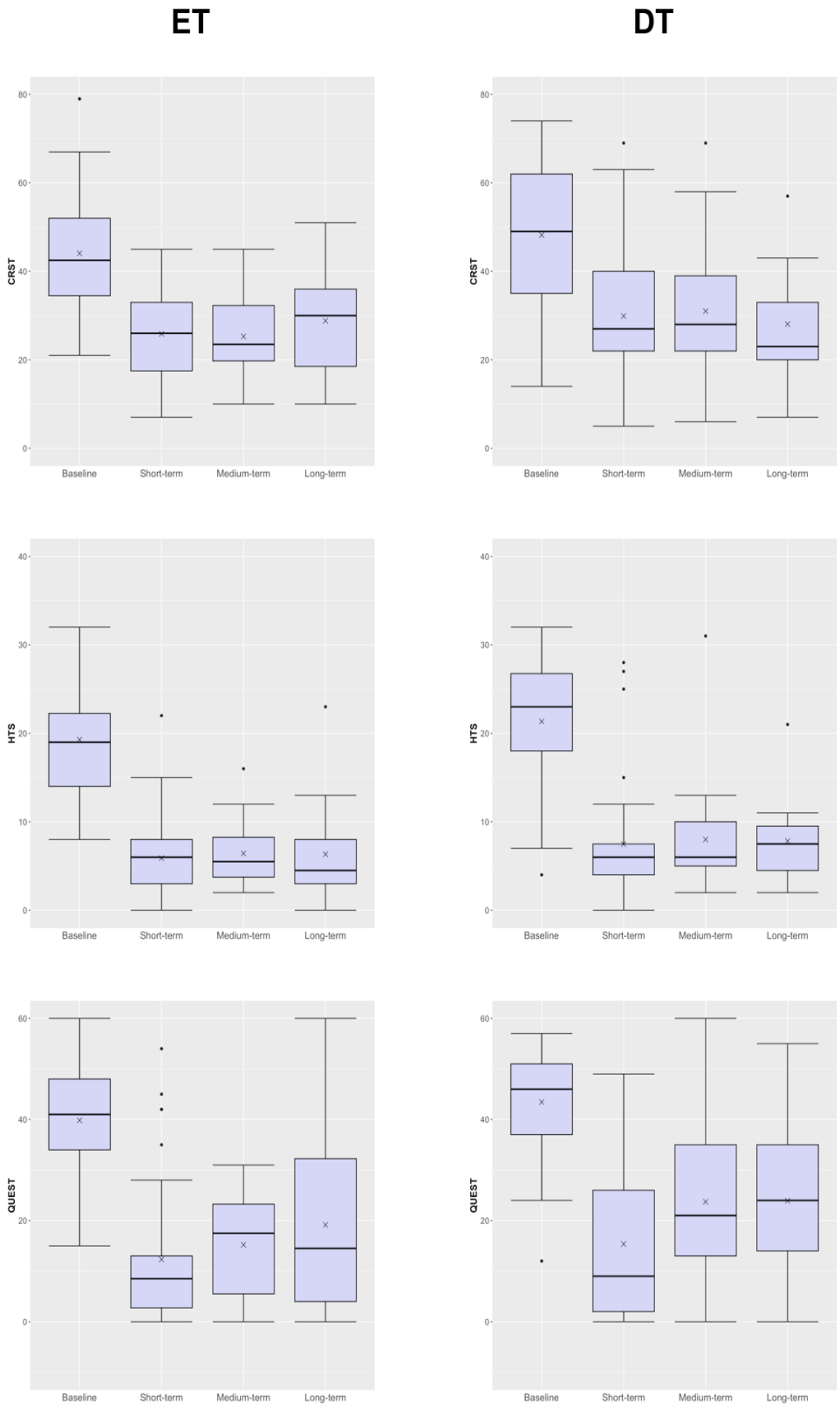

*Figure 2-9 Distribution of HTS (**top**), CRST (**middle**) and QUEST (**bottom**) scores for patients with ET (**left**) and DT (**right**). Upper and lower bounds of box indicate the interquartile range, median value indicated by solid line, mean value indicated by cross. Whiskers indicate the minimum and maximum values, and outliers represented by black dots.*

the difference in QUEST improvement was approaching statistical significance (p=0.08).

When all subjects and timepoints were included in the linear-mixed effects model, a statistically significant effect of disease type on improvement in HTS (β=0.49, p=0.029), CRST (β=0.57, p=0.010) and QUEST (β=0.51, p=0.031) was found, with percentage improvement greater in ET patients for all 3 scores. A significant negative effect of age was found with change in HTS (β=-0.40, p<0.001) and CRST (β=-0.24, p=0.006). Patient sex was also found to have a significant effect on HTS (β=-0.49, p=0.03) and CRST (β=-0.52, p=0.005) improvement, with improvement greater in females than males.

A significant negative effect of time on change in HTS (β=-0.22, p<0.001), CRST (β=-0.17, p<0.001) and QUEST (β=-0.18, p<0.001) was also found. When the analysis was run independently for ET and DT patients, time remained a significant predictor of change in HTS (β=-0.19, p=0.001), CRST (β=-0.20, p<0.001) and QUEST (β=-0.18, p<0.001) in ET patients, while a significant effect of time was not found in patients with DT for any tremor score. Linear mixed-effects model results are summarised in *Table 2-6* and Table 2-7.

Between the short- and long-term visits, HTS improvement was significantly reduced in ET patients (mean change=-9.84 $\pm$ 17.56%, p=0.04). While HTS improvement was also reduced in DT patients (mean change=-6.17 $\pm$ 23.96%), the change was not statistically significant (p=0.41). Similarly, the improvement in QUEST scores for ET patients was significantly reduced at the long-term visit (mean change=-19.26 $\pm$ 27.83%, p=0.01), while the change for DT patients was not significant (mean change=-13.30 $\pm$ 34.41%, p=0.19). The change in CRST improvement between was reduced in ET patients, however, the change was not

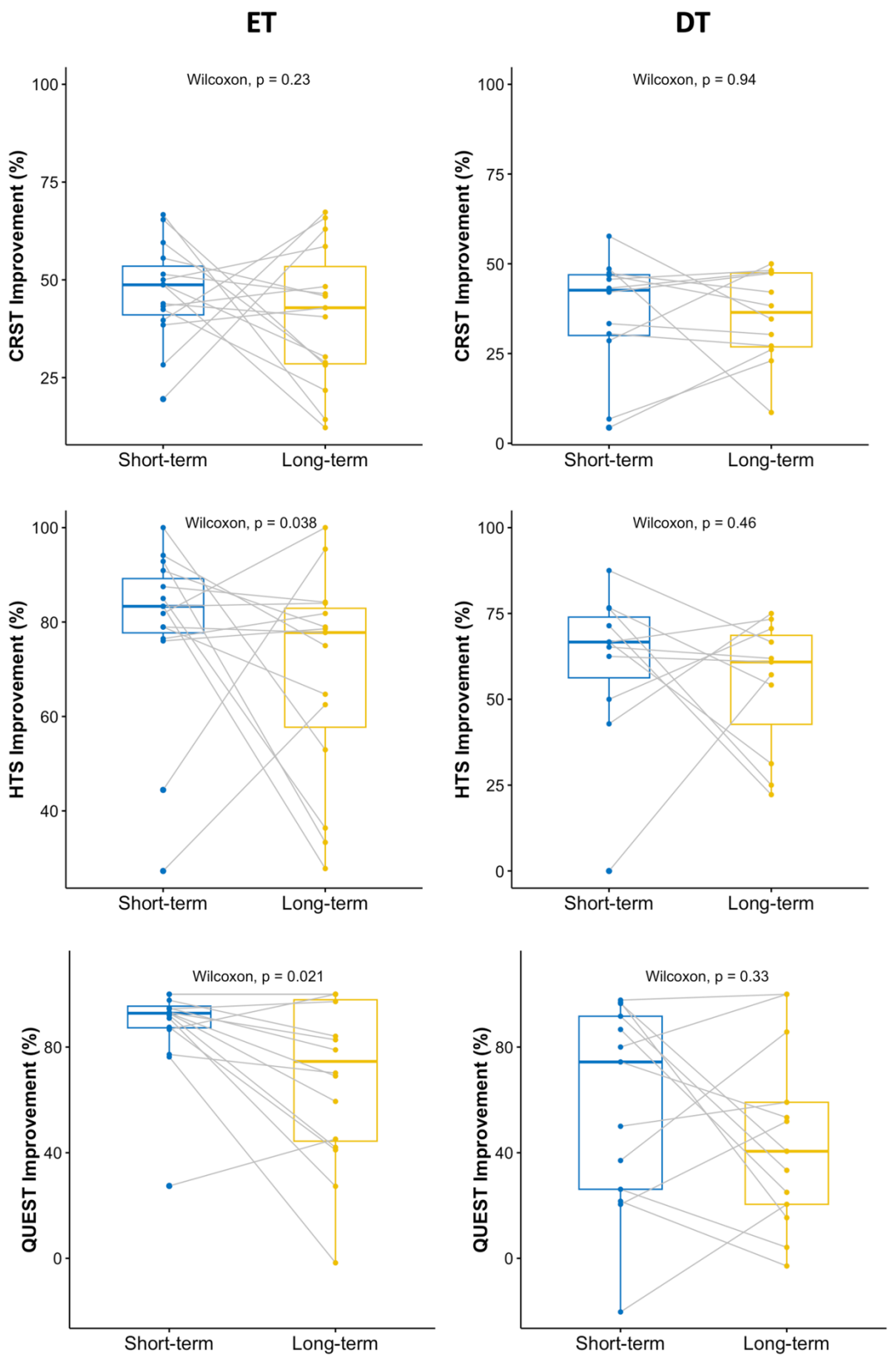

*Figure 2-10 Change in tremor score percentage improvement between short-term (**blue**) and long-term (**yellow**) follow-up visits for patients that returned for both evaluations. Grey line connects scores from each patient across visits. Sold line represent median value.*

statistically significant (mean change=-5.82 ± 15.72%, p=0.17). Paired changes in

improvement for each tremor score are displayed in *Figure 2-10*.

2.4.4 Discussion

The aim of this study was to determine if there was a significant difference in the improvement in tremor scores experienced by ET and DT patients treated with tcMRgFUS. We observed that HTS, CRST and QUEST scores were significantly improved at long-term follow-up in ET patients, with an average percentage improvement of 62.85, 37.59 and 64.53%. Similarly, in DT patients, HTS, CRST and QUEST scores were all significantly improved at long-term follow-up, with an average percentage improvement of 51.93, 31.50 and 34.71%, respectively.

While tremor was significantly improved in both ET and DT patients, the mean percentage improvement in HTS, CRST and QUEST scores was greater in ET patients at every follow-up visit. Direct comparison of tremor improvement at each follow-up visit did not reveal a significant difference between ET and DT patients. However, linear mixed-effects modal analysis, including data from all subjects and timepoints to increase statistical power, did indicate that there may be a significant effect of disease type on improvement in tremor scores, with improvement greater in ET. The difference in improvement was particularly evident in QUEST scores, where the mean long-term improvement was 64% in ET patients, compared with 34% in DT patients.

The improvement in tremor in ET patients observed in this study is consistent with previous reports on long-term outcomes following tcMRgFUS [333,339,340]. There is, however,

comparatively little research reporting outcomes in patients with DT following tcMRgFUS. The results presented here demonstrate a significant improvement in all analysed tremor scores in DT patients, albeit the improvement was lower compared to patients with ET.

Linear mixed effects model analysis also indicated a significant negative effect of time on tremor improvement in ET patients, with tremor scores increasing over time. Time was not, however, found to have a significant effect on the trajectory of tremor improvement in DT patients. Moreover, paired analysis between the short- and long-term visits indicated that HTS and QUEST improvement was significantly reduced in ET patients, while there was not a significant change in the DT cohort.

Tremor reoccurrence over time has been observed in ET patients treated with tcMRgFUS [333,339,340]. However, this phenomenon is not unique to tcMRgFUS, with reports of a similar effect following treatment with GF thalamotomy [341,342] and DBS [343–345]. It is not unexpected that tremor severity may increase over time, despite surgical intervention, in a progressive disease such as essential tremor, particularly in an elderly patient cohort. Pashcen et. al. estimated that following treatment with DBS, 87% of tremor reoccurrence was the result of disease progression, while only 13% was due to the development of a tolerance to chronic stimulation[345]. Importantly, the observed reduction in tremor suppression over time in this patient cohort did not render the treatment effect insignificant at long-term follow-up in either ET or DT. In cases where the treatment effect wanes significantly, re-treatment may be required, which has been demonstrated successfully for tcMRgFUS[346]. Owing to the minimally invasive nature of tcMRgFUS, this represents a distinct advantage over more invasive techniques, where re-treatment may be less appropriate.

Our findings that improvement in tremor scores were not significantly reduced over time in DT patients may indicate that while, on average, tremor suppression is lower in DT, it appears to be sustained over time, and provides further validation of the effectiveness of tcMRgFUS for the treatment of tremor in DT patients. It has been reported that thalamotomy in patients with DT may result in an initial treatment benefit, followed by a worsening of tremor at long-term follow-up [347,348], potentially due to the "unmasking" of dystonia, manifesting as an increase in QUEST score. While we did find QUEST improvement was significantly lower in DT patients, we did not observe a significant increase in QUEST scores between the short and long-term visits, suggesting occurrences of new onset or worsening dystonia may be rare.

This study was not without limitations. Analysis of this cohort was complicated by the high attrition rate in this study, with only 32 of the 66 participants (48%) returning for a clinical evaluation beyond 2 years post-treatment. Halpern et al. addressed this issue by imputation of data, assuming either no change in tremor scores between short- and long-term evaluations, or a return to baseline tremor[253]. Given the expected increase in tremor over time however, it is unrealistic to assume there is no change in tremor scores in the patients that did not return. Similarly, a return to baseline values may represent a pessimistic bias in results. Rather than making any assumptions about the tremor severity in the non-returning patients, we felt the most rigorous means of analysis was by utilisation of a statistical model that can account for missing data points and restriction of longitudinal analysis to patients that returned for long-term follow-up. Comparison of tremor improvement at the short-term visit between returning and non-returning patients did not find a significant difference

between the two groups, providing confidence that the returning patients were representative of the entire cohort.

2.4.5 Conclusion

As a relatively new technique for the treatment of tremor, it is important to report clinical outcomes following treatment with tcMRgFUS, both to identify avenues for improvement of outcomes, and for counselling of patients on the expected outcomes of treatment. To the author's knowledge, this study is the first to directly compare improvement in tremor scores between ET and DT patients treated at a single centre. The results presented here suggest that while tremor suppression is significant in both ET and DT patients, patients with ET may experience greater benefit than patients with DT. Conversely, the reduction in treatment effect over time may be more pronounced in ET patients.

2.5 Chapter Summary

While several studies have reported on the tremor benefit observed in patients with ET treated in tcMRgFUS, there remains comparatively little literature on the improvement in patients with alternative tremor subtype diagnosis, including ET-plus and DT. In this chapter, the observed tremor improvement across these tremor subtypes following treatment with tcMRgFUS was investigated. To aid in the intra-procedural evaluation of tremor improvement, a novel automated algorithm was presented which uses the deviation of the drawn spiral from the intended trajectory as a measure of tremor severity. This algorithm was validated against the current gold-standard manual visual ratings and demonstrated greater correlation with the average expert rating, than the interrater correlation. Results of this analysis suggest that the automated spiral algorithm may provide an unbiased and more reproducible measure of the tremor severity captured by freeform spirals. After the application of the validated automated algorithm to the intraoperative spirals, the analysis revealed a significant effect of tremor subtype on spiral improvement, with patients diagnosed with DT experiencing significantly lower spiral improvement at every evaluation, including the post-treatment evaluation compared to those with pure ET. Similarly, longitudinal analysis of post-treatment tremor score improvement revealed a significant effect of tremor subtype, with patients diagnosed with DT experiencing significantly less tremor benefit compared to those with ET. The results reported in this chapter suggest that tremor subtype may be a significant factor in determining the tremor benefit experienced by patients treated with tcMRgFUS. However, within each tremor subtype there remains a range of tremor improvement which suggests that additional patient-specific factors may

contribute to the observed clinical outcome. Penetration of US waves through the skull is vital for effective treatment with tcMRgFUS, and in the following chapter, the influence of the skull on lesion formation and tremor improvement is investigated.

3 Penetrating the Skull: Influence of Skull Characteristics on Clinical Outcomes

Based on:

- **Kyle, Kain**, Joel Maamary, Benjamin Jonker, James Peters, Yael Barnett, Michael Barnett, Arkiev D'Souza, Jerome Maller, Chenyu Wang, and Stephen Tisch. 2023. "Consistency Is Key: Influence of Skull Density Ratio Distribution on the Formation of Clinically Effective Lesions and Long-Term Tremor Suppression Following Treatment with MR-Guided Focused Ultrasound." *Journal of Neurosurgery* 1–9. doi: https://doi.org/10.3171/2023.6.JNS231153.

3.1 Abstract

In the previous chapter, the influence of tremor subtype was explored, and evidence was presented that indicated patients with DT may experience less tremor benefit, compared with patients diagnosed with ET. However, the observed variation in tremor suppression following treatment with tcMRgFUS is not completely explained by tremor subtype. Within both ET and DT there is a range of observed clinical outcomes, which may be explained by the influence of patient-specific factors. The influence of individual variations in the properties of the skull may influence the efficient delivery of energy to the tissue of the brain, which is crucial for the successful treatment of tremor with tcMRgFUS. The skull is a major impediment to the transmission of US energy into the brain due to the effects of US absorption, reflection and scattering, as well as the introduction of US phase errors. This chapter focuses on the impact of the skull on intraoperative heating efficiency, the formation of clinically effective lesions and the relationship with long-term tremor suppression.

3.2 Background

The therapeutic benefit of lesioning with tcMRgFUS is dependent on the efficient deposition of energy within the tissue at the treatment target region [349–351] to cause adequate tissue heating [246,272,352,353]. One of the key advantages of tcMRgFUS over more invasive options such as RF thalamotomy, is the ability to deliver energy to the brain through an intact skull, without the need for burr holes or removal of sections of the skull. The skull, however, represents a major barrier to the efficient transmission of US into the tissue of the brain. US attenuation through bone is significantly greater than in soft tissue[354], thus a significant amount of energy is lost due to absorption, reflection and refraction by the skull.

The speed of US through a medium is governed by the density of the material. As the US enters the skull, the wave velocity is changed, leading to a change in phase of the US wave. Due to the heterogeneity of density and thickness across the skull, the varying phase change imparted on US waves directed on different regions of the skull leads to a loss of phase coherence, and a reduction in the US intensity at the focal site. To mitigate this issue, tcMRgFUS employs a phase-array of US elements, the phase and amplitude of which can be individually modulated to correct for the phase aberrations introduced by the skull. The phase correction required for each element is estimated on the ExAblate console, using planning computed tomography (CT) imaging acquired prior to treatment together with the treatment target coordinates to estimate the skull density and thickness along the path from each transducer element to the treatment target.

In addition to phase aberrations and energy absorption, mismatches in the density of tissue within the skull also influences the amount of energy reflected by the skull. The skull density ratio (SDR), defined as the ratio of the computed tomography (CT) measured density of the bone marrow to the cortical bone, has been validated as a key factor in predicting the efficiency of energy transmission through the skull [246,250,355]. A greater mismatch in density, which is reflected as a lower SDR, causes a greater amount of energy to be reflected, and thus reduces the energy deposited at the treatment target[356]. To mitigate the lost energy, the ultrasound intensity, or duration, must be increased in order to deliver a therapeutic thermal dose at the target. However, as significant energy is deposited in the skull, increases in US intensity can lead to focal heating of the skull, with associated risk of burns to the scalp[242]. Thus, the SDR value is used as a key metric to predict the amount of energy required to achieve therapeutic heating, and patients with low SDR values may be deemed unsuitable for treatment with tcMRgFUS. The SDR varies with the changes in density and thickness across the skull. The SDR value typically used clinically for patients screening is the mean value across the skull. An SDR value below 0.4 has historically been considered low [357,358], and guidelines from the American Society for Stereotactic and Functional Neurosurgery recommend the patient SDR be greater than 0.4[270]. However, several studies have shown that patients with SDR below 0.4 can be successfully treated with tcMRgFUS by employing longer duration sonications to ensure an adequate thermal dose is delivered [271–275].

The heating efficiency (HE) of tcMRgFUS is defined as the amount of energy required to achieve a given temperature increase. While the negative relationship between patient SDR and sonication HE is well established [271–273,352,359–362], there remains uncertainly around the

factors that influence any changes of HE over the course of the tcMRgFUS procedure. Studies have suggested that patient SDR may contribute to an observed reduction in HE throughout the procedure [361,363–365]. Whether the observed intraoperative reduction in HE is related only to patient characteristics, or factors relating to treatment strategy is an ongoing area of research, which some groups finding the decline in HE was associated with the number of delivered sonications[365].

Any reduction in intraoperative HE may impact the ability to reach therapeutic temperatures during the treatment sonication phase of treatment, thus further investigation of these effects is warranted. Furthermore, while the calculation of the mean SDR values across the skull provides a meaningful indicator of the sonication HE for each patient, there has been little research on the prognostic value of the distribution of SDR values across the skull. Investigation of the factors that influence intraoperative sonication HE, and the formation of clinically effective lesions, may aid clinicians in improving treatment strategy, as well as further refining patient selection during the patient screening process.

3.3 Persistent effects of sonication history on magnetic resonance-guided focused ultrasound heating efficiency

3.3.1 Introduction

To ensure patient safety and treatment target accuracy, the intensity of US delivered during tcMRgFUS is gradually increased over the course of the procedure, with the temperature gradually up titrated until temperatures capable of causing permanent lesioning are reached. Pre-clinical studies suggest that at temperatures above 54°C and sonications between 5 -10 seconds in duration are required to cause tissue necrosis[349]. At lower temperatures (50 - 54°C), lesioning requires significantly longer temperature exposure (10 - 100 seconds) [349,366], which can be associated with increased side effects such as burns, nausea, and vertigo[242]. Successful lesioning under 50°C is generally considered infeasible due to the increased risk of adverse side effects[242].

Critical to the success of tcMRgFUS is the ability to deliver a sufficient thermal dose to the target volume [349–351]. Thermal dose is defined by sonication temperature elevation and duration, which can be manipulated via adjustments to the sonication power and energy. Higher sonication temperatures are associated with larger and circular lesions [271,366–368], and some groups advise reaching temperatures above 54°C in order to achieve adequate lesioning [254,271,272,351,357,358,363]. However, studies have recently demonstrated that sufficient thermal dose can be achieved with sonications between 50 - 54°C in a clinical setting [366]. Given the importance of sonication temperature on treatment success, the impact of individual patient anatomy on sonication heating has been studied extensively [271–273,352,359–

[362]. The skull impedes energy delivery through absorption, reflection, refraction, and scattering [369,370]; and the skull density ratio (SDR) has emerged as the most important physical property in predicting sonication heating. SDR is estimated from preoperative CT imaging and is defined as the ratio between the mean values in Hounsfield units of bone marrow and cortical bone [352]. A higher SDR indicates a smaller mismatch in acoustic impedance within the skull[356] and has been shown to correlate positively with sonication temperatures [271,273,352,359–361,371]. For this reason, patients with a SDR below 0.40 have often been considered unsuitable for treatment with tcMRgFUS [357,358]; however, several groups have demonstrated that despite the impact of SDR on sonication temperatures, satisfactory clinical outcomes can still be achieved in instances of low SDR [271–275].

Heating efficiency (HE), defined as the amount of energy required to reach a given temperature, varies between patients and is dependent on physical properties such as SDR. However, HE also tends to decrease across successive sonications with increasing energy within the same patient [361,363–365], a phenomenon that has not been reproduced in tissue-mimicking phantoms[372]. Biological models of tissue heating suggest that the peak sonication temperature should exhibit a linear relationship with acoustic power[299].

The nature of the non-linear relationship between sonication energy and temperature is an area of active research. Hughes et al. demonstrated that increases in beam dispersion were associated with lower HE at high energies [364], while Yamamoto et al. found that HE decline was associated with greater subtotal temperature delivered in previous sonications [365]. The findings of Yamamotoa et al. are of particular importance for treatment strategy, as their results indicate that early low energy sonication could impact the HE of later high energy

sonications. How SDR values influence the observed decrease in HE with respect to energy also remains uncertain. Yamamotoa et al. reported that HE decline was more rapid in subjects with lower SDR[365], while Yang et. al. reported that SDR was positively correlated with HE loss[373].

In this investigation, the relationship between patient SDR and intraoperative HE is further explored with an independent dataset, building on previous observations of intraoperative HE decline [361,363–365]. Furthermore, a novel paired sonication analysis is conducted to isolate the effects of sonication energy/power on temperature, to determine whether previous sonications have a persistent effect on the HE of successive sonications.

3.3.2 Methods

Subjects

This study was a retrospective analysis of data collected from patients treated with tcMRgFUS for the treatment medication refractory tremor at St Vincent's Hospital, Sydney, Australia between November 2018 and July 2021. Study inclusion criteria included a tremor subtype diagnosis of ET, ETP or DT, TAWD or PD, per the 2018 consensus statement on the classification of tremor[374], as well as the availability of sonication data. Additionally, to remove any confounding effect of the treatment target on HE, analysis was restricted to sonications targeting Vim of the thalamus only, i.e., excluding any sonications targeting additional regions such as PSA or Voa nucleus. Any patients in the which the Vim was not

the first treatment target, or who were not treated in the Vim, were excluded from the study.

Informed consent was obtained from all participating patients, and the study was approved by the St Vincent's Hospital Ethics Review Committee (ETH00670). Patient and treatment characteristics are summarised in *Table 3-1*.

tcMRgFUS Procedure

tcMRgFUS was performed as described in sections 1.2.4 and 2.3.2. All subjects were assessed by a neurologist prior to participation in the study. Preoperative CT and MR imaging was acquired for estimation of SDR and stereotactic target planning. Ultrasonic lesioning was performed using the ExAblate Neuro system (InSightec, Tirat Carmel, Israel) 650kHz, with a 1024-element, phased array ultrasound transducer. Imaging was simultaneously performed on a 3T MRI scanner (SIGNA Architect, General Electric, Milwaukee). During each sonication, single slice two-dimensional MRI thermometry was acquired in 3 second intervals centred on the target region to monitor the temperature of tissue at the target site.

Predictors of Sonication Temperature

As estimated by 2D MRI thermometry, the voxel-wise temperature map was used to determine the maximum sonication temperature (T_{MAX}). At each point of the temperature time series, the average temperature of the 3×3-pixel grid centred at the target coordinates

was taken, and T_{MAX} was defined as the peak average temperature reached throughout the sonication. The energy (E), power (P) and the number of active elements (NAE) for each sonication were extracted directly from the ExAblate console. SDR and skull thickness (ST) values along the line connecting each transducer element and the target coordinates were extracted from the ExAblate console and the mean value was calculated.

Heating Efficiency

Heating efficiency is generally defined as the increase in sonication temperature per unit of applied sonication energy[365,375]. However, sonication temperature is influenced by both the total sonication energy and power, which can both be independently modified on the ExAblate console. To determine which parameter was more relevant for the calculation of HE, data from the final sonication of each subject was examined. Multivariate linear regression was performed with T_{MAX} as the dependent variable and subject SDR, ST, age, NAE, and sonication energy or power as predictors. The final model predictors were chosen via forward selection, where each predictor was added individually to the model, and the predictor with the lowest p-value under 0.05 was included. This process was repeated until all significant predictors were included in the model. Due to the co-linearity of sonication power and energy, multivariate analysis was performed independently with either energy or power included in the model. The model fit using either sonication energy or power as a predictor of temperature were compared with ANOVA comparison of residual sum of squares. Normal distribution of all variables was assessed with Shapiro-Wilk test of normality.

The within-subject change in HE was investigated by examining the slope of the power vs. temperature curve for each subject. While HE can be calculated and modelled directly, we instead defined HE as the slope of the power vs. temperature curve, where a reduction in HE is observed as a reduction in slope. This strategy was chosen as it does not assume the intercept of the power vs. temperature curve to be zero, as is required for direct calculation of HE. The relationship between sonication power and temperature was investigated with a linear mixed-effects model, with a random slope and intercept to account for inter-subject variance. The initial first order model included temperature as the dependent variable and power as the independent variable. An additional second order term was added to the model to determine if the relationship between power and temperature was non-linear. Goodness of fit of the two models was compared with ANOVA.

An interaction term between SDR and both first and second order terms of the model was then added to determine how SDR influenced the slope of the curve (HE) and the rate of slope reduction, respectively. The residuals of each model were manually inspected to ensure normality.

Persistent Effects of Previous Sonications

Given the multi-collinearity present in the sonication data - sonication power, temperature and time all increase and co-vary throughout the procedure - assessing the effect of any single predictor in a truly independent fashion is challenging. To isolate the effect of power and energy on HE, a paired analysis of sonications with identical energy and power was performed. Sonications in the early alignment and verification phases of treatment are

often repeated with unchanged parameters, while the MR thermometry imaging plane is altered. In this analysis, pairs of sonications were identified where the prescribed sonication energy and power were repeated consecutively in the same subject. To exclude any effect of tissue destruction on HE, any pair in which either temperature exceeded 53°C was excluded. T_{MAX} in each of the paired sonications was compared and grouped based on whether the temperature of the second sonication was less than or greater than the first. A paired t-test was used to assess changes in T_{MAX} between the two sonications, and a binomial test of significance was employed to test if the proportion of pairs in which T_{MAX} of the second sonication was less than the first differed significantly from the expected value of 50% if the two sonication temperatures were independent.

All statistical analysis was performed using the R statistical software package with RStudio (Version 1.4.1717, RStudio, Inc., Boston, MA URL, http://www.rstudio.com).

3.3.3 Results

Patients

82 subjects treated with tcMRgFUS meeting the inclusion criteria were identified. One subject where the Vim was the second treatment target was excluded, and 1 subject in whom the Vim was not targeted was excluded. 202 individual sonications from 32 subjects were excluded due to targeting outside of the Vim, and a further 9 sonications from 6

subjects that were prematurely terminated by either the patient, operator or ExAblate software, were excluded from analysis.

Of the 80 included patients, 33 patients were diagnosed with ETP, 22 with DT, 13 with PD and 12 with ET. The mean age at the time of treatment of the entire cohort was 74.612 ± 8.60 years; and the mean SDR was 0.43 ± 0.10. There were no statistically significant differences in the patient age, SDR, or maximum sonication temperature across the different tremor subtypes. Patient and treatment characteristics are summarised in *Table 3-1*.

Prediction of Sonication Temperature

Table 3-1 Patient and procedure characteristics

Variable	**All patients** **N=80**
Sex, n(%)	
Male	60 (75)
Female	20 (25)
Age, mean ± SD, years	74.616 ± 8.594
SDR, mean ± SD	0.428 ± 0.070
Skull Thickness, mean ± SD, mm	6.583 ± 1.034
Sonications ± SD	7.913 ± 2.361*
Time ± SD, minutes	38.668 ± 20.701*
Max. Sonication Temp., °C	60.607 ± 3.503*

Abbreviations used: SDR (Skull Density Ratio), SD (Standard Deviation)

The cross-sectional multivariate linear regression analysis of data from the final sonication in each subject revealed that, as expected, sonication temperature was positively associated with both the subject SDR and sonication power. When the analysis was repeated with sonication energy as a predictor, there was again found to be positive association between subject SDR and sonication temperature, however, a negative relative relationship was found with sonication energy (*Table 3-2*). Given a positive relationship between sonication energy or power, and temperature was expected, for all subsequent analyses HE was defined with respect to sonication power, rather than energy. ANOVA comparison of the first and second order mixed-effects models revealed that adding a second order term significantly improved the model fit (AIC = 2941.3 vs. 2918.4, respectively, $p<0.01$), and both first and second order terms were statistically significant (*Table 3-3*). The second order term

Table 3-2 Multivariate Regression Model Coefficients for Temperature of Final Sonication

Variable	Standardised regression coefficient	Standard error	p-value
SDR	0.260	0.070	<0.001
Power	0.466	0.110	<0.001
NAE	0.008	0.004	<0.001
Energy	-0.129	0.062	<0.001

Note: Age, sex and skull thickness were not selected for final model.
Abbreviations used: SDR (Skull Density Ratio), NAE (Number of Active Elements)

(β_2) coefficient was negative, indicating that at the group level, the slope of the power vs. temperature curves tended to decrease with increasing power. An example of first and second order polynomial models for a single subject are shown in *Figure 3-1*.

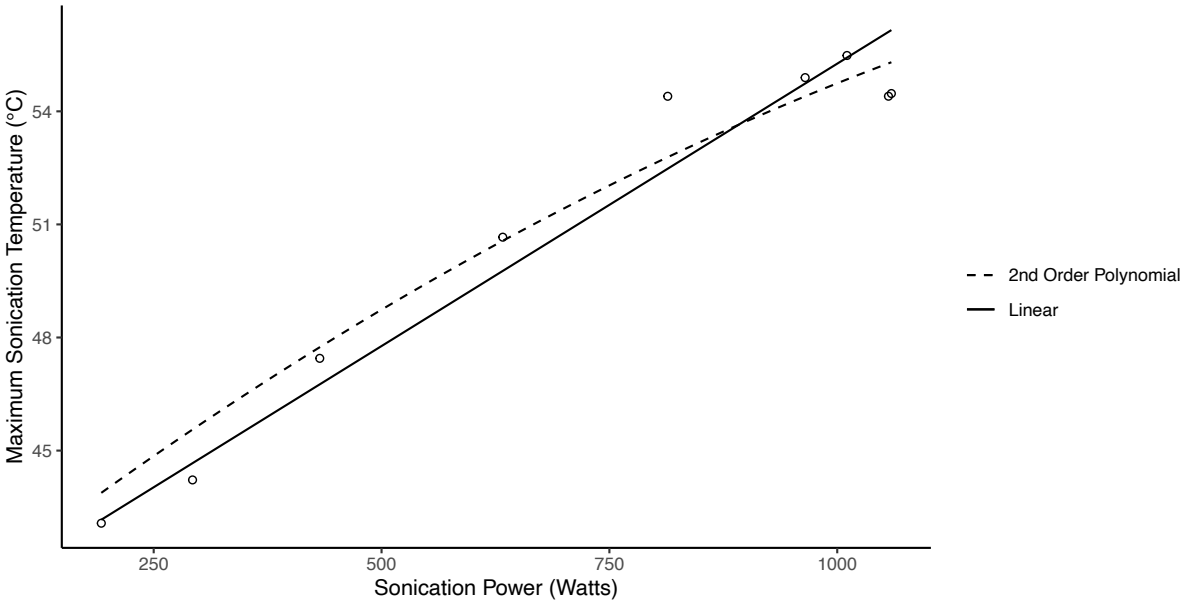

Figure 3-1 Example of sonication power vs. maximum temperature for a single subject. Linear fit is shown with solid line and second order polynomial fit with dashed line.

Table 3-3 Second order mixed effects model for sonication temperature with respect to power.

Variable	Standardised fixed effect coefficient	Standard error	p-value
Power	1.005	0.022	<0.001
$Power^2$	-0.134	0.020	<0.001
[a]SDR:Power	0.099	0.023	<0.001
[a]SDR:$Power^2$	-0.072	0.020	<0.001

Interaction effect with SDR[a]

Abbreviations used: SDR (Skull Density Ratio)

There was a statistically significant and positive interaction effect between SDR and the first order term, indicating that greater SDR was associated with greater HE. Conversely, there was a statistically significant and negative interaction effect between SDR and the second order term, indicating that HE reduction was more pronounced in patients with higher SDR.

Persistent Effects

Seventy-one pairs of sonications with repeated energy and power were identified. Forty-three of the pairs were excluded due to exceeding the threshold temperature of 53°C. For 20 of the 28 (71.43%) remaining pairs, the temperature (T_{MAX}) was lower in the second sonication (*Figure 3-2*), which was a significant deviation from 50% (p=0.016), as determined by binomial test of significance. The mean T_{MAX} of the first and second sonications was 48.61°C and 47.05°C, respectively, and paired t-test confirmed that the difference in T_{MAX} was statistically significant (p=0.005).

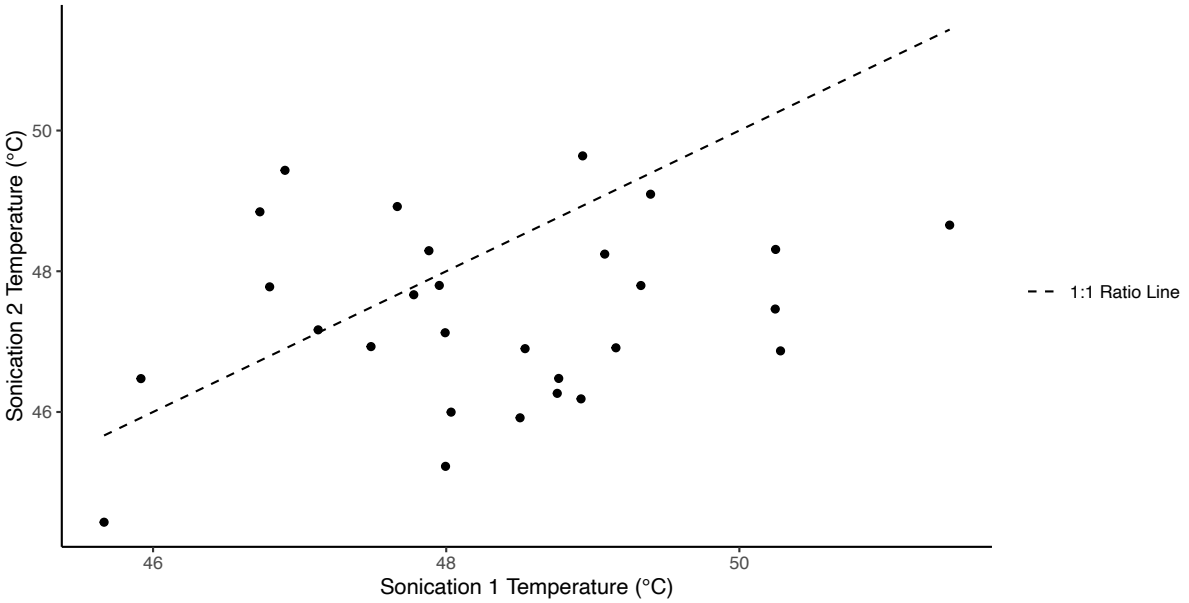

Figure 3-2 Scatter plot of the maximum temperature of each sonication in the paired sonication analysis. Dashed line indicates the 1:1 line. The data points are skewed towards sonication 1, indicating that the temperature of sonication 2 tended to be lower.

3.3.4 Discussion

Sonication heating efficiency is critical factor in the success of tremor treatment with tcMRgFUS. In this study, we identified that sonication power, rather than energy delivered as used in previous investigations of HE [365,373], appears to be a better predictor of sonication temperature elevation across subjects. Furthermore, linear mixed-effects analysis revealed, as expected, patient SDR was associated with greater HE, but also greater HE decline with respect to sonication power increase. Finally, results of the paired sonication indicated that there was a persistent effect historical sonications of the HE of subsequent sonications.

Multi-variate analysis of the final sonication in each subject demonstrated that sonication power provided a more realistic predictor of sonication temperature. While sonication power and energy are strongly correlated, the energy delivered with each sonication can be increased by increasing the sonication duration, while leaving the ultrasound intensity unchanged. At longer sonication durations tissue perfusion effects may be more relevant, leading to the development of a steady state between energy deposition in tissue and heat sink effects via blood perfusion [301]. Subsequently, increases in sonication energy, while increasing the accumulated thermal dose, may not yield increases in the peak sonication temperature. Thus, for analysis of HE with multivariate regression analysis, and mixed effects analysis, HE was defined with respect to power. The negative relationship observed between sonication energy and T_{MAX} is likely explained by the longer duration required to achieve sufficient therapeutic thermal dose in patients where higher temperatures could not be reached. These results highlight the difficulty in extracting the true relationship between sonication parameters and heating efficiency in an observational study, given the collinearity of the variables.

Our finding of a non-linear relationship between sonication temperature and power, with the slope decreasing with increasing power, are consistent with previous reports[363–365]. As expected, the power vs. temperature curve slope was positively correlated with subject SDR, indicating that temperature increases more rapidly for a given increase in power, for subjects with higher SDR. Furthermore, the negative relationship between SDR and the second order term of the mixed-effects model indicates that HE decline is also influenced by SDR, with a more rapid decline in HE associated with higher SDR. This result is consistent with the results reported by Yang et al[373] and contrary to those reported by Yamamoto et

al[365], who observed that the loss of HE with respect to energy was more rapid in subjects with lower SDR. Despite the more rapid loss of HE in patients with higher SDR, therapeutic temperatures were still easily achieved. HE loss may have more clinical significance in subjects with lower SDR who are already at risk of falling below the threshold temperature required for permanent lesioning.

The relationship between power and declining HE might have several causes. Changes in the thermal properties of the tissue at the focal point may lead to a reduction in HE. Volvano et al. demonstrated the changes in thermal conductivity with increasing temperature of various tissues[376]; however, thermal conductivity increased with increasing temperature. Moreover, at temperatures high enough to cause coagulation, it would be expected that perfusion effects would be reduced. Thus, we would expect HE to increase if changes in thermal properties at the focal point were responsible for HE changes. Another hypothesis is that changes in the acoustic properties due to heating along the beam between each transducer element and the target leads to dephasing of the beams at the focal point, causing the focal volume to increase. Several studies have observed the temperature dependence of ultrasound velocity and attenuation [377–379]. The phase correction calculations for each element in the tcMRgFUS array assume that these acoustic parameters do not change, thus if the values are altered due to heating, sub-optimal phase correction could lead to dephasing at the focal point. Indeed, Hughes et al. observed that HE decline was associated with larger focal volumes[364]. It remains unclear whether the observed increase in beam dispersion is generated by the change in acoustic properties of brain tissue or the skull. Skull heating during tcMRgFUS has been well documented [380,381] and temperature-dependent acoustic parameters of the skull have been reported[377]. The reported

relationship between SDR and HE decline suggests that the skull plays an important role in intraoperative HE decline, although the exact mechanism responsible is unknown. Yang et al. speculated that, since heating leads to increased attenuation in bone[377] and decreased attenuation in bone marrow[382], the change in acoustic parameters could be more pronounced in high SDR subjects owing to their lower proportion of bone marrow. Future studies investigating the influence of SDR on beam dispersion at high energy might help explain this phenomenon.

The above explanations assume that the change in HE throughout the procedure is due solely to changes induced by the current sonication. There is increasing interest in determining whether persistent changes due to previous sonications also influence HE decline. Some groups advocate reaching therapeutic temperatures as rapidly as possible to reduce the impact of planning sonications on the HE of later therapeutic sonications.

The motivation of the paired sonication analysis design was to test if the sonication temperature for a given energy and power were independent of previous sonications. The results of this analysis revealed that in a majority of cases (71.43%), the second sonication in the pair achieved a lower temperature than the first, despite the prescription of identical sonication power and energy. If there were no persistent effects from previous sonications, we would not expect to observe a statistically significant temperature difference when comparing the first and second sonication. However, a paired t-test revealed that the drop in T_{MAX}, while small, was statistically significant. By limiting our analysis to sonications below 53°C, we have ruled out the effect of changes in tissue structure at the focal point from influencing HE. Exactly which property of previous sonications has the most significant effect

on heating efficiency remains an open question. However, this finding adds to the evidence that previous sonications may have a persistent effect that influences the HE of subsequent sonications. These results may suggest that there may be an effect of low energy sonications on the acoustic properties of the brain or skull that influence HE. Yamamoto et al. speculate that edema in response to the temperature increase at the focal point may alter the thermal properties at the target site[365], leading to the observed reduction in HE. Future work investigating how edema impacts heating efficiency may help answer this question.

The change in sonication HE during the tcMRgFUS procedure has important implications for treatment strategy. Given the importance of reaching sufficient temperatures for lesion formation, strategies to maximise HE could improve patient outcomes. Our results suggest that limiting the number of planning sonications may contribute to improved HE when therapeutic sonications are applied. Most groups apply multiple therapeutic sonications in the same location, thus maximizing HE could aid in lesion consolidation, particularly in subjects with low SDR. This strategy does, however, have inherent risks. Firstly, the purpose of including low temperature sonications during the early stages of the procedure is to confirm the location of the target region. As MRI thermometry is acquired in a single 2D slice, imaging in different planes requires multiple sonications. By minimising the number of index sonications, the accuracy of the target region could be compromised. Secondly, rapid ramping up to therapeutic temperatures requires accurate knowledge of the energy and power required to reach the target temperature. With fewer incremental temperature increases, it is more difficult to estimate the energy requirements, increasing the risk of adverse side effects due to overheating. Improved treatment targeting procedures may help

reduced the number of index sonications required for target verification, thus improving the sonication HE.

This study is not without limitations. First, the analysis did not include subject characteristics other than SDR, skull thickness, age, and gender that may influence HE. Second, we considered only the maximum sonication temperature in the investigation of HE, which measures the sonication temperature at the centre of a 3×3-pixel grid, however, the 3D distribution of accumulated thermal dose (ATD) may be more relevant to lesion formation. Thus, future studies should investigate the impact of SDR on ATD change over the course of the procedure.

3.3.5 Conclusion

We report a non-linear relationship between sonication power and temperature, with the slope decreasing with increasing power. Heating efficiency was greater in subjects with higher SDR but also declined more rapidly with respect to power. We found that, in pairs of sonications with identical energy and power, the temperature of the second sonication was on average lower than the first. These results suggest that there may be a persistent effect of previous sonications on the HE of subsequent sonications.

3.4 Influence of skull density ratio distribution on long-term tremor suppression

3.4.1 Introduction

As discussed in section 3.3.1, critical to the success of tcMRgFUS is the ability to create temperature increases high enough to cause thermocoagulation at the focal point [246,272,352,353]. The skull is a major impediment to the transmission of energy into the brain, due to refraction, scattering and absorption of the ultrasound waves[191,192,272,383,384]. The SDR, defined as the ratio of the CT measured density of the bone marrow to the cortical bone, has been validated as a key factor in predicting the efficiency of energy transmission through the skull [246,250,355]. SDR values are typically estimated prior to treatment, and then calculated more accurately during treatment by measuring the SDR value along the path traced between each element and the target coordinates. The mean SDR value across all elements in the array is typically used clinically to give an indication of the permeability of the skull to ultrasound[385], and is a key criterion for the evaluation of a patient's suitability for treatment with tcMRgFUS [246,250]. While higher SDR has been shown to be strongly correlated with greater sonication temperatures[272,383], it has not been shown to be associated with long-term clinical outcomes, provided that the total thermal dose delivered over the course of the treatment is sufficient to create a permanent lesion [271,272,274,386,387].

Iijima et. al. investigated how the distribution of SDR values was related to sonication heating and found that the SDR skewness was a better predictor of heating, compared with the mean SDR[385]. The aim of this investigation was to extend this histogram analysis approach to the analysis of clinical outcomes following treatment with tcMRgFUS,

considering recent findings that suggest the distribution of SDR values may predict tremor suppression in ET patients treated with tcMRgFUS[388]. Additionally, we applied a novel approach in which we investigated the individual element SDR values in an element-wise analysis to determine if the SDR values in specific regions of the array were related to clinical outcomes.

3.4.2 Methods

Patient characteristics

Data from 61 patients with either DT (N=27) or ET (N=34) who underwent tcMRgFUS for treatment of tremor at St Vincent's Hospital Sydney, Australia, was retrospectively analysed. All ET patients met 2018 consensus classification criteria[1] for ET or ETP, considered collectively as ET, and all DT patients met the criteria for DT [21]. Informed consent was obtained from all participating patients, and the study was approved by the St Vincent's Hospital Ethics Review Committee (ETH00670).

MRgFUS Procedure

tcMRgFUS targeting the Vim was performed as described in sections 1.2.4 and 2.3.2. In a subset of patients, following incomplete tremor suppression after adequate lesioning of the Vim, the PSA (N=13) or Voa (N=3) was targeted. Planning CT images were acquired prior to treatment for the purpose of SDR estimation and stereotactic planning. All patients had a mean SDR greater than 0.30. MR imaging was acquired pre-treatment and fused to planning

CT imaging to aid in target localisation. In all subjects, the initial treatment target was the Vim, targeted using coordinates of 25% of the anterior commissure–posterior commissure (AC-PC) distance anterior to the PC plus approximately 0.5mm, 14mm lateral to the midline at the level of the intercommissural line and adjusted for individual patient anatomy including width of 3rd ventricle, and proximity to visualised internal capsule.

Clinical Evaluation

Subjects were evaluated clinically by a movement disorders neurologist prior to treatment and again at intervals of 1-, 3-, 6-, 12- and 24-months post treatment. The evaluation included CRST[13,389] and HTS[198,246,247,333,358], as described in section 1.1.5. As CRST part C can be considered a less objective measure of tremor severity, CRST was calculated as the sum of parts A and B only, consistent with previous studies on tcMRgFUS[337]. Tremor scores at follow-up were converted into percentage change from the pre-treatment score and inverted such that a positive percentage indicated a reduction in score, where a value of 100% indicates a tremor score of 0 at follow-up, and negative values indicate tremor increase.

MRI Protocol

MR imaging was acquired 1-7 days prior to treatment, the day immediately following treatment, and 12-months post treatment. The protocol included a 3D T1 weighted image (T1-WI) for assessment of lesion size. The day-1 imaging was acquired on a 3T Philips Ingenia (Philips Inc, Amsterdam, The Netherlands) (sequence: IR-FFE, imaging plane: axial, TI: 450

ms, TR: 7.9 ms, TE:2.6 ms, Flip Angle: 8^{o}, FOV: 240 mm, acquisition matrix: 240 $\times$ 240, slice thickness: 1.0 mm, slices: 170). The pre-treatment and 12-month follow-up imaging was acquired on a 3T GE SIGNA Architect (General Electric, Milwaukee) (sequence: IR-FSPGR, imaging plane: sagittal, TI: 450 ms, TR: 8 ms, TE:3.24 ms, Flip Angle: 10^{o}, FOV: 256 mm, acquisition matrix: 256 $\times$ 256, slice thickness: 1.2 mm, slices: 146). 12-month follow-up imaging was collected for 27 of the 61 patients.

Vim Ablation Volumes

The Vim ablation was manually delineated on the day-1 and 12-month T1-WI and used for calculation of the Vim ablation volume. The follow-up T1-WIs were first linearly co-registered to the pre-treatment T1-WI with FSL-FLIRT[390]. Both the inner most iso-intense lesion core, and hypointense rim, corresponding to zones 1 and 2 respectively[309], were manually segmented by a trained image analysist using ITK-SNAP[335]. While ablation volume can be dependent on the imaging sequence, use of T1-WI for ablation segmentation has been validated [296,391].

SDR Analysis

SDR values were extracted directly from the ExAblate console. SDR values were calculated from the pre-treatment CT image individually for each element in the ultrasound array. Importantly, these SDR values represent the SDR along the beam traced from each element to the sonication target, such that changing the coordinates of the target results in slight changes to the SDR values of each element. The SDR values were extracted for the first Vim

sonication only, resulting in an array of 1024 SDR values per subject. The element array for those treated on the right side (N=14) was flipped so that the focal point location was consistent with those treated on the left. SDR histogram analysis included calculation of the mean (SDR_{Mean}), standard deviation (SDR_{SD}), Shannon entropy ($SDR_{Entropy}$), kurtosis ($SDR_{Kurtosis}$) and skewness (SDR_{Skew}) for each subject, for use in statistical analysis of tremor suppression. SDR histogram metrics were calculated with the stats module in SciPy[392] in Python (version 3.8.15).

To determine if there was a relationship between the SDR values in any subset of transducer elements and treatment outcome, an elementwise SDR analysis was performed. First, patients were split into two groups based on whether they experienced greater or lower than average percentage CRST change at the most recent follow-up. For each of the 1024 elements, the percentage difference in the individual element SDR value from the intra-patient SDR_{Mean} was compared across the two CRST outcome groups via a Student t-test. Elements with a p value < 0.05 were considered statistically significant. False positives due to multiple comparisons were controlled by adjusting the p-values for a false discovery rate of 5%. Statistically significant (SS) elements were isolated and the mean SDR (SDR_{SSM}) and mean percentage difference (MPD) from the intra-patient SDR_{Mean} (SDR_{SSMPD}) was calculated in this element subset.

Statistical Analysis

The relationship between the SDR metrics and change in tremor scores were assessed using a linear mixed-effects model, with percentage change in tremor score from pre-treatment

as the response variable, and a random intercept to account for the repeated tremor score measures for each subject. Patient characteristics including age, sex, and tremor type (ET or DT) were included as predictors. To account for the difference in treatment targets across patients, treatment target (Vim, Vim and PSA or Vim and Voa) was also included in the model as a categorical predictor. Each of the SDR histogram metrics were then individually added to the model to determine if there was an improvement to the model fit. From the element-wise analysis, both SDRSSM and SDRSSPD were also included in the model. The analysis was repeated using percentage change from pre-treatment of CRST and HTS values as the response variable. To isolate any effect of patient sex, the mixed-effects model was then repeated using data from males only. Model goodness of fit was assessed using the Akaike information criterion (AIC). Model residuals were inspected and assessed with a Shapiro-Wilk test of normality to confirm a normal distribution.

Multi-variate regression analysis was performed using the significant predictors identified in the mixed effects model and change in tremor scores collected at 1-month post treatment, and the most recent clinical follow-up, as the dependant variables. $SDR_{Kurtosis}$ cut-off values were estimated by ROC curve analysis using the mean change in CRST or HTS at the most recent follow-up as the threshold. The cut-off value of the ROC curve was defined as the point of maximum specificity and sensitivity. The relationship between SDR kurtosis, sonication temperature and Vim lesion volumes were explored by grouping patients into high and low SDR kurtosis based on the cut-off value estimated in ROC curve analysis.

Table 3-4 . Patient and tcMRgFUS treatment characteristics.

Variable	All patients N=61
Sex, n(%)	
Male	42 (69)
Female	19 (31)
Disease Type, n(%)	
ET	34 (56)
DT	27 (44)
Age, mean ± SD, years	73.23 ± 8.52
Treatment Side, n(%)	
Left	47 (77)
Right	14 (23)
Treatment Target, n(%)	
Vim	45 (74)
Vim & PSA	13 (21)
Vim & Voa	3 (5)
Number of Sonications	9.98 ± 2.79
Max. Temperature (°C)	60.89 ± 3.40
Max. Average Temperature (°C)	56.64 ± 3.02

Abbreviations used: ET (Essential Tremor), DT(Dystonic Tremor), SD (Standard Deviation), Vim (Ventral Intermediate Nucleus), PSA (Posterior Subthalamic Area), Voa (Ventralis Oralis Anterior)

Variables were assessed for normality with a Shapiro-Wilk test of normality. Group differences were assessed using an independent samples t-test or Mann-Whitney U test, for normally or non-normally distributed data, respectively.

All statistical analysis was performed using the R (version 4.2.2) statistical software package in RStudio (Version 1.4.1717, RStudio, Inc., Boston, MA URL, http://www.rstudio.com).

3.4.3 Results

MRgFUS Procedure

An average (± SD) of 9.98 ± 2.79 sonications per patient were delivered over the course of the treatment (*Table 3-4*). The mean peak average sonication temperature (where the average temperature is defined as the average temperature of the 9 voxels centered on the sonication focal spot, and the peak value is the maximum value across all sonications for a given subject) was 56.64° ± 3.02°C, reaching 53°C or greater in all patients. The mean Vim ablation volume measured on the T1-weighted imaging was 129.85 ± 47.65 mm^3 at day-1, and 17.73 ± 17.31 mm^3 at 12 months post-treatment. The mean reduction in lesion volume at 12 months relative to the day-1 lesion was -84.82% ± 16.43%. Lesion volume at 12 months post-treatment was significantly greater in patients with high SDR kurtosis compared with those with low SDR kurtosis (24.87 ± 23.80 vs 12.02 ± 5.66 mm^3, p = 0.040). The reduction in lesion volume at 12 months relative to the day-1 lesion volume was also significantly less in the high kurtosis patients (-77.53% ± 22.38% vs -90.66% ± 5.09%, p = 0.007). No significant difference in lesion volume measured on day-1 was found between the SDR kurtosis groups. The mean peak maximum sonication temperature reached throughout the procedure was significantly lower in patients in the high SDR kurtosis group (55.97° ± 3.36° vs 57.46° ± 2.33°C, p = 0.047).

The mean latest clinical evaluation was 14.14 $\pm$ 8.35 months post treatment. The average change in CRST and HTS scores from pre-treatment to the most recent clinical visit was 43.88% and 61.93% respectively. There was not a significant difference in age between patient sex or disease types. Patient demographic and treatment information is summarised in *Table 3-4*.

SDR Analysis

Table 3-5 Summary of linear mixed effects model results.

Variable	CRST		HTS	
	Beta (p)	**95% CI**	**Beta (p)**	**95% CI**
SDR_{Mean}	-0.01 (0.920)	-0.24, 0.22	0.02 (0.881)	-0.22, 0.26
SDR_{SD}	-0.28 (0.006)*	-0.48, -0.08	-0.30 (0.006)*	-0.51, -0.09
$SDR_{Kurtosis}$	0.33 (0.004)*	0.11, 0.54	0.38 (< .001)*	0.16, 0.60
SDR_{Skew}	0.001 (0.953)	-0.23, 0.24	-0.02 (0.863)	-0.27, 0.23
$SDR_{Entropy}$	0.19 (0.052)	-2×10^{-3}, 0.38	0.24 (0.019)*	0.04, 0.44
SDR_{SSM}	0.12 (0.254)	-0.09, 0.34	0.14 (0.232)	-0.09, 0.37
SDR_{SSMPD}	0.27 (0.008)*	0.07, 0.47	0.27 (0.015)*	0.05, 0.48

*Significant effects

Abbreviations used: SDR (Skull Density Ratio), SD (Standard Deviation), SSM (Statistically Significant elements Mean), SSMPD (Statistically Significant elements Percentage Difference), CRST (Clinical Rating Scale for Tremor), HTS (Hand Tremor Score), CI (Confidence Interval)

The mean SDR_{Mean} across the entire patient cohort was 0.42 ± 0.07, and the mean $SDR_{Kurtosis}$ was 0.0198 ± 0.87. There was a statistically significant ($p<0.001$) difference in $SDR_{Kurtosis}$ between females and males.

(*Figure 3-3*), with females exhibiting greater $SDR_{Kurtosis}$ (0.79), compared with males (-0.33). There was no difference in SDR_{Mean} or $SDR_{Kurtosis}$ between disease types. There was a significant negative correlation between $SDR_{Kurtosis}$ and SDR_{Mean} (β=-0.391, p=0.002). While changes in intraprocedural treatment coordinates did introduce small changes to $SDR_{Kurtosis}$ and SDR_{Mean}, the differences were not statistically significant, thus the values calculated for the first Vim sonication were considered to be representative of each subject.

The linear mixed-effects model results are summarised in *Table 3-5*. The analysis revealed that patient age was significantly negatively associated with CRST and HTS improvement, indicating that older patients experienced poorer outcomes. Disease type also presented a significant effect, with CRST and HTS improvement lower in DT patients, compared with ET patients. SDR_{Mean} was not found to be a statistically significant predictor of improvement in CRST or HTS values post treatment. Treatment target was not found to have a significant effect on tremor score improvement.

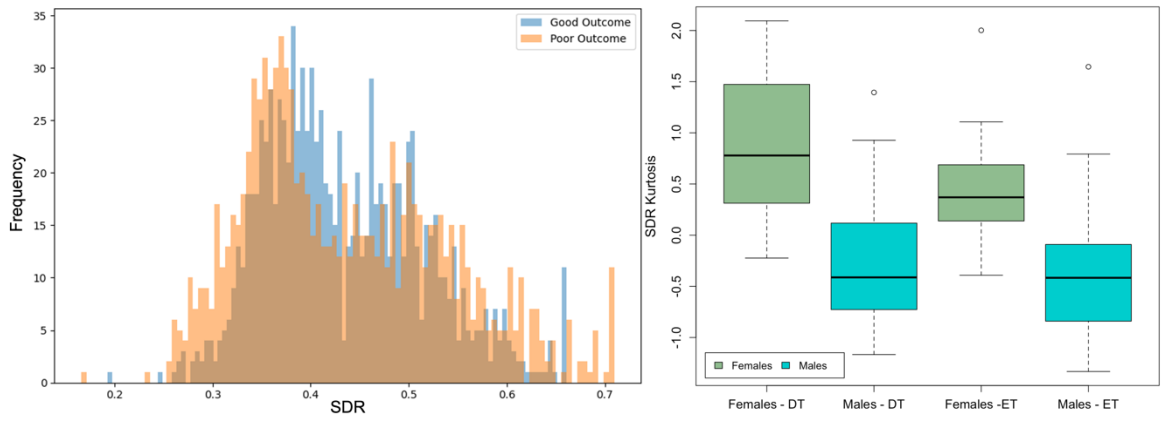

Figure 3-3 ***Left*** *- Averaged SDR histograms of patients with below-average CRST change (orange) overlayed on patients with above-average outcomes (blue).* ***Right -*** *SDR kurtosis by patient sex and disease type.*

A significant negative effect was found between SDR_{SD} and improvement in CRST (β=-0.28, p=0.006) and HTS (β=-0.30, p=0.006). A significant positive effect was also found between $SDR_{Kurtosis}$ and CRST (β=0.33, p=0.004) and HTS (β=0.38, p<0.001) improvement. Using $SDR_{Kurtosis}$ as an effect in the mixed effects model resulted in an improved model fit compared with SDR_{SD} for CRST (AIC = -156.14 vs. -155.17) and HTS (AIC = -116.30 vs. -113.11).

A significant effect between patient sex and improvement in CRST (p=0.016) was observed, while the effect on HTS was approaching significance (p=0.06). When the linear mixed effects model was repeated using data from males only, there was found to be a significant effect between $SDR_{Kurtosis}$ and HTS (p=0.01) improvement, while the effect on CRST improvement was approaching significance (p=0.06).

Multi-variate regression analysis revealed the effect between $SDR_{Kurtosis}$ and tremor improvement was significant both at 1-month (CRST: β=0.415, p=0.008, HTS: β=0.369, p=0.016), and at the most recent follow-up (CRST: β=0.395, p<0.001, HTS: β=0.386, p<0.001). The cut-off $SDR_{Kurtosis}$ value estimated by ROC analysis was -0.26 for CRST change (72.2% sensitivity and 76.0% specificity) and -0.38 for HTS change (70.0% sensitivity and 71.1% specificity). The mean $SDR_{Kurtosis}$ cut-off value between the two tremor scores was -

Table 3-6 Summary of demographic and treatment information by SDR kurtosis group.

Variable	**Low Kurtosis**	**High Kurtosis**
n (%)	27 (44)	34 (56)
Age, mean $\pm$ SD (years)	74.81 $\pm$ 8.34	71.98 $\pm$ 8.57
Disease Type, n(%)		
ET	18 (67)	16 (47)
DT	9 (33)	18 (53)
Treatment Target, n(%)		
Vim	21 (78)	26 (76)
Vim & PSA	5 (19)	7 (21)
Vim & Voa	1 (4)	1 (3)
Mean SDR	0.46 $\pm$ 0.06	0.41 $\pm$ 0.07*
Number of Sonications	9.89 $\pm$ 2.65	10.06 $\pm$ 2.94
Max. Sonication temperature	58.86 $\pm$ 2.11	57.80 $\pm$ 1.76*
Most recent clinical visit (months)	19.04 $\pm$ 11.20	16.00 $\pm$ 11.34
Baseline HTS	18.04 $\pm$ 7.62	20.29 $\pm$ 5.58
Baseline CRST	45.67 $\pm$ 16.62	47.00 $\pm$ 15.22
HTS change at most recent clinical visit (%)	50.91 $\pm$ 25.13	67.58 $\pm$ 18.06*
CRST change at most recent clinical visit (%)	33.16 $\pm$ 15.95	43.39 $\pm$ 15.49*
Day-1 Vim ablation volume (mm^3)	142.56 $\pm$ 52.80	119.75 $\pm$ 41.16
12-month Vim ablation volume (mm^3)	12.02 $\pm$ 5.66 mm^3	24.87 $\pm$ 23.80*

**Statistically significant group differences.*

Abbreviations used: SD (Standard Deviation), ET (Essential Tremor), DT(Dystonic Tremor), Vim (Ventral Intermediate Nucleus), PSA (Posterior Subthalamic Area), Voa (Ventralis Oralis Anterior), CRST (Clinical Rating Scale for Tremor), HTS (Hand Tremor Score)

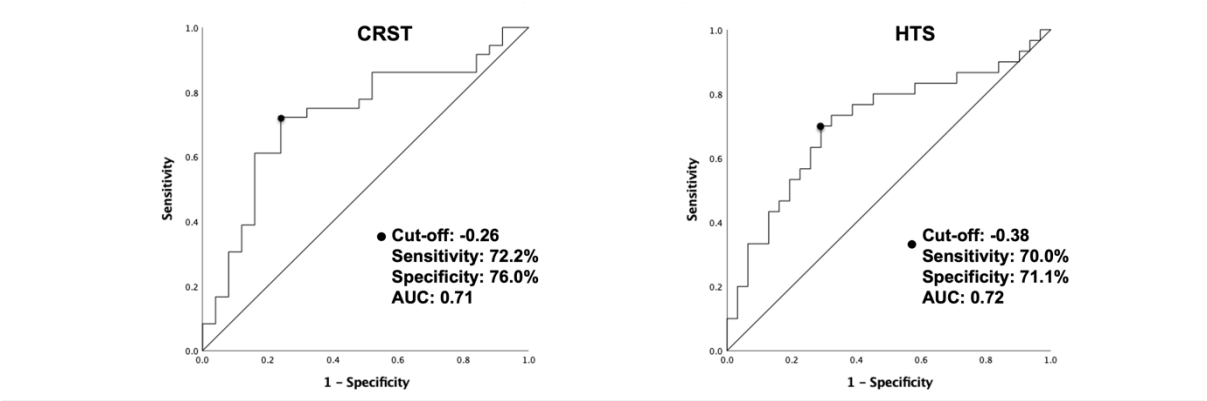

*Figure 3-4 ROC curve analysis for improvement in CRST (**left**) and HTS (**right**) at the most recent clinical follow-up. The black dot in each graph indicates the optimal cut-off value.*

0.32. ROC curves are shown in *Figure 3-4*. Patient demographic, treatment parameters and tremor scores, stratified by $SDR_{Kurtosis}$ group are summarised in *Table 3-6*.

Elementwise SDR Analysis

Figure 3-5 illustrates the average distribution of SDR values over the elements in the array. Across the patient cohort, individual element SDR values ranged between 0.16 to 0.71. When expressed as the percentage difference from SDR_{Mean}, the individual element SDR values ranged from -62.33% to 66.53% of SDR_{Mean}. The distribution of SDR values was not right-left symmetric, reflecting the effect of the target coordinates, and positioning of the transducer array on the SDR value experienced by each element, rather than a true asymmetry in SDR values between the right and left sides of the skull.

Following the element-wise t-test comparing the percentage difference of each element from SDR_{Mean} between the two CRST outcome groups, a total of 171 statistically significant elements were identified (*Figure 3-5*). In both CRST outcome groups, the mean SDR in this

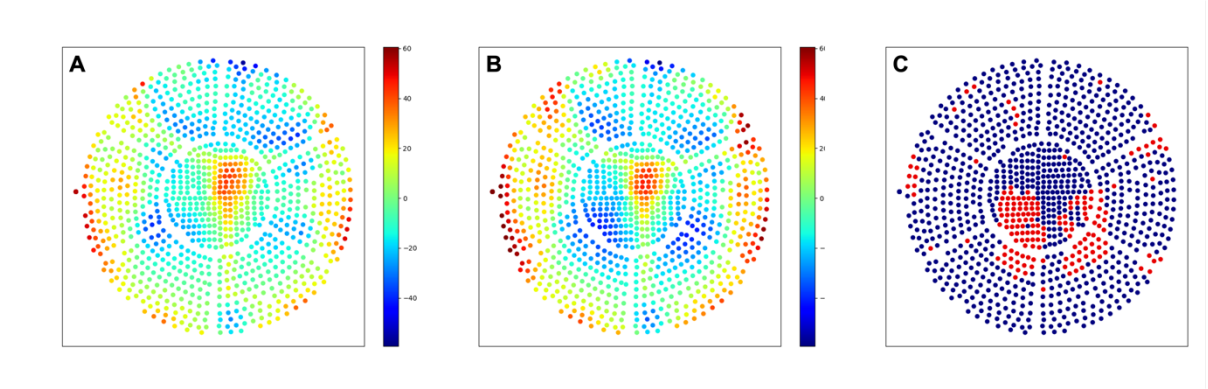

*Figure 3-5 Two-dimensional representation of elements in the ultrasound array. Element-wise average percentage difference from SDR_{Mean} for patients with above-average CRST change (**A**) below-average CRST change (**B**) and statistically significant elements shown in red (**C**). Note elements on the left of the array correspond to elements on the treated side.*

subset of elements was lower than the SDR_{Mean}, however, subjects in the above average outcome group tended to have significantly less deviation from SDR_{Mean} in these elements, when compared with the below average outcome group (-5.70 vs -13.07%, p=0.003). Of the 171 significant elements, 55 (32.16%) were located in the central posterior bank on the treated side. A significant positive effect was found between SDR_{SSPD} in this element subset and improvement in CRST (β=0.27, p<0.008) and HTS (β=0.27, p<0.015). The effect of the

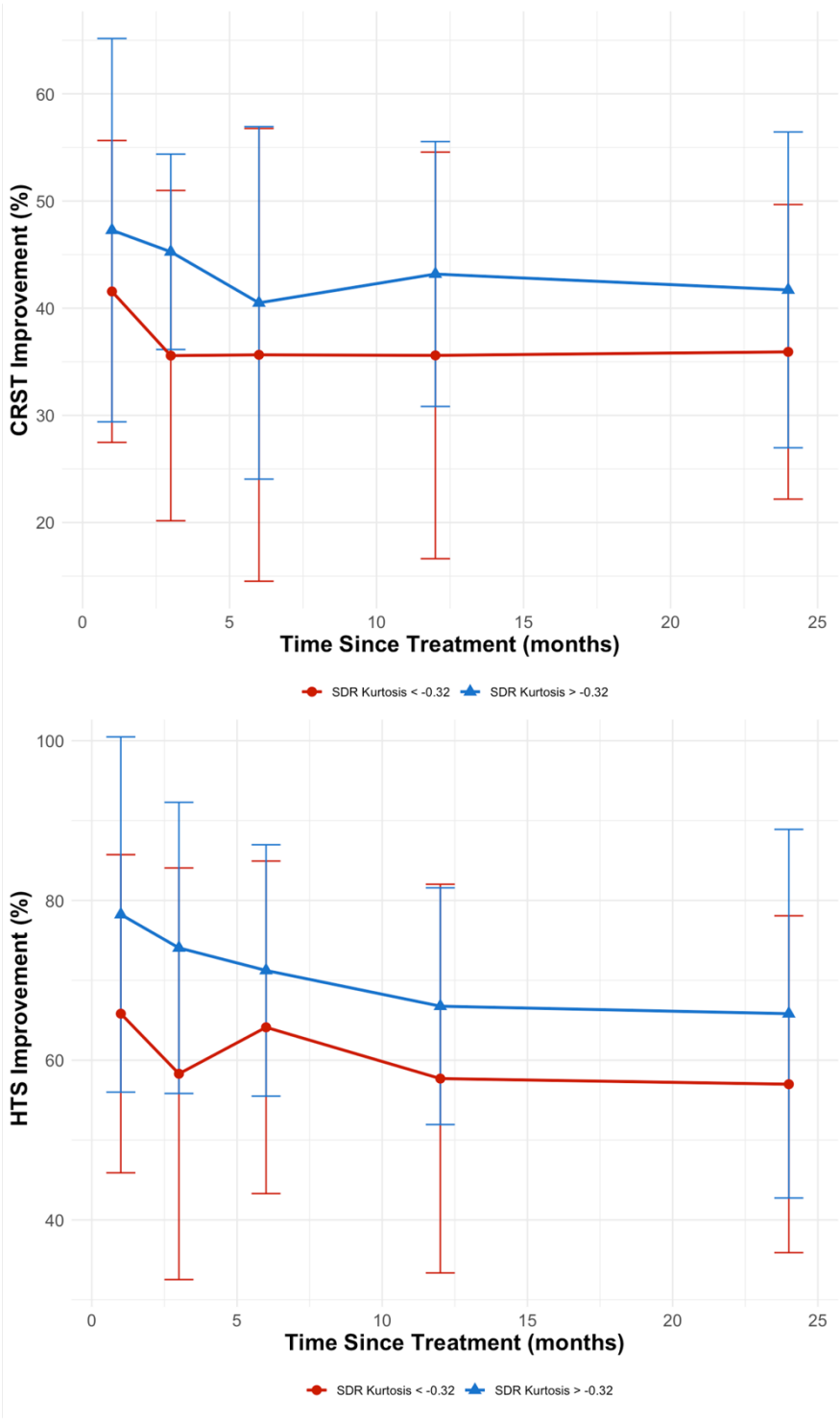

*Figure 3-6 Percentage improvement in CRST (**upper**) and HTS (**lower**) values following treatment with tcMRgFUS for patients in the high (blue) and low SDR kurtosis (red) groups. Mean (dots) and standard deviation (whiskers) are shown.*

mean SDR in this element subset was not found to have a significant effect on any tremor score.

3.4.4 Discussion

The aim of this investigation was to determine if the numerical, or regional, distribution of SDR values calculated for each element in the ultrasound transducer was associated with long-term clinical outcomes in patients with ET or DT, following treatment with tcMRgFUS.

We observed a significant effect of both SDR_{SD} and $SDR_{Kurtosis}$ with tremor improvement following treatment. $SDR_{Kurtosis}$ may provide a more reliable predictor of tremor suppression, as it exhibited a significant relationship with both CRST and HTS (*Figure 3-6*) and provided an improved model fit over SDR_{SD}. Kurtosis describes the distribution of data points in a dataset by measuring the "tailedness" of a distribution, relative to the normal distribution. Increased kurtosis indicates a higher peak and fatter tails, while low kurtosis indicates a lower peak and thinner tails. Averaged histograms of subjects in the two CRST outcome groups are displayed in *Figure 3-3*. The symmetric increase in tail height may account for the observation that the mean SDR value was not predictive of clinical outcome, as SDR_{Mean} is unaffected by a symmetric change in tail height.

The results of the element-wise analysis revealed that the significant elements were, on average, of lower SDR value than the intra-subject SDR_{Mean}, suggesting that it is the increase in number low SDR elements in the left tail of the histogram, that contribute to poorer clinical outcomes. Our findings, however, that the mean SDR in this subset of elements was not predictive of outcome, while the mean difference from SDR_{Mean} was, indicates that it is

not the absolute value of these low SDR elements that is contributing to the poorer outcomes, rather it is the reduction relative to the mean SDR that is more relevant.

Multi-variate regression analysis found that the effect of $SDR_{Kurtosis}$ on tremor suppression was significant both in the early postoperative phase (1-month), and in the long-term (>12 months). This result contrasts with the findings of Torii et al. who observed an effect of mean SDR on clinical outcomes at 1 week post treatment, but no relationship at longer intervals[337]. Our findings suggests that the effect of $SDR_{Kurtosis}$ is observable early, and is sustained over time, despite the observed reduction in treatment effect in both high and low $SDR_{Kurtosis}$ patients over time (*Figure 3-6*). The results presented here are consistent with previous observations that the standard deviation in SDR values was predictive of long-term clinical outcomes in essential tremor[388], and confirms these findings in a larger patient cohort including patients with dystonic tremor.

The results of the analysis of Vim ablations volumes 12-months post treatment are suggestive of an effect of $SDR_{Kurtosis}$ on the formation of clinically effective lesions. Lesion volumes were significantly greater, and the reduction in volume relative to the day-1 volume was less severe, in patients with SDR kurtosis greater than -0.32. Previous studies have found that lesion size was associated with increased tremor suppression[296], thus the relationship between $SDR_{Kurtosis}$ and lesion size may explain the observed effect on clinical outcomes in the present study. While there was not found to be a significant relationship between lesion volumes measured on the day-1 imaging and $SDR_{Kurtosis}$, this may be due to the influence of perilesional oedema on the lesion volume in the early postoperative phase. Future studies examining the quality of the lesion, and the degree to which the lesion

created at the time of treatment leads to permanent alterations of the tissue structure with imaging sensitive to microstructure change, such as diffusion weighted imaging, may help validate these findings.

While the mean SDR value is a useful predictor of sonication thermal increase, the results presented here indicate that the maximum sonication temperature may not be the only factor associated with the formation of clinically effective lesions. Patients in the high SDR kurtosis group tended to experience lower sonication temperatures, yet the lesions were larger at 12-months and the patients experienced superior tremor suppression, compared with those in the low SDR kurtosis group. Sonication temperatures are currently estimated on 2D MR thermometry, and it is possible that the effect of $SDR_{Kurtosis}$ on the 3-dimensional thermal dose distribution is not captured by a 2D cross-section of the heated volume.

Our observation that the distribution of SDR values across the skull, in other words SDR consistency, is a more meaningful prognostic factor, compared to the mean SDR value, may have clinical relevance for the selection of appropriate patients during patient screening. These findings suggest that when evaluating potential patients for treatment with tcMRgFUS, clinicians should look at both the SDR_{Mean} to estimate the likelihood of reaching clinically effective temperatures, and $SDR_{Kurtosis}$ to predict the likely reduction in tremor severity. Results of the ROC analysis suggests that a $SDR_{Kurtosis}$ value of -0.32 may be useful cut-off for predication of clinical outcomes, however, further validation is required before these recommendations should be adopted into clinical practice. It is possible that the current practice of evaluating patients by mean SDR alone, may exclude potentially good candidates for treatment. Evaluation of SDR Kurtosis may enable patients with mean SDRs

below cut-off for treatment to be reconsidered as tcMRgFUS candidates. Conversely, patients with high mean SDR, but low kurtosis, may not experience the optimal clinical benefit.

The element-wise analysis also revealed a regional distribution of statistically significant low SDR elements, primarily in the central posterior element bank on the treated side. This finding suggests that it may be the SDR values in specific regions of the skull that contribute to successful treatment with tcMRgFUS. While the results of the histogram analysis reinforce the importance of examination of the distribution of SDR values, this result suggests evaluation of regional SDR values may also aid in our understanding of the impact of SDR on lesion formation.

Our findings that patient age was negatively associated with tremor improvement is consistent with previous findings[393]. Our analysis also revealed a distinct effect of patient sex on tremor suppression, with females experiencing greater tremor suppression than males, while females also had increased $SDR_{Kurtosis}$ compared to males. Following the statistical analysis in the male only cohort, the effect between $SDR_{Kurtosis}$ and tremor suppression remained significant, suggesting that the observed effect of sex is likely a consequence of the significant difference in $SDR_{Kurtosis}$ between males and females.

These findings are particularly important for treating tremor in patients with dystonic tremor, who may experience less clinical benefit compared with essential tremor patients. These finding may also have implications for bilateral treatments, which are a natural progression of the current unilateral approach, as the SDR values on each side should be

evaluated independently to confirm that both sides of the brain are suitable for treatment with tcMRgFUS.

This investigation had some limitations. The inclusion of patients treated in regions outside of the Vim (PSA or Voa) may have influenced the clinical outcomes, however, investigation of secondary lesions was beyond the scope of this investigation. Inclusion of both ET and DT patients meant the patient cohort was not homogenous, however, this effect was mitigated by inclusion of tremor type in the statistical model.

3.4.5 Conclusion

Our analysis found a significant positive relationship between $SDR_{Kurtosis}$ and percentage improvement in tremor severity, following treatment with tcMRgFUS. Additionally, we found the percentage difference in element SDR from the intra-subject mean SDR in elements near the central posterior region on the treated side were related to tremor improvement, suggesting both SDR distribution and regional SDR values may play a role in the formation of clinically effective lesions.

3.5 Chapter Summary

The most important factor for the successful treatment of tremor with tcMRgFUS is the deposition of adequate energy within the tissue at the treatment target to cause thermocoagulation and tissue necrosis. The skull is known to be a significant impediment to the efficient delivery of US energy at the target site, and thus, investigation of how the skull influences the efficiency of tissue heating and the formation of clinically effective lesions may help improve patient outcomes.

In this chapter, we confirmed that at the group level, the relationship between sonication HE and power was non-linear, with HE decreasing as sonication power was increased during the procedure. The results of linear mixed-effects analysis suggested that the reduction in HE may be linked with patient SDR, with higher SDR associated with more rapid loss of HE, consistent with results reported by Yang et al[373]. Additionally, through a paired sonication analysis where we isolated the effects of sonication power and energy, we demonstrated the presence of a persistent effect of previous sonications on the HE of subsequent sonications. In the paired sonication analysis, we observed that HE was lower in the later sonication in 71% of cases, despite the prescription of identical sonication power and energy. This result may suggest that the temperatures achieved by a given sonication are not truly independent and may be influenced by the effects of previous sonications.

Analysis of the relationship between the distribution of SDR values across the skull and long-term lesion volumes and tremor suppression found that greater lesion volumes and tremor

benefit were associated with more consistent SDR values, as measured by the kurtosis of the distribution. The mean SDR value is a known predictor of sonication HE, however, in this chapter we show that the distribution of SDR values may be a more meaningful prognostic factor.

Together, these findings may contribute to enhancing patient outcomes via an improved understanding of the factors that influence intra-procedure sonication HE, as well as improved identification of appropriate treatment candidates during patient screening.

4 Influence of Treatment Target

Based on:

- **Kyle, Kain**, Jerome Maller, Yael Barnett, Benjamin Jonker, Michael Barnett, Arkiev D. Souza, Fernando Calamante, Joel Maamary, James Peters, and Chenyu Wang. 2023. “Tremor Suppression Following Treatment with MRgFUS : Skull Density Ratio Consistency and Degree of Posterior Dentatorubrothalamic Tract Lesioning Predicts Long-Term Clinical Outcomes in Essential Tremor.” (April):1–10. doi: 10.3389/fneur.2023.1129430.

- **Kyle, Kain**, James Peters, Benjamin Jonker, Yael Barnett, Joel Maamary, Michael Barnett, Jerome Maller, Chenyu Wang PhD, and Stephen Tisch. Magnetic resonance-guided focused ultrasound for treatment of essential tremor: Ventral intermediate nucleus ablation alone or additional posterior subthalamic area lesioning? (In submission with Movement Disorders: Clinical Practice).

4.1 Abstract

In Chapters 2 and 3, the impact of characteristics inherent to the patient, namely tremor subtype and properties of the skull, on tremor suppression was explored. The results of these investigations identified significant relationships between these patient-specific characteristics and the tremor benefit experience following treatment with tcMRgFUS. However, there remains a variance in outcomes not accounted for by these characteristics alone, which we hypothesised may be explained by the choice of treatment target coordinates chosen by the treating team. Despite advances in MRI acquisition and imaging post-processing software, the definition of treatment coordinates continues to be defined with indirect landmark-based methods, whereby the treatment target is defined with coordinates relative to easily identifiable landmarks. Indirect targeting methods do not consider individual variations in anatomy; thus, methods of direct targeting by visualisation of relevant structures on planning MRI are appealing. Several structures and multiple methodologies for direct target visualisation have been proposed in the literature. This chapter focuses on the investigation of the optimal treatment target for tcMRgFUS, as well as the comparison of several automated direct targeting methods.

4.2 Background

A critical determinant of therapeutic success of any stereotactic procedure for the treatment of tremor lies in the accurate targeting of the appropriate structure within the brain. Typically, the Vim of the thalamus has been the most frequently targeted structure in stereotactic interventions for ET[282]. The Vim, a wedge-shaped nucleus in the lateral region of the thalamus, known as the motor thalamus, has long been implicated in tremor and has been the target of many studies with deep brain stimulation (DBS) and radiofrequency (RF) lesioning for the treatment of ET[282].

Histological studies of the thalamus, together with micro-recordings of brain activity and DBS stimulation coordinates[394] have provided approximations for the coordinates of the Vim[395], however, precise localisation is made challenging by the lack of visibility on conventional structural imaging at clinically available field strengths (1.5 or 3.0T). The borders of the individual thalamic nuclei are indistinguishable on conventional structural MRI, thus targeting of the Vim during tcMRgFUS is achieved via landmark based indirect targeting. Indirect targeting relies on the identification of known anatomical landmarks in the brain and defines the coordinates of the Vim relative to these landmarks. Indirect coordinates for the Vim have been refined over years of stereotactic surgery with RF lesioning and DBS, where microelectrode recordings and correlation of stimulation coordinates with intraoperative tremor improvement have helped define the average coordinates of the Vim, typically relative to the anterior and posterior commissure's (AC and PC, respectively) of the brain. Indirect targeting remains the gold-standard method for

targeting of the Vim [283,284], however, the method does not account for individual variations in anatomy, or the effects of global and regional atrophy, which may affect the relationship between structures in the brain, particularly with the nuclei of the thalamus [285–287].

For this reason, several methods of direct targeting have recently been proposed, to aid neurosurgeons in the definition of optimal treatment coordinates for targeting of the Vim. Direct targeting involves the direct visualisation of the Vim itself or the connecting white matter pathways. While the borders of the individual thalamic nuclei are not visible on standard structural T1- or T2-weighted MRI, recent improvements in acquisition and post-processing algorithms may provide improved visualisation. Optimisation of sequence timings of the common MRI sequence magnetisation-prepared rapid acquisition gradient echo (MPRAGE) for improved differentiation of GM and WM has been shown to aid in identification of individual thalamic nuclei[396]. Modulation of this inversion time can be used to alter the contrast in an image, or even null the signal from certain tissue based on the T1-relaxation properties. Sudhyadhom et al. developed the FGATIR sequence for improved differentiation of subcortical structures [289], which was further optimised by Tourdias et al. with the more recently reported a white matter nulled MPRAGE (WMnMPRAGE). This sequence was shown to provide significantly improved intra-thalamic contrast, where the Vim may be directly visualised at 7T [397].

Alternative approaches for direct targeting leverage the directional information of diffusion MRI (dMRI) by mapping the white matter pathways in the brain and using the connections of the thalamus to define the Vim. The Vim receives primarily excitatory input from the cerebellum and projects to the primary motor cortex (M1) of the cerebral cortex. Thus,

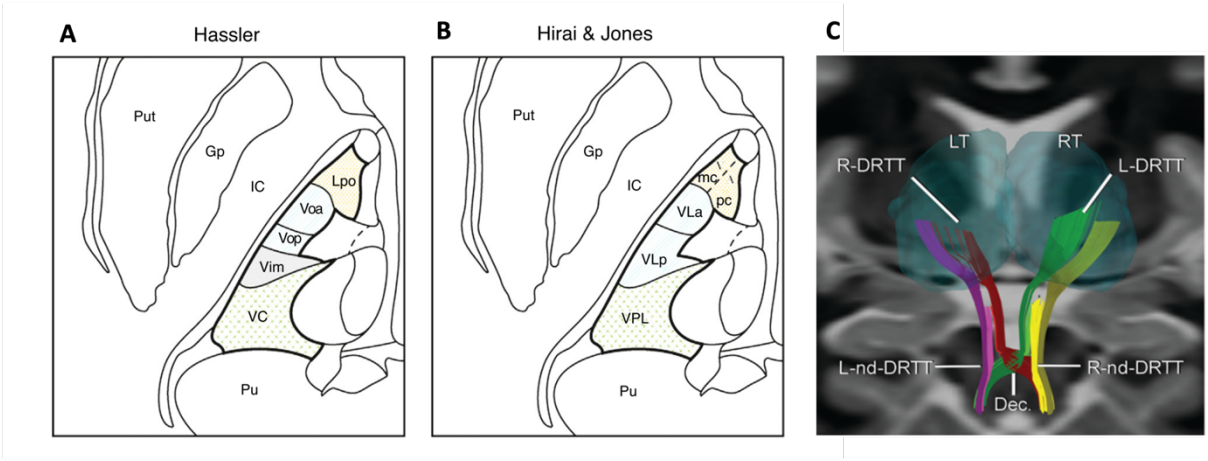

Figure 4-1 ***A*** *- Axial cross section thalamic nuclei labelled with the Hassler atlas.* ***B*** *– Thalamic nuclei labelled with the terminology of Hirai and Jones.* ***C*** *– decussating dentatorubrothalamic tract (DRTT) and non-decussating DRTT (nd-DRTT). Thalamus indicated by blue transparent overlay. Adapted from Petersen et al.* [399].

several methods have been proposed for the use of dMRI to target the Vim via the structural connections to these regions [290,291,398]. The dentatorubrothalamic tract (DRTT), which regulates motor control by linking cerebellar efferents with ascending projections to the primary motor cortex via the Vim of the thalamus[399]. The DRTT runs between the dentate nucleus of the cerebellum, and contralateral thalamus at the level of the Vim (*Figure 4-1*), via the superior cerebellar peduncle and red nucleus. More recently, the non-decussation DRTT (nd-DRTT), which connects with the ipsilateral thalamus has been identified[399,400]. dMRI tractography reconstruction of the dRTT has been demonstrated in several studies [298,401,402], and involvement of the DRTT has been shown to be crucial for achieving tremor suppression in several DBS and tcMRgFUS studies [294–296]. Thus, direct visualisation of the DRTT may provide a useful method of direct target visualisation.

While the Vim has been the most popular treatment target, some centres have begun to experiment with alternative treatment targets for treatment of tremor with tcMRgFUS,

following trends from the RF and DBS literature [403–405]. The posterior subthalamic area (PSA) encompasses the zona incerta (ZI) and highly dense cerebellar afferents to the thalamus via the prelemniscal radiation [248,249,406], and studies have suggested that targeting of the PSA may provide tremor benefit[196], without the sensory adverse effects that may results from incidental lesioning of the VC nucleus of the thalamus while targeting the Vim[276].

Improvements in MRI acquisition and post-processing algorithms may benefit clinicians treating patients with tcMRgFUS by allowing direct visualisation of treatment targets, providing optimal tremor suppression while avoiding the adverse effects associated with the unintended lesioning of surrounding structures. However, there remains uncertainly around both the optimal tcMRgFUS treatment target, as well as the optimal method for direct targeting, thus further research is required to validate proposed direct targeting methodologies before clinical adoption can be expected.

4.3 Evaluation of Automated Thalamic Segmentation and Probabilistic Targeting

4.3.1 Introduction

The Vim of the thalamus as labelled by Hassler, which corresponds approximately to the ventral portion of the ventral lateral posterior (VLp) nuclei[407] of the thalamus per the Morel atlas[408], is a common target for stereotactic treatment of tremor [409–411]. The Vim acts as a junction between cerebellar and cortical pathways, receiving afferent projections from the contralateral deep cerebellar nuclei and connecting to the ipsilateral motor cortex. While the pathophysiology of movement disorders such as ET and DT are known to differ, the Vim remains a central component in both tremor subtypes[412].

The Vim is a common target for treatment of tremor with tcMRgFUS, and accurate localisation of the target is imperative for successful tremor suppression. Complicating this is the fact that the borders of the Vim are not visible on standard structural MRI at 3T. The current gold-standard approach is to use stereotactic landmarks to locate the Vim, however, this approach does not account for individual variations in anatomy or the effects of global or regional brain atrophy [286,287]. Various approaches for improved localisation of the Vim have been investigated, including diffusion MRI (dMRI) to parcellate the thalamus based on the cortical connectivity [290,291,398], clustering of diffusion fibre orientation distributions FODs[293]. While such methods of Vim localisation are promising, they suffer from a lack of consensus on the ideal parameters and methods with which to perform the segmentation, increased MRI acquisition times and reduced spatial resolution and signal-to-noise ratio

(SNR). Moreover, spatial distortions due to the accumulation of phase errors inherent in diffusion imaging, as well as increased acquisition duration make DWI-based methods difficult to implement in clinical practice, thus analysis of conventional structural imaging may be more practical option for target definition. Segmentation of discrete thalamic nuclei with quantitative susceptibility mapping, which exploits the differences in magnetic susceptibility to generate tissue contrast has also been demonstrated [397], however QSM-based methods suffer from long acquisitions times making them difficult to implement clinically.

To aid in neuroimaging studies of thalamic substructures, an automated thalamic segmentation technique was developed by Iglesias et al [413] in 2018 and recently included in the popular neuroimaging software suite FreeSurfer[414]. This technique is based on manual segmentations of histological data and ex-vivo MRI data, which were combined to generate a probabilistic thalamic atlas that is applied to T1-weighted imaging (T1-WI) MRI.

Direct visualisation of thalamic substructures on in-vivo MRI with sequences designed to optimise intra-thalamic contrast may also aid in thalamic segmentation. Modification of the inversion time of a conventional magnetisation-prepared rapid acquisition gradient echo (MPRAGE) MRI sequence has been shown to improve the identification of the individual thalamic nuclei [396]. Tourdias et al. built on this by optimising the inversion pulse to null the signal from white matter with the white matter-nulled MPRAGE (WMnMPRAGE), allowing direct visualisation of the Vim on WMnMPRAGE acquired at 7-tesla (7T) [288]. The thalamic segmentation tool THOMAS was developed to segment the thalamus on WMnMPRAGE images acquired at lower field strengths[415]. Using manual segmentations of 20 manually

labelled 7T WMnMPRAGE images, a probabilistic atlas was built by non-linearly warping the segmentations to a template image. While THOMAS was originally developed for use with a WMnMPRAGE acquisition, it has recently been extended to parcellate the thalamus on conventional T1-WI.

Instead of parcellation of the thalamus into individual nuclei, an alternative targeting strategy recently proposed by Su et al [255] defines a probabilistic target region by combining the ablated volumes from a number of subjects lesioned in the Vim in an unbiased spatially normalised WMnMPRAGE template image with non-linear co-registration. As all subjects who were treated with tcMRgFUS experienced some degree of tremor benefit, the intersection in treated volumes across all subjects is thought to correspond to the optimal treatment target, which the authors report to be associated with greater post-treatment tremor suppression.

While the thalamic parcellations provided by FreeSurfer and THOMAS have been directly compared previously [415], comparison in the context of tcMRgFUS targeting the Vim has not been published. Thus, in the present study, we compare the thalamic parcellations provided by FreeSurfer and THOMAS by examining the overlap between the individual thalamic nuclei and the ablated volume in patients treated with tcMRgFUS targeting the Vim using conventionally defined stereotactic coordinates. Additionally, we replicate and compare the probabilistic target method developed by Su et. al. using imaging data from our patient cohort.

4.3.2 Methods

Subjects

This study was a retrospective analysis of data collected from patients diagnosed with medication-refractory ET, ETP or DT, and treated with tcMRgFUS for tremor at St Vincent's Hospital Sydney between November 2019 and July 2020. Only patients who were targeted in the Vim, and in which requisite pre- and post-treatment MR imaging was acquired were included in the study. The presence of secondary treatment targets such as the PSA or Voa in some subjects was not considered in this study. Informed consent was obtained from all participating subjects, and the study was approved by the St Vincent's Hospital Ethics Review Committee (ETH00670).

tcMRgFUS Procedure

tcMRgFUS was performed as described in sections 1.2.4 and 2.3.2. All subjects were assessed by a neurologist prior to participation in the study. Preoperative CT and MR imaging was acquired for estimation of skull density ratio (SDR) and stereotactic treatment planning. The target coordinates for the Vim were chosen by a neurosurgeon using the conventional stereotactic location 25% of the AC-PC distance anterior to the PC, 14 mm lateral to the midline at the level of the intercommisural line. The target was adjusted for individual patient anatomy including width of the 3rd ventricle and proximity to visualised descending corticospinal tract. A minimum of 2 sonication reaching 53 C targeting the Vim were delivered. In a subset of patients, if tremor suppression was considered incomplete

following adequate lesioning of the Vim, secondary regions such as the PSA or Voa were lesioned. Investigation of these secondary lesions was beyond the scope of this study.

Imaging Protocol

MR imaging was acquired 1-7 days prior to, and immediately following treatment with tcMRgFUS. All imaging data was acquired on a 3 Tesla MRI scanner (SIGNA Architect, General Electric, Milwaukee) using a 48-channel head coil. The pre-treatment and post treatment imaging protocol included a sagittal 3D T1-WI (IR-FSPGR ; TI: 450 ms, TR: 8 ms, TE:3.24 ms, Flip Angle: 10 , FOV: 256 mm, acquisition matrix: 256 $\times$ 256, slice thickness: 1.2 mm, slice number 146) and an axial 2D T2-weighted image (TR: 3785 ms, TE: 118 ms, flip angle: 142 , FOV 180 mm, acquisition matrix: 300 $\times$ 300, slice thickness: 2 mm, slice number 30) with slices covering the level of the thalamus. In a subset of 35 patients, the pre-treatment protocol also included an axial WMnMPRAGE (TI: 410 ms, excitation TR: 8.0 ms, TE:3.24 ms, Flip Angle: 8, FOV: 256 mm, acquisition matrix: 256 $\times$ 256, slice thickness: 1.0 mm, slice number 320).

Thalamic Parcellation

Thalamic parcellation was performed on the pre-treatment MRI data with both FreeSurfer and THOMAS (*Figure 4-2*). FreeSurfer (version 6.0) was run on the T1-WI in all patients, parcellating each thalamus into 26 individual nuclei. In the patients with pre-treatment WMnMPRAGE data, THOMAS (version 2.0) was run on both the T1-WI and WMnMPRAGE

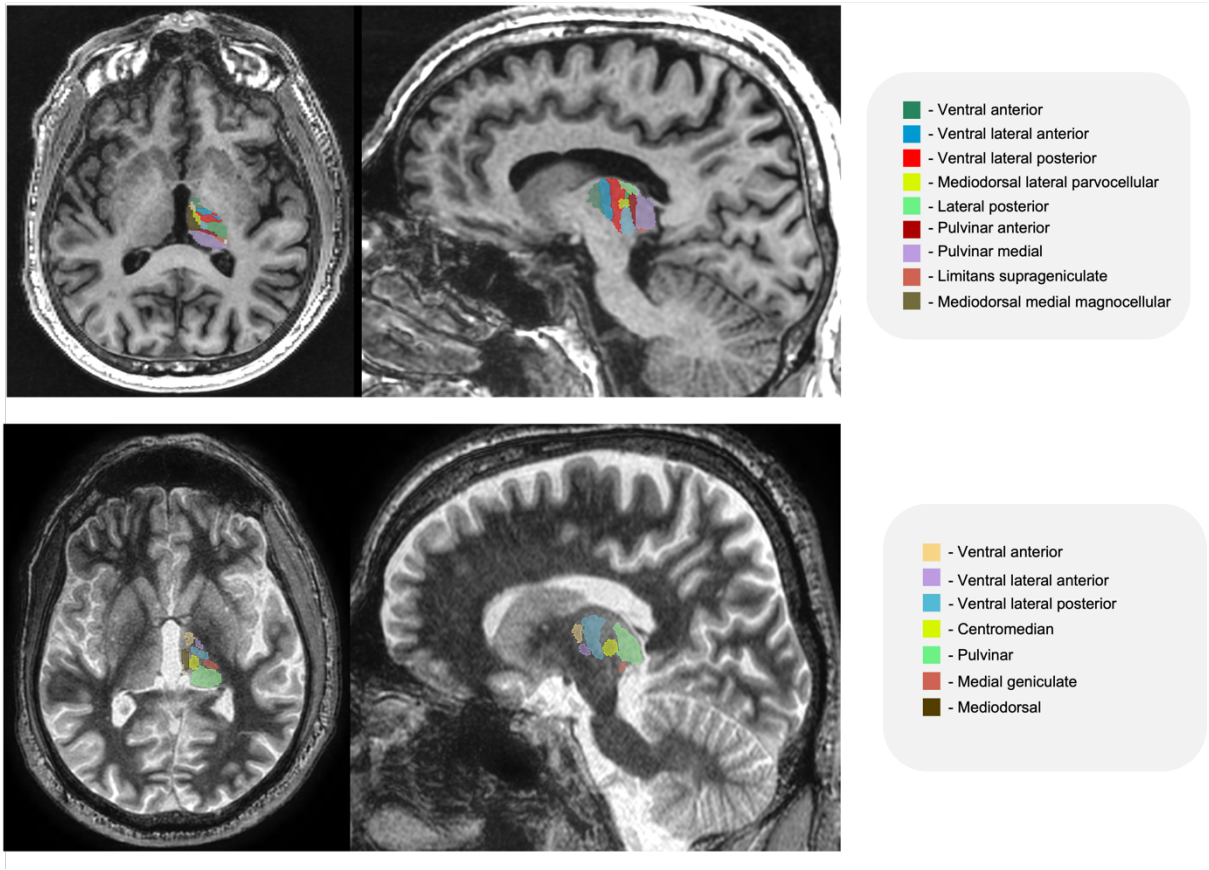

Figure 4-2 ***Top*** *- Axial (****left****) and sagittal (****right****) view of FreeSurfer thalamic segmentation overlayed on T1-WI.* ***Bottom*** *- Axial (****left****) and sagittal (****right****) view of THOMAS thalamic segmentation overlayed on WMnMPRAGE.*

($THOMAS_{T1}$ and $THOMAS_{WMn}$ respectively), parcellating the thalamus into 11 individual nuclei. Both FreeSurfer and THOMAS parcellations schemes included the VLp nucleus, which approximately corresponds to Hassler's Vim[407], with the VLp segmentation generated with THOMAS further subdivided into dorsal (dVLp) and ventral (vVLp) components.

Segmentation of Ablation Site

The tcMRgFUS ablation site was identified on the T1-WI acquired immediately after the tcMRgFUS procedure. The post treatment T1-WI was first linearly co-registered to the pre-treatment T1-WI with FSL-FLIRT (version 6.0)[390]. The post-treatment T2-weighted image was linearly co-registered to the pre-treatment T1-WI and overlayed to assist in demarcation of

the ablation boundary. To avoid including vasogenic oedema in the ablation segmentation, only the T1 iso-intense ablation core and hypointense rim were included in the segmentation, corresponding to ablation zones 1 and 2[309]. Ablation site demarcation was performed with ITK-SNAP (version 3.6.0)[335].

Vim Ablation Overlap Calculation

Following parcellation of the thalamus into the discrete nuclei, the amount of overlap between the tcMRgFUS ablation and each nucleus was calculated by multiplying a binary mask of each nucleus with a binary mask of the ablation site. The volume of non-zero voxels in this overlap mask was calculated to provide the volume of ablated tissue contained within each FreeSurfer/THOMAS derived thalamic nucleus. This overlap volume was then divided by the total ablation volume, to give the fraction of the total ablation volume contained within each thalamic nucleus.

The ablated volume overlapping with the VLp segmented by FreeSurfer $THOMAS_{WMn}$ and $THOMAS_{T1}$, as a fraction of the total ablation volume, were compared with a pairwise t-test. Additionally, the Vim ablation overlap was compared between the dVLp and vVLp segmentations provided by $THOMAS_{WMN}$. Bonferroni correction was applied for multiple comparisons, and the statistical significance level was set to 0.05.

Inter-Subject Registration

For patients in whom an WMnMPRAGE was acquired, a probabilistic target was generated by non-linearly warping the ablated volume to the publicly available WMnMPRAGE group template published by Su et. al. [255]. The non-linear deformation field was generated with ANTS (version 2.2.0)[416], using the WMnMPRAGE template as the registration target, and the pre-treatment WMnMPRAGE as the moving image, masking the voxels within the brain of the group template for inclusion in the registration optimisation. The imaging from any subjects who were treated in the right thalamus were flipped along the L-R axis, so that the ablation site was in the left thalamus for all subjects, consistent with the procedure in the original study [255].

The pre-treatment T1-WI was then linearly co-registered to the pre-treatment WMnMPRAGE, and the resultant transformation matrix was concatenated with the non-

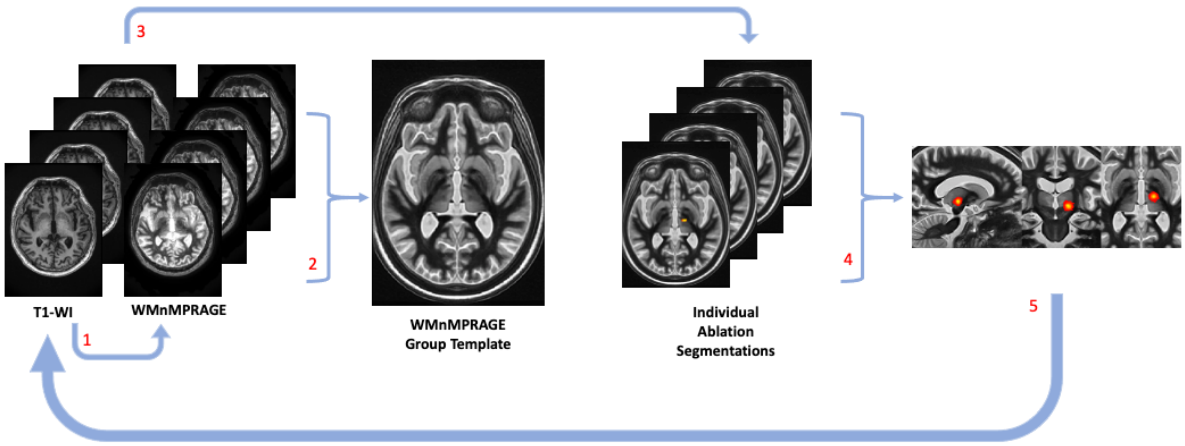

Figure 4-3 Summary of probabilistic target generation. ***1)*** *Pre-treatment T1-WI is linearly registered to pre-treatment WMnMPRAGE.* ***2)*** *Pre-treatment WMnMPRAGE is non-linearly registered to group template.* ***3)*** *Using combined linear and non-linear transformations, ablation segmentation is warped to group template space.* ***4)*** *Ablation segmentations from all subjects are combined in group template space to generate a probabilistic target.* ***5)*** *Probabilistic target is warped back to pre-treatment T1-WI space.*

linear warp of the WMnMPRAGE to the group template, resulting in a single transformation from the pre-treatment T1-WI to the group WMnMPRAGE template. This combined transformation was applied to the ablation segmentation of each subject in the native pre-treatment T1-WI space, warping the ablation segmentation into the group template space (*Figure 4-3*).

The warped ablation segmentations from each subject in the template space were then added together and divided by the number of subjects (N=35). This resulted in a single probabilistic map in which the value of each voxel represents the proportion of subjects for which that voxel was included in the ablation segmentation. The probabilistic target created by Su et al (T_{SU}) was eroded to include only those voxels that were present in the ablations of all subjects. However, as the probabilistic map created in this investigation did not feature any voxels that were present for all 35 subjects, i.e. no voxels with a value of 1, the map was filtered to a threshold value - zeroing those voxels below a certain threshold value, until the volume of the filtered probabilistic map equalled that of T_{SU}. This threshold value was found to be 0.77. The location of the filtered probability map (T_{STUDY}) was compared to T_{SU} by calculating the DICE coefficient and the Euclidian distance between the centre of gravity of the two clusters in the WMnMPRAGE group template space.

4.3.3 Results

Patients and tcMRgFUS Characteristics

73 subjects treated in the defined window were identified. One subject not treated in the Vim was excluded, and 6 subjects in which the post-treatment MRI protocol did not include a 3D volumetric T1-WI were excluded, resulting in a total sample size of 66 subjects. The mean patient age was 73.78 $\pm$ 8.87 years at the time of treatment, and the mean SDR was 0.43 $\pm$ 0.07. An average of 8.48 $\pm$ 2.87 sonications were delivered targeting the Vim, and the average peak sonication temperature reached during the procedure was 62.53 $\pm$ 2.95°C. In 27 of the 66 subjects (41%) additional regions outside of the Vim were also targeted during procedure, however, the effect of these secondary lesions was not considered in this investigation. Patient and treatment characteristics are summarised in *Table 4-1*.

Comparison of Thalamic Segmentations

Table 4-1 Patient and tcMRgFUS treatment characteristics.

Variable	**All patients N=66**
Sex, n(%)	
Male	52 (79)
Female	14 (21)
Age, mean $\pm$ SD, years	73.78 $\pm$ 8.87
Treatment Side, n(%)	
Left	50 (76)
Right	16 (24)
Treatment Target, n(%)	
Vim Only	31 (47)
Vim & Secondary (PSA or Voa)	35 (53)
Number of Vim Sonications	8.48 $\pm$ 2.87
Peak Temperature (°C)	62.53 $\pm$ 2.95

Abbreviations used: SD (Standard Deviation), Vim (Ventral Intermediate Nucleus), PSA (Posterior Subthalamic Area), Voa (Ventralis Oralis Anterior).

An example of the VLp and VLa segmented with $THOMAS_{WMN}$ (VLp_{WMN}) and FreeSurfer (VLp_{FS}) are displayed in *Figure 4-4*. The volume of the VLp segmentations were 764.84 ± 97.54 mm^3, 758.23 ± 98.07 mm^3 and 751.99 ± 123.65 mm^3 for the VLp_{FS}, VLp_{WMN} and the $THOMAS_{T1}$ VLp (VLp_{T1}), respectively, however, these differences were not found to be statistically significant. The VLp_{T1} was generally located laterally and anterior relative to the VLp_{WMN}, however, there was reasonable agreement between the two THOMAS segmentations, with a mean DICE coefficient of 0.72 ± 0.10. Agreement between THOMAS VLp segmentations and the VLp_{FS} was considerably lower, with a mean DICE coefficient of 0.54 ± 0.05 and 0.40 ± 0.07 for the VLp_{WMN} and VLp_{T1}, respectively. For both THOMAS

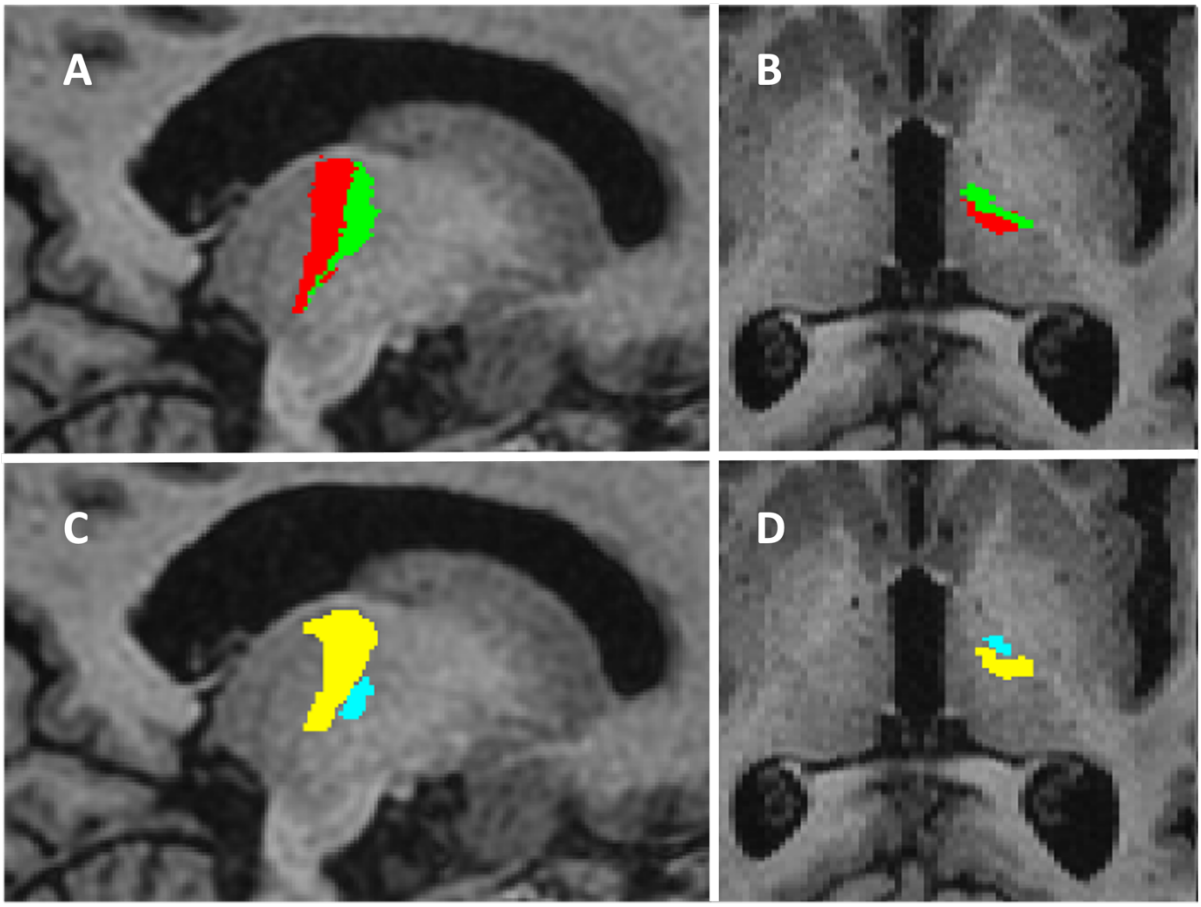

Figure 4-4 Example of FreeSurfer and $THOMAS_{WMn}$ VLp and VLa segmentations, overlayed on the pre-treatment T1-WI. ***A & B*** *– Axial and sagittal view of FreeSurfer VLp (red) and VLa (green).* ***C & D*** *- Axial and sagittal view of $THOMAS_{WMn}$ VLp (yellow) and VLa (blue).*

methods, the VLp was located further anteriorly to the VLp_{FS}, corresponding more closely to the combined FreeSurfer VLa_{FS} and VLp_{FS} (VL_{FS}). There was a greater agreement between the THOMAS VLP and VL_{FS}, with the mean DICE coefficient between the VLp_{WMN} and VL_{FS} of 0.64 ± 0.04, and 0.57 ± 0.07 between the VLp_{T1} and VL_{FS}.

tcMRgFUS Ablation

The mean (± SD) total Vim ablation volume across all patients was 134.33 ± 60.11 mm^3, of which an average of 63.28 ± 41.99 (44.71 ± 19.07%) was within the FreeSurfer defined thalamus. All 66 patients had some degree of lesioning within the FreeSurfer defined Ventral lateral anterior (VLa_{FS}) and Ventral lateral posterior (VLp_{FS}) nuclei. The mean percentage of the ablation volume within these two nuclei, as a proportion of total ablation volume, was 11.97 ± 4.66% and 28.36 ± 13.91%, respectively.

In the subset of subject in which THOMAS was used, of the thalamic nuclei segmented by THOMAS, the Vim ablation site overlapped almost exclusively with the VLp. The mean percentage of total ablation volume within the VLp_{WMN} and VLP_{T1} was 23.02 ± 12.86% and 17.41 ± 11.25% respectively. There was little overlap of the ablation with any other nuclei segmented by THOMAS; no other nuclei had a mean overlap greater than 0.01% of total ablation volume. Pairwise paired t-test analysis of the ablation overlap with the VLp segmented with the 3 methods showed that the overlap as a percentage of the total ablation volume was significantly lower in the VLp_{T1} compared with the VLp_{WMN} ($p<0.001$). The relative overlap was on average lower in the VLp_{FS} (21.83 ± 9.77%), however, this was not significantly lower than the VLp_{WMN} ($p=0.265$). The comparison in ablation overlap with

the VLp segmented with the 3 methods is summarised in *Figure 4-5*. When the overlap with the THOMAS generated dorsal and ventral VLp segmentations was compared, the ablation overlap was shown to overlap exclusively with the vVLp, with 0 overlapping ablation volume found with the dVLp.

Inter-Subject Registration

The two probabilistic targets (T_{STUDY} and T_{SU}) are shown in *Figure 4-6*. The maximum value of the T_{STUDY} was 0.94. A maximum value less than one indicated that there were no voxels that

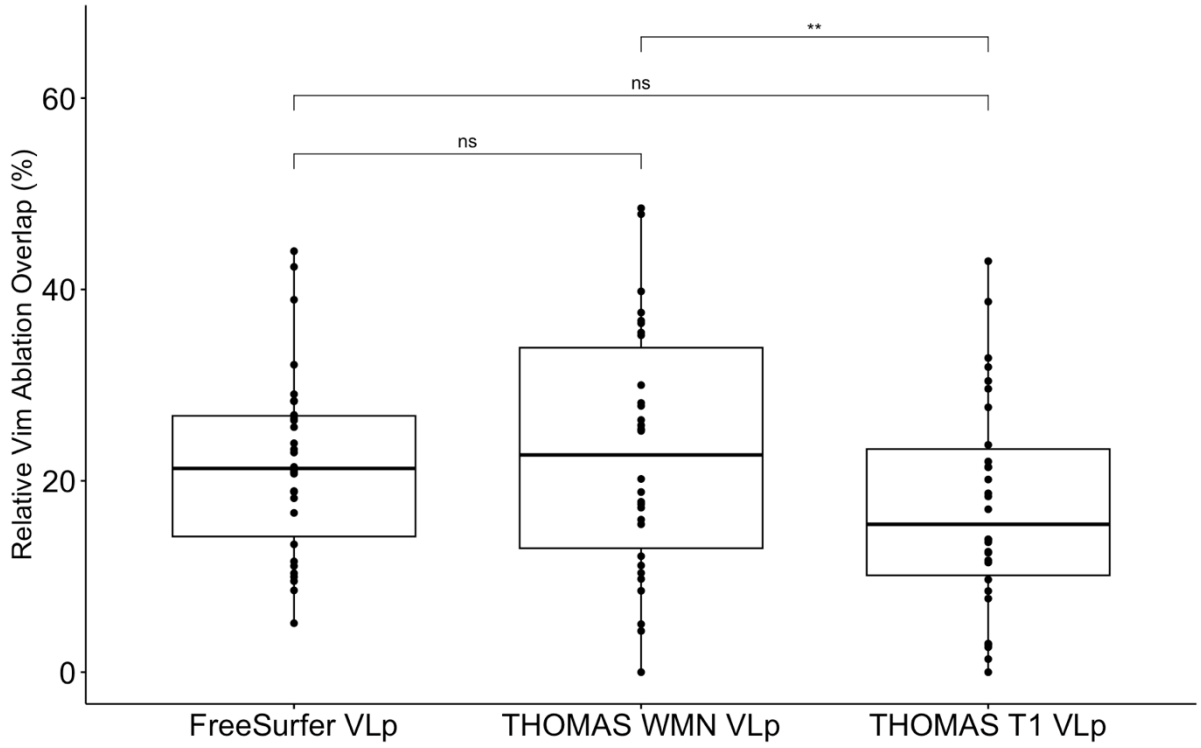

Figure 4-5 Percentage of ablation volume contained within the VLp defined by FreeSurfer, $THOMAS_{WMn}$ and $THOMAS_{T1}$ for the 35 subjects with pre-treatment WMnMPRAGE. Lower and uppers box bounds indicate the interquartile range, solid horizontal line indicates the median value, vertical line indicates the minimum and maximum values.

**indicates significance <0.001, ns indicates no significance.

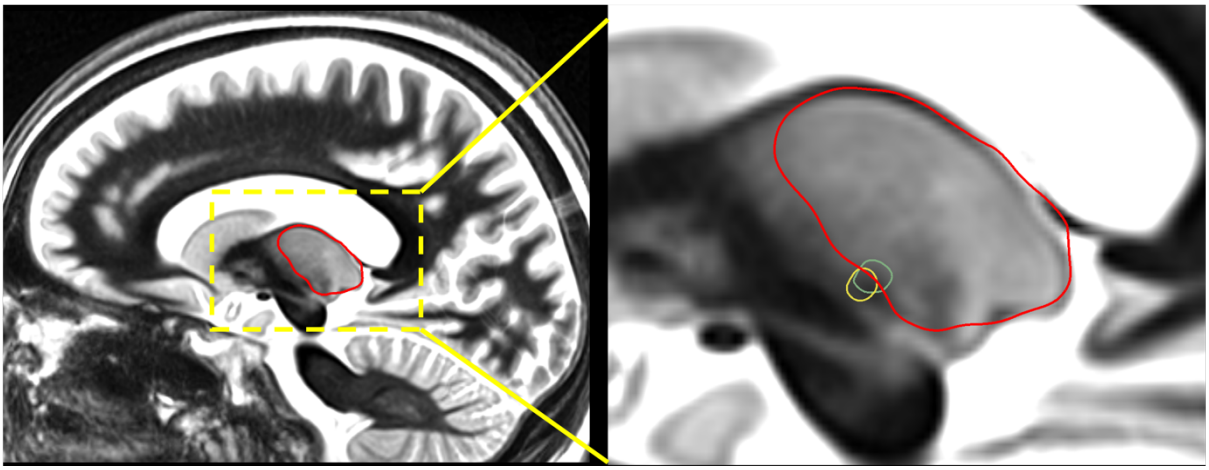

Figure 4-6 Sagittal view of probabilistic target regions in the WMnMPRAGE template space, overlayed on the average FreeSurfer thalamic segmentation (red). T_{SU} shown in green, and T_{STUDY} shown in yellow.

were present in the ablation segmentation of all 35 subjects. The DICE coefficient between T_{STUDY} and T_{SU} was 0.51, and the Euclidian distance between the centre of gravity (COG) of the two clusters in the group template space was 1.33mm. The COG of T_{STUDY} was located lateral, anterior and inferior to T_{SU}.

4.3.4 Discussion

The primary goal of this study was to investigate the potential clinical utility of automated thalamic parcellation of structural imaging for use in tcMRgFUS planning, by retrospectively comparing the degree of overlap between the segmented thalamic nuclei, and the ablated volume in lesions targeting the Vim. Additionally, we sought to generate a probabilistic target, for comparison with the target region published by Su et. al.

The VLp segmentations produced by the two THOMAS methods (VLp_{WMn} and VLp_{T1}) demonstrated the most substantial agreement, with an average DICE of 0.72. This result was expected as the two algorithms are fundamentally the same, only differing in the input image contrast. The agreement between the VLp segmented with THOMAS compared to that of FreeSurfer (VLp_{FS}) was modest. Agreement was greatest between VLp_{FS} and VLp_{WMn}, with an average DICE of 0.54. The observed differences in the boundaries of the VLp between $THOMAS_{WMn}$ and FreeSurfer can likely be attributed to the different segmentation algorithms, with each segmenting on a different image contrast, as well as the different thalamic parcellation schemes employed by the two methods. Without ground-truth histological data, it is not possible to comment on which algorithm provides the most accurate VLp segmentation, however, the overlap with Vim ablation in this study provides an indication of concordance with the conventionally defined Vim coordinates.

When examining only the FreeSurfer thalamic nuclei in all 66 patients, the VLp_{FS} exhibited the greatest overlap with the ablated volume, with 28% of the ablated volume contained within the VLp_{FS}, while the next greatest overlap was with the VLa_{FS} at 11%. Similarly, in the THOMAS segmentation, the Vim ablation overlapped almost exclusively with the VLp, with an overlap of 23.02% in the VLp_{WMn} (compared with 21.83% in the VLp_{FS} for this subset of 35 patients), while no other nuclei had an overlap greater than 0.01% of the total ablation volume. The slightly greater overlap in the VLp segmented with $THOMAS_{WMn}$, compared with FreeSurfer, may indicate that the THOMAS algorithm provides a more accurate VLp segmentation. However, the differences in overlap were not found to be statistically significant, and further validation against clinical tremor improvement is required. The significantly lower overlap with VLp_{T1} may suggest that the thalamic segmentation produced

with THOMAS on a T1-WI is less reliable than that segmented on a WMnMPRAGE, and thus FreeSurfer may present a more reliable option when a WMnMPRAGE is not available.

The low observed ablation overlap values across all examined methods may be a reflection of the treatment targeting strategy employed at this centre, which while including the Vim, also includes the white matter inferior to the thalamus. This was reflected in the low ablation volume contained within the whole FreeSurfer defined thalamus (44%), which ranged between 10 and 80% in this study. The DRTT is a white matter tract connecting the cerebellum with the thalamus via the red nucleus, entering the thalamus at the level of the Vim, and is a key component in the tremor network. Studies investigating DBS treatment have shown that the proximity of the tip of the DBS electrode to the DRTT was significantly correlated with tremor suppression[417–420]. Similarly, it has been shown that tcMRgFUS ablations overlapping with the DRTT correlated with sustained tremor improvement[421,422]. Thus, any tremor suppression observed in this patient cohort may reflect lesioning of the DRTT, rather than the Vim directly. This treatment strategy of targeting the inferior thalamic floor is also reflected in the comparison of the probabilistic target templates, where a DICE of 0.51 was observed, with the probabilistic target generated with the data from the present study was located inferiorly and anterior to the target published by Su et. al. This difference in coordinates likely reflects the difference in treatment strategies between the two groups, rather than an inaccuracy in the target region.

While the importance of the DRTT in achieving tremor suppression may suggest that direct targeting with dMRI tractography based methods may prove more useful, the relatively high overlap with the FreeSurfer and THOMAS VLp, relative to other nuclei segmented by both algorithms, may suggest that the segmented VLp does include the region corresponding to

the Vim, however, further validation with dMRI tractography and comparison with clinical tremor improvement is required. The VLp segmented by FreeSurfer or THOMAS may provide a useful indirect target for neurosurgeons in identifying the point of DRTT entry to the thalamus in cases where dMRI tractography is not available.

The generation of a probabilistic target provides a promising approach to target localisation, and indeed this was the only target shown to correlate with sustained clinical improvement by Su et al[255]. Generation of a probabilistic target can be completely automated and is computationally efficient, using only a single non-linear registration from a template to the subjects structural imaging data. Such a template may also provide a smaller and more specific target, compared with segmenting the entire VLp. However, as demonstrated in this study, the definition of the probabilistic target region may be influenced by differences in centre-specific treatment strategy, and thus more research is needed to define the optimal target for tremor suppression while avoiding adverse effects.

4.3.5 Conclusion

In this investigation, we compare the overlap of tcMRgFUS ablations targeting the Vim, with the VLp segmented with both THOMAS and FreeSurfer. We demonstrate that the degree of VLp overlap was similar between FreeSurfer and THOMAS run on an WMnMPRAGE, while the overlap with the VLp generated by THOMAS on a T1-WI was significantly lower. However, neither method exhibited high agreement with the Vim ablation. The probabilistic target region generated with data from this patient cohort demonstrated only a moderate

agreement with a previously published target, which may reflect differences in treatment strategies between the two centres.

4.4 Clinical utility of dMRI tractography for tcMRgFUS targeting: Comparisons with thalamic segmentation.

4.4.1 Introduction

As discussed in section 4.3.1, the Vim of the thalamus is a common target for treatment of tremor with tcMRgFUS, and accurate localisation of the target is imperative for successful tremor suppression. Direct targeting of the Vim is complicated by the fact that the borders of the Vim are not visible on standard structural imaging using 3T MRI. The traditionally accepted approach is to use indirect targeting, in which the Vim location is inferred by stereotactic landmarks, however, this approach does not fully account for individual variations in anatomy or the effects of global or regional brain atrophy [286,423].

In section 4.3. the automated thalamic segmentation tools THOMAS [415] and the segmentation algorithm developed by Iglesias et al [413], available in FreeSurfer [414], for defining the VLp, the ventral portion of which includes the Vim[407] were investigated for potential use in identifying optimal treatment coordinates. These segmentation algorithms may benefit clinicians by providing additional information on the otherwise indistinguishable boundaries between each thalamic nuclei, however, further validation with clinical tremor improvement data is required. Furthermore, the low overlap between the VLp segmentations and the Vim ablation reported in section 4.3 suggests that a more specific treatment target may be required.

More recently, dMRI tractography has emerged as a useful technique in defining the connectivity of the thalamus to aid in target selection. Many of the findings from studies of DBS have demonstrated proximity to the DWI tractography generated DRTT and the correlation with tremor suppression [424–428], knowledge which has been translated to treatment with tcMRgFUS. In tcMRgFUS studies, the strongest evidence to date of DRTT involvement comes from several studies examining the microstructural changes along the DRTT and the relationship with clinical outcomes. Thaler et. al. observed that fractional anisotropy (FA) changes at the ablation site and along the DRTT correlated with clinical improvement[429]. Similarly, both Kapadia et al.[296] and Pineda-Pardo et. al. [310] found that FA reduction along the DRTT was correlated with tremor improvement, and that these changes were correlated with the overlap between the DRTT and the ablated volume.

While tractography and thalamic segmentation-based methods for treatment targeting are promising, there remains a lack of consensus around the optimal method and parameters for accurate target definition. In this study, we investigated the overlap between the volume of tissue ablated with FUS and both the FreeSurfer and THOMAS thalamic segmentations, as well as with the tractography derived DRTT, to examine any relationship with tremor suppression. Additionally, we apply a streamline clustering algorithm to conventionally generated DRTT streamlines with the aim of probing the relationship between tremor suppression and ablation of streamlines within the DRTT.

Table 4-2 Patient characteristics

Variable	All patients N=31
Sex, n(%)	
Male	23 (74)
Female	8 (26)
Age, mean ±SD, years	75.72 ± 7.20
Treatment Target, n(%)	
Vim	22 (71)
Vim & PSA	8 (26)
Vim, PSA & VOA	1 (3)

Abbreviations used: SD (Standard Deviation), Vim (Ventral Intermediate Nucleus), PSA (Posterior Subthalamic Area), Voa (Ventralis Oralis Anterior).

4.4.2 Methods

Subjects

This study was a retrospective analysis of data collected from 31 ET patients undergoing tcMRgFUS thalamotomy, targeting the Vim, and in a subset of patients either PSA or Voa nucleus, for treatment of tremor at St Vincent's Hospital Sydney (Australia) between March 2019 and February 2021. All patients met 2018 consensus classification criteria [21] for ET or ETP, herein considered collectively as ET. In accordance with 2018 consensus criteria, patients classified as ETP met criteria for ET but had additional features including subtle dystonia, rest tremor, mild gait ataxia or mild Parkinsonian features. Informed consent was obtained from all participating subjects, and the study was approved by the St Vincent's Hospital Ethics Review Committee (ETH00670). Patient characteristics are summarised in *Table 4-2*.

MRgFUS Procedure

tcMRgFUS was performed as described in sections 1.2.4 and 2.3.2. The initial target coordinates for the Vim were chosen by a neurosurgeon using the conventional stereotactic location 25% of the AC-PC distance anterior to the PC, 14mm lateral to the midline at the level of the intercommissural line and adjusted for individual patient anatomy including width of 3rd ventricle, and proximity to visualised internal capsule. In 9 of the 31 participants (*Table 4-2*), the PSA was additionally targeted where intra-procedural tremor suppression was incomplete after adequate VIM lesioning. In these patients additional lesioning in PSA conferred additional tremor suppression, including proximal upper limb tremor, resulting in a greater clinical benefit at the conclusion of treatment. The coordinates of PSA were similar to those used for PSA DBS, targeting the white matter equidistant between the medial border of the STN and lateral border of the red nucleus at its equator, corresponding to AC-PC coordinates of approximately x=9.5 mm, y=-6.0 mm, z=-5.5 mm. The Voa was additionally targeted in 1 ETP patient with dystonic tremor, in whom tremor relief was incomplete after VIM lesioning alone. In this patient the coordinates for Voa lesioning were 12mm right of midline, 11mm anterior to the posterior commissure and 1.5mm above the commissural plane. Analysis of the effect of these secondary lesions was beyond the scope of this investigation.

Imaging Protocol

MR imaging was acquired 1-7 days prior to treatment and again the day after treatment. Pre-treatment imaging was acquired on a 3 Tesla MRI scanner (SIGNA Architect, General

Electric, Milwaukee), and post-treatment imaging was acquired on a 3T Philips Ingenia (Philips Inc, Amsterdam, The Netherlands).

The pre-treatment imaging protocol included a sagittal 3D IR-FSPGR T1-WI (TI: 450 ms, TR: 8 ms, TE:3.24 ms, Flip Angle: 10^{o}, FOV: 256 mm, acquisition matrix: 256 × 256, slice thickness: 1.2 mm, slices: 146). Additionally, 3 different DWI protocols were acquired; Protocol 1 (N=9): b = 0, 1000 s/mm^2, directions = 64, TR: 9100 ms, TE: 90 ms, Flip Angle: 90^{o}, FOV: 230 mm, acquisition matrix: 128 × 128, slice thickness: 1.8 mm, slices: 72. Protocol 2 (N=15): b = 0, 700, 1000, 2800 s/mm^2, directions = 140, TR: 6250 ms, TE: 106 ms, Flip Angle: 90^{o}, FOV: 230 mm, acquisition matrix: 128 × 128, slice thickness: 1.8 mm, slices: 72. Protocol 3 (N=7): b = 0, 700, 1000, 2800 s/mm^2, directions = 140, TR : 7970 ms, TE: 102 ms, Flip Angle: 90^{o}, FOV: 232 mm, acquisition matrix: 116 × 116, slice thickness: 2.0 mm, slices: 70.

The post-treatment protocol included an axial 3D IR-FFE T1-WI (TI: 450 ms, TR: 7.9 ms, TE:2.6 ms, Flip Angle: 8^{o}, FOV: 240 mm, acquisition matrix: 240 × 240, slice thickness: 1.0 mm, slices: 170).

Segmentation of Ablation Site

The FUS ablation site was identified and demarcated on the post-treatment T1-WI. The post treatment T1-WI was first linearly co-registered to the pre-treatment T1-WI with FSL-FLIRT[390]. To avoid including vasogenic and cytotoxic oedema, only the T1 iso-intense lesion core was included in the segmentation (*Figure 4-7*), corresponding to ablation zone 1[430]. The segmentation was performed with ITK-SNAP[335] by a trained neuroimaging analyst. While

zone 2 can also form part of the final lesion necrotic core and is commonly included in ablation segmentations, zone 1 was isolated to improve the specificity of ablation overlap measurements and reduce the risk of artificially inflating overlapping volumes with regions that may not form part of the necrotic core.

Thalamic Parcellation

Two automated methods for segmentation of the thalamus described in section 4.3, THOMAS and FreeSurfer, were applied to the pre-treatment T1-WI: THOMAS and FreeSurfer. The FreeSurfer thalamic segmentation module segments the thalamus into 26 thalamic nuclei, while THOMAS segments the thalamus into 11 nuclei. Both atlases provide a segmentation of the VLp, as per the Morel nomenclature[408], which includes the supposed location of the Vim as labelled by Hassler[431]. Both thalamic segmentation techniques result in a hard segmentation, whereby each voxel in the segmented volume can belong to only one category, i.e., unique thalamic nuclei.

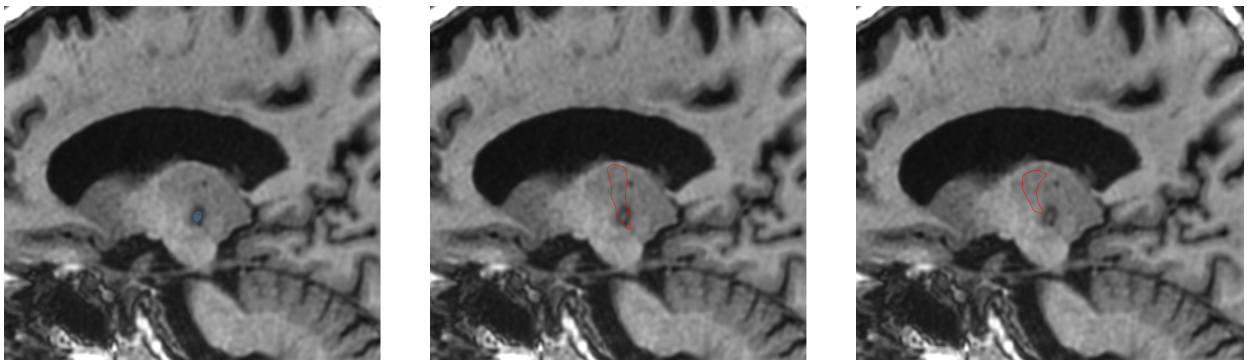

*Figure 4-7 (**Left**). Example of ablation core segmented on T1-WI acquired 1 day post treatment. (**Middle**). FreeSurfer segmented VLp overlayed on day 1 T1-WI. (**Right**). THOMAS VLp overlayed on day 1 T1-WI.*

Brain Tissue Volumes

The T1-WI was n4 bias corrected and skull-stripped using an in-house AI-based brain extraction algorithm, followed by manually correction when necessary. A skull mask was generated using FSL-BET[432], and the images were processed with FSL-SIENAX[433] to derive estimates of absolute and skull size normalised whole brain, and substructure volumes.

The brain extracted T1-WIs from all subjects were combined to generate an unbiased template T1-WI using buildtemplateparallel in ANTS[416]. Region of interest (ROI) masks were generated on the pre-treatment T1-WI for use in diffusion MRI tractography. Masks of the thalamus and precentral gyrus were extracted directly from the FreeSurfer segmentation and transformed to the native DWI space. Masks of the dentate nucleus and red nucleus were defined manually on the template T1-WI and transformed to the native T1-WI via non-linear registration using the inverse warp generated during the T1-WI template construction described above.

Diffusion MRI Processing

The diffusion MRI data was processed using the default MRtrix3[434] pipeline. Briefly, the raw DWI data were denoised, corrected for Gibb's ringing, susceptibility distortion, eddy current corrected and bias field corrected. Fibre orientation distributions (FOD)[435] were estimated using single-shell multi-tissue spherical deconvolution[436] for the single shell data (protocol 1), and multi-shell multi-tissue spherical deconvolution[437] for the multi-shell data (protocols 2 and 3). Probabilistic fibre tracking[438] was used to reconstruct the DRTT, seeding in the

dentate nucleus, with inclusion masks in the contralateral red nucleus, thalamus and pre-central cortex[439]. Fibre tracking was terminated after 3000 streamlines satisfied the inclusion criteria, and then reduced to the 1000 most coherent streamlines with DIPY[440].

DRTT Cluster Segmentation

Due to the large size of the tractography inclusion masks, the path of the resultant streamlines through the thalamus exhibited several common paths, or clusters (*Figure 4-8*). To determine which of these clusters was the most clinically relevant target, we created unbiased template clusters, which were warped and analysed in the individual subject space.

The white matter FOD of each subject was first processed to generate a total apparent fibre density (AFD) map, which gives the total density of all fibre populations within each voxel[441].

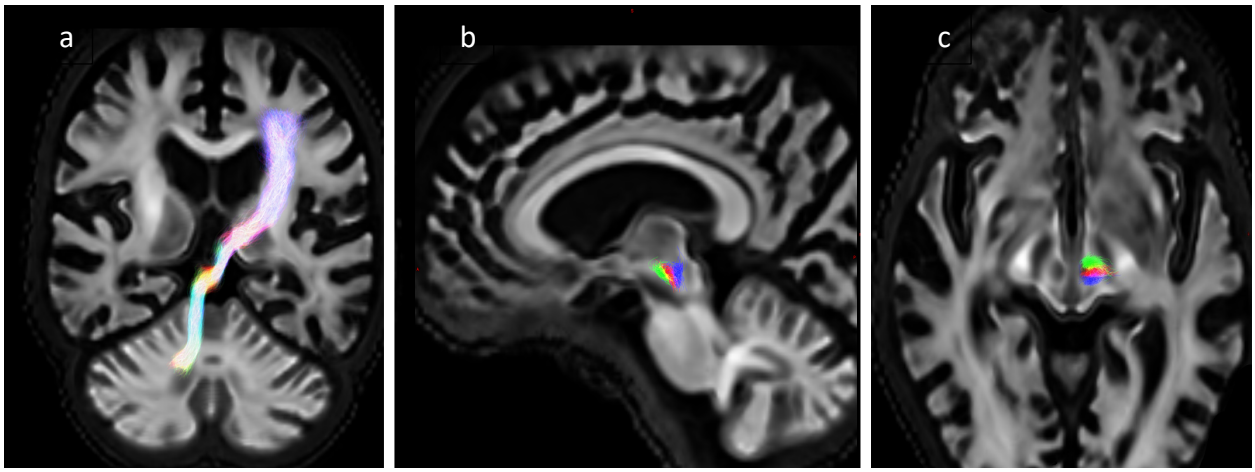

*Figure 4-8 . (**a**) - Obliqued coronal view of native DRTT trajectory. (**b & c**) - Sagittal and axial view of 3 template DRTT clusters in a single slice – anterior (green), middle (red) and posterior (blue).*

The AFD images were combined to generate an unbiased template image using the command buildtemplateparallel in ANTS. Ten subjects were selected at random, and the native DRTT streamlines were warped to the AFD template. For each of the 10 subjects, the DRTT in the template space was split into 3 clusters – anterior (aDRTT), middle (mDRTT) and posterior (pDRTT), based on the trajectory of the streamlines between the red nucleus and thalamus using QuickBundles[442] in DIPY, an automated algorithm that groups streamlines together based on the similarity of location in space of each point along the entire streamline. Anterior, middle, and posterior clusters were chosen due to the simplicity of implementation in a systematic fashion across multiple subjects. Adjustments to the threshold value in QuickBundles can be used to increase/decrease the number of clusters in the data. For each subject, the threshold value was incrementally increased until the resultant clusters included a posterior, middle and anterior component, as determined by manual inspection of the path of the cluster centroids. The selected cluster centroids were isolated, and each streamline in the full warped streamline set was assigned to one of the

three clusters based on the path similarity between each streamline and the cluster centroid. While more than 3 clusters may have been present in the clustered data, streamlines were assigned to only one of the 3 selected clusters, corresponding to posterior, middle and anterior clusters (*Figure 4-8*).

For each cluster, the streamlines from each subject were combined and filtered down to the 1000 most coherent streamlines for that cluster, resulting in 3 template streamline bundles. Each bundle was warped back to the native DWI space of each subject. This process was performed independently for the left and right DRTT.

Ablation Overlap

The overlap between the ablation segmentation and the tractography was assessed by counting the number of streamlines that pass through the segmentation and dividing by the total number of streamlines in the bundle, where an overlap of 100% represents complete transection of the fibre tract. For each subject, there were 4 tracts: the DRTT generated from the native DWI data, and the 3 template bundles described above (aDRTT, mDRTT and pDRTT). An example of the native DRTT, and 3 template clusters is shown in *Figure 4-8*.

The overlap of the ablation segmentation with each of the thalamic nuclei generated by FreeSurfer and THOMAS was calculated by multiplying each nuclei segmentation with the ablation segmentation mask and calculating the volume of the resulting overlap mask. The ablation overlap was calculated individually with all regions defined by the two atlases, to determine if the ablation overlap with any region was predictive of clinical outcome.

MRgFUS Treatment Parameters

Patient skull characteristics such as SDR, are often communicated with a single value, however, these values are not necessarily consistent across the entire skull. Measurements are taken along the beam from each of the 1024 elements in the ultrasound array, and the mean value is typically used clinically. Given the array of values, it is possible to calculate additional summary statistics, such as the standard deviation. For each subject, the tcMRgFUS treatment parameters were extracted from the ExAblate console. The patient specific parameters included the SDR, skull thickness (ST), and inner and outer skull angle. For each parameter, a value was extracted for each of the 1024 elements in the ultrasonic array, and both the mean and standard deviation for each parameter was calculated for use in subsequent statistical analysis.

Treatment specific parameters including the maximum temperature reached during the procedure, the number of active elements of the first sonication, the number of total sonications and the sum of temperature delivered across all sonications were also extracted.

Clinical Assessment

Clinical evaluation of each patient was performed by a neurologist prior to treatment and again at regular intervals up to 36 months following treatment. The mean ($\pm$ SD) length of the clinical follow-up visit from the treatment date was 16.0 $\pm$ 10.9 months. The evaluation

included CRST [336] and HTS [247], as described in section 1.1.5. As not all subjects returned for all follow-up evaluations, the latest available CRST and HTS score for each subject was used to assess tremor change following treatment. As the absolute change in tremor scores can be expected to be greater in subjects with greater pre-treatment scores, percentage change in each tremor score was calculated such that a positive value indicated a reduction in tremor score.

Statistical Analysis

Predictors of tremor suppression were assessed via multivariate linear regression by forward selection. Each predictor was added to the model individually, and the predictor with the lowest p-value under 0.05 was chosen to be included in the model. This process continued iteratively until there were no remaining predictors with a p-value less than 0.05. An initial model was constructed including only patient specific pre-treatment variables including age, sex, brain tissue volumes, SDR, skull thickness, and inner and outer skull angle and pre-treatment tremor scores. Treatment specific parameters including ablation volumes and overlap with the DRTT and thalamic nuclei segmentations, maximum temperature reached during the procedure, the number of active elements, the number of total sonications and the total sum of temperature delivered were then individually added to the model and again chose by forward selection. The goodness of fit of this more complex model was then compared to the baseline model via ANOVA comparison of residual sum of squares.

This process was repeated using all subcomponents of CRST ($CRST_A$, $CRST_B$ and $CRST_C$), CRST, and the dominant and non-dominant hand HTS values (HTS_D and HTS_{ND}) as the dependent variable.

To remove any effect of secondary lesions on the observed statistical relationships, the statistical analysis was repeated for any statistically significant predictors, after exclusion of the 9 subjects who were lesioned in a secondary region outside the Vim.

All statistical analysis was performed using the R (version 4.2.2) statistical software package with RStudio (Version 1.4.1717, RStudio, Inc., Boston, MA URL, http://www.rstudio.com).

4.4.3 Results

Clinical Outcomes

Clinical scores are summarised in *Table 4-3*. The mean reduction in CRST at the most recent follow-up visit was 44.77 $\pm$ 16.6%, while the mean reduction in HTS_D and HTS_{ND} was 62.58 $\pm$ 18.77% and 3.48 $\pm$ 23.90%, respectively. Both CRST and HTS_D were reduced in all 31 participants, while HTS_{ND} was reduced in 17 subjects.

Table 4-3 Mean change in tremor scores between pre-treatment and the most recent clinical visit following treatment with tcMRgFUS

Variable	Pre-Treatment	Post Treatment	Tremor Change (%)
CRST			
Part A	23.10	13.16	41.69
Part B	21.48	13.45	38.60
Part C	14.68	6.67	56.31
Total	60.03	33.68	44.77
HTS			
Dominant Hand	19.03	7.48	62.58
Non-dominant Hand	16.19	15.52	3.48

Abbreviations used: CRST (Clinical Rating Scale for Tremor), HTS (Hand Tremor Score)

Ablation Volumes

The mean ablation core volume at one day post treatment was 11.61 ± 4.82 mm^3. The FreeSurfer defined nuclei with the greatest overlapping ablation volume was the ventral lateral posterior (VLp) nucleus 5.13 ± 3.64 mm^3 followed by the ventral lateral anterior (VLa) 2.30 ± 2.02 mm^3. Similarly, the VLp defined by THOMAS showed the greatest overlap with the ablation (2.51 ± 2.90 mm^3), consistent with the findings reported in section 4.3.

The percentage of streamlines overlapping with the ablated volume are shown in *Figure 4-9*. Overlap with the ablation was greatest in the mDRTT (28.35 ± 11.66%), followed by the pDRTT (25.28 ± 12.14%), and aDRTT (21.79 ± 10.56%) clusters, and the native DRTT (20.86 ± 11.33%). The ablation overlap with the native DRTT was significantly correlated with both the mDRTT and pDRTT clusters (r = 0.445 and 0.473 respectively), per Pearson correlation

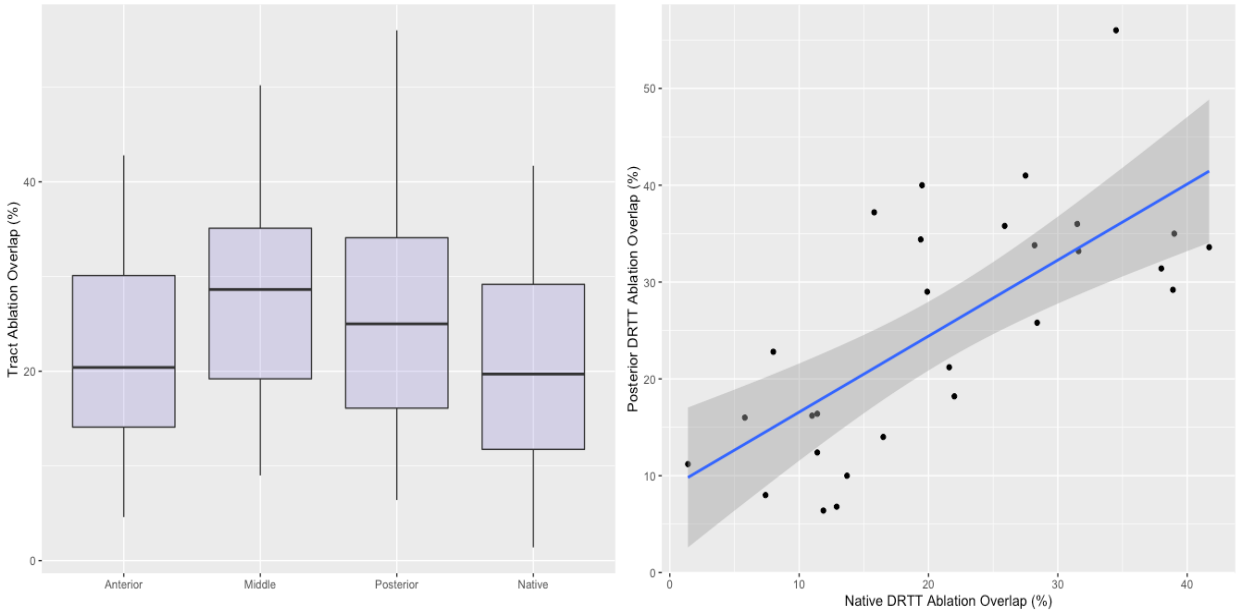

*Figure 4-9 (**Left**). Boxplots displaying the ablation overlap for the native DRTT and 3 template DRTT clusters. (**Right**). Correlation between the ablation overlap between the native DRTT and the posterior template DRTT. Line of best fit indicated by blue line, and 95% confidence interval indicated by shaded region.*

analysis, however, the correlation was stronger with the posterior cluster (R^2=0.224) than the middle cluster (R^2=0.198), indicating that the path of the native DRTT through the thalamus more closely followed that of the pDRTT. Pearson correlation between the ablation overlap of the native DRTT and aDRTT was not statistically significant (r=0.263, p=0.105).

Predictors of Tremor Suppression

Multivariate linear regression, with percentage CRST change as the dependent variable revealed that of the patient specific parameters, age (β=-0.375, p=0.006) and SDR standard deviation (SDR_{SD}) (β=-0.324, p=0.015) were statistically significant predictors. After addition of treatment specific parameters to the model, total ablation core volume (β=0.318,

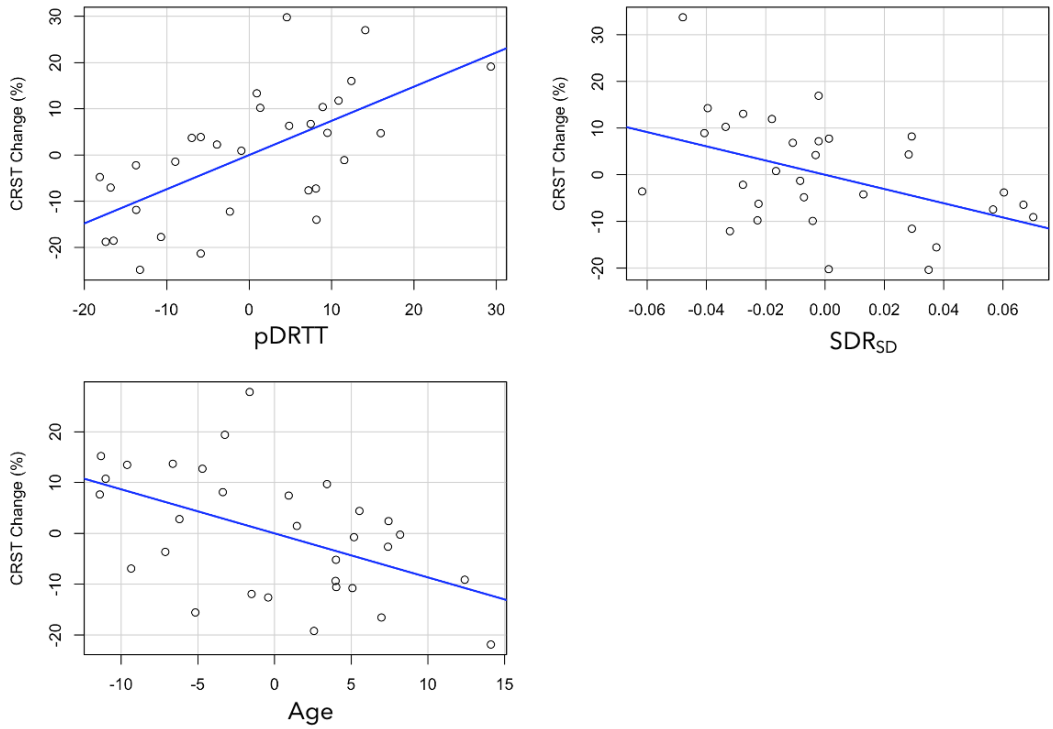

*Figure 4-10 Partial plots from multi-variate regression with CRST change as dependent variable for pDRTT (**top left**), SDR_{SD} (**top right**) and age (**bottom left**). All variables are mean centered.*

p=0.023) and pDRTT overlap (β=0.533, p<0.001) were also statistically significant predictors (*Figure 4-10*), however, the model including pDRTT as a predictor (R^2 = 0.548) provided a significantly better model fit, per ANOVA model comparison (p< 0.001), while the model including the total ablation core volume (R^2 = 0.408) did not provide a significant model improvement (p=0.08).

Replacement of CRST with each of the CRST subcomponents revealed that pDRTT overlap was a significant predictor of $CRST_A$ (β=0.452, p=0.007) and $CRST_B$ (β=0.377, p=0.040) change, while it was not a significant predictor of change in $CRST_C$. SDR_{SD} was approaching significance for $CRST_A$ change (β=-0.319, p=0.052), but was not a significant predictor of

change in $CRST_B$ or $CRST_C$. Patient age was not a significant predictor of change in any CRST subcomponent.

Change in HTS_D was found to be significantly negatively associated with age (β=-0.576, p<0.001) while the relationship with SDR_{SD} was approaching statistical significance (β=-0.256, p<0.081). HTS_{ND} change was found to be significantly associated with pDRTT overlap (β=0.472, p=0.006). No treatment specific metrics, brain tissue volumes or pre-treatment tremor scores were found to be significant predictors of percentage change in CRST or HTS.

When the analysis was repeated excluding the 9 patients with secondary lesions, pDRTT overlap remained a significant predictor of change in $CRST_A$ (β=0.588, p=0.006), CRST (β=0.562, p=0.003) and HTS_{ND} (β=0.522, p=0.016). SDR_{SD} was a significant predictor of change in $CRST_A$ (β=-0.401, p=0.038) and CRST (β=-0.383, p=0.022), and approaching significance for HTS_D change (β=-0.365, p=0.056).

Ablation overlap volumes with the THOMAS and FreeSurfer derived thalamic segmentations were not found to be significant predictors of CRST or HTS change.

4.4.4 Discussion

In this study, we sought to investigate the relationship between the change in tremor scores following treatment with tcMRgFUS, and the location of the ablated volume in relation to a number of potential targeting methods.

We observed a significant relationship between the degree of DRTT lesioning and tremor suppression at follow-up, following treatment with tcMRgFUS. Our results suggest that while the middle DRTT cluster is the region most consistently lesioned across all subjects, it is the degree of posterior DRTT lesioning that has the greatest impact on tremor suppression. These results do not necessarily suggest that surgeons should forgo targeting of the middle DRTT in favour of the posterior region, rather, it is perhaps the extension of the lesion into the posterior fibres that has resulted in the additional clinical benefit observed in this patient cohort, consistent with the findings of Pineda-Pardo et al.[391] and Boutet et al.[276] who found that clinical improvement was corelated with more posteriorly placed lesions.

The presence of the non-decussating DRTT (nd-DRTT) might explain the importance of the posterior region of the DRTT in achieving optimal clinical outcomes. The nd-DRTT consists of fibres that do not decussate from the dentate nucleus to the contralateral red nucleus and thalamus, representing around 20% of the total DRTT fibres[294]. The course of the nd-DRTT is medial and posterior to the d-DRTT[425], and it has been postulated that the Vim is located at the point of anterior-posterior fading between these two tracts[443]. Thus, the results presented here could indicate that extension of the ablation into the posterior region of the DRTT, towards the region typically occupied by fibres of the nd-DRTT could result in improved clinical outcomes. While this hypothesis is supported by our finding that tremor in the non-dominant hand was significantly associated with pDRTT lesioning, while tremor in the dominant hand was not, further studies specifically designed to investigate these findings are warranted.

The methodology presented in this work for isolation of the posterior fibres of the DRTT has the potential to provide a more specific fibre tract than the conventionally generated DRTT. Such methods require extensive validation before they can be adopted for treatment targeting, however, the results presented here suggest further investigation into this method is warranted. We believe that while the native DRTT is not incorrect, the probabilistic tractography algorithm often required to generate the d-DRTT can result in additional unrealistic spurious streamlines that need to be pruned to reveal the true course of the DRTT. By defining this course in a template space and then warping the streamlines to individual subject space, we alleviate the impact of non-realistic streamlines, and through use of the AFD image to generate the non-linear warp field, we retain the intra-thalamic contrast necessary to accurately define the region of interest.

Although not as significant as pDRTT overlap, we observed that the total lesion core volume was also a significant predictor of percentage CRST reduction; however, this relationship is likely owing to the strong correlation between the total lesion core volume and the pDRRT overlap ($r=0.643$, $p<0.001$), which is supported by our finding that inclusion of the total lesion volume did not significantly improve the model for CRST change. Lesion volume in the FreeSurfer and THOMAS-derived VLp segmentation did not correlate with improvement in any tremor score, consistent with the findings of section 4.3, where the agreement with the VLp segmentation and Vim ablation were modest. This result may be a consequence of the fact that both methods segment the entire VLp, rather than the Vim specifically, resulting in a less specific target volume.

In addition to the location of the tcMRgFUS lesion, the effectiveness of treatment is also limited by the ability to achieve sufficient tissue destruction to create long lasting microstructural change. A number of patient characteristics such as SDR [271,352,359–361,371,386], and skull angle[359] have previously been shown to be important factors in the delivery of thermal energy to the treatment target. It is well documented that lower SDR results in less efficient energy transmission across the skull, requiring greater sonication power to achieve the same temperature elevation. However, numerous studies have demonstrated that successful tremor suppression can still be achieved at low SDR, by delivery of longer duration, low temperate doses [271,352,359–362,371,386]. The results of this investigation suggest that it may be the distribution in SDR values across the skull, rather than the mean value, that is more relevant for achieving clinically effective lesions and thus optimal outcomes, consistent with the findings reported in section 3.4.

Our finding that older age was negatively associated with sustained tremor reduction is consistent with previous findings[444] and highlights the importance of patient age as well as SDR, in the screening of appropriate patients for treatment of tremor with tcMRgFUS.

This study had several limitations. The variation in DWI protocol across subjects undoubtedly contributed additional variance to the DRTT measurements, however, ANOVA analysis of the results between the 3 protocols revealed that there was not a systematic difference in metrics derived from the different protocols. Additionally, a lack of follow-up imaging data limited the image analysis to cross-sectional, preventing analysis of microstructure change in the DRTT. The inclusion of subjects treated in additional regions

outside of the Vim may have influenced the results, however, repetition of the statistical analysis with these subjects excluded did not change the outcomes of this investigation.

4.4.5 Conclusion

In this investigation, we report that CRST improvement following lesioning of the Vim with tcMRgFUS was predicted by patient age, SDR standard deviation, and the degree of the lesioning in the posterior DRTT. Lesion volume in the FreeSurfer and THOMAS derived VLp was not associated with change in tremor scores. These results may suggest that tractography-based methods could provide more specific treatment target compared with atlas-based methods, however, further validation is required before such techniques can be adopted clinically.

4.5 Ventral intermediate nucleus ablation alone or additional posterior subthalamic area lesioning?

4.5.1 Introduction

In section 4.4 it was found that in patients treated in the Vim, the degree of lesioning of the posterior DRTT was significantly associated with tremor improvement. However, in this section the presence of secondary lesions in the PSA or Voa was ignored. While it has been demonstrated that targeting the Vim with a tcMRgFUS lesion is an effective strategy for the treatment of ET [192,246,250,445]; other regions of the brain have been explored, that follow trends from the RF and DBS literature [403–405]. There is promising evidence for single tcMRgFUS lesioning of the PSA, which encompasses the zona incerta (ZI) and highly dense cerebellar afferents to the thalamus via the preleminiscal radiation[248,249,406]. It has been suggested that these dense cerebellar afferent projections in the PSA are more important for tremor control, especially those with a proximal origin[446]. Another conceptual motivating factors for targeting the PSA is the avoidance of paresthesia associated with lesions encroaching on the ventralis caudalis (VC) nucleus[276]. Recently, the unit at the Imperial College London have published on a hybrid approach to tcMRgFUS lesioning in ET. This involves a primary lesion to the anterior-Vim, followed by a secondary lesion to the PSA if tremor suppression is considered sub-optimal after anterior-Vim lesioning alone.[196] This strategy has been adopted to the present study with minor differences in VIM and PSA targeting.

As a relatively new technique, literature comparing the clinical and imaging outcomes in ET patients treated with a single tcMRgFUS Vim lesion compared to dual VIM-PSA lesions does not exist. Results of studies employing DBS suggest that tremor suppression following targeting of the PSA may be superior, compared with targeting of the Vim.[403] While the Imperial College unit report their hybrid approach to provide similar tremor suppression at 2-years in comparison to the original multicentre tcMRgFUS VIM study and achieving a more favourable side-effect profile[196]

The aim of the study was to compare the lesion characteristics of patients with ET treated with a single tcMRgFUS Vim lesion or dual Vim-PSA lesions at a single centre, to determine if there was a difference in Vim lesion location in patients requiring additional lesioning in the PSA. Additionally, we compare the long-term improvement in tremor scores, and prevalence of AEs to determine if there was a significant difference in clinical outcomes as a result of the additional PSA lesion.

4.5.2 Methods

Patients

This study was a retrospective analysis of prospectively collected data from patients who underwent tcMRgFUS for treatment of tremor at St Vincent's Hospital, Sydney. The primary aim of this study was to compare the lesion characteristics and tremor suppression following treatment with tcMRgFUS targeting either the Vim only (single-target), or a combination of the Vim and PSA (dual-target). The study consisted of patients with

medication refractory ET or ETP, in accordance with the 2018 Consensus Statement on the classification of Tremors, [1] considered collectively as ET. The hybrid treatment strategy adapted from the Imperial College group, commenced after the first 37 patients had been treated at this site and thus these patients were excluded from the study, to ensure all patients were treated under the same treatment scheme.

In the investigation of AEs, to increase sample size the presence or absence of AEs was assumed to be independent of disease type, and subsequently patients with diseases other than ET who were treated with tcMRgFUS at the same centre, including those with dystonic tremor (DT) and Parkinson's Disease (PD), were included in the analysis of AEs.

Informed consent was obtained from all participating subjects, and the study was approved by the St Vincent's Hospital Ethics Review Committee (ETH00670).

tcMRgFUS Procedure

tcMRgFUS was performed as described in sections 1.2.4 and 2.3.2. The Vim was initially targeted using coordinates of 25% of the AC-PC distance anterior to the PC plus 0.5-1mm, 14mm lateral to the midline at the level of the intercommissural line and adjusted for individual patient anatomy including width of 3rd ventricle, and proximity to visualised internal capsule. Clinical examinations were performed between each sonication to assess for tremor suppression and the presence of side effects.

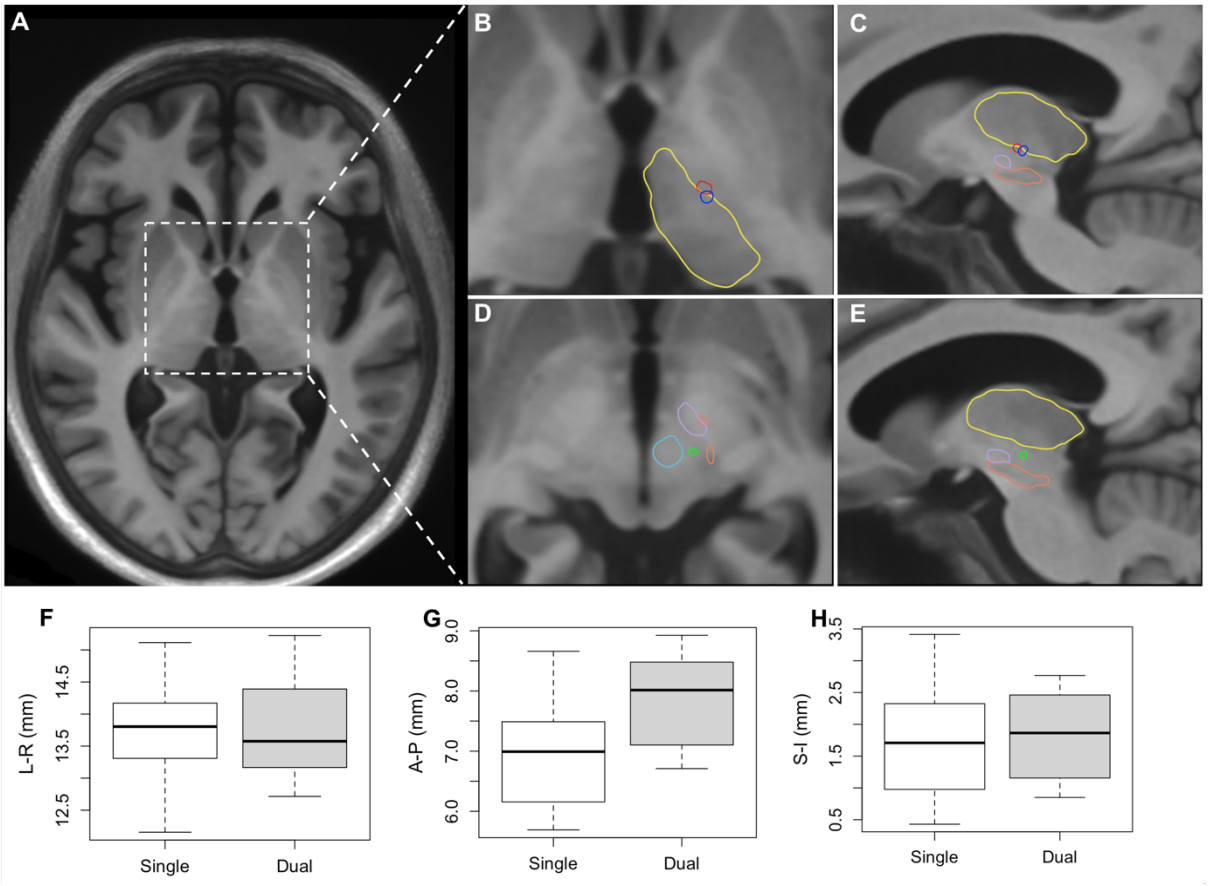

Figure 4-11 ***Top Panel:*** *Vim and PSA ablations in unbiased T1-WI template space.* ***A –*** *T1-WI template.* ***B-*** *Axial view of averaged Vim ablation from single-target patients (blue) and dual-target patients (red).* ***C –*** *Sagittal view of averaged Vim ablation from single-target patients (blue) and dual-target patients (red).* ***D & E*** *- Axial and sagittal view of average PSA lesion (light green). Ablation segmentation overlayed on deep grey matter structures from the PD25 template* (Xiao et al. 2015)*, including the left thalamus (yellow), red nucleus (light blue), subthalamic nucleus (pink) and substantia nigra (orange). Bottom Panel: Coordinates of Vim ablation for patients in the single (white) and dual-target (grey) groups. F – coordinates in the L-R direction, G – coordinates in the A-P direction, and H – coordinates in the S-I direction. All coordinates are relative to the template T1-WI posterior commissure.*

If despite three therapeutic sonications in the Vim, tremor persisted and was considered clinically significant, a second lesion to the PSA (dual-target) would be performed by targeting the white matter equidistant between the medial border of the STN and lateral border of the red nucleus at its equator, corresponding to AC-PC coordinates of approximately lateral=9.5 mm, A-P=-6.0 mm anterior to PC, S-I=-3.5 mm below AC-PC (*Figure*

4-11). The AC-PC distance of each patient was recorded for use in statistical comparison across the two treatment groups.

Clinical Evaluation

Each patient was evaluated by a trained movement disorders specialist prior to treatment, and again at intervals of 1-, 3- 6-, 12-, 24- and 36 months post treatment. Tremor severity was assessed with the CRST [389] and as done in previously tcMRgFUS published studies, the HTS for the 'treated' side [337], as described in section 1.1.5. The patient's quality of life was assessed using the disease specific, self-reported QUEST scores [338,389].

Frequency and severity of AEs were recorded at each time point of follow-up using a standardised template adapted from previously published tcMRgFUS side effects [198]. To standardise the analysis of AEs, the data was regrouped into short-term (up to 1 month), medium term (3-6 months) and long-term (12 months or greater), with data at the most recent visit in each window used for analysis. The AEs in the analysis included the presence of dysarthria, dysmetria, fatigue, gait disturbance, headache, memory, and paresthesia.

Intraoperative spiral assessment

Intraoperative freehand spirals were serially collected from the treated hand prior to the first and then after each sonication. Each patient was asked to draw in the supine position in the MRI scanner, with their head positioned within the ultrasound transducer. Changes in

the spirals formed one part of the on day clinical assessment to help make intraoperative decisions. The spirals were then digitised and analysed with a semi-automated algorithm described in section 2.3, based on the methods described by Kraus et al. and validated against blinded expert visual raters using the validated Bain Finley Spiral score [320,321,338] to give a spiral rating between 0-10.

To compare the intraoperative trajectory of spiral improvement between patients treated with single Vim or dual Vim-PSA lesions, the percentage improvement in spiral rating from baseline was calculated for the spirals drawn at the first and final intraprocedural evaluations, and in the dual-targeted patients, the spiral drawn following the final Vim sonication.

MRI Analysis

MRI data was acquired 1-7 days prior to treatment, and again the day immediately following treatment. Pre-treatment imaging was acquired on a 3T GE Signa Architect (General Electric, Milwaukee), and day-one imaging was acquired on a 3T Philips Ingenia (Philips Inc, Amsterdam, The Netherlands). The pre-treatment protocol included a sagittal 3D IR-FSPGR T1-weighted image (T1-WI) (TI: 450 ms, TR: 8 ms, TE:3.24 ms, Flip Angle: 10^{o}, FOV: 256 mm, acquisition matrix: 256×256, slice thickness: 1.2 mm, slices: 146). Additionally, diffusion weighted imaging (dMRI) was acquired pre-treatment with 1 of 2 DWI protocols; Protocol 1 (N=17): b = 0, 700, 1000, 2800 s/mm^2, directions = 140, TR: 6250 ms, TE: 106 ms, Flip Angle: 90^{o}, FOV: 230 mm, acquisition matrix: 128×128, slice thickness: 1.8 mm, slices: 72. Protocol

2 (N=18): b = 0, 700, 1000, 2800 s/mm^2, directions = 140, TR : 7970 ms, TE: 102 ms, Flip Angle: 90^o, FOV: 232 mm, acquisition matrix: 116 $\times$ 116, slice thickness: 2.0 mm, slices: 70.

The day-1 imaging protocol included an axial 3D IR-FFE T1-WI (TI: 450 ms, TR: 7.9 ms, TE:2.6 ms, Flip Angle: 8^o, FOV: 240 mm, acquisition matrix: 240 $\times$ 240, slice thickness: 1.0 mm, slices: 170). The Vim ablation was segmented on the T1-WI acquired on day-1 with ITK-SNAP[335], after linear registration to the pre-treatment T1-WI with FSL-FLIRT [390]. The isointense ablation core, as well as the hyperintense rim were segmented individually to measure the ablation core, and total ablation volume, respectively.

The DWI data acquired prior to treatment was processed to reconstruct the DRTT, however, this data was used for retrospective analysis only. The DWI data was processed with the default MRtrix3[434] pipeline. Briefly, the raw DWI data was denoised, corrected for Gibb's ringing, susceptibility distortion, eddy current correction and bias field corrected. Fibre orientation distributions (FODs) [435] were estimated with multi-shell multi-tissue spherical deconvolution.[437] The dentatorubrothalamic tract (DRTT) was reconstructed with probabilistic fibre tracking in MRtrix3[438], seeding in the dentate nucleus, with inclusion masks in the contralateral red nucleus, thalamus, and pre-central cortex.[439] Fibre tracking was seeded continuously until 3000 streamlines satisfied the inclusion criteria. The resultant fibre bundle was filtered down to the 1000 most coherent streamlines with DIPY[440]. DRTT fibre bundles representing the anterior, middle, and posterior DRTT components in an unbiased template space, as described in section 4.4 were also generated and used for tractography analysis of the Vim ablation location.

Lesion Location Analysis

To compare the location of the ablations in a standardised space, the pre-treatment T1-WI from each subject was first non-linearly warped to an unbiased T1-WI template, built by combining the pre-treatment T1-WIs from all patients with buildtemplateparallel in ANTS[416]. The generated deformation field from the T1-WI to the template image was then applied to the ablation segmentation for each patient, warping the segmentation into a standard space. The centre of gravity (COG) of each Vim ablation in standardised space relative to the template PC was calculated with SciPy (version 1.10.1) in python (version 3.8.15), to compare the coordinates of the centre of each ablation. For visual comparison of the lesion location, the warped segmentations for patients in each group were combined, and the mean voxel value was calculated for each voxel. A threshold value of 50% was applied to the averaged ablation segmentations, followed by binarization. The T1-WI of any patient treated in the right side of the brain was flipped prior to non-linear registration, so that the ablation appeared on the left side for all patients. The template T1-WI and averaged ablations are shown in *Figure 4-11*

To assess the overlap of the ablation core with the DRTT generated on the pre-treatment imaging, the Vim ablation core was linearly transformed to the DTI image space. The ablation core was used, rather than the whole ablation to improve specificity and reduce the risk of inflating the overlap values with regions that may not form part of the necrotic lesion core. The number of streamlines that traversed the ablated region was calculated in MRTrix3[434] and divided by the total number of streamlines to give the percentage DRTT

transection. This procedure was repeated using the native DRTT, as well as the 3 DRTT clusters (posterior, middle and anterior).

Statistical Analysis

Improvement in tremor scores were assessed by calculating the percentage change in each tremor score at follow-up from baseline and inverting such that a positive value indicates a reduction in tremor score. Due to the number of patients that did not return for each follow-up visit, the change in tremor scores were defined between baseline and the most recent clinical visit. Patients were grouped into those targeted in both the Vim and PSA (dual-target), and those lesioned in the Vim only (single-target) for statistical comparison. Change in tremor severity was assessed by comparing the percentage improvement in CRST, HTS, QUEST and spiral ratings across the two treatment groups with a student's T-Test, or Mann Whitney U Test, for normal and non-normally distributed data, respectfully. Vim ablation volumes, COG coordinates of the spatially standardised ablation segmentations and the overlap between the Vim and the DRTT fibre bundles were also compared across the two treatment groups with a student's T-Test. For comparison of the incidence of AEs, the adverse effect rate (AER) was calculated, defined as the proportion of patients experiencing any AE. The AER was compared across the two treatment groups at each visit with a Chi-squared test.

All statistical analysis was performed using the R (version 4.2.2) statistical software package in RStudio (Version 1.4.1717, RStudio, Inc., Boston, MA URL, http://www.rstudio.com).

4.5.3 Results

Patients

The main study was comprised of a total number of 35 ET patients, of which 21 were treated in the Vim only, and 14 were treated with lesions in both the Vim and PSA. The mean patient age was 77.42 $\pm$ 7.23 years, and the mean disease duration was 39.44 $\pm$ 18.85 years at the time of treatment. The mean SDR was 0.44 $\pm$ 0.08, and the mean clinical follow-up time was 18.80 $\pm$ 12.25 months post-treatment. The baseline tremor severity in the dual-target group (HTS 19.78 $\pm$ 4.32 and CRST 47.89 $\pm$ 12.46) was greater than the single targeted group (HTS 18.68 $\pm$ 6.58 and CRST 42.26 $\pm$ 13.06), however, the difference was not statistically significant. Other baseline measurements, including age, disease duration, SDR or follow-up times between the dual and single target groups did not differ. Patient characteristics are summarised in *Table 4-4*.

Table 4-4 Patient and tcMRgFUS treatment characteristics.

Variable	**All patients N=35**
Sex, n(%)	
Male	26 (74)
Female	9 (26)
Age, mean ± SD, years	77.42 ± 7.23
Treatment Side, n(%)	
Left	31 (89)
Right	4 (11)
Treatment Target, n(%)	
Vim	21 (60)
Vim & PSA	14 (40)
Number of Sonications	10.11 ± 3.28
Max. Temperature (°C)	59.49 ± 3.18°C

Abbreviations used: SD (Standard Deviation), Vim (Ventral Intermediate Nucleus), PSA (Posterior Subthalamic Area).

Across the entire patient cohort, an average of 10.11 ± 3.28 sonications were delivered, with an average maximum sonication temperature of 59.49 ± 3.18°C. Patients treated in the Vim only received an average of 8.30 ± 2.18 sonications, with an accumulated therapeutic thermal dose (ATTD), defined as the sum of sonication temperatures over 53°C, of 287.53 ± 73.80°C. Dual targeted patients received on average 7.80 ± 1.97 sonications targeting the Vim, with a ATTD of 214.43 ± 75.53°C, and an additional 4.73 ± 1.49 sonications targeting the PSA, with an ATTD of 107.14 ± 29.36°C.

The mean total Vim ablation volume across all patients was 122.41 ± 37.23 mm^3, and the mean ablation core volume was 10.71 ± 4.53 mm^3. The total Vim ablation, and ablation core volumes were greater in single-target patients (131.87 ± 35.35 and 11.54 ± 4.41 mm^3), compared with dual-targeted patients (108.21 ± 36.62 and 9.45 ± 4.59 mm^3), however, the difference in volumes were not statistically significant (p=0.065 and p=0.185, respectively).

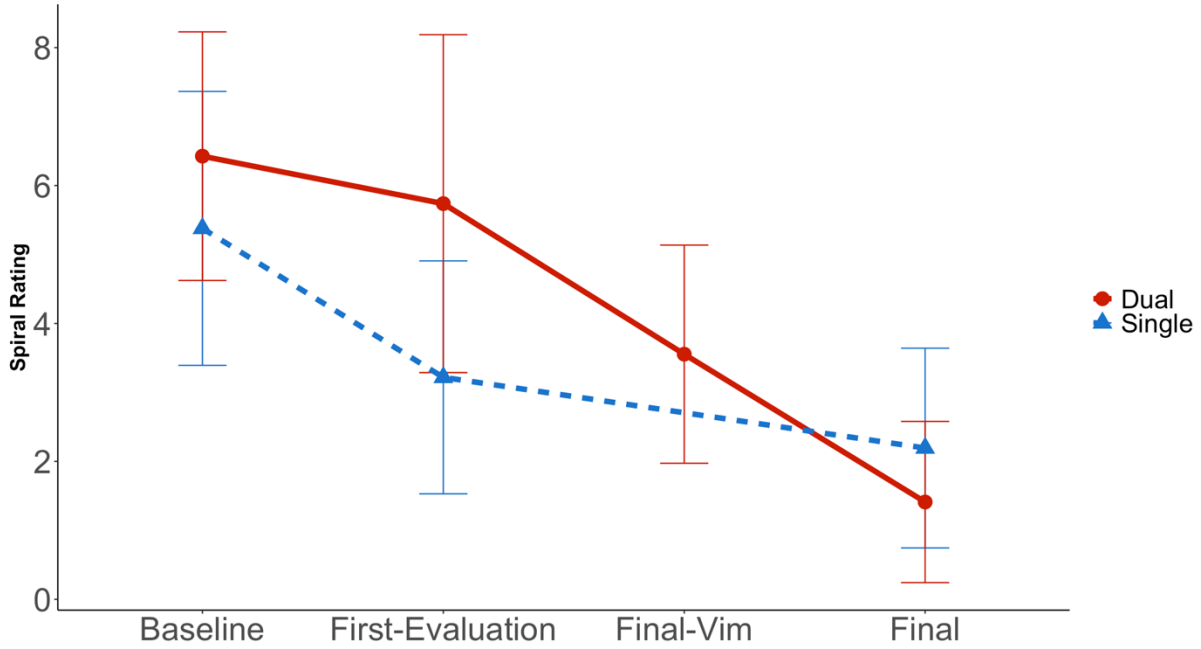

*Figure 4-12 Mean absolute spiral rating at each evaluation, including baseline, the first evaluation, the final Vim evaluation (dual-target only), and the final treatment evaluation for dual-target patients (**red**) and single-target patients (**blue**). Mean value indicated by dot, and whiskers represent the standard deviation.*

PSA ablation volume was typically smaller, with a mean total PSA ablation volume of 74.04 ± 29.30 mm^3, and a core volume of 7.89 ± 4.70 mm^3.

Intraoperative spiral assessment

Pre-treatment, the mean spiral rating in the single-target group was 5.38 ± 1.99, which improved to 3.21 ± 1.69, (percentage improvement 37.77 ± 26.93%) at the first evaluation, and 2.19 ± 1.45 (percentage improvement 58.21 ± 24.63%) following the final sonication. The absolute pre-treatment spiral rating in the dual-targeted group was greater at 6.43 ± 1.80, improving to 5.74 ± 2.45 (percentage improvement 9.69 ± 35.90%) at the first evaluation, and 3.55 ± 1.58 (percentage improvement 43.25 ± 24.08%) following the final Vim sonication. Following subsequent lesioning of the PSA, the spiral rating improved to

1.41 ± 1.16 (percentage improvement 77.31 ± 18.04%), with the percentage improvement following the final treatment sonication found to be significant greater compared to the single target group (p=0.04). Dual targeted patients experienced an average of 34.06 ± 30.68% additional improvement in spiral rating after shifting target coordinates to the PSA (*Figure 4-12*).

Tremor Scores

The mean HTS, CRST and QUEST values pre-treatment were 19.04 ± 5.90, 44.07 ± 12.92 and 48.77 ± 15.37, respectively. At the most recent follow-up, HTS, CRST and QUEST in the single-target group improved by 57.97 ± 22.24±, 36.71 ± 12.30% and 58.26 ± 31.28%, respectively. In the dual-target group, HTS, CRST and QUEST improved by 68.34 ± 14.99%, 35.37 ± 15.64% and 46.97 ± 32.16%, respectively. There was not found to be significant

Table 4-5 Summary of tremor scores at baseline and the most recent clinical follow-up, for patients in the single and dual-target groups.

	Baseline	**Follow-up**	**Improvement (%)**
Single			
HTS	18.68 ± 6.58	8.64 ± 5.56	57.97 ± 22.24
CRST	42.26 ± 13.06	30.50 ± 11.65	36.71 ± 12.30
QUEST	48.65 ± 18.04	21.00 ± 19.53	58.26 ± 31.28
Dual			
HTS	19.78 ± 4.32	7.73 ± 4.03	68.35 ± 14.99
CRST	47.89 ± 12.46	32.36 ± 9.59	35.37 ± 15.64
QUEST	49.00 ± 9.54	25.37 ± 17.30	46.97 ± 32.16

Abbreviations used: HTS (Hand Tremor Score), CRST (Clinical Rating Scale for Tremor), QUEST (Quality of Life in Essential Tremor).

difference in pre-treatment tremor scores, or percentage improvement in tremor scores at follow-up, between the two treatment groups. Tremor scores are summarised in *Table 4-5*.

Adverse Effects

In the investigation of AEs, a total of 43 patients with AE data were identified, including 21 patients with ET, 13 patients with DT and 9 patients with PD. Of those patients, 8 (38%) patients with ET, 3 (23%) patients with DT and 5 (56%) patients with PD were treated in the Vim and PSA, with the remainder treated in the Vim only.

Table 4-6 Summary of adverse events for single and dual-targeted patients at short-term (up to 1 month), medium-term (3-6 months) and long-term (12 months or greater) follow-up visits.

	Short-term	Medium-term	Long-term
Single-Target			
Subjects	27	24	23
Dysarthria, N(%)	4 (15)	2 (8)	0
Disequilibrium, N(%)	0	0	0
Dysmetria, N(%)	2 (7)	1 (4)	0
Fatigue, N(%)	4 (15)	0	0
Gait Disturbance, N(%)	15 (56)	7 (29)	9 (39)
Headache, N(%)	0	0	0
Memory , N(%)	0	0	0
Paresthesia, N(%)	2 (7)	0	0
Dyskinesia, N(%)	0	0	0
AER	**62.96**	**29.17**	**39.13**
Dual-Target			
Subjects	16	17	15
Dysarthria, N(%)	2 (13)	0	0
Disequilibrium, N(%)	1 (6)	0	0
Dysmetria, N(%)	1 (6)	2 (12)	1 (7)
Fatigue, N(%)	2 (13)	1 (6)	0
Gait Disturbance, N(%)	12 (75)	9 (53)	5 (33)
Headache, N(%)	0	0	0
Memory, N(%)	0	0	0
Paresthesia, N(%)	1 (6)	0	0
Dyskinesia, N(%)	0	0	1 (7)
AER	**87.50**	**58.82**	**33.33**

Abbreviations used: AER (Adverse Effect Rate).

At short-term (up to 1-month post-treatment), the most common AEs experienced were gait disturbance (N=27, 63%), dysarthria (N=6, 14%), fatigue (N=6, 14%) and paresthesia (N=3, 7%), while 12 patients (28%) reported no AEs. At the medium-term visit (3-6 months), gait disturbance was again the most common AE, affecting 16 (39%) patients, while dysarthria was reported in 2 (5%) patients, no cases of paresthesia were reported, and 24 (57%) of patients reporting no AEs. At long-term follow-up (12 months or greater), there were 14 (37%) cases of gait disturbance, no cases of paresthesia or dysarthria, and 24 (63%) of patients reporting no AEs.

When the AER was compared across the two treatment groups, it was observed that dual targeted patients experienced greater proportion of patients with short-term AEs, with 87.50% of patients experiencing an AE, compared with 62.96% in the single target group. This result, however, did not reach a statistical significance level of 0.05 (p=0.083), per Chi-squared analysis. At the medium term-visit, 58.82% of patients in the dual-target group reported an AE, compared with 29.17% in the single-target group, which was approaching statistical significance (p=0.056). At the long-term visit, there was not found to be a significant difference in the proportion of patients reporting AEs, with 33.33% of the dual-targeted patients reporting an AE, compared with 39.13% of single-target patients (p=0.717). A summary of the AEs at each visit are shown in *Table 4-6*.

Lesion Location Analysis

The AC-PC distance of the template T1-WI was 27.67mm. Analysis of the location of the Vim ablation in the spatially normalised template image revealed that the COG coordinates in

single-targeted patients were further posterior, with average coordinates of lateral: 13.74 ± 0.70 mm, A-P: 6.92 ± 0.84 mm and S-I: 1.69 ± 0.93 mm, relative to the PC. The coordinates in dual targeted patients were lateral: 13.83 ± 0.88 mm, A-P: 7.84 ± .80 mm and S-I: 2.04 ± 1.01 mm SI. The difference in coordinates in the A-P direction between the two groups was significant per Students t-test (p=0.003), while the differences in coordinates in the L-R and S-I directions were not found to be statistically significant (p=0.761 and p=0.304, respectively). The A-P coordinates of the Vim ablation in the single target group

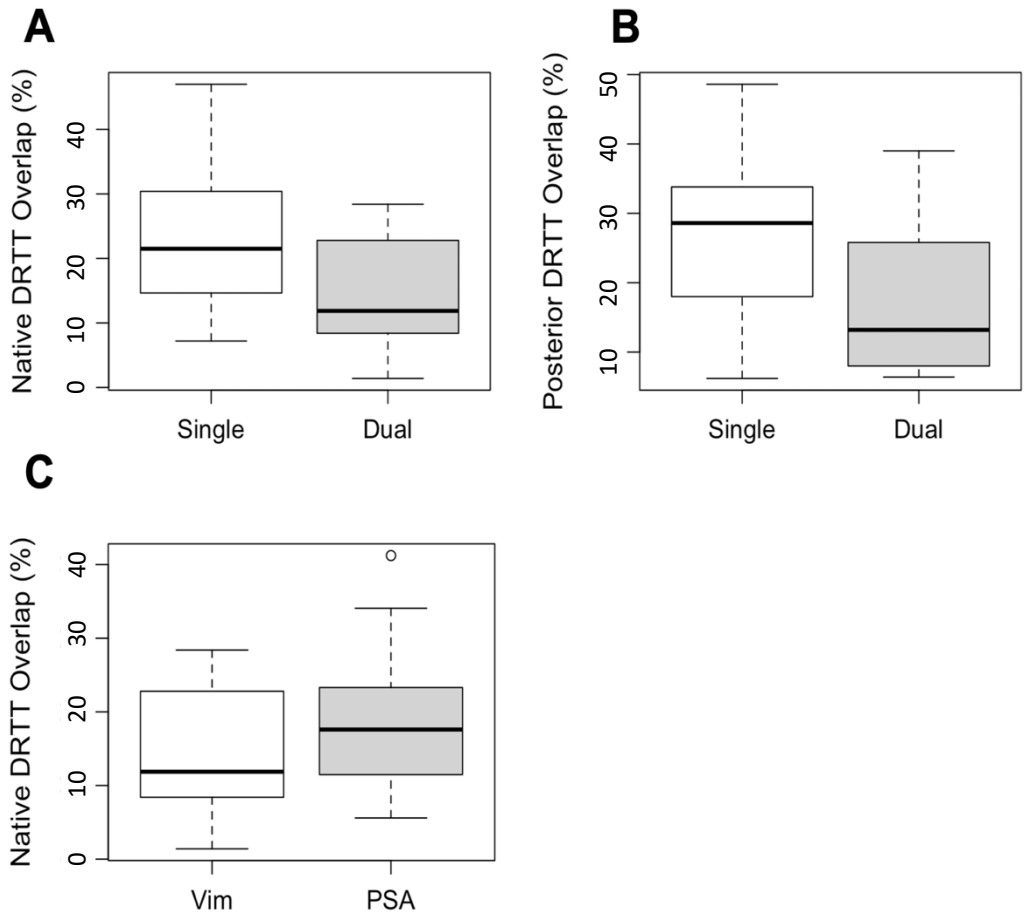

Figure 4-13 ***A*** *- Mean overlap between the Vim ablation core and the native DRTT.* ***B*** *– Mean overlap between the Vim ablation core and posterior DRTT cluster.* ***C*** *- Mean overlap between the native DRTT, and the Vim and PSA ablation cores in dual-targeted patients.*

corresponded to 25.01% of the ACPC distance, while in the dual targeted group the A-P coordinates were 28.33% of the ACPC distance. The distribution of coordinates are shown in *Figure 4-11*.

Analysis of the AC-PC distance measured on the pre-treatment T1-WI found that while there was not a statistically significant difference in the mean values (27.64 vs 27.54mm, p=0.883), there was significantly more variance in the AC-PC distance in the dual targeted group, with a standard deviation of 2.37mm, compared with 1.44mm in the single target group. Bartlett's test indicated the difference in variance was statistically significant (p=0.039).

Overlap between the Vim ablation core and the native DRTT was found to be significantly greater in the single targeted patients, with a mean overlap of 23.21 $\pm$ 1.13%, compared with 14.85 $\pm$ 9.03% in dual targeted patients, p=0.029 (*Figure 4-13*). When examining the overlap between the Vim ablation core and the clustered DRTT, the overlap with the posterior cluster was found to be significantly greater in the single target patients (26.33 $\pm$ 12.77%) compared with the dual targeted patients (16.79 $\pm$ 10.09%, p=0.025). Overlap with the middle and anterior clusters of the DRTT were not found to be significantly different across the treatment type groups (p=0.077 and p=0.485, respectively). The overlap between the Vim ablation and the DRTT is shown in Figure 4-14, as well as examples of patients with low and high overlap. In the dual-targeted patients, the mean overlap between the PSA ablation and the native DRTT was greater (19.00 $\pm$ 9.66%), however, paired t-test analysis with the Vim ablation did not reach statistical significance (p=0.070).

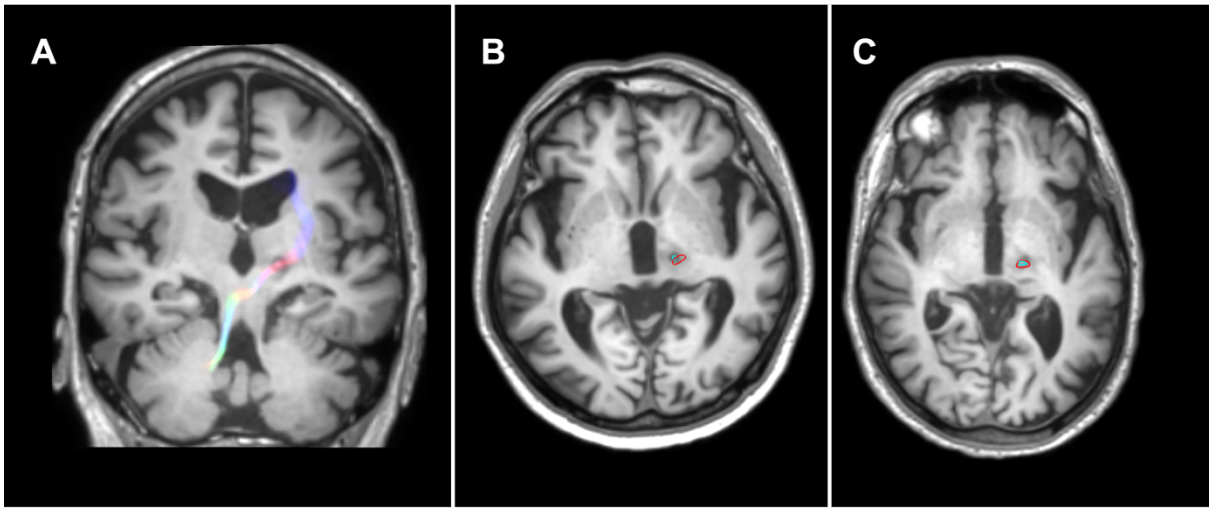

Figure 4-14 **A** - *Obliqued coronal view of native DRTT overlayed on the day-one T1-WI from a single subject.* ***B & C*** *– Axial cross section showing example of subjects with low and high overlap between the DRTT (red) and Vim ablation core (blue), respectively.*

4.5.4 Discussion

In the present study, we conducted a comparative analysis of the lesion characteristics and clinical outcomes among patients treated with tcMRgFUS, targeting either the Vim exclusively, or a combination of lesions in both the Vim and PSA. While the decision to target the PSA was a clinical judgment made at the time of treatment, predicated upon the patient's tremor response to targeting of the Vim alone rather than a predetermined experimental design, the two treatment groups represent some of the emerging treatment strategies currently being employed in the tcMRgFUS community for the treatment of tremor.

Analysis of the spirals drawn during treatment showed that, as expected, patients who required lesioning of the PSA experienced less spiral improvement at the early intra-

procedural evaluations, compared with patients lesioned in the Vim only. In dual-targeted patients, ablation of the PSA conferred an additional 34.06% improvement in spiral rating, a similar result to the 27.9% spiral improvement observed by Jameel et al[196]. Furthermore, the percentage improvement in post-treatment spiral rating was significantly greater in the dual targeted patients, compared to the single-target group. However, comparison of tremor severity in the long-term did not reveal a statistically significant difference between the two groups, though there remain a trend of greater improvement to the treated hand in the dual-targeted group.

This short-term advantage in tremor suppression observed in the dual targeted patients that was subsequently lost in the long term; may have been due to in-complete thermocoagulation of the prelemniscal fibre tract in the PSA, which has been suggested to require more thermal application than nuclei such as the Vim[447]. Further, the intraoperative semi-automated digital spiral assessments which detected the difference between the two groups were unable to be applied in the long-term, and thus tremor assessment relied on validated rating scales that were possibly inferior to the computerised method[320].

Comparison of the COG of the Vim ablations across the two patient groups revealed that there was a systematic difference in the location of the Vim ablation between the two groups. The Vim ablation of patients who did not require an additional lesion in the PSA was situated further posteriorly than the dual-targeted patients, with COG coordinates significantly closer to the PC. As demonstrated in section 4.4, there is a growing body of evidence that lesions with more posterior extension may provide improved tremor suppression in patients with ET [276,388,448]. The COG coordinates of the Vim ablation in the

single target group were approximately 25% of the AC-PC distance, anterior to the PC, consistent with the coordinates conventionally used to target the Vim, compared with 28% in patients that required a lesion in the PSA. This finding was confirmed with analysis of the Vim ablation overlap with the tractography derived DRTT, where patients who required lesioning of the PSA had significantly lower Vim ablation overlap with the DRTT, particularly in the posterior fibres, and on average greater overlap between the PSA ablation and the DRTT. The results of the tractography analysis may explain why lesions placed further anteriorly tend to be less effective, as they may not be ideally placed to transect the DRTT, which several studies have shown is crucial for achieving more complete tremor suppression[294–296]. These findings support the view that lesions placed further posteriorly provide superior tremor suppression, consistent with the findings presented in section 4.4.

The excellent early tremor suppression observed in patients treated in the PSA, following inadequate suppression from Vim lesioning alone, begs the question of whether lesioning of the Vim directly is necessary at all, given similar outcomes have been observed in patients lesioned in the PSA alone[248,249]. Consensus on the optimal target for tcMRgFUS may hinge on the differences in adverse effect profiles between the two strategies. Holcomb et al. advise against direct lesioning of the PSA due to the increased risk of AEs. Analysis of the AER in this study found that patients whose Vim lesion inadvertently extended inferiorly into the PSA experienced a higher proportion of gait disturbance in the short and medium-term compared with patients whose lesion remained confined to the VIM. However, this difference was largely resolved by 12-months[297]. This contrasts with the single PSA target and dual VIM-PSA target studies by Galley et and Jameel et al., that report fewer AE than the original multicentre tcMRgFUS VIM study, including gait disturbance[196,248].

An alternative treatment pathway to a secondary PSA lesion, faced with residual clinically significant residual tremor, despite 'adequate' Vim lesioning, is to provide further thermal application, to enlarge the initial lesion posteriorly. This posterior lesioning strategy is not without risk. Boutet et al. demonstrated that posterior encroachment of the VC nucleus of the thalamus was associated with a 38% increase acute sensory adverse effects[276], which was cited by the Imperial College group as one of the motivations for placing lesions 2.7-3.7mm anterior to the conventional coordinates[196]. Extension into the VC is likely the explanation for 7% of patients in the single target group who experienced paraesthesia, which had resolved by the medium-term visits. The sample size in this study is not large enough to draw definitive conclusions regarding the AE profile of each targeting strategy, the high proportion of short-term gait disturbance observed in the dual-targeted group might suggest that this strategy is associated with a higher risk of acute motor AEs.

Given patients in both groups of this study were subject to the same initial targeting coordinates of approximately 25% of the AC-PC distance posterior to the PC, it is unclear why in a subset of patients this did not result in a lesion covering the posterior portion of the Vim. Analysis of the AC-PC distance in the two groups indicated that there was significantly greater variance in the dual targeted group, which may have contributed to the anterior lesion placement. This observation highlights the challenge of applying landmark based targeting in the presence of individual variation in anatomy, and the potential role for tractography in providing direct targeting of the DRTT and surrounding white matter tracts.

This study has several limitations. The number of patients treated with lesions in the PSA was relatively small compared with other studies on tcMRgFUS, which was further diminished by the high attrition rate in clinical follow-up. However, despite the small sample size, the findings presented here were statistically significant and provide meaningful data on the outcomes of each treatment strategy. Future studies, with randomised, blinded comparison of VIM versus PSA lesioning will be required to adequately compare the effectiveness and side-effect profile of the two targets.

4.5.5 Conclusion

Targeting the PSA with MRgFUS lesioning in ET represent a valid treatment strategy when faced with residual tremor despite 'adequate' Vim lesioning. This approach will likely avoid sensory side effects, have comparable long-term tremor suppression effects to single MRgFUS Vim targeting and possible increase the risk of gait disturbance in the short-term. Further, under this treatment strategy, patients who required ablation of the PSA are more likely to have a Vim ablation situated further anteriorly, with less DRTT involvement.

4.6 Chapter Summary

The successful treatment of tremor with tcMRgFUS relies on the accurate targeting of the appropriate region of the brain. Stereotactic interventions targeting the Vim have traditionally relied on indirect targeting methods that despite achieving tremor suppression in many patients, fail to account for individual variations in anatomy or the effects of brain atrophy and may be responsible for the suboptimal tremor benefit observed in some patients treated with tcMRgFUS. Direct targeting may aid neurosurgeons during treatment with tcMRgFUS by providing more accurate target coordinates to achieve suppression of tremor while avoiding lesioning of surrounding structures that may lead to adverse effects.

In this chapter, several automated methods for direct targeting were investigated. Two automated thalamic segmentation tools, FreeSurfer and THOMAS, which provide direct segmentation of the VLp of the thalamus, which approximately corresponds to the Vim, were compared to the location of the Vim ablation chosen with conventional indirect methods. A high degree of overlap with the VLp, relative to other defined nuclei, was observed with both FreeSurfer and THOMAS-based methods, however, the overall concordance with the indirect target was moderate. This finding may be due to the targeting methodology that prioritises lesioning the white matter pathway that connects the cerebellum and the thalamus at the level of the Vim, the DRTT, rather than the Vim directly. dMRI tractography was employed to reconstruct the DRTT, and compare the involvement of this white matter tract, as well as the overlap with the FreeSurfer and THOMAS-defined VLp, with the improvement in tremor experienced following treatment with tcMRgFUS. We

observed that tremor suppression was significantly correlated with lesioning of the posterior portion of the DRTT, while overlap with the THOMAS and FreeSurfer-defined VLp was not found to be associated with tremor improvement. This finding supports the concept that lesioning of the DRTT is critical to achieving optimal tremor suppression. While segmentation of the thalamic nuclei may provide an indication of the entry point of the DRTT to the thalamus, dMRI tractography may represent the direct targeting method with the strongest relationship with tremor benefit.

The importance of lesioning of the DRTT is further validated by our observation that in patients who required secondary lesion of the PSA, following sub-optimal tremor suppression after adequate lesioning of the Vim, DRTT involvement was lower, particularly in the posterior region. This finding emphasises the importance of DRTT involvement for achieving maximum tremor suppressing effects and supports the application of dMRI tractography for direct treatment targeting.

5 Conclusion

There is a long history of stereotactic interventions for the treatment of tremor, particularly in patients with ET. Many of the disadvantages inherent to the traditional invasive methods, such as DBS and RF lesioning[222], have been mitigated with the development of tcMRgFUS, which offers an incisionless surgical option through an intact skull, with immediate treatment benefit[192,238]. However, compared to existing methodologies, tcMRgFUS is a relatively new procedure, with the first pilot trial undertaken in 2013[192], and FDA approval for the treatment of ET granted in 2018[354]. As such, there is comparatively little literature on the long-term tremor benefits or the factors that influence successful treatment with tcMRgFUS. While several studies have reported significant tremor benefit following tcMRgFUS [198,240], there remains a spectrum of observed clinical improvement; continued research is needed to identify the key factors that may contribute to improving patient outcomes. The research presented in this thesis explored some of the main factors that may contribute to optimal outcomes, starting with the characteristics inherent to the patient and finishing with the targeting decisions made by the treating team.

In **Chapter 2**, the influence of the tremor subtype diagnosis (ET, ETP or DT) on the clinical outcomes following treatment with tcMRgFUS is investigated. In section 2.3, the intraoperative tremor improvement was analysed by the development of a novel algorithm for automated analysis of freeform Archimedes spirals drawn by patients during tcMRgFUS. This algorithm may provide clinicians with an unbiased and reproducible estimate of tremor severity, which could aid in the evaluation of intraoperative tremor improvement, as well as

an assessment tool for future research into tremor. The analysis of intraoperative spirals found that patients with DT tended to experience less spiral improvement compared to patients with pure ET, and tremor improvement measured immediately post-treatment was associated with long-term outcomes, suggesting that patients with DT may experience poorer long-term tremor suppression. These findings were confirmed in section 2.4, where long-term improvement in tremor scores and quality of life metrics were investigated over a 3-year period post-treatment. The results revealed a significant improvement in both tremor scores and quality-of-life metrics for most patients. Longitudinal analysis of the percentage improvement in tremor scores over time showed a significant effect of tremor subtype on tremor improvement, with DT patients experiencing less improvement than patients with ET. Taken together, the findings presented in **Chapter 2** suggest that both the acute and long-term tremor benefit following treatment with tcMRgFUS may be less significant in patients with DT, compared to those with ET.

In **Chapter 3,** the influence of the skull is explored. The effects of the skull on the efficient deposition of US energy within the tissue of the brain are well established, with SDR used as a critical indicator of sonication thermal increase. In section 3.3, building on published reports of intraoperative reduction in heating efficiency (HE), the influence of patient SDR on the change in HE over the course of the tcMRgFUS procedure was investigated. The relationship between HE and sonication power was found to follow a non-linear pattern, with the slope of the sonicate temperature vs. power curve decreasing as sonication power is increased, with greater patient SDR associated with a more rapid decline in intraoperative HE.

While the impact of patient SDR on thermal increase is well known[269], no studies have linked patient SDR with long-term treatment outcomes, provided sonication temperatures are high enough to create a permanent lesion. However, the SDR values reported in the literature are typically the average of several SDR values measured across different regions of the skull; thus, the distribution of SDR values is generally ignored clinically. Section 3.4 investigated how the distribution of SDR values was related to patient outcomes, revealing that patients with more consistent SDR across the skull, as measured by the distribution kurtosis, tended to have larger lesions at 12-month follow-up and experienced significantly greater long-term tremor suppression. This finding may suggest the regional distribution of SDR values across the skull influences lesion formation, and patients with consistent SDR may be more promising candidates than those with greater SDR heterogeneity. This finding has the potential to significantly improve patient screening and may help identify potential treatment candidates who would be considered unsuitable for treatment by evaluation of the average SDR alone.

In **Chapter 4**, the placement of the tcMRgFUS lesion was investigated. The Vim of the thalamus is the most widely targeted region in stereotactic interventions for tremor, including with tcMRgFUS. However, the boundaries of the Vim are not visible on conventional structural MRI; thus, indirect targeting using easily identifiable landmarks in the brain is commonly used to target the Vim. Advanced MRI acquisition and post-processing may aid clinicians in the identification of the ideal target coordinates to target the Vim and its connecting white matter pathways, ultimately leading to improved tremor suppression.

In section 4.3, two automated thalamic segmentation tools, both of which include segmentation of the VLp, which includes the region approximately corresponding to the Vim, were investigated. The agreement between the Vim ablation and the VLp segmented with the two methods was found to be relatively modest compared with the total ablation volume. This discrepancy was theorised to be due to a treatment strategy that prioritises lesioning of the DRTT, which connects the Vim with the cerebellum, rather than lesioning of the Vim itself. Thus, in section 4.4 dMRI tractography was investigated as a targeting method and compared with thalamic segmentation. In this section, the involvement of the DRTT, and the overlap with the segmentation defined VLp, was compared to the clinical tremor improvement experienced by patients treated with tcMRgFUS. Lesioning of the posterior portion of the tractography-defined DRTT was found to be associated with improved long-term tremor suppression. In contrast, no relationship between the VLp segmentations and tremor benefit was found. This result supports the potential clinical utility of dMRI tractography for the identification of the optimal treatment target, and the clustering method proposed in this chapter to isolate the posterior portion of the DRTT may provide a more clinically relevant target compared with previously published methods.

In section 4.5, the location of the Vim lesion was compared across two groups of patients: those lesioned in the Vim alone (single-target), and those who required additional lesioning if the posterior subthalamic area (PSA), following suboptimal tremor improvement after sonications targeting the Vim (dual-target).

The study found that in dual-targeted patients, the Vim lesion overlapped less with the DRTT, particularly in the posterior portion. Tremor severity, as measured on intraoperative

spirals, was found to improve in the dual-targeted patients after sonications targeting the PSA. Long-term tremor suppression was not found to differ significantly across the two groups. However, the results suggested dual-targeted patients may experience a greater incidence of acute motor adverse effects. The results of this section further emphasise the potential utility of dMRI tractography for target localisation, and may aid clinicians during treatment planning by providing targeting coordinates of the DRTT, obviating the need to lesion the PSA.

In summary, this thesis identified several factors that significantly influence patient outcomes following treatment of tremor with tcMRgFUS, namely the diagnosis of tremor subtype, the distribution of SDR values across the skull, and the treatment coordinates chosen by the neurosurgeon. In **Chapter 2**, we show that patients with a diagnosis of DT may experience lesser improvement in intraoperative spirals and less long-term improvement in clinical tremor scores. In **Chapter 3**, we show that patient SDR influences the intraoperative HE and that greater SDR consistency across the skull is associated with larger lesions and greater tremor suppression at long-term follow-up. In **Chapter 4**, we show that patients who are lesioned in the posterior portion of the DRTT when targeting the Vim are less likely to require additional lesioning in secondary areas and experience greater long-term tremor benefit. Taken together, these findings may help improve clinical outcomes following treatment with tcMRgFUS by improving the identification of potential candidates for treatment, where our findings suggest both the tremor subtype diagnosis and the distribution of SDR values should be considered. Outcomes can be further improved by employing dMRI tractography to target the posterior region of the DRTT, which this thesis has demonstrated is associated with improved tremor benefit.

The research presented in this thesis lays the foundation for several future research directions. The results reported in **Chapter 2** indicate that tremor subtype may influence the tremor improvement experienced following tcMRgFUS. However, the sample size used in this analysis was relatively low, thus a more rigorous longitudinal trial designed to compare outcomes across the different tremor subtypes may improve our understanding of the effect of tremor subtype on clinical improvement. DBS studies have indicated that the optimal target in the treatment of DT may differ from ET[138], thus similar tremor subtype-specific treatment targeting strategies should be explored in the context of tcMRgFUS. Accurate and reproducible diagnosis of tremor subtypes, however, is notoriously difficult and remains controversial[105]. Advanced image processing techniques such as dMRI-based structural connectomics and graph theory[449] may assist in tremor classification and build towards the achievement of a truly-patient specific, personalised treatment strategy. The results presented in **Chapter 3** indicate an intriguing influence of SDR distribution on lesion formation, however, the exact mechanism that drives this influence remains unclear. Further investigation of how regional SDR values may affect the distribution delivered thermal dose and the subsequent change in tissue microstructure may help elucidate this relationship. The results of **Chapter 4** support the use of tractography for treatment planning, however, the challenge remains in the validation of tractography in an N=1 setting, as opposed to group level studies. Prospective studies comparing tractography against conventional indirect targeting should be performed to determine the optimal targeting strategy.

In conclusion, the research presented in this thesis identifies several factors relevant to patient screening and treatment strategy that contribute to the successful treatment of tremor with tcMRgFUS. Continued research into these areas may contribute to further improving patient outcomes.

References

1. Bhatia, K. P. *et al.* Consensus Statement on the classification of tremors. from the task force on tremor of the International Parkinson and Movement Disorder Society. *Movement disorders* **33**, 75–87 (2018).
2. Lorenz, D., Schwieger, D., Moises, H. & Deuschl, G. Quality of life and personality in essential tremor patients. *Movement Disorders* **21**, 1114–1118 (2006).
3. Louis, E. D. *et al.* Correlates of functional disability in essential tremor. *Movement Disorders* **16**, 914–920 (2001).
4. Lorenz, D., Schwieger, D., Moises, H. & Deuschl, G. Quality of life and personality in essential tremor patients. *Movement Disorders* **21**, 1114–1118 (2006).
5. Woods, S. P., Scott, J. C., Fields, J. A., Poquette, A. & Tro¨ster, A. I. *Executive Dysfunction and Neuropsychiatric Symptoms Predict Lower Health Status in Essential Tremor*. (2008).
6. Bain, P. G. *et al. A study of hereditary essential tremor*. *Brain* vol. 117 https://academic.oup.com/brain/article/117/4/805/285617 (1994).
7. Rajput, A., Robinson, C. A. & Rajput, A. H. *Essential tremor course and disability A clinicopathologic study of 20 cases*. www.neurology.org (2002).
8. Louis, E. D., Ford, B. & Barnes, L. F. *Clinical Subtypes of Essential Tremor*. https://jamanetwork.com/.
9. Louis, E. D. The primary type of tremor in essential tremor is kinetic rather than postural: cross-sectional observation of tremor phenomenology in 369 cases. *Eur J Neurol* **20**, 725–727 (2013).

10. Schnitzler, A. & Gross, J. Normal and pathological oscillatory communication in the brain. *Nat Rev Neurosci* **6**, 285–296 (2005).

11. Deuschl, G. *et al.* Consensus statement of the Movement Disorder Society on tremor. in *Movement Disorders* vol. 13 2–23 (Lippincott Williams and Wilkins, 1998).

12. Elias, W. J. & Shah, B. B. Tremor. *JAMA* **311**, 948–954 (2014).

13. Fahn, S., Tolosa, E., Marin, C., Jankovic, J. & Tolosa, E. *Clinical rating scale for tremor*. (Urban & Schwarzenberg, 1988).

14. Lombardi, W., Woolston, D., Roberts, J. & Gross, R. *Cognitive deficits in patients with essential tremor*. www.neurology.org (2001).

15. Zubair, A. *et al.* What Predicts Mortality in Essential Tremor? A Prospective, Longitudinal Study of Elders. *Front Neurol* **9**, 1077 (2018).

16. Louis, E. D., Benito-León, J., Ottman, R. & Bermejo-Pareja, F. A population-based study of mortality in essential tremor. *Neurology* **69**, 1982–1989 (2007).

17. Burresi, P. Sopra un caso di tremore essenziale. Memore originali. Conferenza raccolta dallo studente Alfredo Rubini (22 febbraio 1874, Siena). *Sperimentale* **33**, 475–481 (1874).

18. CRITCHLEY, M. OBSERVATIONS ON ESSENTIAL (HEREDOFAMILIAL) TREMOR. *Brain* **72**, 113–139 (1949).

19. Marsden, C. D. Benign essential tremor is not a single entity. *Current concepts in Parkinson's disease* 31–46 (1983).

20. Deuschl, G., Zimmermann, R., Genger, H. & Lücking, C. H. Physiological classification of essential tremor. *Neurological Disease and Therapy* **30**, 195 (1994).

21. Bhatia, K. P. *et al.* Consensus Statement on the classification of tremors. from the task force on tremor of the International Parkinson and Movement Disorder Society. *Movement Disorders* **33**, 75–87 (2018).

22. Pandey, S., Bhattad, S. & Hallett, M. The Problem of Questionable Dystonia in the Diagnosis of 'Essential Tremor-Plus'. *Tremor Other Hyperkinet Mov (N Y)* **10**, 27 (2020).

23. Rajalingam, R., Breen, D. P., Lang, A. E. & Fasano, A. Essential tremor plus is more common than essential tremor: Insights from the reclassification of a cohort of patients with lower limb tremor. *Parkinsonism & related disorders* vol. 56 109–110 Preprint at https://doi.org/10.1016/j.parkreldis.2018.06.029 (2018).

24. Deuschl, G., Bain, P. & Brin, M. Consensus statement of the Movement Disorder Society on Tremor. Ad Hoc Scientific Committee. *Mov Disord* **13 Suppl 3**, 2–23 (1998).

25. Louis, E. D., Ottman, R. & Allen Hauser, W. How common is the most common adult movement disorder? Estimates of the prevalence of essential tremor throughout the world. *Movement Disorders* vol. 13 5–10 Preprint at https://doi.org/10.1002/mds.870130105 (1998).

26. Rautakorpi, I., Takala, J., Marttila, R. J., Sievers, K. & Rinne, U. K. Essential tremor in a Finnish population. *Acta Neurol Scand* **66**, 58–67 (1982).

27. Louis, E. D. & Ferreira, J. J. How common is the most common adult movement disorder? Update on the worldwide prevalence of essential tremor. *Movement Disorders* **25**, 534–541 (2010).

28. St Vincent's Hospital Sydney. About tremor. https://www.svhs.org.au/focussed-ultrasound/about-tremor (2023).

29. Song, P. *et al.* The global prevalence of essential tremor, with emphasis on age and sex: A meta-analysis. *J Glob Health* **11**, 4028 (2021).

30. Louis, E. D. *et al.* Older onset essential tremor: More rapid progression and more degenerative pathology. *Movement Disorders* **24**, 1606–1612 (2009).

31. Louis, E. D. The Roles of Age and Aging in Essential Tremor: An Epidemiological Perspective. *Neuroepidemiology* **52**, 111–118 (2019).

32. Hubble, J. P., Busenbark, K. L., Pahwa, R., Lyons, K. & Koller, W. C. Clinical expression of essential tremor: effects of gender and age. *Mov Disord* **12**, 969–972 (1997).

33. Louis, E. D., Ford, B. & Frucht, S. Factors associated with increased risk of head tremor in essential tremor: a community-based study in northern Manhattan. *Mov Disord* **18**, 432–436 (2003).

34. Sullivan, K. L., Hauser, R. A. & Zesiewicz, T. A. Essential tremor. Epidemiology, diagnosis, and treatment. *Neurologist* **10**, 250–258 (2004).

35. Louis, E. D. *et al.* Risk of tremor and impairment from tremor in relatives of patients with essential tremor: a community-based family study. *Ann Neurol* **49**, 761–769 (2001).

36. Deng, H., Wu, S. & Jankovic, J. Essential tremor: genetic update. *Expert Rev Mol Med* **21**, e8 (2019).

37. Benito-León, J., Louis, E. D. & Bermejo-Pareja, F. Risk of incident Parkinson's disease and parkinsonism in essential tremor: a population based study. *J Neurol Neurosurg Psychiatry* **80**, 423–425 (2009).

38. Tanner, C. M. *et al.* Essential tremor in twins: an assessment of genetic vs environmental determinants of etiology. *Neurology* **57**, 1389–1391 (2001).

39. Lorenz, D. *et al.* High concordance for essential tremor in monozygotic twins of old age. *Neurology* **62**, 208–211 (2004).

40. Scarmeas, N. & Louis, E. D. Mediterranean diet and essential tremor. A case-control study. *Neuroepidemiology* **29**, 170–177 (2007).

41. Jiménez-Jiménez, F. J. *et al.* Environmental risk factors for essential tremor. *Eur Neurol* **58**, 106–113 (2007).

42. Azevedo, M. F. A. de & Meyer, A. [Essential tremor in endemic disease control agents exposed to pesticides: a case-control study]. *Cad Saude Publica* **33**, e00194915 (2017).

43. Yao, Y., Wang, Y. & Yang, X. [Related factors and prevalence for the essential tremor disease of Uygur residents in Hetian, Xinjiang UygurAutonomous Region]. *Zhonghua Yi Xue Za Zhi* **95**, 69–72 (2015).

44. Louis, E. D. *et al.* Association between essential tremor and blood lead concentration. *Environ Health Perspect* **111**, 1707–1711 (2003).

45. Dogu, O. *et al.* Elevated blood lead concentrations in essential tremor: a case-control study in Mersin, Turkey. *Environ Health Perspect* **115**, 1564–1568 (2007).

46. Shimohama, S. Nicotinic receptor-mediated neuroprotection in neurodegenerative disease models. *Biol Pharm Bull* **32**, 332–336 (2009).

47. Benito-León, J., Louis, E. D. & Bermejo-Pareja, F. Population-based case-control study of cognitive function in essential tremor. *Neurology* **66**, 69–74 (2006).

48. Louis, E. D., Benito-León, J. & Bermejo-Pareja, F. Population-based prospective study of cigarette smoking and risk of incident essential tremor. *Neurology* **70**, 1682–1687 (2008).

49. Benito-León, J., Louis, E. D. & Bermejo-Pareja, F. Short sleep duration heralds essential tremor: a prospective, population-based study. *Mov Disord* **28**, 1700–1707 (2013).

50. Mostile, G. & Jankovic, J. Alcohol in essential tremor and other movement disorders. *Mov Disord* **25**, 2274–2284 (2010).

51. Boecker, H. *et al.* The effect of ethanol on alcohol-responsive essential tremor: a positron emission tomography study. *Ann Neurol* **39**, 650–658 (1996).

52. Kralic, J. E. *et al.* Genetic essential tremor in gamma-aminobutyric acidA receptor alpha1 subunit knockout mice. *J Clin Invest* **115**, 774–779 (2005).

53. Louis, E. D. *et al.* Semiquantitative study of current coffee, caffeine, and ethanol intake in essential tremor cases and controls. *Mov Disord* **19**, 499–504 (2004).

54. Andersen, B. B. Reduction of Purkinje cell volume in cerebellum of alcoholics. *Brain Res* **1007**, 10–18 (2004).

55. Louis, E. D., Agnew, A., Gillman, A., Gerbin, M. & Viner, A. S. Estimating annual rate of decline: prospective, longitudinal data on arm tremor severity in two groups of essential tremor cases. *J Neurol Neurosurg Psychiatry* **82**, 761–765 (2011).

56. Louis, E. D., Kuo, S.-H., Vonsattel, J.-P. G. & Faust, P. L. Torpedo Formation and Purkinje Cell Loss: Modeling their Relationship in Cerebellar Disease. *The Cerebellum* **13**, 433–439 (2014).

57. Louis, E. D. & Faust, P. L. Essential tremor pathology: neurodegeneration and reorganization of neuronal connections. *Nat Rev Neurol* **16**, 69–83 (2020).

58. Quattrone, A. *et al.* Essential Head Tremor Is Associated with Cerebellar Vermis Atrophy: A Volumetric and Voxel-Based Morphometry MR Imaging Study. *American Journal of Neuroradiology* **29**, 1692–1697 (2008).

59. Cerasa, A. *et al.* Cerebellar Atrophy in Essential Tremor Using an Automated Segmentation Method. *American Journal of Neuroradiology* **30**, 1240–1243 (2009).

60. Luo, R., Pan, P., Xu, Y. & Chen, L. No reliable gray matter changes in essential tremor. *Neurol Sci* **40**, 2051–2063 (2019).

61. Saini, J. *et al.* Diffusion tensor imaging: tract based spatial statistics study in essential tremor. *Parkinsonism Relat Disord* **18**, 477–482 (2012).

62. Klein, J. C. *et al.* Diffusion tensor imaging of white matter involvement in essential tremor. *Hum Brain Mapp* **32**, 896–904 (2011).

63. Shin, D. H., Han, B. S., Kim, H. S. & Lee, P. H. Diffusion tensor imaging in patients with essential tremor. *AJNR Am J Neuroradiol* **29**, 151–153 (2008).

64. Jia, L., Jia-Lin, S., Qin, D., Qing, L. & Yan, Z. A diffusion tensor imaging study in essential tremor. *J Neuroimaging* **21**, 370–374 (2011).

65. Pietracupa, S. *et al.* White matter rather than gray matter damage characterizes essential tremor. *Eur Radiol* **29**, 6634–6642 (2019).

66. Revuelta, G., McGill, C., Jensen, J. H. & Bonilha, L. Characterizing Thalamo-Cortical Structural Connectivity in Essential Tremor with Diffusional Kurtosis Imaging Tractography. *Tremor Other Hyperkinet Mov (N Y)* **9**, (2019).

67. Mueller, K. *et al.* General and selective brain connectivity alterations in essential tremor: A resting state fMRI study. *Neuroimage Clin* **16**, 468–476 (2017).

68. Yin, W., Lin, W., Li, W., Qian, S. & Mou, X. Resting State fMRI Demonstrates a Disturbance of the Cerebello-Cortical Circuit in Essential Tremor. *Brain Topogr* **29**, 412–418 (2016).

69. Wang, L. *et al.* Resting-state fMRI study on drug-naive patients of essential tremor with and without head tremor. *Sci Rep* **8**, 1–8 (2018).

70. Broersma, M. *et al.* Bilateral cerebellar activation in unilaterally challenged essential tremor. *Neuroimage Clin* **11**, 1–9 (2016).

71. Gallea, C. *et al.* Intrinsic signature of essential tremor in the cerebello-frontal network. *Brain* **138**, 2920–2933 (2015).

72. Benito-León, J. *et al.* Altered Functional Connectivity in Essential Tremor: A Resting-State fMRI Study. *Medicine* **94**, e1936 (2015).

73. Li, J.-Y. *et al.* Patterns of intrinsic brain activity in essential tremor with resting tremor and tremor-dominant Parkinson's disease. *Brain Imaging Behav* **14**, 2606–2617 (2020).

74. Buijink, A. W. G. *et al.* Motor network disruption in essential tremor: a functional and effective connectivity study. *Brain* **138**, 2934–2947 (2015).

75. Bucher, S. F., Seelos, K. C., Dodel, R. C., Reiser, M. & Oertel, W. H. Activation mapping in essential tremor with functional magnetic resonance imaging. *Ann Neurol* **41**, 32–40 (1997).

76. Buijink, A. W. G. *et al.* Rhythmic finger tapping reveals cerebellar dysfunction in essential tremor. *Parkinsonism Relat Disord* **21**, 383–388 (2015).

77. Neely, K. A. *et al.* Functional Brain Activity Relates to 0-3 and 3-8 Hz Force Oscillations in Essential Tremor. *Cereb Cortex* **25**, 4191–4202 (2015).

78. Fang, W. *et al.* Multiple Resting-State Networks Are Associated With Tremors and Cognitive Features in Essential Tremor. *Mov Disord* **30**, 1926–1936 (2015).

79. Archer, D. B. *et al.* A widespread visually-sensitive functional network relates to symptoms in essential tremor. *Brain* **141**, 472–485 (2018).

80. Raethjen, J. & Deuschl, G. The oscillating central network of Essential tremor. *Clinical Neurophysiology* **123**, 61–64 (2012).

81. Raethjen, J., Govindan, R. B., Kopper, F., Muthuraman, M. & Deuschl, G. Cortical involvement in the generation of essential tremor. *J Neurophysiol* **97**, 3219–3228 (2007).

82. Albanese, A. *et al.* Phenomenology and classification of dystonia: a consensus update. *Mov Disord* **28**, 863–873 (2013).

83. Fahn, S. Concept and classification of dystonia. *Adv Neurol* **50**, 1–8 (1988).

84. Tarsy, D. & Simon, D. K. Dystonia. *N Engl J Med* **355**, 818–829 (2006).

85. Geyer, H. L. & Bressman, S. B. The diagnosis of dystonia. *Lancet Neurol* **5**, 780–790 (2006).

86. Albanese, A. & Del Sorbo, F. Dystonia and tremor: The clinical syndromes with isolated tremor. *Tremor and Other Hyperkinetic Movements* **2016**, 1–10 (2016).

87. Kassavetis, P. *et al.* Secondary and primary dystonia : pathophysiological differences. 2038–2049 (2013) doi:10.1093/brain/awt150.

88. Albanese, A. The clinical expression of primary dystonia. *J Neurol* **250**, 1145–1151 (2003).

89. Gövert, F. & Deuschl, G. Tremor entities and their classification: an update. *Curr Opin Neurol* **28**, 393–399 (2015).

90. Klein, C. & Fahn, S. Translation of Oppenheim's 1911 paper on dystonia. *Mov Disord* **28**, 851–862 (2013).

91. Sjögren, G. Dystonia musculorum deformans. A genetic and clinical population study of 121 cases. *Acta Neurol Scand* **42**, Suppl-17 (1966).

92. Yanagisawa, N. & Goto, A. Dystonia musculorum deformans: Analysis with electromyography. *J Neurol Sci* **13**, 39–65 (1971).

93. MARSDEN, C. D. & HARRISON, M. J. G. IDIOPATHIC TORSION DYSTONIA (DYSTONIA MUSCULORUM DEFORMANS): A REVIEW OF FORTY-TWO PATIENTS. *Brain* **97**, 793–810 (1974).

94. Fahn, S. Classification and investigation of dystonia. *Movement disorders* **2**, 332–358 (1987).

95. Shaikh, A. G., Zee, D. S. & Jinnah, H. A. Oscillatory head movements in cervical dystonia: Dystonia, tremor, or both? *Movement Disorders* **30**, 834–842 (2015).

96. Erro, R. *et al.* Rest and other types of tremor in adult-onset primary dystonia. *J Neurol Neurosurg Psychiatry* **85**, 965–968 (2014).

97. Gigante, A. F., Berardelli, A. & Defazio, G. Rest tremor in idiopathic adult-onset dystonia. *Eur J Neurol* **23**, 935–939 (2016).

98. Haggstrom, L., Darveniza, P. & Tisch, S. Mild parkinsonian features in dystonia: Literature review, mechanisms and clinical perspectives. *Parkinsonism Relat Disord* **35**, 1–7 (2017).

99. Shaikh, A. G. *et al.* Dystonia and Tremor. *Neurology* **96**, e563 LP-e574 (2021).

100. Svetel, M., Pekmezovic, T., Tomic, A., Kresojevic, N. & Kostic, V. S. The spread of primary late-onset focal dystonia in a long-term follow up study. *Clin Neurol Neurosurg* **132**, 41–43 (2015).

101. Norris, S. A. *et al.* Clinical and demographic characteristics related to onset site and spread of cervical dystonia. *Mov Disord* **31**, 1874–1882 (2016).

102. Panyakaew, P., Jinnah, H. A. & Shaikh, A. G. Clinical features, pathophysiology, treatment, and controversies of tremor in dystonia. *J Neurol Sci* **435**, 120199 (2022).

103. Münchau, A. *et al.* Arm tremor in cervical dystonia differs from essential tremor and can be classified by onset age and spread of symptoms. *Brain* **124**, 1765–1776 (2001).

104. Defazio, G., Conte, A., Gigante, A. F., Fabbrini, G. & Berardelli, A. Is tremor in dystonia a phenotypic feature of dystonia? *Neurology* **84**, 1053–1059 (2015).

105. Becktepe, J. *et al.* Exploring Interrater Disagreement on Essential Tremor Using a Standardized Tremor Elements Assessment. *Mov Disord Clin Pract* **8**, 371–376 (2021).

106. Tisch, S. Recent advances in understanding and managing dystonia [version 1; referees: 2 approved]. *F1000Res* **7**, (2018).

107. di Biase, L. *et al.* Tremor stability index: a new tool for differential diagnosis in tremor syndromes. *Brain* **140**, 1977–1986 (2017).

108. Panyakaew, P., Cho, H. J., Lee, S. W., Wu, T. & Hallett, M. The Pathophysiology of Dystonic Tremors and Comparison With Essential Tremor. *J Neurosci* **40**, 9317–9326 (2020).

109. Jedynak, C. P., Bonnet, A. M. & Agid, Y. Tremor and idiopathic dystonia. *Mov Disord* **6**, 230–236 (1991).

110. Warner, T. T. & Bressman, S. B. *Clinical diagnosis and management of dystonia* . (CRC Press, 2007). doi:10.3109/9780203640487.

111. Butler, A. G., Duffey, P. O., Hawthorne, M. R. & Barnes, M. P. An epidemiologic survey of dystonia within the entire population of northeast England over the past nine years. *Adv Neurol* **94**, 95–99 (2004).

112. Sex-related influences on the frequency and age of onset of primary dystonia. Epidemiologic Study of Dystonia in Europe (ESDE) Collaborative Group. *Neurology* **53**, 1871–1873 (1999).

113. Nakashima, K., Kusumi, M., Inoue, Y. & Takahashi, K. Prevalence of focal dystonias in the western area of Tottori Prefecture in Japan. *Mov Disord* **10**, 440–443 (1995).

114. A prevalence study of primary dystonia in eight European countries. *J Neurol* **247**, 787–792 (2000).

115. Kandil, M. R., Tohamy, S. A., Fattah, M. A., Ahmed, H. N. & Farwiez, H. M. Prevalence of chorea, dystonia and athetosis in Assiut, Egypt: a clinical and epidemiological study. *Neuroepidemiology* **13**, 202–210 (1994).

116. Korczyn, A. D. *et al.* Torsion dystonia in Israel. *Ann Neurol* **8**, 387–391 (1980).

117. Duffey, P. O., Butler, A. G., Hawthorne, M. R. & Barnes, M. P. The epidemiology of the primary dystonias in the north of England. *Adv Neurol* **78**, 121–125 (1998).

118. Li, S. C. *et al.* A prevalence survey of Parkinson's disease and other movement disorders in the People's Republic of China. *Arch Neurol* **42**, 655–657 (1985).

119. Müller, J. *et al.* The prevalence of primary dystonia in the general community. *Neurology* **59**, 941–943 (2002).

120. Castelon Konkiewitz, E. *et al.* Service-based survey of dystonia in munich. *Neuroepidemiology* **21**, 202–206 (2002).

121. Steeves, T. D., Day, L., Dykeman, J., Jette, N. & Pringsheim, T. The prevalence of primary dystonia: a systematic review and meta-analysis. *Mov Disord* **27**, 1789–1796 (2012).

122. de Carvalho Aguiar, P. M. & Ozelius, L. J. Classification and genetics of dystonia. *Lancet Neurol* **1**, 316–325 (2002).

123. Pandey, S. & Sarma, N. Tremor in dystonia. *Parkinsonism Relat Disord* **29**, 3–9 (2016).

124. Pal, P. K., Samii, A., Schulzer, M., Mak, E. & Tsui, J. K. Head tremor in cervical dystonia. *Can J Neurol Sci* **27**, 137–142 (2000).

125. Ferraz, H. B., De Andrade, L. A., Silva, S. M., Borges, V. & Rocha, M. S. [Postural tremor and dystonia. Clinical aspects and physiopathological considerations]. *Arq Neuropsiquiatr* **52**, 466–470 (1994).

126. Defazio, G. *et al.* Tremor in primary adult-onset dystonia: prevalence and associated clinical features. *J Neurol Neurosurg Psychiatry* **84**, 404–408 (2013).

127. Charlesworth, G., Bhatia, K. P. & Wood, N. W. The genetics of dystonia: new twists in an old tale. *Brain* **136**, 2017–2037 (2013).

128. Martino, D. *et al.* Extragenetic factors and clinical penetrance of DYT1 dystonia: an exploratory study. *J Neurol* **260**, 1081–1086 (2013).

129. Jankovic, J. & Van der Linden, C. Dystonia and tremor induced by peripheral trauma: predisposing factors. *J Neurol Neurosurg Psychiatry* **51**, 1512–1519 (1988).

130. Defazio, G. *et al.* Possible risk factors for primary adult onset dystonia: a case-control investigation by the Italian Movement Disorders Study Group. *Journal of Neurology, Neurosurgery & Psychiatry* **64**, 25 LP – 32 (1998).

131. Jinnah, H. A., Neychev, V. & Hess, E. J. The Anatomical Basis for Dystonia: The Motor Network Model. *Tremor Other Hyperkinet Mov (N Y)* **7**, 506 (2017).

132. Lehéricy, S., Tijssen, M. A. J., Vidailhet, M., Kaji, R. & Meunier, S. The anatomical basis of dystonia: Current view using neuroimaging. *Movement Disorders* **28**, 944–957 (2013).

133. Conte, A. *et al.* Somatosensory temporal discrimination in essential tremor and isolated head and voice tremors. *Movement Disorders* **30**, 822–827 (2015).

134. Cerasa, A. *et al.* Neuroanatomical correlates of dystonic tremor: A cross-sectional study. *Parkinsonism Relat Disord* **20**, 314–317 (2014).

135. Nisticò, R. *et al.* Blink reflex recovery cycle in patients with dystonic tremor: a cross-sectional study. *Neurology* **78**, 1363–1365 (2012).

136. Tinazzi, M. *et al.* Temporal discrimination in patients with dystonia and tremor and patients with essential tremor. *Neurology* **80**, 76–84 (2013).

137. Rudzińska, M., Krawczyk, M., Wójcik-Pędziwiatr, M., Szczudlik, A. & Wasielewska, A. Tremor associated with focal and segmental dystonia. *Neurol Neurochir Pol* **47**, 223–231 (2013).

138. Tsuboi, T. *et al.* Comparative connectivity correlates of dystonic and essential tremor deep brain stimulation. *Brain* **144**, 1774–1786 (2021).

139. Madelein van der Stouwe, A. M., Nieuwhof, F. & Helmich, R. C. Tremor pathophysiology: lessons from neuroimaging. *Curr Opin Neurol* **33**, (2020).

140. Nieuwhof, F., Panyakaew, P., van de Warrenburg, B. P., Gallea, C. & Helmich, R. C. The patchy tremor landscape: recent advances in pathophysiology. *Curr Opin Neurol* **31**, (2018).

141. Alarcón, F., Tolosa, E. & Muñoz, E. Focal limb dystonia in a patient with a cerebellar mass. *Arch Neurol* **58**, 1125–1127 (2001).

142. LeDoux, M. S. & Brady, K. A. Secondary cervical dystonia associated with structural lesions of the central nervous system. *Mov Disord* **18**, 60–69 (2003).

143. Sethi, K. D. & Jankovic, J. Dystonia in spinocerebellar ataxia type 6. *Mov Disord* **17**, 150–153 (2002).

144. Hagenah, J. M., Zühlke, C., Hellenbroich, Y., Heide, W. & Klein, C. Focal dystonia as a presenting sign of spinocerebellar ataxia 17. *Mov Disord* **19**, 217–220 (2004).

145. Le Ber, I. *et al.* Predominant dystonia with marked cerebellar atrophy: a rare phenotype in familial dystonia. *Neurology* **67**, 1769–1773 (2006).

146. Kirke, D. N. *et al.* Neural correlates of dystonic tremor: a multimodal study of voice tremor in spasmodic dysphonia. *Brain Imaging Behav* **11**, 166–175 (2017).

147. Merola, A. *et al.* Head tremor at disease onset: an ataxic phenotype of cervical dystonia. *J Neurol* **266**, 1844–1851 (2019).

148. Batla, A. *et al.* The role of cerebellum in patients with late onset cervical/segmental dystonia?--evidence from the clinic. *Parkinsonism Relat Disord* **21**, 1317–1322 (2015).

149. Ma, K., Babij, R., Cortés, E., Vonsattel, J.-P. G. & Louis, E. D. Cerebellar pathology of a dual clinical diagnosis: patients with essential tremor and dystonia. *Tremor Other Hyperkinet Mov (N Y)* **2**, (2012).

150. Park, Y.-G. *et al.* Ca(V)3.1 is a tremor rhythm pacemaker in the inferior olive. *Proc Natl Acad Sci U S A* **107**, 10731–10736 (2010).

151. Llinás, R. R. The intrinsic electrophysiological properties of mammalian neurons: insights into central nervous system function. *Science* **242**, 1654–1664 (1988).

152. Llinás, R. R. The olivo-cerebellar system: a key to understanding the functional significance of intrinsic oscillatory brain properties. *Front Neural Circuits* **7**, 96 (2013).

153. Louis, E. D. & Lenka, A. The Olivary Hypothesis of Essential Tremor: Time to Lay this Model to Rest? *Tremor Other Hyperkinet Mov (N Y)* **7**, 473 (2017).

154. Houk, J. C. & Wise, S. P. Distributed modular architectures linking basal ganglia, cerebellum, and cerebral cortex: their role in planning and controlling action. *Cereb Cortex* **5**, 95–110 (1995).

155. Milner, T. E., Cadoret, G., Lessard, L. & Smith, A. M. EMG analysis of harmaline-induced tremor in normal and three strains of mutant mice with Purkinje cell degeneration and the role of the inferior olive. *J Neurophysiol* **73**, 2568–2577 (1995).

156. Pan, M.-K. *et al.* Cerebellar oscillations driven by synaptic pruning deficits of cerebellar climbing fibers contribute to tremor pathophysiology. *Sci Transl Med* **12**, (2020).

157. Colebatch, J. G., Findley, L. J., Frackowiak, R. S., Marsden, C. D. & Brooks, D. J. Preliminary report: activation of the cerebellum in essential tremor. *Lancet* **336**, 1028–1030 (1990).

158. Jenkins, I. H. *et al.* A positron emission tomography study of essential tremor: evidence for overactivity of cerebellar connections. *Ann Neurol* **34**, 82–90 (1993).

159. Schnitzler, A., Münks, C., Butz, M., Timmermann, L. & Gross, J. Synchronized brain network associated with essential tremor as revealed by magnetoencephalography. *Movement Disorders* **24**, 1629–1635 (2009).

160. Buijink, A. W. G., Van Rootselaar, A. F. & Helmich, R. C. Connecting tremors - A circuits perspective. *Curr Opin Neurol* **35**, 518–524 (2022).

161. Nieuwhof, F. *et al.* Cerebello-thalamic activity drives an abnormal motor network into dystonic tremor. *Neuroimage Clin* **33**, 102919 (2022).

162. Desimone, J. C., Archer, D. B., Vaillancourt, D. E. & Shukla, A. W. Network-level connectivity is a critical feature distinguishing dystonic tremor and essential tremor. *Brain* **142**, 1644–1659 (2019).

163. Eidelberg, D. *et al.* Functional brain networks in DYT1 dystonia. *Ann Neurol* **44**, 303–312 (1998).

164. Argyelan, M. *et al.* Cerebellothalamocortical connectivity regulates penetrance in dystonia. *J Neurosci* **29**, 9740–9747 (2009).

165. Bradnam, L. V, McDonnell, M. N. & Ridding, M. C. Cerebellar Intermittent Theta-Burst Stimulation and Motor Control Training in Individuals with Cervical Dystonia. *Brain Sci* **6**, (2016).

166. Koch, G. *et al.* Effects of two weeks of cerebellar theta burst stimulation in cervical dystonia patients. *Brain Stimul* **7**, 564–572 (2014).

167. Bertrand, G., Jasper, H., Wong, A. & Mathews, G. Microelectrode recording during stereotactic surgery. *Clin Neurosurg* **16**, 328–355 (1969).

168. Ferreira, F. *et al.* Ventralis intermedius nucleus anatomical variability assessment by MRI structural connectivity. *Neuroimage* **238**, (2021).

169. Marsden, J. F., Ashby, P., Limousin-Dowsey, P., Rothwell, J. C. & Brown, P. Coherence between cerebellar thalamus, cortex and muscle in man: Cerebellar thalamus interactions. *Brain* **123**, 1459–1470 (2000).

170. Pedrosa, D. J. *et al.* Thalamomuscular coherence in essential tremor: hen or egg in the emergence of tremor? *J Neurosci* **34**, 14475–14483 (2014).

171. Lenz, F. A. *et al.* Single unit analysis of the human ventral thalamic nuclear group. Tremor-related activity in functionally identified cells. *Brain* **117 (Pt 3**, 531–543 (1994).

172. Hua, S. E. & Lenz, F. A. Posture-related oscillations in human cerebellar thalamus in essential tremor are enabled by voluntary motor circuits. *J Neurophysiol* **93**, 117–127 (2005).

173. Iorio-Morin, C., Fomenko, A. & Kalia, S. K. Deep-Brain Stimulation for Essential Tremor and Other Tremor Syndromes: A Narrative Review of Current Targets and Clinical Outcomes. *Brain Sci* **10**, (2020).

174. Tsuboi, T. *et al.* Longitudinal follow-up with VIM thalamic deep brain stimulation for dystonic or essential tremor. *Neurology* **94**, e1073–e1084 (2020).

175. Hirai, T., Miyazaki, M., Nakajima, H., Shibazaki, T. & Ohye, C. The correlation between tremor characteristics and the predicted volume of effective lesions in stereotaxic nucleus ventralis intermedius thalamotomy. *Brain* **106 (Pt 4**, 1001–1018 (1983).

176. Milosevic, L. *et al.* Physiological mechanisms of thalamic ventral intermediate nucleus stimulation for tremor suppression. *Brain* **141**, 2142–2155 (2018).

177. Anderson, T., Hu, B., Pittman, Q. & Kiss, Z. H. T. Mechanisms of deep brain stimulation: an intracellular study in rat thalamus. *J Physiol* **559**, 301–313 (2004).

178. Battistella, G. & Simonyan, K. Top-down alteration of functional connectivity within the sensorimotor network in focal dystonia. *Neurology* **92**, e1843–e1851 (2019).

179. Dembek, T. A. *et al.* PSA and VIM DBS efficiency in essential tremor depends on distance to the dentatorubrothalamic tract. *Neuroimage Clin* **26**, 102235 (2020).

180. Barbe, M. T. *et al.* DBS of the PSA and the VIM in essential tremor: A randomized, double-blind, crossover trial. *Neurology* **91**, e543–e550 (2018).

181. Percheron, G., François, C., Talbi, B., Yelnik, J. & Fénelon, G. The primate motor thalamus. *Brain Res Brain Res Rev* **22**, 93–181 (1996).

182. Hellwig, B. *et al.* Tremor-correlated cortical activity in essential tremor. *The Lancet* **357**, 519–523 (2001).

183. Britton, T. C. *et al.* Modulation of postural wrist tremors by magnetic stimulation of the motor cortex in patients with Parkinson's disease or essential tremor and in normal subjects mimicking tremor. *Ann Neurol* **33**, 473–479 (1993).

184. Pascual-Leone, A., Valls-Solé, J., Toro, C., Wassermann, E. M. & Hallett, M. Resetting of essential tremor and postural tremor in Parkinson's disease with transcranial magnetic stimulation. *Muscle Nerve* **17**, 800–807 (1994).

185. Chuang, W.-L., Huang, Y.-Z., Lu, C.-S. & Chen, R.-S. Reduced cortical plasticity and GABAergic modulation in essential tremor. *Movement Disorders* **29**, 501–507 (2014).

186. Hellriegel, H., Schulz, E. M., Siebner, H. R., Deuschl, G. & Raethjen, J. H. Continuous theta-burst stimulation of the primary motor cortex in essential tremor. *Clin Neurophysiol* **123**, 1010–1015 (2012).

187. Sharifi, S. *et al.* Intermittent cortical involvement in the preservation of tremor in essential tremor. *J Neurophysiol* **118**, 2628–2635 (2017).

188. Ondo, W. *et al.* Comparison of the Fahn-Tolosa-Marin Clinical Rating Scale and the Essential Tremor Rating Assessment Scale. *Mov Disord Clin Pract* **5**, 60–65 (2018).

189. Sarica, C. *et al.* Clinical Rating Scale for Tremor: a needed clarification. *J Neurosurg* **136**, 932–933 (2022).

190. Fahn, S., Tolosa, E., Marin, C., Jankovic, J. & Tolosa, E. *Clinical rating scale for tremor*. (Williams & Wilkins, 1993).

191. Chang, W. S. *et al.* Unilateral magnetic resonance guided focused ultrasound thalamotomy for essential tremor: practices and clinicoradiological outcomes. *J Neurol Neurosurg Psychiatry* **86**, 257–264 (2015).

192. Elias, W. J. *et al.* A pilot study of focused ultrasound thalamotomy for essential tremor. *N Engl J Med* **369**, 640–648 (2013).

193. Fukutome, K., Kuga, Y., Ohnishi, H., Hirabayashi, H. & Nakase, H. What factors impact the clinical outcome of magnetic resonance imaging-guided focused ultrasound thalamotomy for essential tremor? *J Neurosurg* **134**, 1618–1623 (2020).

194. Gasca-Salas, C. *et al.* Cognitive safety after unilateral magnetic resonance-guided focused ultrasound thalamotomy for essential tremor. *J Neurol Neurosurg Psychiatry* **90**, 830–831 (2019).

195. Huss, D. S. *et al.* Functional assessment and quality of life in essential tremor with bilateral or unilateral DBS and focused ultrasound thalamotomy. *Mov Disord* **30**, 1937–1943 (2015).

196. Jameel, A. *et al.* Double lesion MRgFUS treatment of essential tremor targeting the thalamus and posterior sub-thalamic area: preliminary study with two year follow-up. *Br J Neurosurg* **36**, 241–250 (2022).

197. Jung, N. Y., Park, C. K., Chang, W. S., Jung, H. H. & Chang, J. W. Effects on cognition and quality of life with unilateral magnetic resonance-guided focused ultrasound thalamotomy for essential tremor. *Neurosurg Focus* **44**, E8 (2018).

198. Elias, W. J. *et al.* A Randomized Trial of Focused Ultrasound Thalamotomy for Essential Tremor. *New England Journal of Medicine* **375**, 730–739 (2016).

199. Calne, D. B., Deutch, A. Y. & Wolters, E. C. Parkinsonism & Related Disorders. *Parkinsonism Relat Disord* **13**, i (2007).

200. Tröster, A. I., Pahwa, R., Fields, J. A., Tanner, C. M. & Lyons, K. E. Quality of life in Essential Tremor Questionnaire (QUEST): Development and initial validation. *Parkinsonism Relat Disord* **11**, 367–373 (2005).

201. Haubenberger, D. *et al.* Validation of digital spiral analysis as outcome parameter for clinical trials in essential tremor. *Movement disorders* **26**, 2073–2080 (2011).

202. HORSLEY, V. & CLARKE, R. H. THE STRUCTURE AND FUNCTIONS OF THE CEREBELLUM EXAMINED BY A NEW METHOD. *Brain* **31**, 45–124 (1908).

203. Spiegel, E. A., Wycis, H. T., Marks, M. & Lee, A. J. Stereotaxic Apparatus for Operations on the Human Brain. *Science* **106**, 349–350 (1947).

204. GILDENBERG, P. L. Studies in stereoencephalotomy. VIII. Comparison of the variability of subcortical lesions produced by various procedures (radio-frequency coagulation, electrolysis, alcohol injection). *Confin Neurol* **17**, 299–309 (1957).

205. RIECHERT, T. Long term follow-up of results of stereotaxic treatment in extrapyramidal disorders. *Confin Neurol* **22**, 356–363 (1962).

206. COOPER, I. S. Chemopallidectomy: an investigative technique in geriatric parkinsonians. *Science* **121**, 217–218 (1955).

207. SPIEGEL, E. A. & WYCIS, H. T. Pallidothalamotomy in chorea. *Arch Neurol Psychiatry* **64**, 295–296 (1950).

208. SPIEGEL, E. A. *et al.* CAMPOTOMY IN VARIOUS EXTRAPYRAMIDAL DISORDERS. *J Neurosurg* **20**, 871–884 (1963).

209. GUIOT, G., HARDY, J. & ALBE-FESSARD, D. [Precise delimitation of the subcortical structures and identification of thalamic nuclei in man by stereotactic electrophysiology]. *Neurochirurgia (Stuttg)* **5**, 1–18 (1962).

210. Hassler, R. & Hess, W. R. Experimentelle und anatomische Befunde über die Drehbewegungen und ihre nervösen Apparate. *Arch Psychiatr Nervenkr* **192**, 488–526 (1954).

211. TALAIRACH, J., DE ALJURIAGUERRA, J. & DAVID, M. [A stereotaxic study of the deep encephalic structures in man; technic; physiopathologic and therapeutic significance]. *Presse Med* **60**, 605–609 (1952).

212. Hassler, R. Architectonic organization of the thalamic nuclei.: InG. Schaltenbrand, AE Walker (eds): Stereotaxy of the Human Brain. Preprint at (1982).

213. Spiegel, E. A. Methodological problems in stereoencephalotomy. *Confin Neurol* **26**, 125–132 (1965).

214. Ahmed, H. *et al.* Evolution of Movement Disorders Surgery Leading to Contemporary Focused Ultrasound Therapy for Tremor. *Magn Reson Imaging Clin N Am* **23**, 515–522 (2015).

215. Marsden, C. D. & Parkes, J. D. 'On-off' effects in patients with Parkinson's disease on chronic levodopa therapy. *Lancet* **1**, 292–296 (1976).

216. Laitinen, L. V, Bergenheim, A. T. & Hariz, M. I. Ventroposterolateral pallidotomy can abolish all parkinsonian symptoms. *Stereotact Funct Neurosurg* **58**, 14–21 (1992).

217. Laitinen, L. V, Bergenheim, A. T. & Hariz, M. I. Leksell's posteroventral pallidotomy in the treatment of Parkinson's disease. *J Neurosurg* **76**, 53–61 (1992).

218. Yamashiro, K. & Tasker, R. R. Stereotactic thalamotomy for dystonic patients. *Stereotact Funct Neurosurg* **60**, 81–85 (1993).

219. Shahzadi, S., Tasker, R. R. & Lozano, A. Thalamotomy for essential and cerebellar tremor. *Stereotact Funct Neurosurg* **65**, 11–17 (1995).

220. Lozano, A. M. *et al.* Globus pallidus internus pallidotomy for generalized dystonia. *Mov Disord* **12**, 865–870 (1997).

221. Goldman, M. S. & Kelly, P. J. Symptomatic and functional outcome of stereotactic ventralis lateralis thalamotomy for intention tremor. *J Neurosurg* **77**, 223–229 (1992).

222. Pahwa, R. *et al.* Comparison of thalamotomy to deep brain stimulation of the thalamus in essential tremor. *Mov Disord* **16**, 140–143 (2001).

223. Fodstad, H. & Hariz, M. Electricity in the treatment of nervous system disease. *Acta Neurochir Suppl* **97**, 11–19 (2007).

224. Tasker, R. R. Deep brain stimulation is preferable to thalamotomy for tremor suppression. *Surg Neurol* **49**, 144–145 (1998).

225. Tasker, R. R. *et al.* Deep brain stimulation and thalamotomy for tremor compared. *Acta Neurochir Suppl* **68**, 49–53 (1997).

226. Fenoy, A. J. & Simpson, R. K. J. Risks of common complications in deep brain stimulation surgery: management and avoidance. *J Neurosurg* **120**, 132–139 (2014).

227. Ohye, C. & Shibazaki, T. Treatment of functional disorders with gamma knife thalamotomy. *Prog Neurol Surg* **22**, 170–181 (2009).

228. Niranjan, A., Kondziolka, D., Baser, S., Heyman, R. & Lunsford, L. D. Functional outcomes after gamma knife thalamotomy for essential tremor and MS-related tremor. *Neurology* **55**, 443–446 (2000).

229. Duma, C. M. *et al.* Gamma knife radiosurgery for thalamotomy in parkinsonian tremor: a five-year experience. *J Neurosurg* **88**, 1044–1049 (1998).

230. Lynn, J. G. & Putnam, T. J. Histology of Cerebral Lesions Produced by Focused Ultrasound. *Am J Pathol* **20**, 637–649 (1944).

231. Burgess, A. & Hynynen, K. Noninvasive and targeted drug delivery to the brain using focused ultrasound. *ACS Chem Neurosci* **4**, 519–526 (2013).

232. Barile, A. *et al.* Minimally invasive treatments of painful bone lesions: state of the art. *Med Oncol* **34**, 53 (2017).

233. Masciocchi, C. *et al.* Radiofrequency ablation versus magnetic resonance guided focused ultrasound surgery for minimally invasive treatment of osteoid osteoma: a propensity score matching study. *Eur Radiol* **26**, 2472–2481 (2016).

234. Barile, A. *et al.* Present role and future perspectives of interventional radiology in the treatment of painful bone lesions. *Future Oncol* **14**, 2945–2955 (2018).

235. Masciocchi, C. *et al.* Uterine fibroid therapy using interventional radiology mini-invasive treatments: current perspective. *Medical Oncology* **34**, 52 (2017).

236. Arrigoni, F. *et al.* Developments in the management of bone metastases with interventional radiology. *Acta Biomed* **89**, 166–174 (2018).

237. Masciocchi, C. *et al.* Critical role of HIFU in musculoskeletal interventions. *Radiol Med* **119**, 470–475 (2014).

238. Lipsman, N. *et al.* MR-guided focused ultrasound thalamotomy for essential tremor: a proof-of-concept study. *Lancet Neurol* **12**, 462–468 (2013).

239. Fasano, A. *et al.* MRI-guided focused ultrasound thalamotomy in non-ET tremor syndromes. *Neurology* **89**, 771–775 (2017).

240. Zaaroor, M. *et al.* Magnetic resonance-guided focused ultrasound thalamotomy for tremor: a report of 30 Parkinson's disease and essential tremor cases. *J Neurosurg* **128**, 202–210 (2018).

241. Schlesinger, I. *et al.* MRI Guided Focused Ultrasound Thalamotomy for Moderate-to-Severe Tremor in Parkinson's Disease. *Parkinsons Dis* **2015**, 219149 (2015).

242. Zaaroor, M. *et al.* Magnetic resonance–guided focused ultrasound thalamotomy for tremor: a report of 30 Parkinson's disease and essential tremor cases. *J Neurosurg* **128**, 1–9 (2017).

243. Meng, Y. *et al.* Technical Principles and Clinical Workflow of Transcranial MR-Guided Focused Ultrasound. *Stereotact Funct Neurosurg* **99**, 329–342 (2020).

244. Bond, A. E. *et al.* Safety and Efficacy of Focused Ultrasound Thalamotomy for Patients With Medication-Refractory, Tremor-Dominant Parkinson Disease: A Randomized Clinical Trial. *JAMA Neurol* **74**, 1412–1418 (2017).

245. Li, C. *et al.* Cost-Effectiveness of Magnetic Resonance-Guided Focused Ultrasound for Essential Tremor. *Mov Disord* **34**, 735–743 (2019).

246. Elias, W. J. *et al.* A Randomized Trial of Focused Ultrasound Thalamotomy for Essential Tremor. *N Engl J Med* **375**, 730–739 (2016).

247. Elias, W. J. *et al.* A Randomized Trial of Focused Ultrasound Thalamotomy for Essential Tremor. *N Engl J Med* **375**, 730–739 (2016).

248. Gallay, M. N. *et al.* Incisionless transcranial MR-guided focused ultrasound in essential tremor: Cerebellothalamic tractotomy. *J Ther Ultrasound* **4**, (2016).

249. Schreglmann, S. R. *et al.* Unilateral cerebellothalamic tract ablation in essential tremor by MRI-guided focused ultrasound. *Neurology* **88**, 1329–1333 (2017).

250. Chang, J. W. *et al.* A prospective trial of magnetic resonance-guided focused ultrasound thalamotomy for essential tremor: Results at the 2-year follow-up. *Ann Neurol* **83**, 107–114 (2018).

251. Sinai, A. *et al.* Magnetic resonance-guided focused ultrasound thalamotomy for essential tremor: a 5-year single-center experience. *J Neurosurg* 1–8 (2019) doi:10.3171/2019.3.JNS19466.

252. Park, Y.-S., Jung, N. Y., Na, Y. C. & Chang, J. W. Four-year follow-up results of magnetic resonance-guided focused ultrasound thalamotomy for essential tremor. *Mov Disord* **34**, 727–734 (2019).

253. Halpern, C. H. *et al.* Three-year follow-up of prospective trial of focused ultrasound thalamotomy for essential tremor. *Neurology* **93**, e2284–e2293 (2019).

254. Krishna, V. *et al.* Predictors of outcomes after focused ultrasoun thalamotomy. *Neurosurgery* **87**, 229–237 (2020).

255. Su, J. H. *et al.* Improved Vim targeting for focused ultrasound ablation treatment of essential tremor: A probabilistic and patient-specific approach. *Hum Brain Mapp* **41**, 4769–4788 (2020).

256. Zur, G. *et al.* Tremor Relief and Structural Integrity after MRI-guided Focused US Thalamotomy in Tremor Disorders. *Radiology* **294**, 676–685 (2020).

257. Wu, P. *et al.* Focused Ultrasound Thalamotomy for the Treatment of Essential Tremor: A 2-Year Outcome Study of Chinese People. *Front Aging Neurosci* **13**, 697029 (2021).

258. Purrer, V. *et al.* Transcranial high-intensity Magnetic Resonance-guided focused ultrasound (tcMRgFUS) - safety and impacts on tremor severity and quality of life. *Parkinsonism Relat Disord* **100**, 6–12 (2022).

259. Yamamoto, K. *et al.* Ipsilateral and axial tremor response to focused ultrasound thalamotomy for essential tremor: clinical outcomes and probabilistic mapping. *J Neurol Neurosurg Psychiatry* **93**, 1049–1058 (2022).

260. Kato, S. *et al.* Magnetic resonance-guided focused ultrasound thalamotomy restored distinctive resting-state networks in patients with essential tremor. *J Neurosurg* **138**, 306–317 (2023).

261. Pae, C. *et al.* Differences in intrinsic functional networks in patients with essential tremor who had good and poor long-term responses after thalamotomy performed using MR-guided ultrasound. *J Neurosurg* **138**, 318–328 (2023).

262. Harary, M. *et al.* Focused ultrasound in neurosurgery: a historical perspective. *Neurosurgical Focus FOC* **44**, E2 (2018).

263. Abu-Zidan, F. M., Hefny, A. F. & Corr, P. Clinical ultrasound physics. *J Emerg Trauma Shock* **4**, 501–503 (2011).

264. Harary, M. *et al.* Focused ultrasound in neurosurgery: a historical perspective. *Neurosurgical Focus FOC* **44**, E2 (2018).

265. Kobus, T. & McDannold, N. Update on Clinical Magnetic Resonance-Guided Focused Ultrasound Applications. *Magn Reson Imaging Clin N Am* **23**, 657–667 (2015).

266. Ghanouni, P. *et al.* Transcranial MRI-guided focused ultrasound: A review of the technologic and neurologic applications. *American Journal of Roentgenology* **205**, 150–159 (2015).

267. Fry, F. J. & Barger, J. E. Acoustical properties of the human skull. *J Acoust Soc Am* **63**, 1576–1590 (1978).

268. Arvanitis, C. D. & McDannold, N. Integrated ultrasound and magnetic resonance imaging for simultaneous temperature and cavitation monitoring during focused ultrasound therapies. *Med Phys* **40**, 112901 (2013).

269. Tsai, K. W. K. *et al.* The Distribution of Skull Score and Skull Density Ratio in Tremor Patients for MR-Guided Focused Ultrasound Thalamotomy. *Front Neurosci* **15**, (2021).

270. Pouratian, N., Baltuch, G., Elias, W. J. & Gross, R. American Society for Stereotactic and Functional Neurosurgery Position Statement on Magnetic Resonance-Guided Focused Ultrasound for the Management of Essential Tremor. *Neurosurgery* **87**, E126–E129 (2020).

271. Fukutome, K., Kuga, Y., Ohnishi, H., Hirabayashi, H. & Nakase, H. What factors impact the clinical outcome of magnetic resonance imaging–guided focused ultrasound thalamotomy for essential tremor? *J Neurosurg* **134**, 1618–1623 (2021).

272. D'Souza, M. *et al.* Impact of skull density ratio on efficacy and safety of magnetic resonance–guided focused ultrasound treatment of essential tremor. *J Neurosurg* **132**, 1392–1397 (2020).

273. Pineda-Pardo, J. A. *et al.* Letter: The Role of Skull Thickness beyond the Skull Density Ratio on MRgFUS Thalamotomy Feasibility: Which Patients Should We Exclude? *Neurosurgery* **86**, E477–E479 (2020).

274. Boutet, A. *et al.* The relevance of skull density ratio in selecting candidates for transcranial MR-guided focused ultrasound. *J Neurosurg* **132**, 1785–1791 (2020).

275. Yamamoto, K. *et al.* Ventralis intermedius thalamotomy with focused ultrasound for patients with low skull density ratio. *Movement Disorders* **34**, 1239–1240 (2019).

276. Boutet, A. *et al.* Focused ultrasound thalamotomy location determines clinical benefits in patients with essential tremor. *Brain* **141**, 3405–3414 (2018).

277. White, J., Clement, G. T. & Hynynen, K. Transcranial ultrasound focus reconstruction with phase and amplitude correction. *IEEE Trans Ultrason Ferroelectr Freq Control* **52**, 1518–1522 (2005).

278. Connor, C. W. & Hynynen, K. Patterns of thermal deposition in the skull during transcranial focused ultrasound surgery. *IEEE Trans Biomed Eng* **51**, 1693–1706 (2004).

279. Gaur, P. *et al.* Correcting heat-induced chemical shift distortions in proton resonance frequency-shift thermometry. *Magn Reson Med* **76**, 172–182 (2016).

280. Iacopino, D. G. *et al.* Preliminary experience with a transcranial magnetic resonance-guided focused ultrasound surgery system integrated with a 1.5-T MRI unit in a series of patients with essential tremor and Parkinson's disease. *Neurosurg Focus* **44**, E7 (2018).

281. Louis, E. D. Utility of the hand-drawn spiral as a tool in clinical-epidemiological research on essential tremor: Data from four essential tremor cohorts. *Neuroepidemiology* **44**, 45–50 (2015).

282. Dallapiazza, R. F. *et al.* Outcomes from stereotactic surgery for essential tremor. 474–482 (2019) doi:10.1136/jnnp-2018-318240.

283. Vassal, F. *et al.* Direct stereotactic targeting of the ventrointermediate nucleus of the thalamus based on anatomic 1.5-T MRI mapping with a white matter attenuated inversion recovery (WAIR) sequence. *Brain Stimul* **5**, 625–633 (2012).

284. Tsolaki, E., Downes, A., Speier, W., Elias, W. J. & Pouratian, N. The potential value of probabilistic tractography-based for MR-guided focused ultrasound thalamotomy for essential tremor. *Neuroimage Clin* **17**, 1019–1027 (2018).

285. Spiegelmann, R., Nissim, O., Daniels, D., Ocherashvilli, A. & Mardor, Y. Stereotactic targeting of the ventrointermediate nucleus of the thalamus by direct visualization with high-field MRI. *Stereotact Funct Neurosurg* **84**, 19–23 (2006).

286. Abosch, A., Yacoub, E., Ugurbil, K. & Harel, N. An Assessment of Current Brain Targets for Deep Brain Stimulation Surgery With Susceptibility-Weighted Imaging at 7 Tesla. *Neurosurgery* **67**, 1745–1756 (2010).

287. Anthofer, J. *et al.* The variability of atlas-based targets in relation to surrounding major fibre tracts in thalamic deep brain stimulation. *Acta Neurochir (Wien)* **156**, 1497–504; discussion 1504 (2014).

288. Tourdias, T., Saranathan, M., Levesque, I. R., Su, J. & Rutt, B. K. Visualization of intra-thalamic nuclei with optimized white-matter-nulled MPRAGE at 7T. *Neuroimage* **84**, 534–545 (2014).

289. Sudhyadhom, A., Haq, I. U., Foote, K. D., Okun, M. S. & Bova, F. J. A high resolution and high contrast MRI for differentiation of subcortical structures for DBS targeting: The Fast Gray Matter Acquisition T1 Inversion Recovery (FGATIR). *Neuroimage* **47**, T44–T52 (2009).

290. Middlebrooks, E. H. *et al.* A method for pre-operative single-subject thalamic segmentation based on probabilistic tractography for essential tremor deep brain stimulation. *Neuroradiology* **60**, 303–309 (2018).

291. Middlebrooks, E. H. *et al.* Structural connectivity–based segmentation of the thalamus and prediction of tremor improvement following thalamic deep brain stimulation of the ventral intermediate nucleus. *Neuroimage Clin* **20**, 1266–1273 (2018).

292. Akram, H. *et al.* Connectivity derived thalamic segmentation in deep brain stimulation for tremor. *Neuroimage Clin* **18**, 130–142 (2018).

293. Duan, Y., Li, X. & Xi, Y. Thalamus segmentation from diffusion tensor magnetic resonance imaging. *Int J Biomed Imaging* **2007**, (2007).

294. Bruno, F. *et al.* Comparative evaluation of tractography-based direct targeting and atlas-based indirect targeting of the ventral intermediate (Vim) nucleus in MRgFUS thalamotomy. *Sci Rep* **11**, 13538 (2021).

295. Parras, O., Domínguez, P., Tomás-Biosca, A. & Guridi, J. The role of tractography in the localisation of the Vim nucleus of the thalamus and the dentatorubrothalamic tract for the treatment of tremor. *Neurologia* (2021) doi:10.1016/j.nrleng.2019.09.008.

296. Kapadia, A. N. *et al.* Multimodal MRI for MRgFUS in essential tremor: Post-treatment radiological markers of clinical outcome. *J Neurol Neurosurg Psychiatry* **91**, 921–927 (2020).

297. Holcomb, J. M. *et al.* Improving tremor response to focused ultrasound thalamotomy. *Brain Commun* fcad165 (2023) doi:10.1093/braincomms/fcad165.

298. Krishna, V. *et al.* Prospective Tractography-Based Targeting for Improved Safety of Focused Ultrasound Thalamotomy. *Neurosurgery* **84**, 160–168 (2019).

299. Pennes, H. H. Analysis of tissue and arterial blood temperatures in the resting human forearm. *J Appl Physiol* **85**, 5–34 (1998).

300. Billard, B. E., Hynynen, K. & Roemer, R. B. Effects of physical parameters on high temperature ultrasound hyperthermia. *Ultrasound Med Biol* **16**, 409–420 (1990).

301. Jolesz, F. A. MRI-guided focused ultrasound surgery. *Annu Rev Med* **60**, 417–430 (2009).

302. Sapareto, S. A. & Dewey, W. C. Thermal dose determination in cancer therapy. *Int J Radiat Oncol Biol Phys* **10**, 787–800 (1984).

303. Roizin-Towle, L. & Pirro, J. P. The response of human and rodent cells to hyperthermia. *Int J Radiat Oncol Biol Phys* **20**, 751–756 (1991).

304. Huang, Y. *et al.* Predicting lesion size by accumulated thermal dose in MR-guided focused ultrasound for essential tremor. *Med Phys* **45**, 4704–4710 (2018).

305. Jones, R. M. *et al.* Accumulated thermal dose in MRI-guided focused ultrasound for essential tremor: repeated sonications with low focal temperatures. *J Neurosurg* **132**, 1802–1809 (2019).

306. Tomlinson, F. H., Jack, C. R. J. & Kelly, P. J. Sequential magnetic resonance imaging following stereotactic radiofrequency ventralis lateralis thalamotomy. *J Neurosurg* **74**, 579–584 (1991).

307. Ram, Z. *et al.* Magnetic resonance imaging-guided, high-intensity focused ultrasound for brain tumor therapy. *Neurosurgery* **59**, 946–949 (2006).

308. Chen, L., Bouley, D. M., Harris, B. T. & Butts, K. MRI study of immediate cell viability in focused ultrasound lesions in the rabbit brain. *J Magn Reson Imaging* **13**, 23–30 (2001).

309. Wintermark, M. *et al.* Imaging findings in MR imaging-guided focused ultrasound treatment for patients with essential tremor. *AJNR Am J Neuroradiol* **35**, 891–896 (2014).

310. Pineda-Pardo, J. A. *et al.* Microstructural changes of the dentato-rubro-thalamic tract after transcranial MR guided focused ultrasound ablation of the posteroventral VIM in essential tremor. *Hum Brain Mapp* **40**, 2933–2942 (2019).

311. Hubble, J. P. *et al.* Deep brain stimulation for essential tremor. *Neurology* **46**, 1150–1153 (1996).

312. Haubenberger, D. *et al.* Validation of digital spiral analysis as outcome parameter for clinical trials in essential tremor. *Movement Disorders* **26**, 2073–2080 (2011).

313. Stacy, M. A., Elble, R. J., Ondo, W. G., Wu, S.-C. & Hulihan, J. Assessment of interrater and intrarater reliability of the Fahn-Tolosa-Marin Tremor Rating Scale in essential tremor. *Movement disorders* **22**, 833–838 (2007).

314. Louis, E. D. Essential tremor. *Lancet Neurology* **4**, 100–110 (2005).

315. Panyakaew, P., Cho, H. J., Lee, S. W., Wu, T. & Hallett, M. The pathophysiology of dystonic tremors and comparison with essential tremor. *Journal of Neuroscience* **40**, 9317–9326 (2020).

316. Louis, E. D. *et al.* Correlates of functional disability in essential tremor. *Mov Disord* **16**, 914–920 (2001).

317. Legrand, A. P. *et al.* New insight in spiral drawing analysis methods – Application to action tremor quantification. *Clinical Neurophysiology* **128**, 1823–1834 (2017).

318. Elble, R. J. & Ellenbogen, A. Digitizing tablet and Fahn–Tolosa–Marín ratings of archimedes spirals have comparable minimum detectable change in essential tremor. *Tremor and Other Hyperkinetic Movements* **7**, 8–11 (2017).

319. Lak, A. M., Segar, D. J., McDannold, N., White, P. J. & Cosgrove, G. R. Magnetic Resonance Image Guided Focused Ultrasound Thalamotomy. A Single Center Experience With 160 Procedures. *Front Neurol* **13**, 1–7 (2022).

320. Kraus, P. H. & Hoffmann, A. Spiralometry: Computerized assessment of tremor amplitude on the basis of spiral drawing. *Movement Disorders* **25**, 2164–2170 (2010).

321. Bain, P. G. *et al.* Assessing tremor severity. *J Neurol Neurosurg Psychiatry* **56**, 868–873 (1993).

322. Dehaene, S. The neural basis of the Weber–Fechner law: a logarithmic mental number line. *Trends Cogn Sci* **7**, 145–147 (2003).

323. Elble, R. J. *et al.* Tremor amplitude is logarithmically related to 4- and 5-point tremor rating scales. *Brain* **129**, 2660–2666 (2006).

324. Louis, E. D. *et al.* Essential tremor-plus: a controversial new concept. *Lancet Neurol* **19**, 266–270 (2020).

325. Koller, W. C. & Rubino, F. A. Combined resting-postural tremors. *Arch Neurol* **42**, 683–684 (1985).

326. Rajput, A. H., Rozdilsky, B., Ang, L. & Rajput, A. Significance of Parkinsonian Manifestations in Essential Tremor. *Canadian journal of neurological sciences* **20**, 114–117 (1993).

327. Buijink, A. W. G. *et al.* Motor network disruption in essential tremor: A functional and effective connectivity study. *Brain* **138**, 2934–2947 (2015).

328. Fang, W. *et al.* Multiple Resting-State Networks Are Associated With Tremors and Cognitive Features in Essential Tremor. *Movement Disorders* **30**, 1926–1936 (2015).

329. Schnitzler, A., Münks, C., Butz, M., Timmermann, L. & Gross, J. Synchronized brain network associated with essential tremor as revealed by magnetoencephalography. *Movement Disorders* **24**, 1629–1635 (2009).

330. Blomstedt, P. & Hariz, M. I. Deep brain stimulation for movement disorders before DBS for movement disorders. *Parkinsonism Relat Disord* **16**, 429–433 (2010).

331. Fasano, A., Bove, F. & Lang, A. E. The treatment of dystonic tremor: a systematic review. *J Neurol Neurosurg Psychiatry* **85**, 759–769 (2014).

332. Fasano, A. *et al.* MRI-guided focused ultrasound thalamotomy in non-ET tremor syndromes. *Neurology* **89**, 771–775 (2017).

333. Elias, W. J. *et al.* A Randomized Trial of Focused Ultrasound Thalamotomy for Essential Tremor. *New England Journal of Medicine* **375**, 730–739 (2016).

334. Halpern, C. H. *et al.* Three-year follow-up of prospective trial of focused ultrasound thalamotomy for essential tremor. *Neurology* **93**, e2284–e2293 (2019).

335. Yushkevich, P. A. *et al.* User-guided 3D active contour segmentation of anatomical structures: Significantly improved efficiency and reliability. *NeuroImage (Orlando, Fla.)* **31**, 1116–1128 (2006).

336. Fahn, S., Tolosa, E. & Marin, C. Clinical Rating Scale for Tremor. *Parkinson's disease and movement disorders* 225–234 Preprint at (1988).

337. Torii, J. *et al.* Cutoff values for the best management strategy for magnetic resonance–guided focused ultrasound ablation for essential tremor. *J Neurosurg* **138**, 38–49 (2023).

338. Elble, R. *et al.* Task force report: scales for screening and evaluating tremor: critique and recommendations. *Mov Disord* **28**, 1793–1800 (2013).

339. Halpern, C. H. *et al.* Three-year follow-up of prospective trial of focused ultrasound thalamotomy for essential tremor. *Neurology* **93**, e2284–e2293 (2019).

340. Miller, W. K. *et al.* Magnetic resonance-guided focused ultrasound treatment for essential tremor shows sustained efficacy: a meta-analysis. *Neurosurg Rev* **45**, 533–544 (2022).

341. Higuchi, Y., Matsuda, S. & Serizawa, T. Gamma knife radiosurgery in movement disorders: Indications and limitations. *Movement Disorders* **32**, 28–35 (2017).

342. Campbell, A. M., Glover, J., Chiang, V. L. S. S., Gerrard, J. & Yu, J. B. Gamma knife stereotactic radiosurgical thalamotomy for intractable tremor: A systematic review of the literature. *Radiotherapy and Oncology* **114**, 296–301 (2015).

343. Shih, L. C., LaFaver, K., Lim, C., Papavassiliou, E. & Tarsy, D. Loss of benefit in VIM thalamic deep brain stimulation (DBS) for essential tremor (ET): how prevalent is it? *Parkinsonism Relat Disord* **19**, 676–679 (2013).

344. Nazzaro, J. M., Pahwa, R. & Lyons, K. E. Long-term benefits in quality of life after unilateral thalamic deep brain stimulation for essential tremor: Clinical article. *Journal of Neurosurgery JNS* **117**, 156–161 (2012).

345. Pilitsis, J. G. *et al.* Factors involved in long-term efficacy of deep brain stimulation of the thalamus for essential tremor. *J Neurosurg* **109**, 640–646 (2008).

346. Weidman, E. K., Kaplitt, M. G., Strybing, K. & Chazen, J. L. Repeat magnetic resonance imaging-guided focused ultrasound thalamotomy for recurrent essential tremor: case report and review of MRI findings. *J Neurosurg* 1–6 (2019) doi:10.3171/2018.10.JNS181721.

347. Picillo, M. *et al.* Dystonia as complication of thalamic neurosurgery. *Parkinsonism Relat Disord* **66**, 232–236 (2019).

348. Martino, D. *et al.* Dystonia following thalamic neurosurgery: A single centre experience with MR-guided focused ultrasound thalamotomy. *Parkinsonism & related disorders* vol. 71 1–3 Preprint at https://doi.org/10.1016/j.parkreldis.2019.11.019 (2020).

349. Dewhirst, M. W., Viglianti, B. L., Lora-Michiels, M., Hanson, M. & Hoopes, P. J. Basic principles of thermal dosimetry and thermal thresholds for tissue damage from hyperthermia. *International Journal of Hyperthermia* **19**, 267–294 (2003).

350. Sapareto, S. A. & Dewey, W. C. Thermal dose determination in cancer therapy. *Int J Radiat Oncol Biol Phys* **10**, 787–800 (1984).

351. Huang, Y. *et al.* Predicting lesion size by accumulated thermal dose in MR-guided focused ultrasound for essential tremor. *Med Phys* **45**, 4704–4710 (2018).

352. Chang, W. S. *et al.* Factors associated with successful magnetic resonance–guided focused ultrasound treatment: efficiency of acoustic energy delivery through the skull. *J Neurosurg* **124**, 411–416 (2016).

353. Jones, R. M. *et al.* Accumulated thermal dose in MRI-guided focused ultrasound for essential tremor: repeated sonications with low focal temperatures. *Journal of Neurosurgery JNS* **132**, 1802–1809 (2020).

354. Harary, M. *et al.* Focused ultrasound in neurosurgery: a historical perspective. *Neurosurgical Focus FOC* **44**, E2 (2018).

355. Park, Y. S., Jung, N. Y., Na, Y. C. & Chang, J. W. Four-year follow-up results of magnetic resonance-guided focused ultrasound thalamotomy for essential tremor. *Movement Disorders* **34**, 727–734 (2019).

356. Pichardo, S., Sin, V. W. & Hynynen, K. Multi-frequency characterization of the speed of sound and attenuation coefficient for longitudinal transmission of freshly excised human skulls. *Phys Med Biol* **56**, 219–250 (2011).

357. Bond, A. E. *et al.* Safety and efficacy of focused ultrasound thalamotomy for patients with medication-refractory, tremor-dominant Parkinson disease a randomized Clinical trial. *JAMA Neurol* **74**, 1412–1418 (2017).

358. Elias, W. J. *et al.* A Randomized Trial of Focused Ultrasound Thalamotomy for Essential Tremor. *New England Journal of Medicine* **375**, 730–739 (2016).

359. Jung, N. Y. *et al.* Factors related to successful energy transmission of focused ultrasound through a skull: A study in human cadavers and its comparison with clinical experiences. *J Korean Neurosurg Soc* **62**, 712–722 (2019).

360. Gagliardo, C. *et al.* Transcranial Magnetic Resonance Imaging-Guided Focused Ultrasound Treatment at 1.5 T: A Retrospective Study on Treatment- and Patient-Related Parameters Obtained From 52 Procedures. *Front Phys* **7**, 1–9 (2020).

361. Caballero-Insaurriaga, J. *et al.* Zero TE MRI applications to transcranial MR-guided focused ultrasound: Patient screening and treatment efficiency estimation. *Journal of Magnetic Resonance Imaging* **50**, 1583–1592 (2019).

362. Wilson, D. N., Barnett, Y., Kyle, K., Tisch, S. & Jonker, B. P. Predictors of thermal response and lesion size in patients undergoing magnetic resonance-guided focused ultrasound thalamotomy. *Journal of Clinical Neuroscience* **91**, 75–79 (2021).

363. Bond, A. E. & Elias, W. J. Predicting lesion size during focused ultrasound thalamotomy: A review of 63 lesions over 3 clinical trials. *Neurosurg Focus* **44**, 1–6 (2018).

364. Hughes, A., Huang, Y., Schwartz, M. L. & Hynynen, K. The reduction in treatment efficiency at high acoustic powers during MR-guided transcranial focused ultrasound thalamotomy for Essential Tremor. *Med Phys* **45**, 2925–2936 (2018).

365. Yamamoto, K. *et al.* Factors associated with heating efficiency in transcranial focused ultrasound therapy. *Neurol Med Chir (Tokyo)* **60**, 594–599 (2020).

366. Pineda-Pardo, J. A. *et al.* Transcranial magnetic resonance-guided focused ultrasound thalamotomy in essential tremor: A comprehensive lesion characterization. *Neurosurgery* **87**, 256–265 (2020).

367. Yang, A. I. *et al.* Letter: Lesion Shape and Size in MRgFUS Thalamotomy: Predictors and Implications. *Neurosurgery* **89**, E198–E200 (2021).

368. López-Aguirre, M. *et al.* Lesion 3D modeling in transcranial MR-guided focused ultrasound thalamotomy. *Magn Reson Imaging* **80**, 71–80 (2021).

369. Fry, F. J. & Barger, J. E. Acoustical properties of the human skull. *Journal of the Acoustical Society of America* **63**, 1576–1590 (1978).

370. Nicholson, P. H. F., Strelitzki, R., Cleveland, R. O. & Bouxsein, M. L. Scattering of ultrasound in cancellous bone: Predictions from a theoretical model. *J Biomech* **33**, 503–506 (2000).

371. Davidson, B. *et al.* Technical and radiographic considerations for magnetic resonance imaging–guided focused ultrasound capsulotomy. *J Neurosurg* **135**, 291–299 (2021).

372. Eames, M. D. C., Hananel, A., Snell, J. W., Kassell, N. F. & Aubry, J. F. Trans-cranial focused ultrasound without hair shaving: Feasibility study in an ex vivo cadaver model. *J Ther Ultrasound* **1**, 2–7 (2014).

373. Yang, A. I. *et al.* Patient-specific effects on sonication heating efficiency during magnetic resonance-guided focused ultrasound thalamotomy. *Med Phys* **48**, 6588–6596 (2021).

374. Shantanam, S. & MUELLER. Consensus Statement on the Classification of Tremors. From the Task Force on Tremor of the International Parkinson and Movement Disorder Society. *Physiol Behav* **176**, 139–148 (2018).

375. Hughes, A., Huang, Y., Schwartz, M. L. & Hynynen, K. The reduction in treatment efficiency at high acoustic powers during MR-guided transcranial focused ultrasound thalamotomy for Essential Tremor. *Med Phys* **45**, 2925–2936 (2018).

376. Valvano, J. W., Cochran, J. R. & Diller, K. R. Thermal Conductivity and Diffusivity of Biomaterials Measured with Self-Heated Thermistors. **6**, 301–311 (1985).

377. Nicholson, P. H. F. & Bouxsein, M. L. Effect of temperature on ultrasonic properties of the calcaneus in situ. *Osteoporosis International* **13**, 888–892 (2002).

378. Wilson, W. D. The Journal of the Acoustical Society Of America Volume 31 Number 8 August 1959:Speed of Sound in Distilled Water as a Function of Temperature and Pressure. *Journal of the Acoustical Society of America* **31**, 1067–1072 (1959).

379. El-Sariti, A. A., Evans, J. A. & Truscott, J. G. The temperature dependence of the speed of sound in bovine bone marrow at 750 kHz. *Ultrasound Med Biol* **32**, 985–989 (2006).

380. McDannold, N., King, R. L. & Hynynen, K. MRI Monitoring of Heating Produced by Ultrasound Absorption in the Skull: In Vivo Study in Pigs. *Magn Reson Med* **51**, 1061–1065 (2004).

381. Schwartz, M. L. *et al.* Skull bone marrow injury caused by MR-guided focused ultrasound for cerebral functional procedures. *J Neurosurg* **130**, 1–5 (2018).

382. Souza, R. M., Costa-Felix, R. P. B. & Alvarenga, A. V. Attenuation Coefficient Variation as a Function of Temperature in a Cortical Bone Phantom. in vol. 70 807–810 (Springer Singapore, 2019).

383. Chang, W. S. *et al.* Factors associated with successful magnetic resonance–guided focused ultrasound treatment: efficiency of acoustic energy delivery through the skull. *J Neurosurg* **124**, 411–416 (2016).

384. Jung, H. H. *et al.* Different magnetic resonance imaging patterns after transcranial magnetic resonance-guided focused ultrasound of the ventral intermediate nucleus of the thalamus and anterior limb of the internal capsule in patients with essential tremor or obsessive-com. *J Neurosurg* **122**, 162–168 (2015).

385. Iijima, K. *et al.* Predictors of thermal increase in magnetic resonance-guided focused ultrasound treatment for essential tremor: histogram analysis of skull density ratio values for 1024 elements. *J Neurosurg* **136**, 1381–1386 (2022).

386. Pineda-Pardo, J. A. *et al.* Letter: The Role of Skull Thickness beyond the Skull Density Ratio on MRgFUS Thalamotomy Feasibility: Which Patients Should We Exclude? *Neurosurgery* **86**, E477–E479 (2020).

387. Yamamoto, K. *et al.* Ventralis intermedius thalamotomy with focused ultrasound for patients with low skull density ratio. *Movement disorders : official journal of the Movement Disorder Society* vol. 34 1239–1240 Preprint at https://doi.org/10.1002/mds.27726 (2019).

388. Kyle, K. *et al.* Tremor suppression following treatment with MRgFUS: skull density ratio consistency and degree of posterior dentatorubrothalamic tract lesioning predicts long-term clinical outcomes in essential tremor. *Front Neurol* **14**, 1–10 (2023).

389. Fahn, S., Tolosa, E. & Marin, C. Clinical Rating Scale for Tremor. *Parkinson's disease and movement disorders* 225–234 Preprint at (1988).

390. Jenkinson, M. & Smith, S. *A global optimisation method for robust affine registration of brain images*. *Medical Image Analysis* vol. 5 www.elsevier.com/locate/media (2001).

391. Pineda-Pardo, J. A. *et al.* Transcranial Magnetic Resonance-Guided Focused Ultrasound Thalamotomy in Essential Tremor: A Comprehensive Lesion Characterization. *Neurosurgery* **87**, 256–265 (2020).

392. Virtanen, P. *et al.* SciPy 1.0: fundamental algorithms for scientific computing in Python. *Nat Methods* **17**, 261–272 (2020).

393. Meng, Y. *et al.* Magnetic resonance–guided focused ultrasound thalamotomy for treatment of essential tremor: A 2-year outcome study. *Movement Disorders* **33**, 1647–1650 (2018).

394. King, N. K. K. *et al.* Microelectrode recording findings within the tractography-defined ventral intermediate nucleus. *J Neurosurg* **126**, 1669–1675 (2017).

395. Obwegeser, A. A. *et al.* Quantitative and qualitative outcome measures after thalamic deep brain stimulation to treat disabling tremors. *Neurosurgery* **48**, 274 (2001).

396. Bender, B., Mänz, C., Korn, A., Nägele, T. & Klose, U. Optimized 3D magnetization-prepared rapid acquisition of gradient echo: Identification of thalamus substructures at 3T. *American Journal of Neuroradiology* **32**, 2110–2115 (2011).

397. Corona, V., Lellmann, J., Nestor, P., Schönlieb, C. B. & Acosta-Cabronero, J. A multi-contrast MRI approach to thalamus segmentation. *Hum Brain Mapp* **41**, 2104–2120 (2020).

398. Akram, H. *et al.* Connectivity derived thalamic segmentation in deep brain stimulation for tremor. *Neuroimage Clin* **18**, 130–142 (2018).

399. Petersen, K. J. *et al.* Structural and functional connectivity of the nondecussating dentato-rubro-thalamic tract. *Neuroimage* **176**, 364–371 (2018).

400. Coenen, V. A., Allert, N. & Mädler, B. A role of diffusion tensor imaging fiber tracking in deep brain stimulation surgery: DBS of the dentato-rubro-thalamic tract (drt) for the treatment of therapy-refractory tremor. *Acta Neurochir (Wien)* **153**, 1579–1585 (2011).

401. Sammartino, F. *et al.* Tractography-Based Ventral Intermediate Nucleus Targeting: Novel Methodology and Intraoperative Validation. *Mov Disord* **31**, 1217–1225 (2016).

402. Fan, H. *et al.* Which one is the superior target? A comparison and pooled analysis between posterior subthalamic area and ventral intermediate nucleus deep brain stimulation for essential tremor. *CNS Neurosci Ther* (2022) doi:10.1111/cns.13878.

403. Kvernmo, N. *et al.* Deep Brain Stimulation for Arm Tremor: A Randomized Trial Comparing Two Targets. *Ann Neurol* **91**, 585–601 (2022).

404. Hariz, G.-M., Blomstedt, P. & Koskinen, L.-O. D. Long-term effect of deep brain stimulation for essential tremor on activities of daily living and health-related quality of life. *Acta Neurol Scand* **118**, 387–394 (2008).

405. Blomstedt, P., Sandvik, U., Fytagoridis, A. & Tisch, S. THE POSTERIOR SUBTHALAMIC AREA IN THE TREATMENT OF MOVEMENT DISORDERS: PAST, PRESENT, AND FUTURE. *Neurosurgery* **64**, (2009).

406. Mai, J. K. & Majtanik, M. Toward a common terminology for the Thalamus. *Frontiers in Neuroanatomy* vol. 12 Preprint at https://doi.org/10.3389/fnana.2018.00114 (2019).

407. Morel, A. *Stereotactic atlas of the human thalamus and basal ganglia*. (CRC Press, 2007).

408. Tani, N., Morigaki, R., Kaji, R. & Goto, S. Current Use of Thalamic Vim Stimulation in Treating Parkinson's Disease. *A Synopsis of Parkinson's Disease* (2014) doi:10.5772/57105.

409. Meng, F.-G. G., Zhang, J.-G. G., Kao, C. C., Klein, J. C. & Hilker, R. The tremor network targeted by successful VIM deep brain stimulation in humans. *Neurology* **79**, 953; author reply 953 (2012).

410. Telford, R. & Vattoth, S. MR anatomy of deep brain nuclei with special reference to specific diseases and deep brain stimulation localization. *Neuroradiology Journal* **27**, 29–43 (2014).

411. Cagnan, H. *et al.* The nature of tremor circuits in parkinsonian and essential tremor. *Brain* **137**, 3223–3234 (2014).

412. Iglesias, J. E. *et al.* A probabilistic atlas of the human thalamic nuclei combining ex vivo MRI and histology. *Neuroimage* **183**, 314–326 (2018).

413. Fischl, B. *et al.* Automatically Parcellating the Human Cerebral Cortex. *Cerebral Cortex* **14**, 11–22 (2004).

414. Su, J. H. *et al.* Thalamus Optimized Multi Atlas Segmentation (THOMAS): fast, fully automated segmentation of thalamic nuclei from structural MRI. *Neuroimage* **194**, 272–282 (2019).

415. Avants, B. B. *et al.* A reproducible evaluation of ANTs similarity metric performance in brain image registration. *Neuroimage* **54**, 2033–2044 (2011).

416. Coenen, V. A. *et al.* The dentato-rubro-thalamic tract as the potential common deep brain stimulation target for tremor of various origin: an observational case series. *Acta Neurochir (Wien)* **162**, 1053–1066 (2020).

417. Fenoy, A. J. & Schiess, M. C. Deep Brain Stimulation of the Dentato-Rubro-Thalamic Tract: Outcomes of Direct Targeting for Tremor. *Neuromodulation* **20**, 429–436 (2017).

418. Sweet, J. A. *et al.* Fiber tractography of the axonal pathways linking the basal ganglia and cerebellum in Parkinson disease: Implications for targeting in deep brain stimulation: Clinical article. *J Neurosurg* **120**, 988–996 (2014).

419. Coenen, V. A. *et al.* Modulation of the cerebello-thalamo-cortical network in thalamic deep brain stimulation for tremor: a diffusion tensor imaging study. *Neurosurgery* **75**, 657–670 (2014).

420. Tian, Q. *et al.* Diffusion MRI tractography for improved transcranial MRI-guided focused ultrasound thalamotomy targeting for essential tremor. *Neuroimage Clin* **19**, 572–580 (2018).

421. Zur, G., Lesman-segev, O. & Schlesinger, I. Structural integrity following focused ultrasound thalamotomy and its correlation with tremor relief. **17**, (2019).

422. Anthofer, J. *et al.* The variability of atlas-based targets in relation to surrounding major fibre tracts in thalamic deep brain stimulation. *Acta Neurochir (Wien)* **156**, 1497–1504 (2014).

423. Deuter, D., Torka, E., Kohl, Z., Schmidt, N.-O. & Schlaier, J. Mediation of Tremor Control by the Decussating and Nondecussating Part of the Dentato-Rubro-Thalamic

Tract in Deep Brain Stimulation in Essential Tremor: Which Part Should Be Stimulated? *Neuromodulation* (2022) doi:10.1016/j.neurom.2022.04.040.

424. Middlebrooks, E. H. *et al.* Directed stimulation of the dentato-rubro-thalamic tract for deep brain stimulation in essential tremor: a blinded clinical trial. *Neuroradiol J* **35**, 203–212 (2022).

425. Middlebrooks, E. H. *et al.* Connectivity correlates to predict essential tremor deep brain stimulation outcome: Evidence for a common treatment pathway. *Neuroimage Clin* **32**, 102846 (2021).

426. Riskin-Jones, H. H., Kashanian, A., Sparks, H., Tsolaki, E. & Pouratian, N. Increased structural connectivity of thalamic stimulation sites to motor cortex relates to tremor suppression. *Neuroimage Clin* **30**, 102628 (2021).

427. Dembek, T. A. *et al.* PSA and VIM DBS efficiency in essential tremor depends on distance to the dentatorubrothalamic tract. *Neuroimage Clin* **26**, 102235 (2020).

428. Thaler, C. *et al.* Changes In The Cerebello-thalamo-cortical Network After MR- guided Focused Ultrasound Thalamotomy. **1**, 1–34 (2021).

429. Wintermark, M. *et al.* Imaging Findings in MR Imaging-Guided Focused Ultrasound Treatment for Patients with Essential Tremor. *American journal of neuroradiology : AJNR* **35**, 891–896 (2013).

430. Hassler, R. Architectonic organization of the thalamic nuclei. *Stereotaxy of the Human Brain, Anatomical, Physiological and Clinical Application* 140–180 (1982).

431. Smith, S. M. Fast robust automated brain extraction. *Hum Brain Mapp* **17**, 143–155 (2002).

432. Smith, S. M. *et al.* Accurate, robust, and automated longitudinal and cross-sectional brain change analysis. *Neuroimage* **17**, 479–489 (2002).

433. Tournier, J. D. *et al.* MRtrix3: A fast, flexible and open software framework for medical image processing and visualisation. *Neuroimage* **202**, 116137 (2019).

434. Tournier, J. D., Calamante, F., Gadian, D. G. & Connelly, A. Direct estimation of the fiber orientation density function from diffusion-weighted MRI data using spherical deconvolution. *Neuroimage* **23**, 1176–1185 (2004).

435. Dhollander, T. & Connelly, A. A novel iterative approach to reap the benefits of multi-tissue CSD from just single-shell (+ b = 0) diffusion MRI data A novel iterative approach to reap the benefits of multi-tissue CSD. (2016).

436. Jeurissen, B., Tournier, J. D., Dhollander, T., Connelly, A. & Sijbers, J. Multi-tissue constrained spherical deconvolution for improved analysis of multi-shell diffusion MRI data. *Neuroimage* **103**, 411–426 (2014).

437. Tournier, J.-D. & , F. Calamante, and a. C. Improved probabilistic streamlines tractography by 2 nd order integration over fibre orientation distributions. *Ismrm* **88**, 2010 (2010).

438. Yamada, K. *et al.* MR imaging of ventral thalamic nuclei. *American Journal of Neuroradiology* **31**, 732–735 (2010).

439. Garyfallidis, E. *et al.* Dipy, a library for the analysis of diffusion MRI data. *Front Neuroinform* **8**, 1–17 (2014).

440. Calamante, F., Smith, R. E., Tournier, J. D., Raffelt, D. & Connelly, A. Quantification of voxel-wise total fibre density: Investigating the problems associated with track-count mapping. *Neuroimage* **117**, 284–293 (2015).

441. Garyfallidis, E. Towards an Accurate Brain. 1–181 (2012).

442. Petersen, K. J. *et al.* Structural and functional connectivity of the nondecussating dentato-rubro-thalamic tract. *Neuroimage* **176**, 364–371 (2018).

443. Meng, Y. *et al.* Magnetic resonance-guided focused ultrasound thalamotomy for treatment of essential tremor: A 2-year outcome study. *Mov Disord* **33**, 1647–1650 (2018).

444. Lipsman, N. *et al.* MR-guided focused ultrasound thalamotomy for essential tremor: A proof-of-concept study. *Lancet Neurol* **12**, 462–468 (2013).

445. Murata, J. *et al.* Electrical stimulation of the posterior subthalamic area for the treatment of intractable proximal tremor. *J Neurosurg* **99**, 708–715 (2003).

446. Magara, A. *et al.* First experience with MR-guided focused ultrasound in the treatment of Parkinson's disease. *J Ther Ultrasound* **2**, 1–8 (2014).

447. Holcomb, J. M. *et al.* Improving tremor response to focused ultrasound thalamotomy. doi:10.1093/braincomms/fcad165/7175205.

448. Sporns, O. The human connectome: origins and challenges. *Neuroimage* **80**, 53–61 (2013).

449. Welton, T. *et al.* Essential tremor. *Nat Rev Dis Primers* **7**, (2021).

450. Sadikot, A. F. *et al.* Creation of computerized 3D MRI-integrated atlases of the human basal ganglia and thalamus. *Front Syst Neurosci* **5**, 1–8 (2011).

451. Osenbach, R. K. & Burchiel, K. J. Thalamotomy: indications, techniques, and results. *Neurosurgical Treatment of Movement Disorders. Park Ridge, AANS* 107–129 (1998).